Single-ion conducting polymer and hybrid electrolyte for high-energy density lithium-metal batteries

Zur Erlangung des akademischen Grades eines

DOKTORS DER NATURWISSENSCHAFTEN

(Dr. rer. nat.)

von der KIT-Fakultät für Chemie und Biowissenschaften des Karlsruher Instituts für Technologie (KIT)

genehmigte

DISSERTATION

von

Grégoire Vansse

1. Referent: Prof. Dr. Dominic Bresser
2. Referent: Prof. Dr. Patrick Théato
Tag der mündlichen Prüfung: 2. Dezember 2024

Abstract

The future of electrochemical energy storage depends on the advancement of science and technology concerning safer recharge-able batteries with enhanced energy densities. With respect to the anode, the maximum energy density is eventually obtained when employing the reactive metal itself. For rechargeable lithium-based batteries, for instance, the metallic anode would allow for a tenfold increase in specific capacity compared to the current state of the art lithium-ion anode, graphite. However, multiple issues, e.g., the parasitic reactions of Li metal with liquid organic electrolytes and the unstable and dendritic lithium deposition, posing the risk of dendrite-induced short circuits, have to be overcome prior to the potential commercialization of secondary lithium metal batteries. These issues are largely associated to the presently used meta-stable electrolytes, suffering low cationic transference numbers, and in case of polymer-based ones, additionally, relatively low ionic conductivities and poor mechanical properties.

My PhD project addressed these issues by employing highly stable and conductive single-ion polymer electrolytes to realize safe, sustainable and cost-efficient high-energy density batteries. The project was grounded in the appealing potentialities of polyaromatic polymers and multiblock copolymers, which provide good ionic conductivity, high thermal stability (>300 °C), and excellent electrochemical stability (>4.0 V). These polymers were processed as solid electrolyte membranes and, in combination with (optimized) high-energy lithium-ion cathode materials like $Li[Ni_8Mn_1Co_1]O_2$), as polymer-cathode tapes. The polymer electrolyte serves simultaneously as binder and ion transport pathway towards the active material particles. The thermomechanical, electrochemical, and structural properties were systematically explored as a function of the versatile molecular architecture and plasticizer such as polyethylene glycol and propyle carbonate. The concept of a hybride membrane was also explored.

Furthermore, we addressed the issue of ether-bound stability by designing a new ether-free single-conducting polymer electrolyte that provides good thermal stability, excellent ionic

conductivity, and a high electrochemical stability window when dopped with propylene carbonate. However, the cyclability in Li/Li symmetrical cells appears to be rather poor when using high current density even after a short time. Hence, we introduced a thin PEO-based protective layer between the single-ion conducting polymer layer and the lithium metal. We found that this multilayer system exhibits excellent cyclability in lithium symmetrical cells at various current densities but also at constant current density for more than 500 hours and could be cycled in full-cells, using lithium metal anode and LFP cathodes, for more than 200 cycles with no particular capacity drop.

In sum, the results reported herein contribute to the development of high-performance polymer electrolytes for long-term stable, high-energy lithium-metal batteries.

Résumé

L'avenir du stockage d'énergie électrochimique dépend des avancées scientifiques et technologiques, notamment du développement de batteries rechargeables plus sûres, avec de meilleures densités d'énergie. Du côté de l'anode, la densité d'énergie maximale peut être obtenue en utilisant directement le métal réactif, et non un matériau à intercalation. Par exemple, pour les batteries rechargeables à base de lithium, l'anode métallique permettrait d'augmenter la capacité spécifique par un facteur dix par rapport au graphite, actuellement utilisé comme anode dans les batteries lithium-ion. Cependant, plusieurs problèmes, tels que les réactions du lithium métallique avec les électrolytes à base de solvants organiques, la déposition inhomogène du lithium et la formation de dendrites pouvant induire un risque de courts-circuits, doivent être surmontés avant une éventuelle commercialisation de batteries basées sur le lithium métallique. Ces problèmes sont largement liés aux électrolytes actuellement utilisés, qui souffrent de faibles nombres de transfert cationique et, dans le cas des électrolytes polymères, de conductivités ioniques relativement faibles et de mauvaises propriétés mécaniques.

Dans cette thèse nous avons abordé ces problèmes en utilisant des électrolytes polymères ionomères, hautement stables et conducteurs, pour fabriquer des batteries à haute densité d'énergie qui seraient sûres, durables et économiques. Le projet s'est appuyé sur les propriétés prometteuses des polymères polyaromatiques et des copolymères multiblocs, qui offrent de hautes conductivités ioniques, une grande stabilité thermique (> 300 °C) et une excellente stabilité électrochimique (> 4 V). Ces polymères ont été préparés sous forme de membranes d'électrolytes solides et combiné avec des matériaux cathodiques à haute énergie en lithium-ion (optimisés) tels que Li[Ni8Mn1Co1]O2, pour former des électrodes positives. Dans ce dernier cas, l'électrolyte polymère sert simultanément de liant et de voie de transport ionique vers les particules de matériau actif. Les propriétés thermomécaniques, électrochimiques et structurales ont été systématiquement explorées en fonction de l'architecture moléculaire et des plastifiants

tels que le polyéthylène glycol et le carbonate de propylène. Des membranes hybrides ont également été étudiées, et d'excellentes stabilités électrochimiques anodiques ont été obtenues. Dans une seconde partie de la thèse, nous avons abordé la question de la stabilité liée aux liaisons éther du squelette polymère en synthétisant un nouvel électrolyte polymère ionomère. Ce nouveau matériau offre une bonne stabilité thermique, une excellente conductivité ionique et une large fenêtre de stabilité électrochimique lorsqu'il est dopé avec du carbonate de propylène. Cependant, la cyclabilité dans des piles symétriques Li/Li s'est révélée faible sous une forte densité de courant, même après un court laps de temps. Nous avons donc introduit une fine couche de protection à base de PEO entre la couche de polymère et le lithium métallique. Ce système multicouche présente une excellente cyclabilité dans des piles symétriques à différentes densités de courant, mais également à densité de courant constante pendant plus de 500 heures. Ce système a également été cyclé dans une batterie composée d'une anode en lithium métallique et d'une cathode LFP, pendant plus de 200 cycles sans chute particulière de capacité.

En résumé, les résultats rapportés ici contribuent au développement d'électrolytes polymères haute performance pour des batteries lithium-métal à haute énergie et haute stabilité.

Kurzfassung

Ziel der weiteren Entwicklung elektrochemischer Energiespeicher ist nicht zuletzt eine Verbesserung der Sicherheit und eine Steigerung der Energiedichte. Was die Anode betrifft, so wird die maximale theoretische Energiedichte durch die Verwendung des reaktiven Metalls selbst erreicht. Bei wiederaufladbaren Batterien auf Lithiumbasis würde die metallische Anode beispielsweise eine Verzehnfachung der spezifischen Kapazität im Vergleich zum derzeitigen Stand der Technik (Graphit) ermöglichen. Vor der potenziellen Vermarktung von Lithium-Metall-Sekundärbatterien müssen jedoch noch mehrere Probleme gelöst werden, z. B. die parasitären Reaktionen von Li-Metall mit flüssigen organischen Elektrolyten und die instabile und dendritische Lithiumablagerung, die das Risiko von Dendriten-induzierten Kurzschlüssen birgt. Diese Probleme stehen größtenteils im Zusammenhang mit den derzeit verwendeten metastabilen Elektrolyten, die eine begrenzte elektrochemische Stabilität, eine relativ niedrige Kationenüberführungszahl und, insbesondere bei Elektrolyten auf Polymerbasis, auch eine relativ geringe Ionenleitfähigkeit aufweisen.

Mein Dissertationsprojekt befasste sich mit diesen Problemen, indem ich hochstabile und leitfähige Einzelionen-Polymerelektrolyte einsetzte, um sichere, nachhaltige und kosteneffiziente Batterien mit hoher Energiedichte zu realisieren. Das Projekt basierte auf den attraktiven Möglichkeiten von polyaromatischen Polymeren und Multiblock-Copolymeren, die eine hohe Ionenleitfähigkeit, eine hohe thermische Stabilität (>300 °C) und eine ausgezeichnete elektrochemische Stabilität (>4 V) aufweisen. Diese Polymere wurden zu Festelektrolytmembranen und in Kombination mit (optimierten) hochenergetischen Lithium-Ionen-Kathodenmaterialien wie Li[$Ni_{0.8}Mn_{0.1}Co_{0.1}$]O_2) zu Polymer-Kathodenmembranen verarbeitet. Die Polymerelektrolyte dienen hierin gleichzeitig als Bindemittel und Ionentransportweg zu den aktiven Materialpartikeln. Ihre thermomechanischen, elektrochemischen und strukturellen Eigenschaften wurden systematisch in Abhängigkeit von der vielseitigen molekularen Architektur und den eingebauten kleineren Molekülen zur

Unterstützung des Ladungstransports untersucht. Darüber hinaus wurden auch hybride Systeme erforscht.

Schließlich wurde ein neuer etherfreier, einfach leitender Polymerelektrolyt entwickelt, der eine gute thermische Stabilität, eine ausgezeichnete Ionenleitfähigkeit und ein breites elektrochemisches Stabilitätsfenster aufweist. Allerdings war die Zyklenstabilität in symmetrischen Li‖Li-Zellen bei hohen Stromdichten vergleichsweise verbesserungsfähig im Vergleich zu den anderen Polymerelektrolyten. Daher haben wir eine dünne Schutzschicht auf PEO-Basis zwischen dem einzelionenleitenden Polymerelektrolyten und der Lithium-Metallelektrode eingebracht. Dieses Mehrschichtsystem weist eine ausgezeichnete Zyklenstabilität in symmetrischen Li‖Li-Zellen für mehr als 500 Stunden und in Li‖LiFePO$_4$-Vollzellen für mehr als 200 Zyklen auf.

Insgesamt tragen die hier vorgestellten Ergebnisse zur Entwicklung von Hochleistungspolymerelektrolyten für langzeitstabile, hochenergetische Lithium-Metall-Batterien bei.

Content

1. Motivation

In 2022, almost 82% of the world's energy consumption came from fossil fuels such as oil, gas, and coal, (**Figure 1-1**) but these energy sources are non-renewable due to their limited natural reserves[1,2]. Furthermore, they are accountable for most CO_2 emissions and contribute to global warming[3]. The Paris Agreement, established in 2015, settled the targeted temperature increase to a maximum of 2 °C compared to the preindustrial level and ideally only 1.5 °C[4]. Unfortunately, our actual extraction and consumption of the resources will render this objective unreachable, and studies suggest that nearly 40% of the committed emissions from existing reserves must be avoided to stay below 1.5 °C[5].

The part of renewable energy has been increasing in the last 20 years, but it is still a relatively small share of the global energy mix. The main advantages of these energy sources are the essentially unlimited resources and the resulting decarbonization. Nevertheless, renewable energy sources such as solar and wind power are intermittent, leading to fluctuating and unpredictable production. To ensure a continuous energy distribution when replacing fossil fuels with renewable sources, stationary energy storage devices are needed. These storage technologies mainly rely on mechanical, electrical, chemical, or electrochemical storage mechanisms[6].
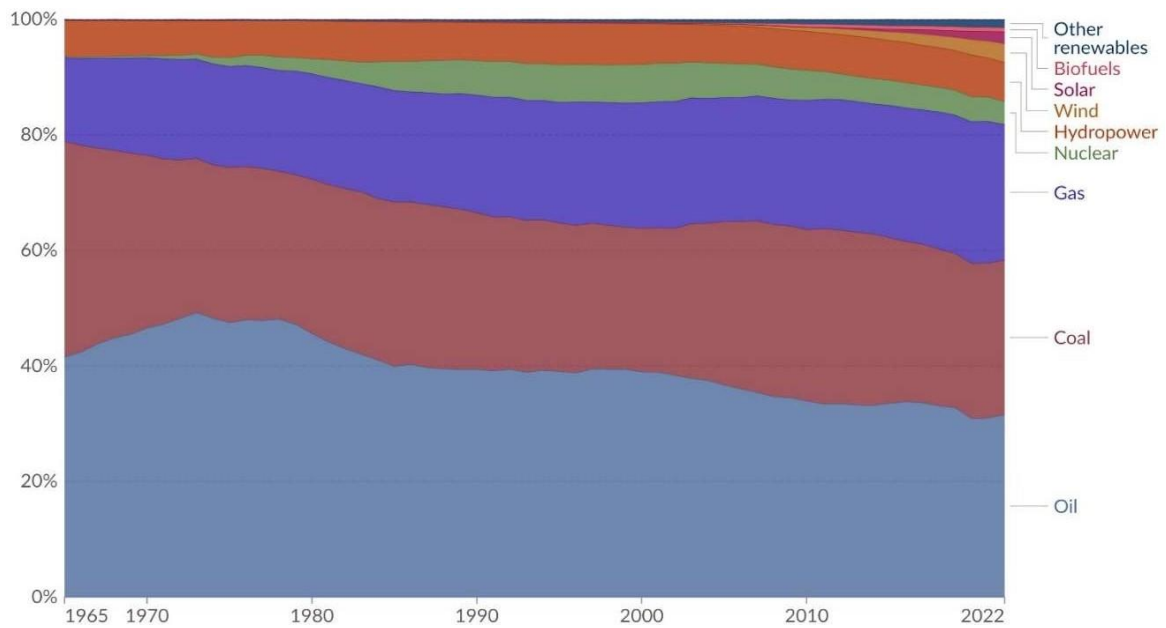
Figure 1-1. Worldwide energy consumption by sources from 1965 to 2022.

Moreover, the consumption of energy by sector (**Figure 1-2.a**) and energy consumption of the transportation sector by energy source (**Figure 1-2.b**) show that the world mainly depends on non-renewable fuels for transportation. Therefore, energy storage technologies for mobile applications are also highly needed to stick to the objectives of the Paris Agreement. The use of electric vehicles is a potential solution for reducing the use of fossil fuels in the transportation sector, which accounts for approximately 30% of the global energy mix.
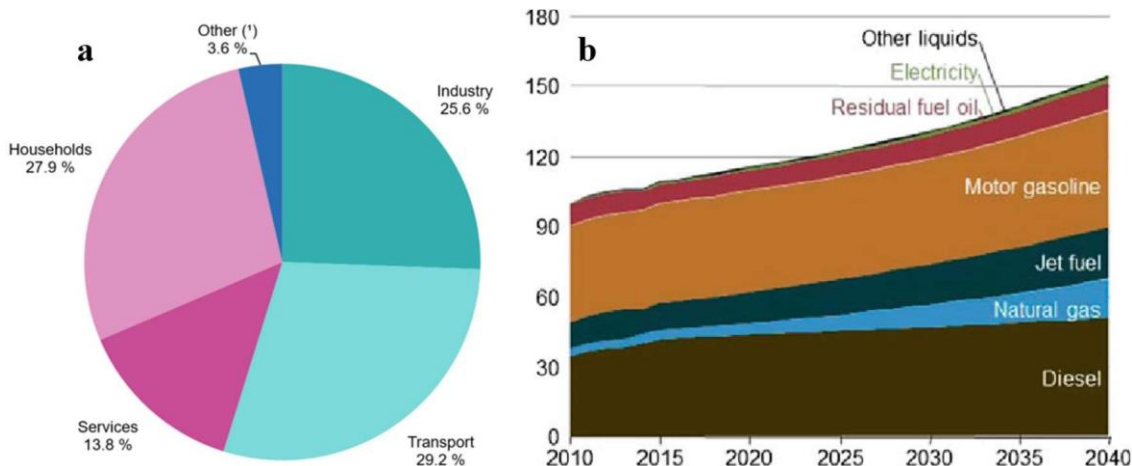
Figure 1-2. Energy consumption by sector in the European Union in 2021 (% of the total, based on tetra joules)[7] and world transportation sector consumption by energy source (in quadrillion Btu)[8].

To achieve the planned substitution of internal combustion engine-powered vehicles by electric vehicles, the batteries powering these vehicles require higher gravimetric and volumetric energy densities due to the space and weight limitations in these vehicles. But they also need to, at least, match the performances of fossil fuel-based systems in terms of cost, cycle life, refueling time, and reliability. Without these prerequisites, commercialization and widespread market penetration will remain hard to achieve.

In this context, the development of advanced batteries with higher energy density is crucial for decarbonizing the transportation sector. Among different technologies, lithium-ion batteries (LIBs) are the most used today, but their energy density is limited by the use of graphite anode. To overcome this, the use of lithium metal anode is the holy grail of researchers. However, these lithium metal batteries (LMBs) still suffer from certain drawbacks due to the use of liquid electrolytes in combination with lithium metal. Therefore, the implementation of solid electrolytes, which can be inorganic solids or polymers, appears to be a suitable approach for further improvement.

2. Introduction

The growth of the global battery market [9] and the demand for always better performances have motivated the development of a new battery technology, first commercialized by SONY in 1991, the lithium-ion battery. This secondary battery allows much higher specific energy and specific power than the previous technologies (**Figure 2-1**) and can respond to the growing energy storage demand. In fact, the invention and development of lithium-ion batteries is sometimes considered as the technology that could have one of the biggest impacts of all technology in human history. This was recognized by John B. Goodenough, M. Stanley Whittingham and Akira Yoshino receiving the 2019 Nobel Prize in Chemistry[10].
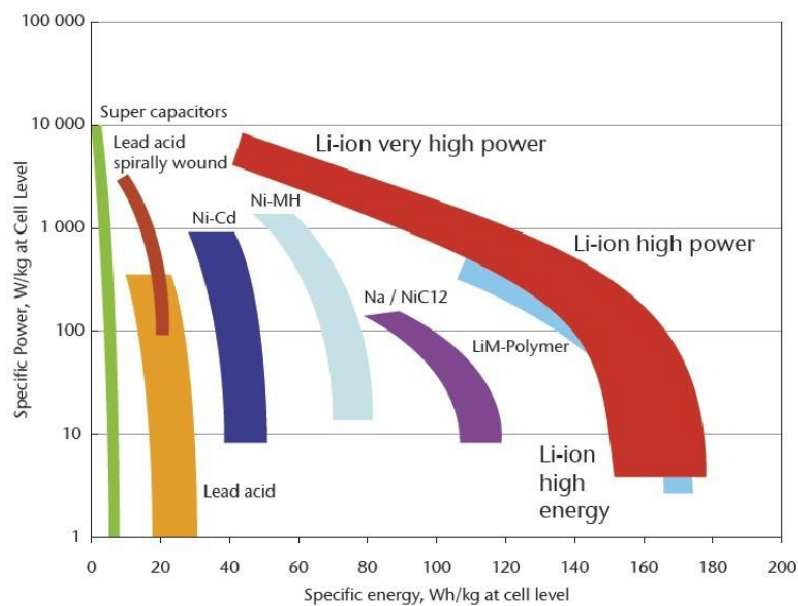
Figure 2-1. Comparison of the different secondary battery technologies[11].

2.1 Secondary Batteries

2.1.1 Working Principle

Secondary batteries are devices used to store energy electrochemically. They consist of essentially three elements: a positive and a negative electrode where the electrochemical processes (oxidation or reduction) occur during charge or discharge, and an electrolyte that ensures the transport of the ions between the two electrodes. In the case of liquid electrolytes, the liquid is contained within a thin polymer microporous membrane that acts as an electronically insulating separator between the two electrodes (**Figure 2-2**). Reversible electrochemical processes in both electrodes enable these batteries to be recharged when a voltage or current is applied to the battery cell. This is different from primary batteries, which can only be discharged once.

During the discharge process. i.e., the spontaneous process, the oxidation reaction occurs at the negative electrode. Therefore, it is commonly called the anode. Conversely, the positive electrode is referred to as the cathode because it is the site of the reduction process during discharge. On the contrary during the charge process, the reduction and oxidation occur at the negative and the positive electrode, respectively. Usually, these electrodes are made of a blend of an active material, carbon, and a polymer binder. This blend is coated on a current collector made of aluminum (cathode) or copper (anode).
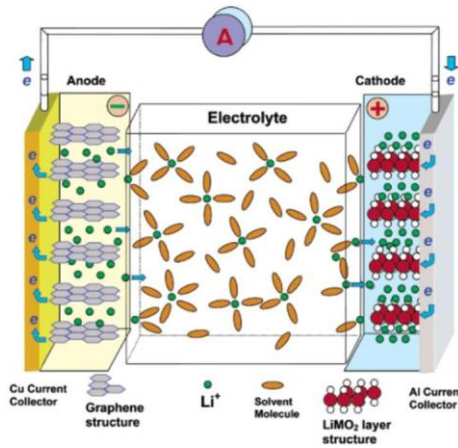
Figure 2-2. Representation of a lithium-ion battery during discharge[12].

2.1.2   Characteristic Parameters

To characterize and evaluate the performances of the different types of batteries, several parameters have been set:

-The nominal cell voltage (V) represents the potential difference between the positive and the negative electrode. It mainly depends on the chemical composition of the active material used in each electrode.

-The energy density and specific energy represent the amount of energy stored in a system respectively, per unit of volume (Wh m^{-3}) and per unit of mass (Wh kg^{-1}).

-The capacity, represents the quantity of charge stored in a unit of mass (C g^{-1} or A s g^{-1} or commonly mAh g^{-1})

-The C rate is the speed at which the battery can be charged and discharged (C rate of 0.1C corresponds to the current needed to fully charge the battery in 10 hours)

-The Coulombic efficiency is the ratio between the capacity delivered by the system during the discharge and the energy used to charge the system. If the efficiency is less than 100%, it implies that some of the charge carriers are consumed by side reactions during discharge or that other (detrimental) side reactions occur such as electrolyte decomposition.

2.2 Lithium Batteries

With the increasing development and practical application of portable electronics, most of us come into contact with lithium batteries daily. Nevertheless, the potential of this technology could have a much bigger impact on our modern society. Lithium-ion batteries are the preferred technology for replacing internal combustion engine-powered vehicles with electric vehicles in the near future. This change will ensure a significant reduction in greenhouse gas emissions. The need to generally improve the storage of intermittent renewable energy (wind, solar, geothermal, …) makes the development of lithium batteries a key factor for the successful transition to a more sustainable future.

The first lithium battery used a lithium metal negative electrode combined with a titanium sulfide positive electrode and an electrolyte made of $LiPF_6$ dissolved in propylene carbonate[13]. This initial chemistry, developed by Whittingham and colleagues, was not suitable for industrial use but laid the groundwork for further research. These lithium batteries are commonly referred to as "rocking chair" batteries, due to the displacement of the lithium ions from the anode to the cathode. These electrodes have undergone significant development, and various chemistries are now available.

2.2.1 Cathode Materials

Since the first lithium battery proposed by Whittingham, the reversible intercalation of lithium in cathodic oxide materials has been demonstrated by Besenhard[14]. The intercalation materials have been the preferred choice for the cathode in most lithium batteries. They consist of a solid network in which ions can be inserted and removed reversibly. These networks can have multiple chemistries, some of them will be presented below.

2.2.1.a   Lithium Transition Metal Oxides

In 1980, Goodehough[15] proposed $LiCoO_2$ (LCO) as a new layered transition metal oxide cathode with the crystal structure presented in **Figure 2-3**. Lithium and cobalt are situated in octahedral sites within alternating layers that are separated by layers of oxygen. This material is very attractive due to its high theoretical specific capacity of 274 mAh g^{-1}, low self-discharge, high discharge voltage, and excellent cycling performance. LCO was the material originally used by SONY in the first commercial lithium battery in 1991 and is still one of the most used materials in commercial batteries, specifically in mobile phones[16].
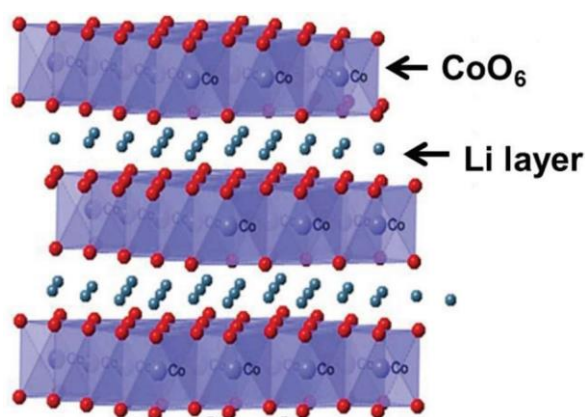
Figure 2-3. Crystal structure of $LiCoO_2$[17].

The major disadvantages of LCO materials are a fast fade capacity at high current rates and deep cycling[18], a rather low thermal stability[19], and the use of a high amount of cobalt resulting in a high cost and issues since cobalt is on the critical raw material list of the European Union[20]. Therefore, research has been focused on reducing or replacing the cobalt in the cathode materials. $LiNiO_2$ (LNO) has a similar crystal structure and theoretical specific capacity compared to LCO (275 mAh g^{-1}), but with a lower cost as it uses nickel instead of cobalt. However, LNO cathodes have two main drawbacks, first their thermal stability is even lower than the one of LCO[21], second the Ni^{2+} ions tend to substitute the Li^+ ions during synthesis and delithiation resulting in a lower cyclability of LNO cathodes[22].

Manganese has been a transition metal of interest to substitute nickel and/or cobalt in cathode materials because of its lower cost and lower toxicity compared to Co and Ni. Nevertheless, the resulting LiMnO$_2$ (LMO) material was still not satisfying because of the change in the crystal structure observed during cycling[23] and the dissolution of Mn in the electrolyte that was observed for manganese-rich cathodes[24].

The further efforts in research on cathode material resulted in the combination of the different transition metals in materials such as LiNi$_{0.8}$Co$_{0.15}$Al$_{0.05}$O$_2$ (NCA) Li(Ni$_{0.5}$Mn$_{0.5}$)O$_2$ (NMO), and LiNi$_x$Co$_y$Mn$_z$O$_2$ (NCM). The NCA cathode was already commercialized and has a high discharge capacity (200 m Ah g^{-1}) but suffers from a severe capacity fade at temperatures higher than 40 °C[25]. NMO suffers from the same drawback as LMO, mainly due to the high amount of manganese that can be dissolved in the electrolyte, resulting in capacity fade and lower cyclability.
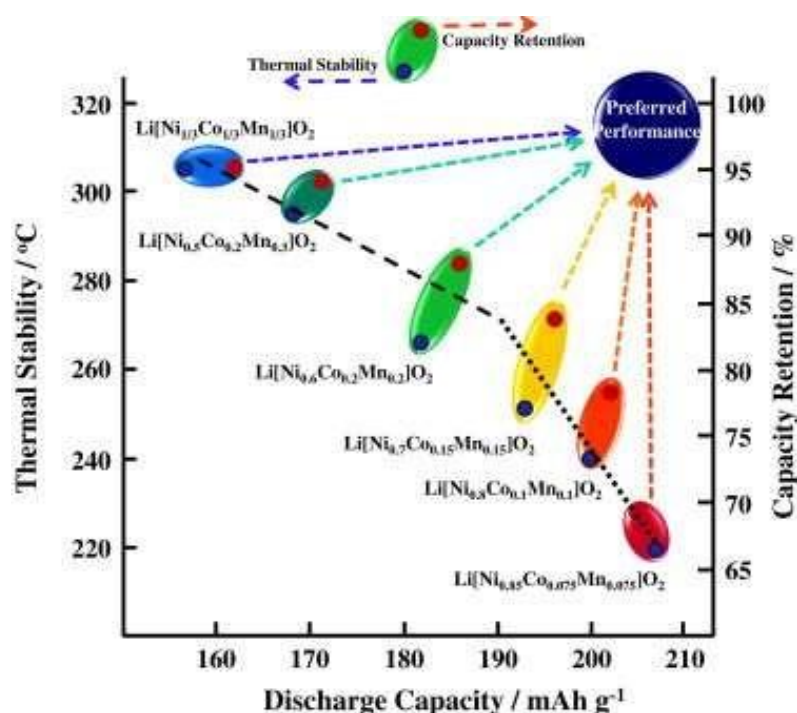

Figure 2-4. Comparison of the properties of Li(Ni$_{1-x-y}$Co$_x$Mn$_y$)O$_2$ with (x=1/3, 0.5, 0.6, 0.7, 0.8, 0.85)[26].

NCM is a very promising material for high-energy-density batteries required for electric vehicles. A big advantage is the multiple compositions that are accessible for this type of material and that results in different electrochemical and thermal properties as shown in **Figure 2-4**. The $LiNi_{1/3}Co_{1/3}Mn_{1/3}O_2$ material has already been used in commercial cells due to its relatively high discharge capacity (around 160 mAh g^{-1}), good capacity retention, and the highest thermal stability among the NCM compositions. However, its discharge capacity is considered low for the next generation of electric vehicles. Therefore, materials richer in nickel were investigated. These materials can achieve higher capacities, up to approximately 200 mAh g^{-1} for $LiNi_{0.8}Co_{0.1}Mn_{0.1}O_2$. However, as mentioned earlier, the thermal stability is reduced by the higher nickel content in the material. Ultimately, choosing the ideal NCM material always involves a trade-off between thermal stability and capacity for the intended application.

2.2.1.b   Polyanionic Compounds

In this class of compound, large $(XO_4)^{3-}$ (with X = S, P, Si, Mo) polyanions occupy a lattice position in the crystal structure, this helps to stabilize the structure and increase the redox potential of the material[27]. In the late 1980s, Manthiram and Goodenough studied the insertion of lithium in 3D frameworks such as $Fe_2(SO_4)_3$ or $Fe_2(WO_4)_3$ and proposed their use as cathode material for rechargeable batteries[28,29]. In 1997 Padhi et al.[30] reported the first use of $LiFePO_4$ (LFP) as a positive electrode material in a rechargeable battery. Since then, this type of polyanion material has been the subject of intensive research but nowadays LFP is still the most used at an industrial scale for example by Tesla for it Model 3 car[31].
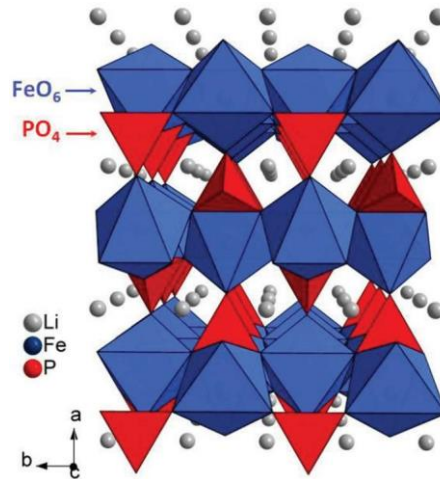
Figure 2-5. Olivine crystal structure with $LiFePO_4$ as an example[17].

LFP exhibits an olivine structure, with iron and lithium located in octahedral sites and phosphate located in tetrahedral sites as shown in **Figure 2-5**. This cathode material presents several advantages such as low cost, abundance and non-toxicity of the components, a low volume expansion, a low capacity fade upon cycling and better safety than the layered transition metal oxide[19]. Nevertheless, due to the discharge plateau around 3.4 V, the theoretical specific capacity of 170 mAh g$^{-1,}$ and the low electronic and ionic conductivity of $LiFePO_4$, the energy density is lower than that of batteries using transition metal oxides as the cathode materials. Intensive research has been conducted to improve this aspect of LFP, for example by reducing the particle size[32] or by using a carbon coating at the surface of the particles[33].
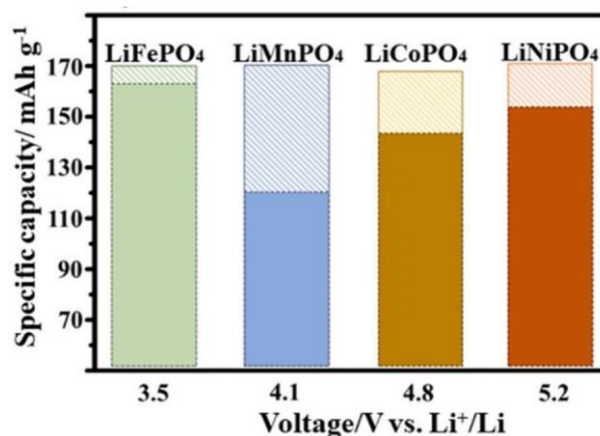
Figure 2-6. Specific capacity *vs.* the average potential for several olivine structures (the total column corresponds to the theoretical capacity and the saturated colors to the actual practical capacity)[34].

Recently the use of manganese ($LiMnPO_4$), cobalt ($LiCoPO_4$), or nickel ($LiNiPO_4$) in olivine structure has been intensively studied, these materials have a theoretical specific capacity very similar to LFP, but they could be very useful to improve the energy density since their average potential is higher than the one of LFP (**Figure 2-6**). However, the practical capacity obtained for these "high-voltage" olivine materials is still much lower than LFP and they suffer from poor cycling stability and rate performances[34]. Some work also reported the use of vanadium in polyanion material like $Li_3V_2(PO_4)_3$ or $LiVPO_4F$ with an average voltage of 3.85 V and 4.2, respectively, with specific capacity of 197 mAh g^{-1} and 140 mAh g^{-1} [35,36]. However, these vanadium-containing materials raise concerns about toxicity and environmental impact and are not yet commercialized.

2.2.2 Anode Materials

Whittingham's initial lithium battery design utilized lithium metal as the negative electrode material. While this battery served as a proof of concept for subsequent research, it was not suitable for industrial use. Since then, in addition to the research on cathode materials

mentioned previously, researchers have been concentrating on various anode materials for lithium batteries.

2.2.2.a   Graphite Anodes

The commercialization of lithium-ion batteries in the early 90s was enabled by carbon anode material. This material is still the most used in today's commercial batteries against a lot of different cathode materials. The electrochemical process occurring involves the intercalation of lithium between the graphene layers, and it has been studied since the 1950s[37]. This intercalation can be up to one Li atom for 6 C atoms (**Figure 2-7**).
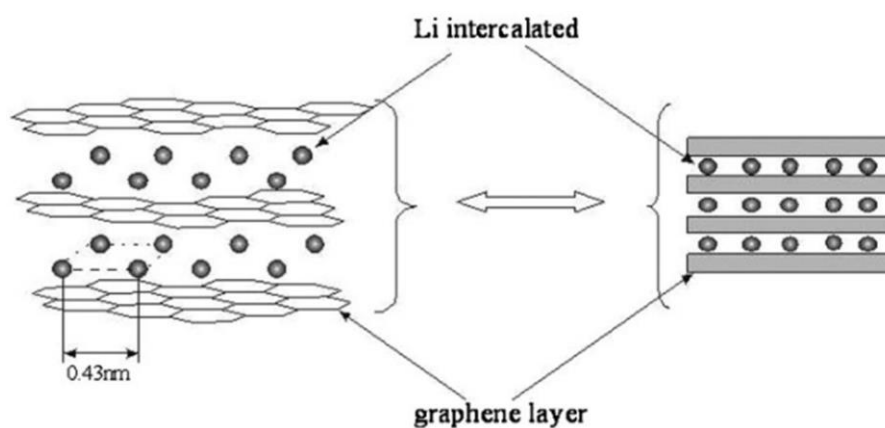
Figure 2-7. Schematic representation of lithium intercalated in graphite carbon anodes[38].

This type of carbon material has many advantages such as the low cost, the abundance of carbon on earth, the high electrical conductivity, the low delithiation potential vs. lithium ($\sim$0.2 V[39]), the high lithium diffusion ($\sim$10^{-6} cm^2 s^{-1} [40]), the high electrical conductivity, the high theoretical capacity (372 mAh g^{-1} [39]) and the rather low volume change during the lithiation/delithiation process ($\sim$10%[41]) enabling long cycling stability compared to other intercalation materials (for example silicon has a volume expansion up to 300%[42]). However, graphite suffers from two main drawbacks: i) the possible co-intercalation of solvent molecules, resulting in the exfoliation of the graphite and loss of capacity[43], and ii) the volume change that can, despite its rather low value, generate damage in the solid-electrolyte interface (SEI) and reduce the cycle

24

life of the battery. Safety concern also arises from the possible lithium dendrite formation due to the low intercalation voltage. [44].

2.2.2.b   Lithium Metal

Lithium is an alkali metal that is highly reactive with air and any common solvent. As said earlier, it was used as the negative electrode material in the first proof of concept for lithium batteries, but its use in commercial batteries remained very limited owing to severe safety issues, as will be discussed in the following. With the continual demand for an increase in the energy density, though the research on lithium metal as an anode material has recently increase again and is now of great interest to replace conventional graphite anodes. Lithium metal has an extremely high theoretical specific capacity of 3860 mAh g^{-1}, which is about an order of magnitude higher than that of graphite, accompanied by a very low redox potential of -3.04 V vs. the standard hydrogen electrode[45]. Paired with the previously mentioned cathode material, it could result in a battery with the highest energy density, making it suitable for electric vehicle applications. However, the development of Li-metal batteries (LMB) has been hindered by two main issues. First, the inhomogeneous deposition of lithium leads to dendrite growth and subsequently to a short circuit, resulting in a thermal run-away and causing the battery to catch fire. The second issue is the low coulombic efficiency of the lithium stripping and plating and the formation of "dead lithium" owing to the high reactivity with essentially any electrolyte (**Figure 2-8**), reducing the battery's capacity and shortening its cycle life.
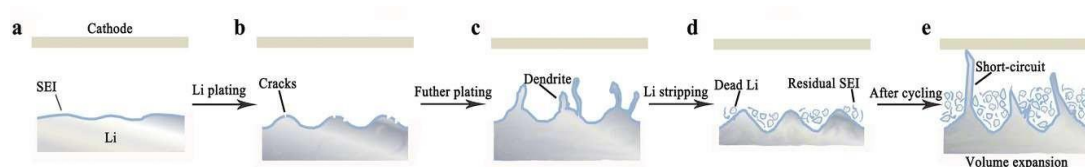

Figure 2-8. Representation of the formation of dendrites and 'dead' lithium during the deposition and dissolution of lithium[46].

During the initial stages of development, this issue has been addressed by using an excess amount of lithium. However, the problem of dendrite growth and safety concerns persists. Despite this, lithium metal is still considered the holy grail of anode materials, especially for enabling high energy density, and will continue to be highly investigated in the future.

2.2.3 Liquid Electrolytes

2.2.3.a   Organic Solvents

In the actual commercial lithium-ion batteries, liquid electrolytes are still the main used technologies. They are conventionally made of a lithium salt dissolved in an organic solvent or a mixture of organic solvents.

Organic solvents have a higher electrochemical stability than water and are therefore highly used in lithium batteries. In addition to this basic requirement, the solvent, or solvent mixture, needs to meet several criteria, i) a high dielectric constant to enable a high concentration of dissolved salt, ii) a low viscosity, resulting in an easier Li^+ transport, iii) a good compatibility with booth anode and cathode within the voltage range of the battery, iv) good thermal properties to increase the safety, v) non-toxicity and low-cost for potential industrial use. In the 1980s, ethers were the most studied solvent for lithium batteries. The ionic conductivity of these electrolytes was high and the deposition of lithium was reported to be homogenous[47]. Nevertheless, the implementation of this type of electrolyte in batteries was unsuccessful due to the poor capacity retention and the low life cycle[48] and their limited stability until 4 V *vs.* Li^+/Li[49]. In this case, the stability of carbonate solvents up to 5 V has made these solvents very interesting for electrolyte applications. The electrodeposition of lithium, from a LiBr in propylene carbonate electrolyte, has been demonstrated already in 1958[50]. Propylene carbonate has been used as an electrolyte solvent in the first lithium battery commercialized by SONY. Nowadays, liquid electrolytes are typically composed of at least two different types of carbonate solvents, a linear carbonate such as dimethyl carbonate (DMC), diethyl carbonate (DEC), with very low viscosity and a cyclic carbonate such as ethylene carbonate (EC) or propylene

carbonate (PC) for their high dielectric constant. PC would be a better solvent mainly because of its much lower melting point compared to EC but the poor ability to generate a proper SEI with graphite anodes hampers its use in lithium batteries[51]. EC, on the other hand, can form a stable SEI with graphite anodes and therefore reduce the solvent co-intercalation and the graphite exfoliation upon cycling[52]. The drawbacks of EC are related to the high melting point (~35 °C) and viscosity, therefore linear carbonates mixed with EC are used to lower the melting point and viscosity and make the electrolytes high conducting at lower temperature[53]. The LP30 electrolyte, made of 1M $LiPF_6$ in 1:1 wt:wt EC:DMC, is commonly used in scientific labs and has shown good cyclability.

2.2.3.b   Lithium Salt

The second main component of liquid electrolytes is lithium salts. For battery applications, the criteria are, i) high solubility in the common organic solvent with easy dissociation of Li^+, ii) high electrochemical stability, iii) no side reaction with solvent, electrode material, or current collector, iv) easy preparation and purification at low costs. Some of the most common lithium salts are presented in **Table 2-1**.

Lithium salt	Conductivity in EC/DMC (mS cm^{-1})	Electrochemical stability vs. lithium	Advantages	disadvantages
$LiClO_4$[12,54]	8.4	5.1 V	Good SEI formation	Explosive
$LiBF_4$[12,54]	4.9	5 V	No aluminum corrosion and performs on the largest range of temperature	Low ionic conductivity
$LiAsF_6$[12,54]	11.1	4.5 V	Highest ionic conductivity and stable rate cyclability	Toxicity
$LiPF_6$[12,54]	10.7	5.1 V	Most well-balances properties	Poor thermal stability and decomposition
LiFSI[55,56]	12.3	5.6	Good thermal stability and ionic conductivity	Can corrode aluminum at voltage > 3.3 V

Table 2-1. Comparison of different lithium salts for lithium battery applications.

Nonetheless, the conventional liquid electrolytes are not usable with the "holy grail" of anode materials, Li metal. The organic solvents are highly flammable, toxic, corrosive, and unstable against Li metal[57]. It is also reported that the lithium deposition with these electrolytes is inhomogeneous and leads to lithium dendrite growth, short-circuit, and loss of performance.

2.3 Solid-State Electrolytes

To overcome these issues, solid state electrolytes are investigated. Their fundamental structure is mechanically more stable and is supposed to prevent the growth of lithium dendrites, improving the safety of lithium batteries. Such electrolytes must be characterized by wide electrochemical window stability (of 4.5-5.0V), possess good compatibility with both electrodes, have high mechanical strength, and provide high ionic conductivity ($> 4.10^{-4}$ S.cm^{-1} at 25 °C) while being electrically insulating. The two main classes of solid-state electrolytes are inorganic and polymer materials.

2.3.1 Inorganic Solid-State Electrolytes

Inorganic solid-state electrolytes present a high shear modulus, excellent thermal stability, and a lithium-ion transference number close to one. The most investigated classes of inorganic ion conductors are presently oxides-based and sulfides-based. The structure of these materials can be crystalline or amorphous, having an impact on the electrochemical properties. The ionic conductivity, advantages, and drawbacks of some inorganic ion conductors are presented in **Table 2-2**.

Ion conductor type	Ion conductor structure	Conductivity	Advantages	Drawbacks
Sulfide	ThioLISICON[58] $Li_{11}Si_2PS_{12}$	10^{-4} S cm^{-1}	-high ionic conductivity	-unstable vs. lithium metal
	Amorphous glasses[59] Li_2S-SiS_2-Li_4SiO_4	10^{-3} S cm^{-1}	-high ionic conductivity -high thermal stability	-highly hygroscopic -low compatibility with cathode materials
Oxide	Perovskite (LLTO) $Li_xLa_{(2-x)/3}TiO_3$ [60]	10^{-3} S cm^{-1}	High stability against oxidation	-Ti^{4+} reduction at the interface with lithium metal
	LISICON[61] $Li_{14}ZnGe_4O_{16}$	10^{-7} S cm^{-1}	-stability against oxidation -mechanical resistance	-highly reactive with lithium metal
	LIPON[62] $Li_{2.88}PO_{3.73}N_{0.14}$	10^{-6} S cm^{-1}	-stable with battery materials -easy thin-film fabrication	-high cost
	Garnet structure[63] $Li_5La_3M_2O_{12}$ (M=Ta, Nb)	10^{-5} S cm^{-1}	-high stability against lithium metal -thermal stability	-unstable with cathode materials
	NASICON (LATP)[64] $Li_{1+x}Al_xTi_{2-x}(PO_4)_3$	10^{-3} S cm^{-1}	-very high ionic conductivity	-reactive with lithium metal

Table 2-2. Overview of selected inorganic solid-state ion conductors.

Despite their promising electrochemical and mechanical properties, inorganic solid-state electrolytes suffer from brittleness and rigidity. This results in a poor solid-solid interface with a lithium metal anode or any cathode material. It can also lead to fragmentation of the electrolyte and therefore even poorer interfaces and low cycle life for the battery. Research on interface modification has been carried out to improve the electrode/electrolyte interface. They mainly focus on adding a polymer[65], metal[66,67], or metal oxide layer[68] between the inorganic solid electrolyte and the positive and/or negative electrodes.

2.3.2 Solid Polymer Electrolytes and PEO-Based Polymer Electrolytes

Solid polymer electrolytes (SPEs) typically consist of an inorganic salt dissolved in a polymer matrix. Armand et al.[69] proposed the use of polymeric ion conductors as solid electrolytes for safer rechargeable batteries in the late 1970s. Moreover, they have many other advantages such as good mechanical strength, ease of thin film fabrication with desirable shapes, and the ability to form a good electrode/electrolyte contact and interface with a much better lithium dendrites inhibition as compared to the liquid electrolytes. Nevertheless, the main drawback is the low ionic conductivity. Since then, different polymer matrices have been investigated (polyethylene oxide, polycarbonate, etc.) but also different formulations such as gel polymer electrolytes (GPEs), composite polymer electrolytes (CPEs), or solvent-free, i.e., solid polymer electrolytes (SPEs). These formulations combined with the number of available polymer matrix allow for a lot of possibilities to develop polymer electrolytes (**Figure 2-9**). Nevertheless, these polymers must fulfill several criteria for SPE applications, i) good cation solvation, which means a balanced polymer-cation interaction to allow the salt to dissolve and the cation to move from one coordination site to the other; ii) a high dielectric constant to have an effective charge separation of the salt; iii) a flexible backbone to ensure an easy motion of the polymer chains; iv) good mechanical stability, mainly insured by a high molecular weight[70].
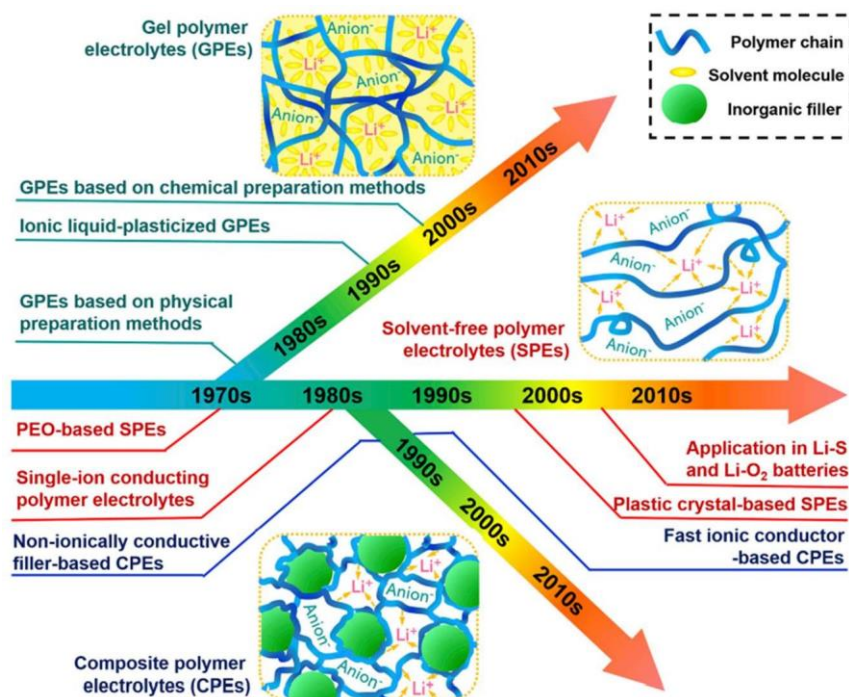
Figure 2-9. Chronological developments of polymer electrolytes for lithium batteries[70].

Poly(ethylene oxide) (PEO) is a polymer prepared by ring-opening polymerization of ethylene oxide. Its chemical structure is $H-(O-CH_2-CH_2)_n-OH$ and its molecular weight is usually above 20 000 g mol^{-1}. This structure with lower molecular weight is commonly referred as poly(ethylene glycol) (PEG). These polymers are available commercially with varying molecular weights and terminal groups (**Figure 2-11**), resulting in different properties. It is also known for its low toxicity.

PEG/PEO   **PEGME**   **PEGDME**

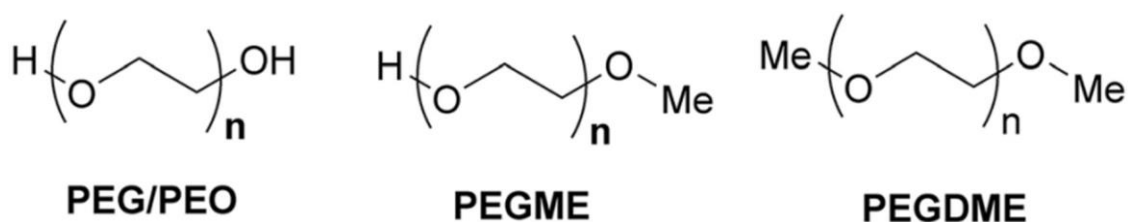**Figure 2-10.** Different structure of linear PEO[71].

PEO is a very flexible semi-crystallin polymer with $T_g < -60$ °C and $T_m < 66$ °C (both temperatures are depending on the polymer chain length), and has a strong ability to solvate the

lithium cation (Li^+). Its ethylene oxide units have a high donor number and ability to complex Li^+ cations and its dielectric constant allows for a good charge separation of the ions. The conduction mechanism takes place via the segmental motion of the Li^+ coordinating polymer chains, as schematically illustrated in **Figure 2-11**. The PEO properties made PEO one of the most investigated polymer matrices so far for battery applications.
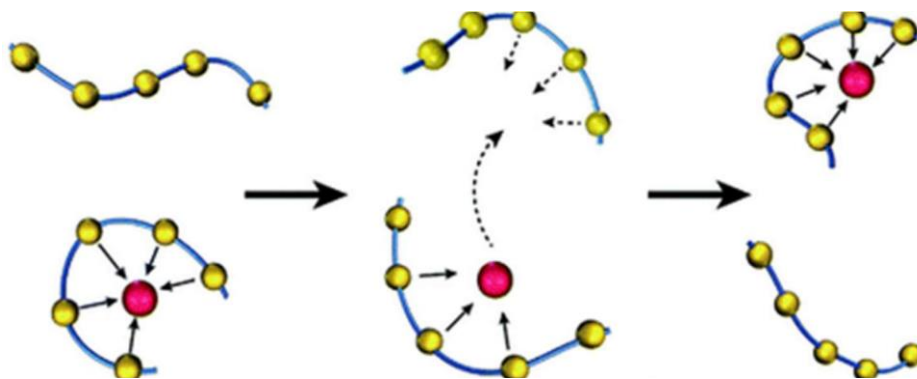

Figure 2-11. Schematic illustration of Li^+ ions transport mechanisms in PEO electrolyte[70].

Since Fenton et al.[72] reported the first conductivity of alkali metal salts in PEO, the main drawback of PEO-based SPEs has been the low ionic conductivity ($\sim 10^{-6}$ S cm^{-1}) at room temperature[73] due to the semi-crystalline character of the polymer. It has been reported that the ion transport occurs mainly in the amorphous region, while the crystalline phase was considered to be only poorly conducting due to the high energy barrier for the Li^+ transport and the required cooperative motion Li^+ between the preferred sites[74]. After the polymer melting, a high increase in ionic conductivity is reported for PEO at 80 °C ($\sim 10^{-3}$ S cm^{-1} [75]). However, the use of polymer in a molten state results in loss of the mechanical properties affecting the membrane's ability to stop dendrites growth and subsequent short-circuit, thus impacting performance and safety of the battery. Consequently, several methods have been explored to enhance the conductivity at low temperatures, including adding organic plasticizers, blending PEO with other polymers, and modifying the PEO polymer structure.

Plasticization is a common method for reducing the crystallinity and increasing the amount of amorphous region in PEO electrolytes. The first idea was to plasticize with the organic solvent

used for liquid electrolytes, as presented earlier. In addition to the plasticization effect, they have the advantage of enhancing the lithium salt dissociation in the SPEs. The plasticization of a PEO-LiCF$_3$SO$_3$ with EC and PC was studied by Frech et al.[76,77]. They concluded that when adding EC or PC, the plasticizer mostly interacts with the crystalline phase and changes it to an amorphous phase. The polymer-salt complexes become more amorphous at room temperature, resulting in an increase by 2 orders of magnitude in the ionic conductivity. The mixture of PC and EC as a plasticizer was also studied. Nan et al.[78] prepared a polymer electrolyte presenting a high ionic conductivity and mechanical stability by mixing PEO and poly(vinylidene fluoride-co hexafluoropropylene) (PVDF-HFP) with LiClO$_4$ plasticized with a mixture of EC and PC. Lang-sheng et al.[79] investigated full-cells made of Li as the anode, PEO-LiClO$_4$+EC as the electrolyte, and polyaniline as the cathode material. At room temperature, this cell performed for more than 250 cycles but presented a low specific capacity (~45 mAh g^{-1}) with a Coulombic efficiency of 98%. Despite these quite low performances, this cell proves that these PEO+EC are suitable for LMBs.

The second approach is to use low molecular weight PEO (PEG) as a plasticizer. Unfortunately, the PEG molecule possesses a hydroxyl end group that might react with lithium metal. The modification of the end groups resulted in two plasticizers, poly(ethylene glycol) monomethyl ether (PEGME) and poly(ethylene glycol) dimethyl ether (PEGDME), both were employed to improve the conductivity of PEO-based SPEs[80] at low temperature. Wang et al.[81] studied the conductivity of a PEO-LiTFSI system with different amounts of PEGDME and highlighted an increase in the ionic conductivity but also in the lithium transference number. Following the same idea, tetraethylene glycol (TEG) and tetraethylene glycol dimethyl ether (TEGDME) were investigated[76]. For booth systems, PEO-LiCF$_3$SO$_3$ with TEG and PEO-LiCF$_3$SO$_3$ with TEGDME, the ionic conductivity was much higher than that of (PEO)$_9$LiCF$_3$SO$_3$ at 30 °C.

The modification of the PEO structure has been another approach to improve the ionic conductivity of these SPEs. The aim is to obtain a new PEO with a less regular structure, by introducing some "defects" in the PEO main chain or by making a PEO with a side chain. The presence of these moieties will impact PEO's ability to crystallize, reduce the transition

temperature, and thus enhance conductivity. For example, Watanabe et al.[82] synthesized a high-molecular-weight branched polyethers P(EO/MEEGE) by ring-opening copolymerization of ethylene oxide (EO) with 2-(2-methoxyethoxy) ethyl glycidyl ether (MEEGE). An ionic conductivity of 3.3 x 10^{-4} S cm^{-1} at 30 °C and a good compatibility with lithium metal electrodes was obtained.

The synthesis of copolymers involving PEO and another linear polymer was also largely investigated. Poly(acrylonitrile) is a good candidate for SPEs with an ionic conductivity of 9.2 x 10^{-4} S cm^{-1} and excellent stability toward lithium metal[83]. Therefore Yuan et al. proposed to use it in combination with PEO in a graft copolymer prepared by reaction of PEO with methacryloyl chloride in a toluene solution with pyridine. They used LiClO$_4$ as lithium salt to build the SPE membrane and obtained an ionic conductivity of 6.79 x 10^{-4} S cm^{-1} at 25 °C and an electrochemical stability until 4.8V versus Li$^+$/Li, making it a potentially usable SPE for high energy density applications[84].

Block copolymers are another possible approach. The idea is to combine two dissimilar polymers bonded end to end. Generally, a lithium-salt-solvating polymer is chosen as one block to ensure ionic conductivity and a second block to ensure mechanical stability. It has been observed that a micro-phase separation occurs in this type of material, creating nanoscopic domains that enable continuous conductivity pathways in the membrane[85]. For instance Niitani et al.[86] reported a lock copolymer synthesized by living radical polymerization between poly(ethylene glycol) methyl ether methacrylate and styrene. The nano structuration of this polymer was observed via TEM images (**Figure 2-12.a**). They prepared the SPE by mixing this polymer with LiClO$_4$ and obtained an ionic conductivity of 2 x 10^{-4} S cm^{-1} at 30 °C and electrochemical stability until 4.3 V. They investigated this SPE in a full-cell with lithium metal as anode material and LiCoO$_2$ cathode material between 3.0 and 4.3 V at 0.1C. This cell showed a discharge capacity of ~100 mAh g^{-1} with a Coulombic efficiency of 99% after 4 cycles (**Figure 2-12.b**).
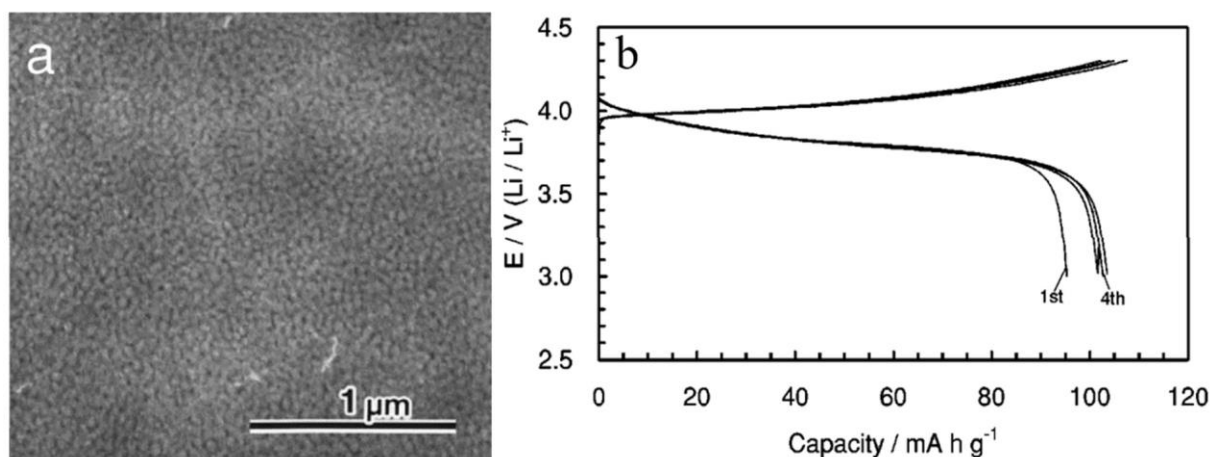
Figure 2-12. (a) TEM images of block copolymers composed of PEO and polystyrene; (b) charge and discharge curves for $LiCoO_2$/SPE/Li cell at 30 °C and 0.1C[86].

The last approach to improve the ionic conductivity of PEO-based SPEs relies on increasing the percentage of amorphous domains by blending PEO with other polymers. The main advantage of this approach is that similar results to the structure modification approach can be obtained but without the need for nontrivial synthesis. This results in easier preparation and better composition control. Tanaka et al.[87] proposed a system composed of a PEO-LiClO$_4$ blend with polyethylenimine (PEI). They showed that with the composition $[(8:2)PEO/PEI]_{10}$-LiClO$_4$ the crystallization of PEO was drastically reduced and a conductivity of $\sim10^{-4}$ S cm^{-1} was achieved at room temperature. Another polymer of interest is Poly(vinylidene fluoride) (PVDF) which has been investigated for lithium batteries applications for a long time, although it suffers from poor ionic conductivity. The blend of PEO with PVDF was studied by Jacob et al.[88]. They incorporated different amounts of PEO in a PVDF-LiClO$_4$ system and obtained an increase in ionic conductivity by more than one order of magnitude for the PVDF-LiClO$_4$:PEO (80:20) composition. Another direction is the use of biopolymers which has gained interest over the last two decades for various applications, and the field of battery technology has not been an exception to this trend. Cellulose is an abundant biodegradable and low-cost material and was already used as a separator for batteries working with liquid electrolyte[89]. Samad et al.[90] prepared a blend of PEO and networked cellulose (NC) with different compositions and 20

wt.% of LiClO$_4$. These blends presented excellent thermal and mechanical stability compared to pure PEO and an acceptable ionic conductivity of ~10^{-5} S cm^{-1} at 60 °C for the PEO/NC(85:15)-LiClO$_4$.

2.4 Single-Ion Conducting Polymer Electrolytes

Nevertheless, all the solid polymer electrolytes discussed earlier suffer from the same drawback, they are dual-ion conductors containing free inorganic salt which leads to a low Li$^+$ transference number. Brissot et al.[91] studied an SPE made of PEO mixed with LiTFSI/LiNPSI (50/50 mol %) and using *in situ* imaging, they demonstrated that this free inorganic salt, particularly the free-anions that are not involved in the electrochemical reactions, results in a concentration gradient in the electrolyte (**Figure 2-13**).
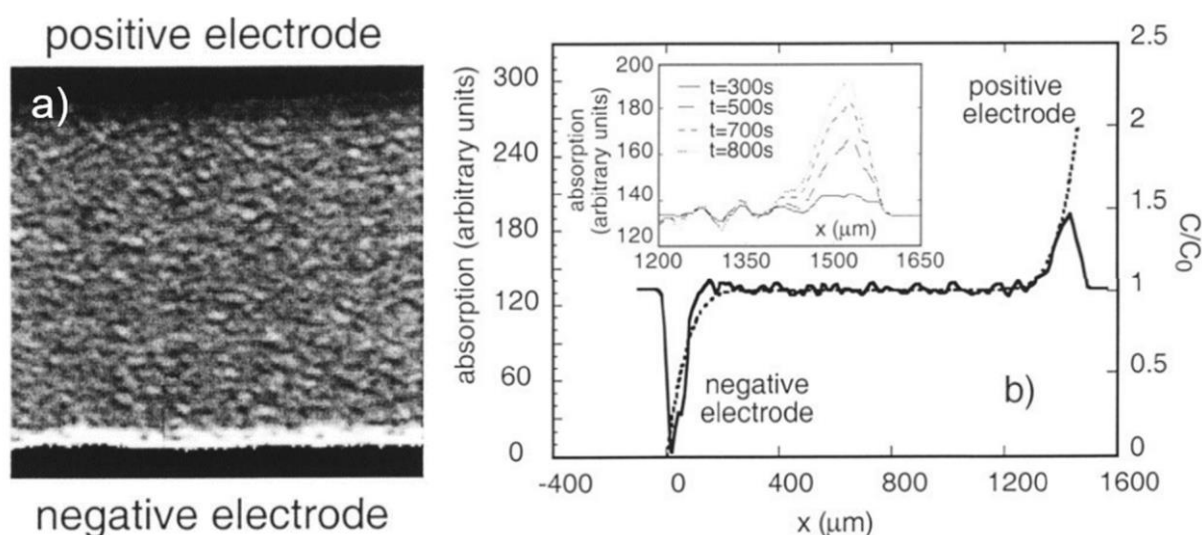

Figure 2-13. (a) Optical absorption in a PEO-LiTFSI/LiNPSI electrolyte, the light region corresponds to the low TFSI-anion concentration region, whereas the dark region corresponds to the high TFSI-anion concentration region. (b) Absorption profile in the PEO-LiTFSI electrolyte and the corresponding concentration profile[91].

This concentration gradient results in a polarization of the cell, which is considered to be a driving factor for the dendrite growth[92], leads to an undesirable change in the electrolyte (phase

transition, salt precipitation, etc.) and therefore is responsible for the loss of performances in lithium solid-state battery[93].

To overcome this issue, the use of single-ion conductors has been proposed. This type of polymer aims to reduce to zero the transference number of the anions, hence the transference number of the Li-ion is theoretically equal to one. Using simulation, it has been demonstrated that, in the case of $t^+_{Li} = 1$, no concentration gradient should occur[94], more homogenous lithium deposition with no dendrite growth should be obtained[95], and higher state-of-charge and current density could be achieved[96]. On the other hand, simulations also reveal lower conductivity for this type of material because of slower polymer mobility and a lower Li^+ diffusion coefficient[96,97].

2.4.1 How to Design a Single-Ion Conductor?

2.4.1.a Immobilization of the Anion

As mentioned earlier, the goal of single-ion conducting polymer electrolytes (SIPEs) is to minimize the transport number of the anions to zero. Therefore, the first design parameter of SIPEs is the immobilization of the anion. There are two strategies in this direction: using anion acceptors or covalently bonding the anions.

An anion acceptor, is a neutral molecules that can, at least partially, immobilize the anionic movement in the electrolyte by interactions between the acceptor and the anion of the lithium salt. Here the Lewis acid-base theory is used. After dissociation, the cation of the lithium salt is an electron pair acceptor whereas the anion is an electron pair donor (Lewis base) by using an acceptor that is also an electron pair acceptor (Lewis acid), a strong Lewis acid-base interaction can be formed and suppress the movement of the anion. In 2005, Blazejczyk et al.[98] synthesized different calix[4]arene derivatives and used them as an additive in common SPEs containing PEO as polymer matrix and LiI or $LiCF_3SO_3$ as lithium salt. They obtained an ionic conductivity of ~10^{-6} S cm^{-1} as expected for this type of PEO-based SPEs but they also demonstrated a lithium transport number up to 1 for certain ratios. Boron compound can also be used in the

matter, Abe et al.[99] prepared a common SPE containing PEO and LiCF$_3$SO$_3$, but they used tris(pentafluorophenyl)borane (TPFB) as an additive. Their results also proved that adding an anion acceptor can improve the lithium transport properties of SPE. These anion acceptors can also be bonded directly on the polymer backbone. Matsumi et al.[100] synthesized an organoboron polymer based on PEO (**Figure 2-14**).
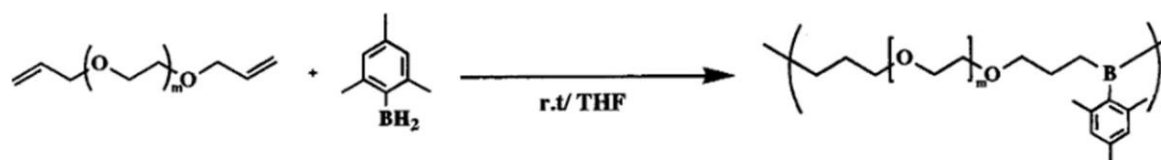

Figure 2-14. Polymerization of PEO-based monomer with mesityl borane to form an organoboron polymer[100].

This polymer exhibited an ionic conductivity of 2.11 x 10^{-6} S cm^{-1} when mixed with 10% LiCF$_3$SO$_3$, the lithium transport number also exhibited a higher value (0.50) than the conventional PEO-based SPEs.

The second approach is the most common one and involves covalently bonding the anionic part of the salt to the polymer backbone. This will avoid the anionic movement in the electrolyte and drastically reduce the anion transport number. Herath et al.[101] prepared ionic melts by bonding a phenyl sulfonyl (trifluoromethylsulfonyl)imide to a low molecular weight PEG chain and investigated the properties of these oligomers, called ionic melts in the article. These melts exhibited a conductivity of ~10^{-4} S cm^{-1} 60 °C but unfortunately no t$^+$ measurements were presented in the work.

2.4.1.b   Dissociation of Lithium Ions

The first step in creating a single-ion conductor is to immobilize the anion, but this alone is not enough to achieve the desired properties for lithium battery applications. To achieve sufficient lithium cation conductivity and migration, it is important to minimize the interaction between

the anion and cation as much as possible. To ensure the best dissociation of Li^+, the negative charge density of the anion must be dispersed.

The first strategy was to synthesize a copolymer with one unit containing the anion bonded to the backbone and a second unit containing electron-withdrawing groups to enhance the ion dissociation. Cao et al.[102] synthesized a SIPE by copolymerization of maleic anhydride (MA) with a lithium 4-styrene sulfonyl (phenylsulfonyl)imide ion conductor monomer. The obtained copolymer was mixed with PVDF-HFP in DMSO, and a self-standing membrane was obtained after solvent evaporation. Excellent values for t^+ (~0.9) and ionic conductivity (2.67 x 10^{-3} S cm^{-1} at room temperature with EC:PC as plasticizer) were reported. They concluded that the alternating arrangement of MA with a high dielectric constant and the styrene-based unit results in a high and uniform dissociation of the lithium ions.

A second strategy was focused on the anionic part of the single-ion conductor. As shown earlier, many lithium salts are available for liquid electrolytes and a lot of similar structures can be used to design a single-ion conductor.

The first investigated anions were **-CO_2^-** (carboxylate anions). Already in the 80s, Tsuchida et al.[103] reported a single-ion conducting homopolymer synthesized from lithium salts of poly[(o-carboxy)oligo(oxyethylene) methacrylate], the oligo(oxyethylene) side chain stand for the lithium transportation when the -CO_2Li side chain termination provides the lithium cations. In the end, a rather low ionic conductivity of ~10^{-9} S cm^{-1} at room temperature reaches for this homopolymer. This conductivity value was increased to ~10^{-7} S cm^{-1} by using a random copolymer synthesized from oligo(oxyethylene) methacrylate with lithium acrylamidocaproate[104]. Even if other works focus on the optimization of the backbone structure[105,106], the conductivity reported is still rather low. The negative charge of -CO_2^- is not well dispersed, resulting in a strong anion-cation interaction between Li^+ and -CO_2^- and a poor ability for lithium cations to migrate. Additionally, -CO_2^- groups are reported to be electrochemically unstable at high voltage, limiting their potential applications.

Therefore, the next anion structure of interest was **-SO_3^-** (sulfonate anions). With the three oxygen atoms surrounding the sulfur, the delocalization of the electron is much higher which

should result in a weaker anion-cation interaction. Park et al.[107] prepared a blend of PEO with a single-ion conducting homopolymer based on lithium 4-vinylbenzenesulfonate. Despite the excellent value for the lithium transport number (t^+=0.85), the maximum conductivity measured was 3.0×10^{-8} S cm^{-1} at room temperature. The use of copolymer structures once again helps to increase the ionic conductivity, but only to values close to 10^{-7} S cm^{-1} [108]. Studies from Cowie et al.[109] and Snyder et al.[110] also confirm an improvement in conductivity with the use of a copolymer containing a PEO-based unit for Li$^+$ transportation. But more interesting, they also showed that including fluorine atoms in the anionic side chains has a significant effect on improving the conductivity of these polymers to 10^{-6} to 10^{-5} S cm^{-1}. Fluorine is known to have a strong electron-withdrawing behavior, in this case, it helps for the electron delocalization of sulfonate anions and therefore for the dissociation of lithium cations, resulting in a higher conductivity. These indicate that improvements were still needed in the choice of anions in single-ion conductors.

A third anion of interest is **-SO$_2$N$^-$SO$_2$-CF$_3$** (trifluoromethane sulfonyl imide anions). It was already the main lithium salt anion used in liquid electrolytes and for conventional SPEs for its good electrochemical properties. In this structure, the four oxygen atoms ensure a high delocalization of the electrons and the -CF$_3$ has a high inductive electron-withdrawing behavior that will increase the delocalization of the negative charges. A homopolymer was synthesized by Feng et al.[111] based on lithium (4-styrenesulfonyl)(trifluoromethanesulfonyl)imide. A self-standing SIPE was prepared by mixing this polymer with PEO and a transference number of 0.92 was measured with ionic conductivity of ~10^{-7} S cm^{-1} at 40 °C. In the same study, they also prepared a random copolymer based on lithium (4-styrene sulfonyl)(trifluoromethane sulfonyl)imide and methoxy polyethylene glycol acrylate and almost managed to match the ionic conductivity of the conventional PEO:LiTFSI SPE with a transport number equal to 0.93[111]. The anionic group was also bonded to other types of backbone, Siska et al.[112] prepared a copolymer based on polysiloxane with anionic and oligoether side chains. They obtained a maximum conductivity of 1.2×10^{-6} S cm^{-1} at room temperature but did not measure the lithium transport number. Ma et al.[113] tried to further modify the anionic group by replacing one of the

=O by a =NSO$_2$CF$_3$ to obtain what they called a super-delocalized polyanion. Practically, they synthesized lithium (4- styrene sulfonyl)(trifluoromethyl(S-trifluooromethylsulfonylimino)sulfonyl)imide and managed to polymerize this monomer in a homopolymer similar to the one made by Feng et al[111]. The blend of their super-delocalized homopolymer with PEO exhibited an ionic conductivity higher than 10^{-5} S cm^{-1} with t$^+$= 91 at 60 °C. These results once again tend to confirm that the higher the delocalization, the higher the conductivity. In this matter, -SO$_2$N$^-$SO$_2$-CF$_3$ is a candidate of choice for research on SIPEs since it combines a high enough delocalization with a rather easy synthesis method.

2.4.1.c   Optimization of the Ion-Polymer Interaction

Once the anions were immobilized and the lithium cation dissociation was optimized, the last important design factor was the interaction between the lithium cation and the polymer backbone. A strong interaction helps the anion-cation dissociation but slows the cation's transport and vice versa. A lot of SIPE presented until now incorporate PEO in a blend[122,126] or as a side chain in the polymer structure[118,124,125,126]. This PEO addition is supposed to transport the lithium cations by ion-dipole interactions between -O- and Li$^+$ like in the conventional PEO:lithium salt SPEs, but this interaction in PEO was demonstrated to be strong and therefore reduces the transport of Li$^+$ [114]. Wen et al.[115] proposed to regulate this ion-dipole interaction by adding other types of units for copolymers. They synthesized a copolymer based on vinyl ethylene carbonate (VEC) and lithium 3-sulfonyl(trifluoromethanesulfonyl)imide propyl methacrylate (MASTFSILi). The obtained polymer was mixed with PVDF for mechanical stability and plasticized with succinonitrile. This SIPE exhibited a maximal ionic conductivity of 1.72 x 10^{-4} S cm^{-1} with a lithium transport number of 0.93. They combined these results with the investigation of the ion-dipole interactions by FTIR and concluded that this behavior is mainly due to the C=O$\cdots$Li$^+$ ion-dipole interaction that provides a better cations transport than C-O$\cdots$Li$^+$ in PEO.

Anions also interact with the polymer backbone and can impact conductivity and transport properties in general. For example, several SIPEs that have been presented so far feature a side

chain consisting of a phenyl group positioned between the backbone and the anionic part[122,126]. This group is rather rigid, which impacts the mobility of the chains and, therefore, the transport of cations[116]. There are also short groups, resulting in a short distance between the backbone and the anion and rather strong interaction. The easiest way to increase the mobility of the chain and reduce the anion-backbone interactions is the incorporation of spacer groups. The efficiency of this technique had been demonstrated with simulation[117] but also by experimentation. Devaux et al.[118] studied the differences between SIPEs with polystyrene-TFSI and polymethacrylate-TFSI structural blocks. Their results show a better ionic conductivity for polymethacrylate, suggesting a real impact of the spacer groups on the transport properties.

2.4.2 Structure and Performances of SIPEs in Lithium Batteries

Although the concept of single-ion conductors for batteries and studies on the design of SIPEs have been reported for about 30 years, most of the works only focused on improving ionic conductivity. However, as mentioned earlier, good ionic conductivity is not the only key factor for potential use in lithium batteries. An electrolyte must also exhibit good compatibility with both anode and cathode, a good electrochemical stability window, and proper mechanical stability.

Several groups have investigated grafted polymers as single-ion conductors. Chen et al.[119] used a commercially available poly(ethylene-co-vinyl alcohol) (EVOH) and grafted a lithium 3-chloropropanesulfonyl(trifluoromethane sulfonyl)imide (LiCPSI) side chain to obtain EVOH-*graft*-LiCPSI polymer (**Figure 2-15.b**). They prepared their membrane by solution casting a mixture of EVOH-*graft*-LiCPSI with PVDF-HFP (50:50 wt.%) and NMP. The obtained membrane was then soaked with EC/DMC (v/v, 1:1) and subjected to electrochemical test. This grafted polymer exhibited an ionic conductivity of 5.7×10^{-5} S cm^{-1} at 25 °C with an electrochemical stability until 4.8 V vs. Li$^+$/Li and a lithium transport number of 0.88. They then demonstrated the good compatibility of their SIPE with lithium metal anode by conducting a lithium stripping-plating test in symmetrical Li-Li cells. These results also confirm that this

SIPE can effectively suppress lithium dendrite growth. They finally investigated the performances in Li/SIPE/LiFePO$_4$ cells, which showed a really good C rates capability (**Figure 2-15.a**) and an initial discharge capacity of 100 mAh g^{-1} at 1C with an excellent capacity retention of 95% after 500 cycles (**Figure 2-15.c**). The SIPE also demonstrated excellent performance in C rate capability testing, displaying good reversibility (**Figure 2-15.a**). Another example of a grafted polymer was reported by Du et al.[120]. They used a commercial and extremely rigid polymer backbone (poly(4,4′-(diphenyl ether)-5,5′- bibenzimidazole) (PBI)) and grafted lithium 3-chloropropanesulfonyl(trifluoromethyl sulfonyl)imide (**Figure 2-15.d**). The thus obtained PBI-*g*-LiPSTFSI polymer formed a self-standing membrane with no addition of a supporting polymer (like PVDF or PEO) and was soaked with an EC/DMC (v/v 1:1) solution and subjected to electrochemical test. Excellent compatibility with lithium metal anodes was demonstrated from the stripping-plating test. The ionic conductivity was measured to be 1.5 x 10^{-4} S cm^{-1} with stability until 4.2 V vs. Li$^+$/Li. C rates capability test exhibited a really good reversibility and long-term cycling with an initial discharge capacity of 144 mAh g^{-1} and a capacity of 122 mAh g^{-1} after 50 cycles (85% capacity retention) suggesting good compatibility with LFP cathodes (**Figure 2-15.e and 2-15.f**).
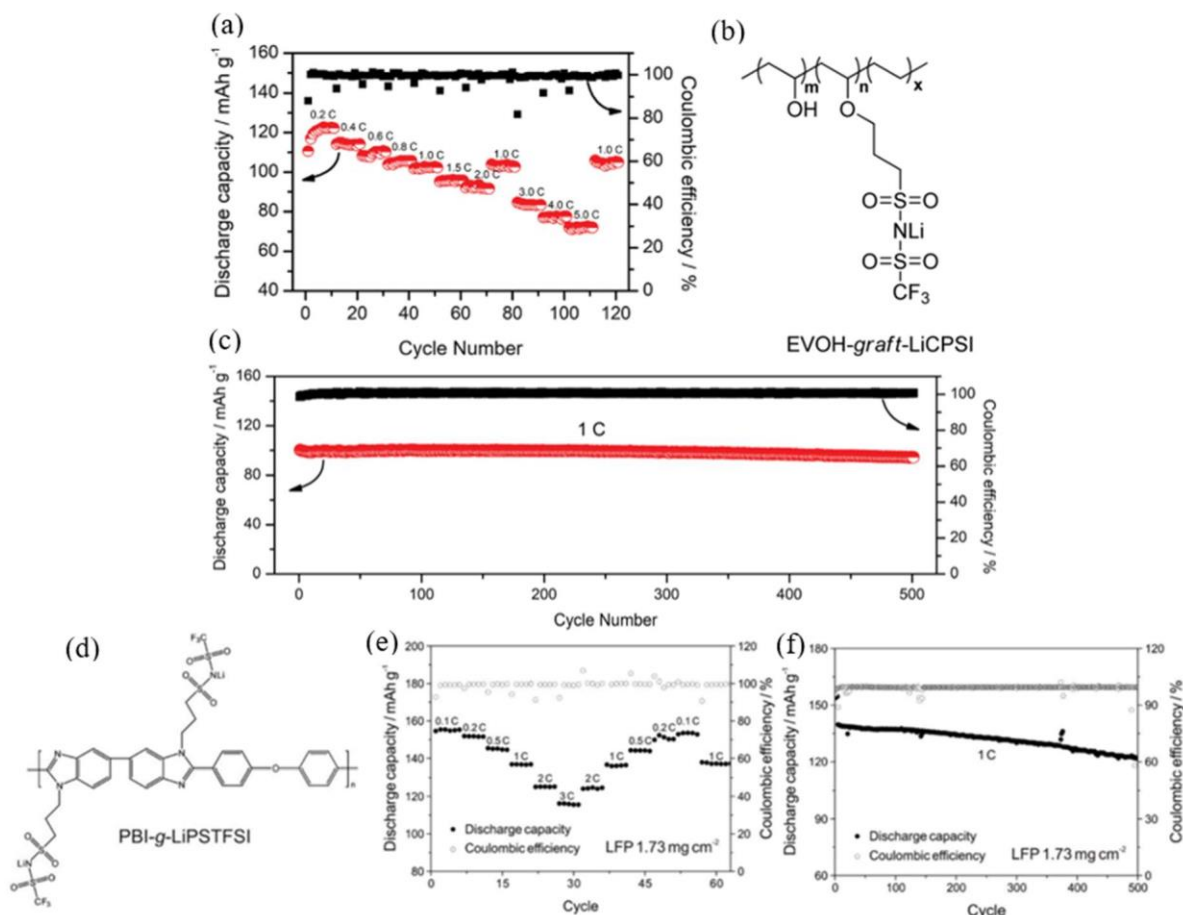
Figure 2-15. C rates capability (a) and long-term cycling stability (c) tests for Li/SIPE/LFP full-cell comprising the polymer structure (b) as single-ion polymer electrolyte at room temperature. C rates capability (e) and long-term cycling (f) stability for PBI-g-LiPSTFSI (d) in lithium metal/LFP full-cells.

Another well-investigated structure for SIPEs is the cross-linked network. In this type of structure, the cross-linked polymer matrix is designed to provide mechanical stability, while the pendant chains ensure segmental mobility and transport of lithium cations. Zhang et al.[121] prepared a single-ion conducting polymer by cross-linking lithium (4-styrenesulfonyl) (trifluoromethanesulfonyl) imide (LiSTFSI), pentaerythritol tetraacrylate (PETA) and Pentaerythritol tetrakis(3- mercaptopropionate) (PTMP) under UV for 30 min (**Figure 16.a**). The obtained membrane was soaked with EC/DMC (v/v 1:1) and used as a SIPE in Li/Li

symmetric cells and Li/LFP full-cells. They measured a lithium transference number of 0.93, and strong compatibility with both cathode and anode materials was demonstrated (**Figure 2-16.b and 2-16.c**).
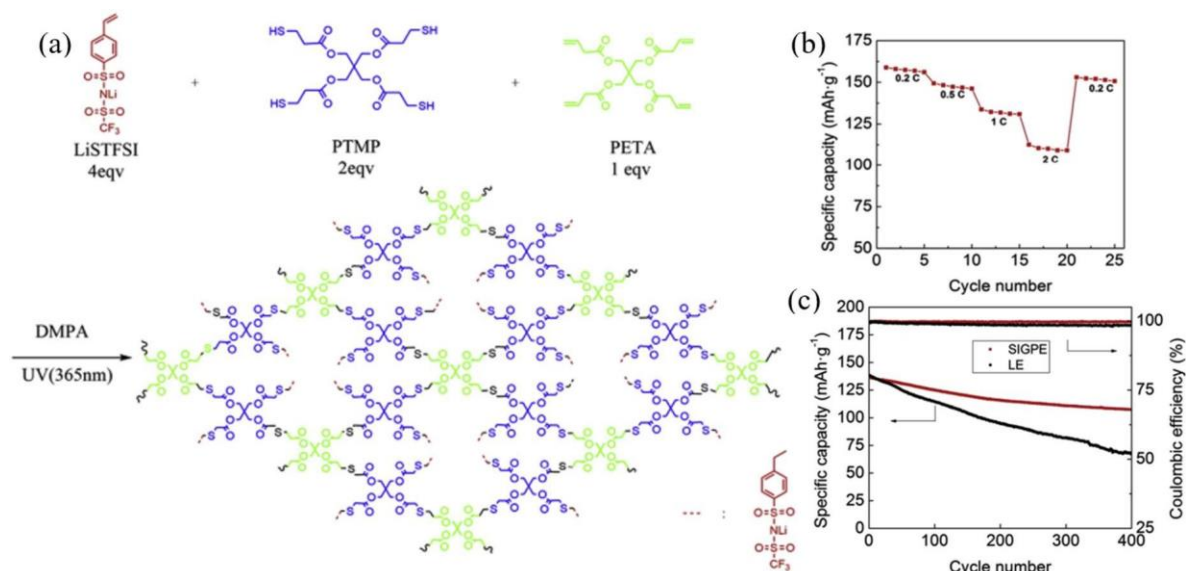
Figure 2-16. (a) Schematic illustration of the synthesis route of the SIPE; (b) C rates capability test with a Li/SIGPE/LFP full-cell at room temperature; (c) long-term cycling stability test for Li/SIGPE/LFP compared with the same test for a standard liquid electrolyte (LE).

Liang et al.[122] used the same UV technique to cross-link with pentaerythritol tetraacrylate (PETA) and lithium (3-methacryloyloxypropylsulfonyl)-(trifluoromethylsulfonyl)imide (LiMTFSI). This anionic chain was chosen because of its better flexibility than the one containing a phenyl group. After cross-linking, they were able to adjust the thickness of the membrane easily by hot-pressing. The SIPE was obtained by soaking the membrane with PC and exhibited an ionic conductivity of 2.1×10^{-4} S cm^{-1} at 20 °C with electrochemical stability of up to 4.4 V upon oxidation. The lithium stripping-plating test demonstrated a good compatibility of the electrolyte with lithium metal anodes and the SIPE was tested vs LFP and NMC$_{622}$ in full-cells. Results with both cathode materials reveal a good C rates capability with good reversibility. For LFP, excellent capacity retention at 0.5C after 300 cycles was measured despite the initial discharge capacity of 108 mAh g^{-1} being lower than the theoretical capacity

(**Figure 2-1.a**). The test with NMC$_{622}$ (**Figure 2-17.b**) showed an initial discharge capacity of 123 mAh g^{-1}, but a faster decrease in capacity retention (~90% after 200 cycles at 0.3C). An even faster loss of capacity retention was observed when using a higher cut-off voltage, probably due to the decomposition of the electrolyte.
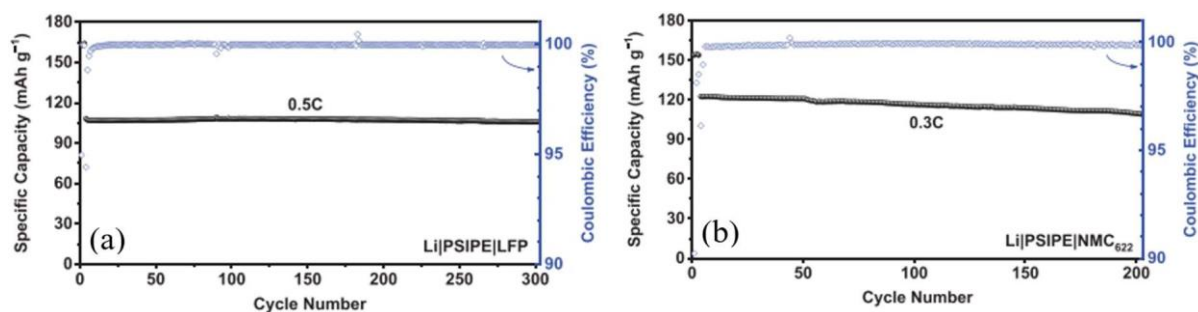
Figure 2-17. Long-term cycling test at 40 °C for a) Li/SIPE/LFP and b) Li/SIPE/NMC$_{622}$ at respectively 0.5 and 0.3C[122].

Finally, one of the most investigated structures for SIPEs are block copolymers. They consist of two or more monomer units that are covalently bonded together in a specific arrangement. For example, a triblock copolymer comprising monomer units A and B can be depicted as -A-A-A-A-A-B-B-B-B-B--A-A-A-A-A-. These polymers are usually synthesized by living polymerization technics in which a first polymerization of A will be conducted followed by the addition and polymerization of B to obtain the block copolymer -A-A-A-A-A-A-B-B-B-B-B-B-[123]. Generally, the design of each block is chemically sufficiently different to make them immiscible. This immiscibility leads to one of the main features of these materials: their ability to phase separate and therefore to self-assemble in nanostructured domains (**Figure 2-18**)[124].
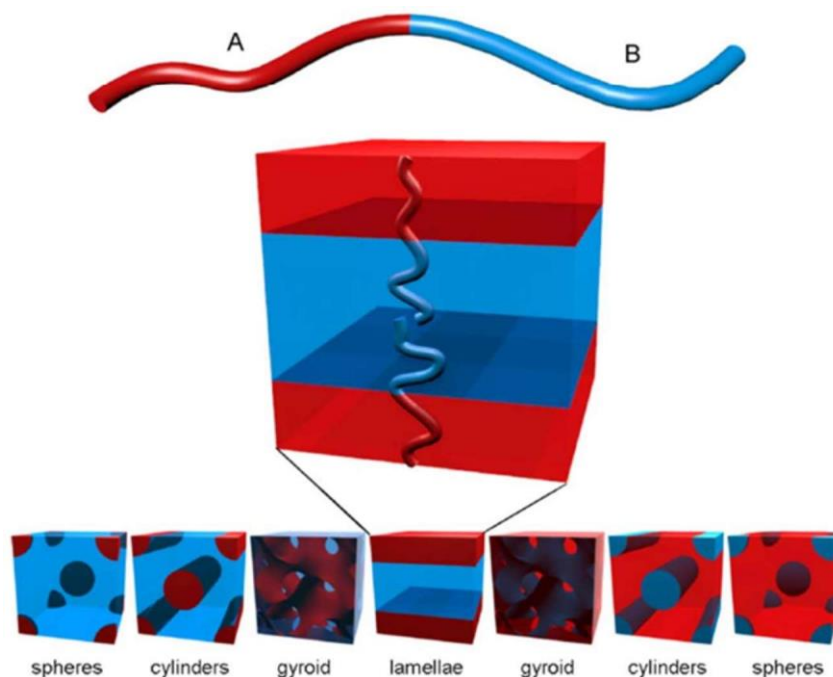
Figure 2-18. Schematic illustration of the potential phase separation in block copolymer materials[124].

In the case of single-ion conducting polymer for lithium battery applications, one block is usually responsible for the mechanical stability of the SIPEs while the other ensures a good segmental motion to help the charge transport. The nano-structuration results then in a pathway for lithium that ensures a good transport through the electrolyte. Bouchet et al.[125] prepared a triblock copolymer with two lithium poly(styrene sulfonyl(trifluoromethane sulfonyl)imide) blocks surrounding a PEO block, which is responsible for the ions dissociation and lithium cations transport. The block made of polystyrene ensures good mechanical stability, allowing for the preparation of a self-standing membrane without the need for additional polymers. The basic electrochemical characterizations revealed a good electrochemical stability window (~4 V), a decent ionic conductivity at 60 °C (10^{-5} S cm^{-1}), and a good lithium transport number (0.85). The results are impressive, especially since the polymer membrane was not supplemented with any plasticizers. The authors also tested this block copolymer in full-cells comprising lithium metal as anode and LFP as cathode, and reported good cycling stability at

60 °C and multiples C rates. Lingua et al.[126] synthesized a diblock copolymer based on polycarbonate and lithium 1-[3-(methacryloyloxy)propylsulfonyl]-1-(trifluoromethylsulfonyl)imide (LiMTFSI). First poly(trimethyl carbonate) (TMC) was synthesized by ring-opening polymerization with 4-cyano-4-(dodecyl sulfanyl thiocarbonyl)-sulfanyl pentanol as initiator. Afterward, on the one hand, a diblock copolymer was prepared by RAFT polymerization between TMC and LiMTFSI (poly[TMC_n-b-LiM_m]) and on the other hand another diblock copolymer, but with one block being a random copolymer, was also prepared by RAFT polymerization from TMC with LiMTFSI and poly(ethylene glycol) methyl ether methacrylate (poly[TMC_n-b-(LiM_m-r-$PEGM_k$)]). The two polymer structures are shown in **Figure 2-19a and 2-19b**.
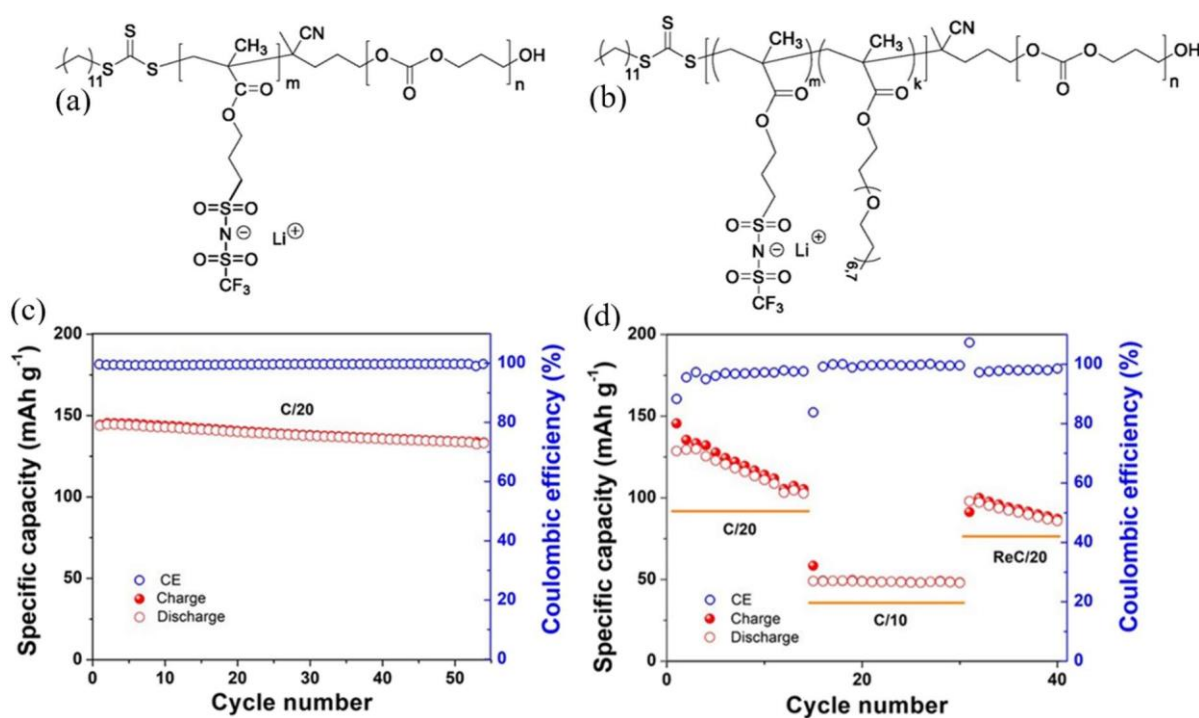
Figure 2-19. poly[TMC_n-b-LiM_m] (a) and poly[TMC_n-b-(LiM_m-r-$PEGM_k$)] (b) structures and cycling performances of Li/ poly[TMC_n-b-(LiM_m-r-$PEGM_k$)]/LFP (c) and Li/poly[TMC_n-b-(LiM_m-r-$PEGM_k$)]/NMC(d).

The electrochemical characterization was performed without the addition of any other polymer or plasticizer. Despite a rather low ionic conductivity (4 x 10^{-6} S cm^{-1} at 70 °C), excellent

electrochemical stability until 5 V vs Li$^+$/Li was reported. Furthermore, the compatibility with lithium metal electrodes was demonstrated to be excellent during the lithium stripping-plating test. Tests with LFP and NMC cathodes were performed at 70 °C with lithium metal as anode. The Li/poly[TMC$_n$-b-(LiM$_m$-r-PEGM$_k$)]/LFP full-cell delivered an initial specific discharge capacity of ~150 mAh g^{-1} and the long-term cycling exhibited a good capacity retention after more than 50 cycles with a Coulombic efficiency of nearly 100% for all cycles. The cycling with NCM revealed a rather fast decrease of the capacity after only 10 cycles at 0.05C. At 0.1C better capacity retention was obtained but the specific discharge capacity was only ~50 mAh g^{-1} (**Figure 2-19.c and 2-19.d**) showing that improvements are still needed for high-energy-density batteries.

Several groups proposed adding small organic carbonate solvents (such as EC or PC) to enhance the properties of these single-ion conductors. In this matter, Zhang et al.[127] reported a new diblock copolymer. Two different homopolymers were synthesized separately, a PEO-based one (poly((2,20 -ethylenedioxy)- bis(ethylamine)isophthalic acid amide) (PEEIA)) and a lithiated one (lithium poly((2,20 -ethylenedioxy)bis(ethylamine)bis(phenylsulfonyl imide)- isophthalate amide) (PEEPSI)). These two homopolymers were then linked to obtain the block copolymer abbreviated PEEIA-co-LiPEEPSI (**Figure 2-20**). The polymer was mixed with PVDF-HFP to ensure good mechanical stability and a self-standing membrane was prepared by solution casting. This resulting membrane was soaked with a solution of EC/PC (v/v 1:1) and subjected to electrochemical tests. In comparison with other block copolymers, the higher ionic conductivity value (3.39 x 10^{-4} S cm^{-1}) at 25 °C is a result of soaking with EC/PC. Indeed, these molecules act as molecular transporters by facilitating the movement of the cation from one coordination site to the other[128]. The use of these carbonate solvents does not affect the single-ion behavior of the polymer (t$^+$=91) or the electrochemical stability (4.3 V).
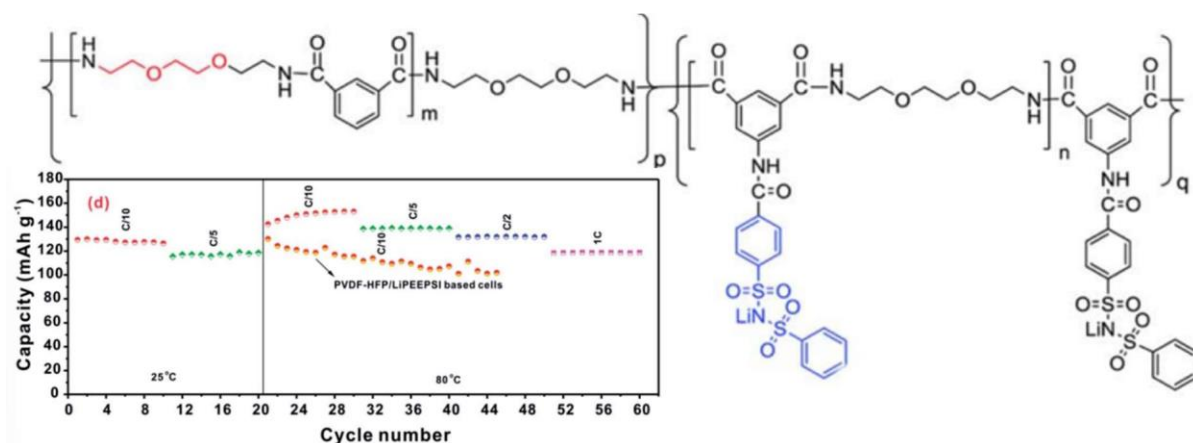
Figure 2-20. Structure and cycling performances PEEIA-*co*-LiPEEPSI in a Li/SIPE/LFP full-cell.

PEEIA-*co*-LiPEEPSI was able to perform at room temperature in full-cells comprising LFP as cathode material. The cell exhibited a specific discharge capacity of ~130 mAh g^{-1} at room temperature and 0.5C, unfortunately no long-term cycling stability results were presented by the authors. At 80 °C and 0.1C, a specific capacity of 150 mAh g^{-1} was fairly close to the theoretical capacity of LFP material. Other C rates also yield high specific discharge capacity, yet long-term cycling stability results were not provided.
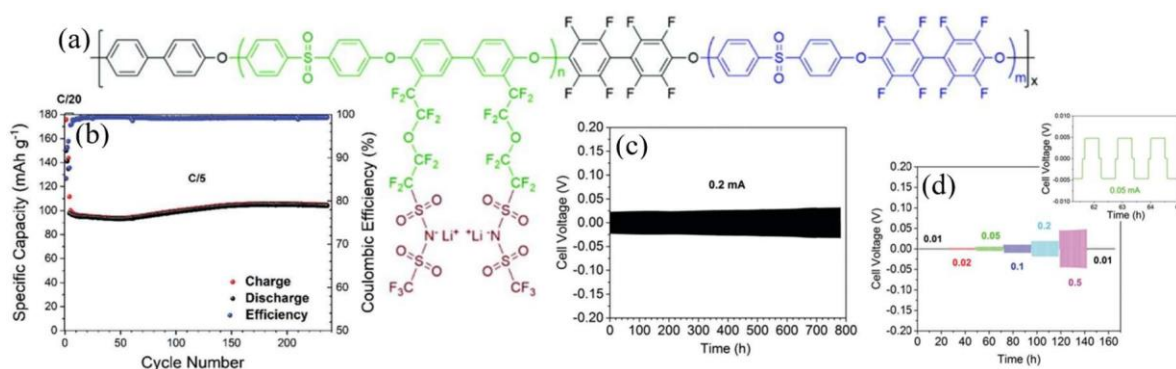
Figure 2-21. (a) structures of the partially fluorinated multi-block copoly(arylene ether sulfone) single-ion conductor; (b) cycling stability test of Li/SIPE/NMC cell, (c) and (d) lithium stripping plating performances of symmetrical lithium-lithium cells with SIPE.

Finally, Nguyen et al.[129] synthesized a partially fluorinated multi-block copoly(arylene ether sulfone) backbone by a one-pot polycondensation reaction with covalently attached TFSI-like side chains (**Figure 2-21.a**). A self-standing membrane was obtained by solution casting and the dry polymer was then soaked with EC. They studied the conductivity of the SIPE as a function of the EC content and observed an increase until 50% EC. At higher EC content, an increase was still observed but not as pronounced as before. The authors concluded that the EC is mainly located in the ionic domains, formed during the nano structuration of the block copolymer. These ionic domains are mostly responsible for the lithium cation transport and therefore it was suggested that EC act as a cation transporter as it was already observed before [128]. The compatibility of this SIPE with lithium metal was once again demonstrated by excellent lithium stripping-plating performances (**Figure 2-21.c and 2-21.d**) and the battery performances were investigated with NMC cathodes. The results at 0.2C and 40 °C exhibited excellent cycling stability with even an increase in capacity before stabilization around 150 cycles and an excellent Coulombic efficiency (99.5%) for all cycles (**Figure 2-21.b**). Nevertheless, the discharge capacity was measured at around 100 mAh g^{-1}. The authors continued to investigate this polymer structure and managed to improve the performances to higher specific discharge capacity and longer cycling stability[130,131].

3. Aim of this Work

Through this review, we saw that despite their excellent ionic conductivity values and their ease of preparation, the actual commercial liquid electrolytes are not stable at high voltage, they are corrosive, flammable, and cannot be used with lithium metal.

Therefore, developing suitable solid electrolytes with high electrochemical stability, high ionic conductivity, and good mechanical stability is crucial for implementing high-energy-density batteries. Inorganic solid electrolytes meet most of these criteria but largely struggle to form smooth interfaces with cathode and anode materials. Salts in polymer solid electrolytes solve this issue but present much lower ionic conductivity and the low cation transport number affects the battery's performance. Due to their t_{Li}^+ close to unity, their good mechanical stability, and easy film fabrication, SIPEs have been of great interest but their commercialization was hindered by low conductivity values for dry SIPEs (10^{-7} to 10^{-5} S cm^{-1}). Higher conductivity values were achieved by immersing the SIPE membrane in a liquid carbonate solvent (such as EC, PC, DMC, etc.), which raises again concerns about flammability. In this context, one aim of this thesis is to obtain a "true" SIPE from the already studied partially fluorinated multi-block copoly(arylene ether sulfone) polymer. For this, membranes containing the multi-block copolymer and PEG as plasticizers were prepared, and their electrochemical performances were studied. The addition of inorganic particles (LATP) to this "true" solid-state electrolyte was also studied.

A second aim was to continue the development of new polymer structures for SIPEs. We designed a new ether-free backbone that was then coupled with a LiTFSI-like side chain. Self-standing membranes of this polymer were obtained, and its electrochemical properties were investigated. Finally, we developed a new multilayer polymer electrolyte combining the previously synthesized ether-free single-ion conducting polymer with a conventional PEO:LiTFSI electrolyte as an interlayer to enhance the charge transport at the interface with lithium metal and obtain a well-performing membrane.

4. Theoretical Part: Instrumentation & Techniques

4.1 Physicochemical Characterization Techniques

4.1.1 Nuclear Magnetic Resonance Spectroscopy

Nuclear magnetic resonance (NMR) spectroscopy is a characterization technique with many potential application fields (chemistry, medicine, physics, biochemistry, …). The determination of the chemical structure of organic molecules in solution is the main use of NMR in chemistry[132]. NMR spectroscopy is suitable for nuclei having a spin number, I, different from zero. Nuclei with $I = 0$ (^{12}C, ^{16}O, …) cannot be characterized by NMR spectroscopy. When applying an external magnetic field to a nucleus with $I \neq 0$, a transition can be observed between the nuclear spin states, called Zeeman levels (**Figure 4-1.a**). This energy transition is highly dependent on the studied nuclei and the chemical environment of the nuclei which is characterized by a resonance frequency called Larmor Frequency.

Figure 4-1.b represents a schematic NMR spectrometer. In a typical NMR measurement, a fixed magnetic field is first applied to the sample to align the nuclei magnetic spins, this results in a magnetic moment. Once the spins are aligned, they are perturbated by a radio frequency pulse. This will induce a change in the magnetic moment that can be detected as a tension by induction and a tension vs. frequency signal is measured. The NRM signal (intensity vs. frequency) is then obtained by a Fournier transformation. Since this frequency is highly influenced by the chemical environment (chemical bond, interaction with neighbor atoms, …), the NMR signal provides insights into the chemical structure of the studied material.
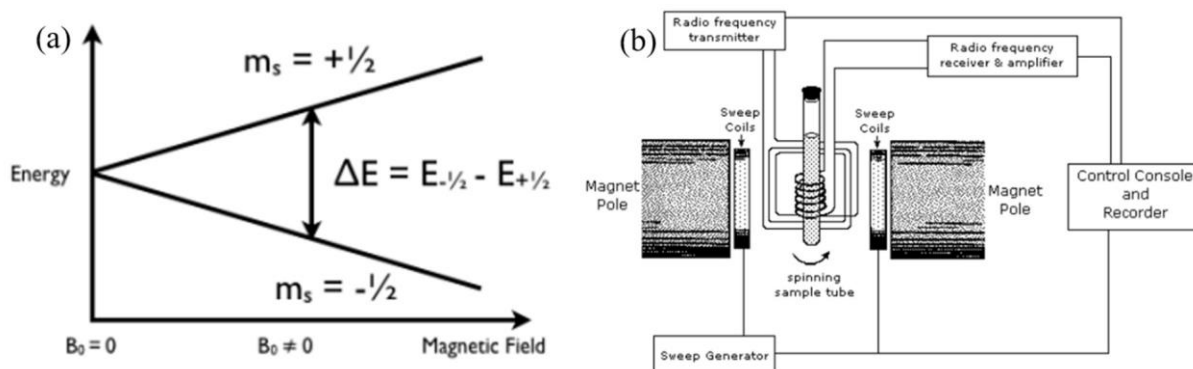
Figure 4-1. (a) energy split of spins in function of the applied magnetic field, (b) schematic representation of an NMR spectrometer[133].

Despite the ease of use and the very reliable results obtainable, certain limitations remain. Some elements are difficult or even impossible to analyze with NMR for two main reasons: first, because of the very low natural abundance of the active isotopes (for example ^{17}O which is only 0.035% abundant) and, second, because of the extremely low magnetic moment of some elements that do not allow for enough detection[133].

4.1.2 Thermogravimetric Analysis

Thermogravimetric Analysis (TGA) is a quantitative technique, which serves to investigate the mass loss processes and obtain information such as the water content, solvent uptake, or thermal stability of materials. In the case of battery research, thermal stability is a key factor for materials, considering the thermal runaway that can occur in a battery when short-circuited, for example, by dendrite growth. **Figure 4-2** represents a scheme of the instrument.
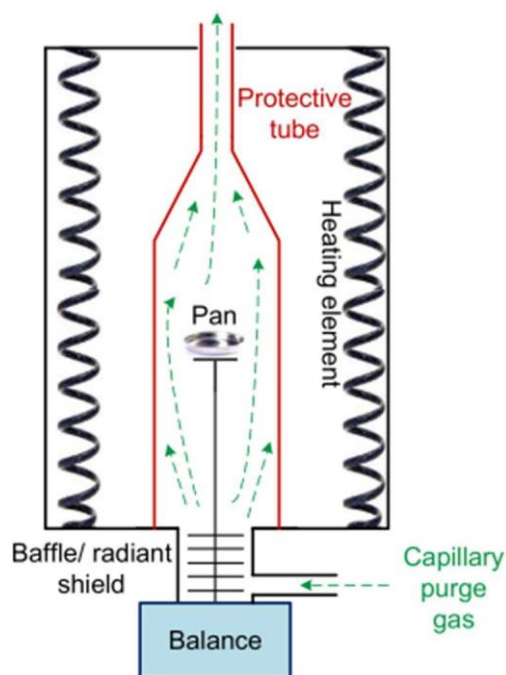
Figure 4-2. Schematic representation of TGA equipment[134].

In a typical measurement, a sample from several milligrams to several grams is placed in a pan and introduced into the instrument. The sample will be subjected to a temperature program under a controlled atmosphere and the mass of the sample will be measured as a function of time or temperature. The choice of the controlled atmosphere is important: inert gas such as argon or helium will avoid any reaction with the sample and enable thermal stability and more accurate and readable analysis. On the other hand, the use of oxidizing gases (air or oxygen) will combust and/or oxidize the material which can be useful to study the mass evolution or the mechanism happening during thermal treatment, for example, carbonization or pyrolysis of material[135,136]. The limitation of this technique is mainly for the study of high-mass samples (>50 mg). In this case, the heating rates are not fast enough in the bulk of the sample and a gradient of concentration occurs and therefore uncertainty in the results[134].

4.1.3 Differential Scanning Calorimetry

Differential scanning calorimetry (DSC) is one of the most commonly used thermoanalytical techniques. It serves to investigate structural transformations such as phase transitions or crystallization. In the case of polymers, the crystallinity and the glass transition temperature (T_g) are key factors for the ionic conductivity of a solid-state polymer electrolyte and these characteristics can be determined by DSC[137].
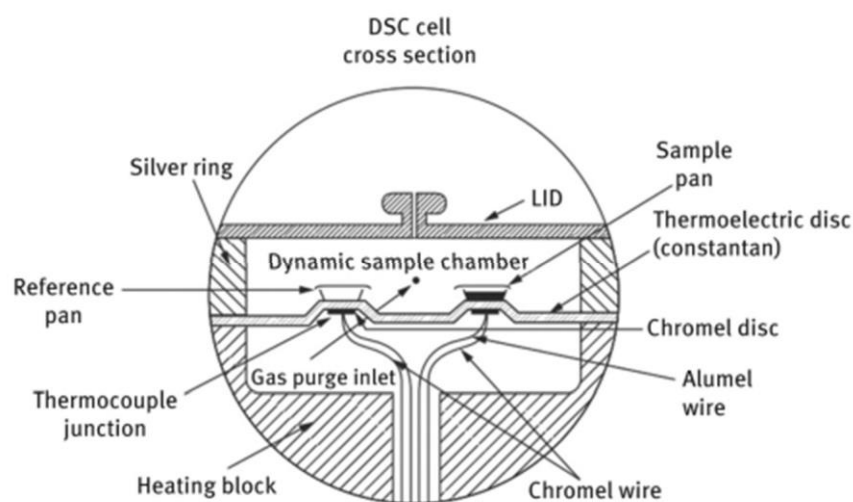
Figure 4-3. Schematic cross-section of a DSC instrument.

In a thermally isolated chamber, two identical pans (one reference and one containing the sample) are subjected to the same heating rate. When the sample undergoes a transition, more or less heat will flow through the sample compared to the reference. These differences in the heat flow are reported vs. temperature to obtain the DC thermograms. The only limitation of this technique is that it does not provide information on the material structure.

4.1.4 Scanning Electron Microscopy

Scanning electron microscopy (SEM) is a microscopy technique not using light but a focused electron beam instead to scan the surface of a sample. This technique has been used worldwide

in many fields to analyze organic and inorganic materials at the nanometer to micrometer scale. The primary electrons are produced by an electron emitter, usually a tungsten wire with a sharp tip. These electrons accelerate to a voltage comprised between 1 to 40 kV by an electric field and are focused by lenses until a narrow beam (**Figure 4-4**). The sample is scanned by the beam and the primary electrons interact with the electron at the surface of the sample, producing a new electron signal that is detected by an electron detector. This signal provides information about the morphology and composition of the material.
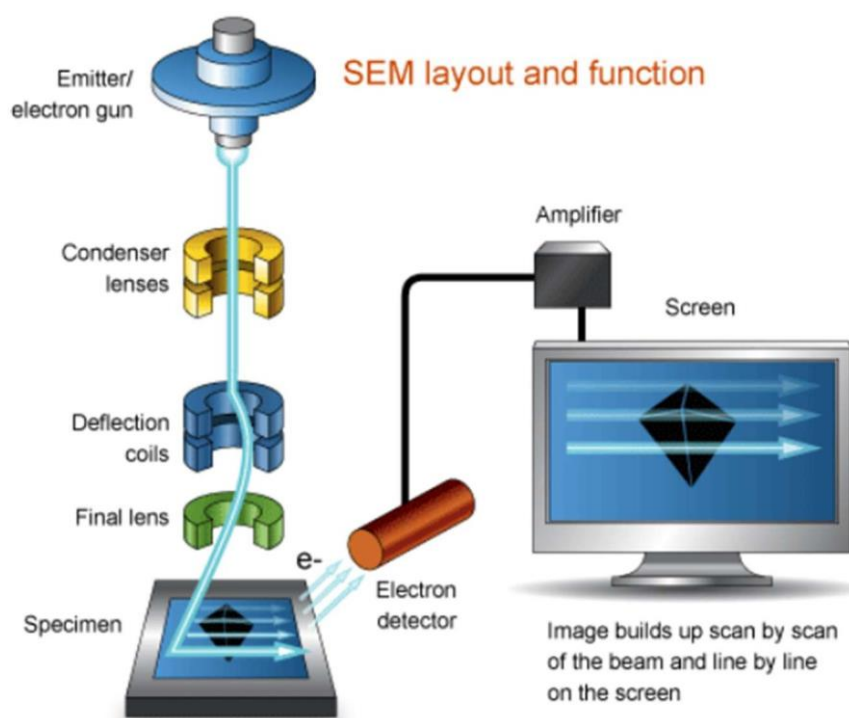
Figure 4-4. Schematic of the different components of SEM microscope[138].

The interactions between the primary electrons and the sample can produce different types of electrons. First, the secondary electrons: are typically weak valence electrons from the material. These electrons usually have low kinetic energy which is limited by the depth from which they can escape from the sample to a few nanometers (**Figure 4-5**), and they give topographic information. Second, backscattered electrons result from the elastic scattering between electrons from the beam with the atomic electric field, which allows for reaching deeper parts

of the sample (**Figure 4-5**). The electrons come from a direct interaction with the material and therefore provide information about the composition of the sample.
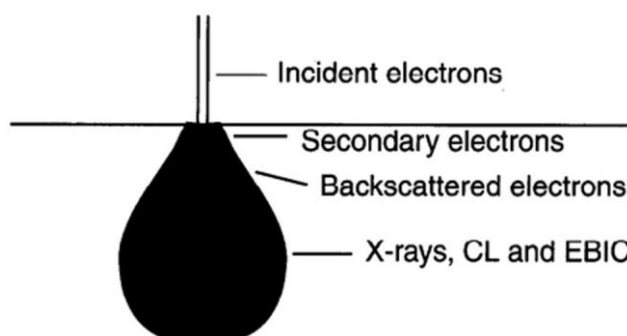
Figure 4-5. Scheme of the different sample-beam interactions at the surface[139].

4.2 Electrochemical Characterization Techniques

4.2.1 Voltammetric and Potentiostatic Methods

Linear sweep voltammetry (LSV) is a voltammetric method to measure the current at a working electrode (WE) while the potential between the WE and the reference electrode (RE) is swept linearly as a function of time between two defined potentials. Cyclic voltammetry (CV) is based on linear sweep voltammetry, but the experiment does not end after a single sweep in the voltage range but returns to the initial potential after reaching the end potential. This will then be repeated for a certain number of cycles (**Figure 4-6**).
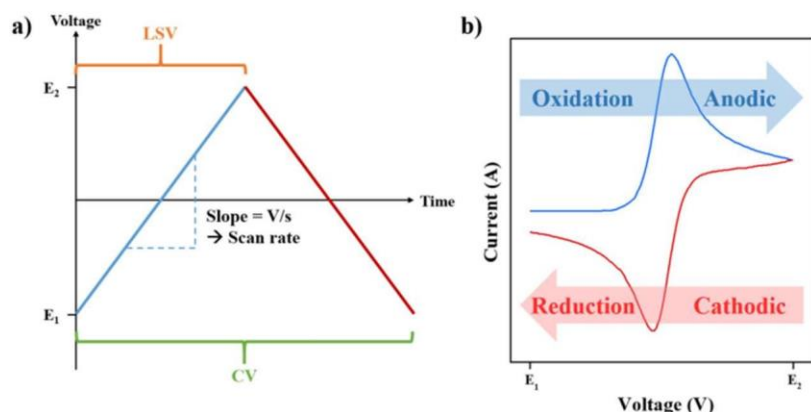
Figure 4-6. (a) Voltage vs. time profile for linear sweep and cyclic voltammetry and (b) example of cyclic voltammogram with anodic and cathodic peaks[140].

The result for LSV presented either an anodic peak or a cathodic peak depending on the sweep direction giving information about oxidation or reduction potentials for the material or process studied. The CV can provide also other information like the reversibility or the cyclability of an electrochemical process. In both cases, a very important parameter is the sweep rate (V s^{-1} or mV s^{-1}), and modifying it can provide information on the kinetics.

The potentiostatic technique consists of applying a constant potential between the WE and the RE and recording the current at the WE in function of time (chronoamperometry). The obtained current depends on the electrochemically active substances and can be used in combination with other methods like electrochemical impedance spectroscopy for example to determine lithium transference number[141].

4.2.2 Electrochemical Impedance Spectroscopy

Electrochemical impedance spectroscopy (EIS) is the technique of choice to investigate the electrochemical processes occurring at the interfaces in batteries. This technique consists of the perturbation of an electrochemical system in equilibrium by applying a small amplitude sinusoidal voltage signal over a large range of frequencies. The corresponding current signal is

recorded. This current signal commonly presents a phase shift that allows calculation of the impedance $Z(\omega)$ via Euler's equation (with Φ = phase shift and j = imaginary number):

$$Z(\omega) = Z_0 \cos(\Phi) + Z_0 j sin(\Phi)$$

The most common way to present impedance data is to use a Nyquist plot, representing the imaginary part of the impedance ($Z'' = Z_0 sin(\Phi)$, representing capacitance and inductance) as a function of the real part of the impedance ($Z' = Z_0 cos(\Phi)$, representing resistance).

An advantage of EIS is the possibility of simulating a Nyquist plot from an equivalent electrical circuit (**Figure 4-7**). When fitting the experimental impedance plots with an equivalent circuit, it is possible to relate the values of the different circuit components to the properties of the cells.
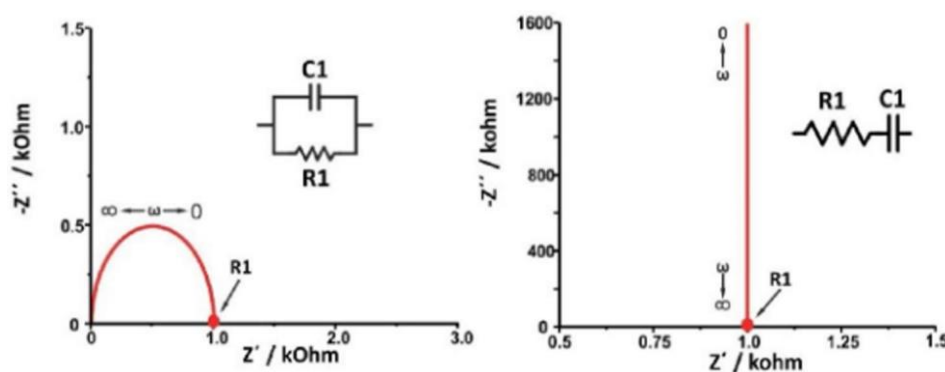
Figure 4-7. Examples of simulated Nyquist plots with their equivalent circuit[142].

The Nyquist plots can usually be separated into two main domains, one at low frequencies where the electrochemical processes are controlled by charge transfer phenomena and another at high frequencies where the electrochemical processes are controlled by mass transfer phenomena[142]. Characteristics such as the resistance of the electrolyte (R_E), the resistance of the electrolyte/electrode interfacial SEI (R_{SEI}), or diffusion of the Li^+ cations can be determined from EIS spectra.

4.2.3 Galvanostatic Techniques

The galvanostatic measurements consist of recording the voltage response between the working electrode (WE) and the counter electrode (CE) under a constant current with defined cut-off voltages. The voltage response is plotted versus time or capacity and voltage or dis-/charge profiles are obtained (**Figure 4-8**). This technique is the most fundamental and practical one to study the capacity, reversibility, stability, and rate capability of electrode materials. From the dis-/charge profiles, important information about the cell performances is accessible.
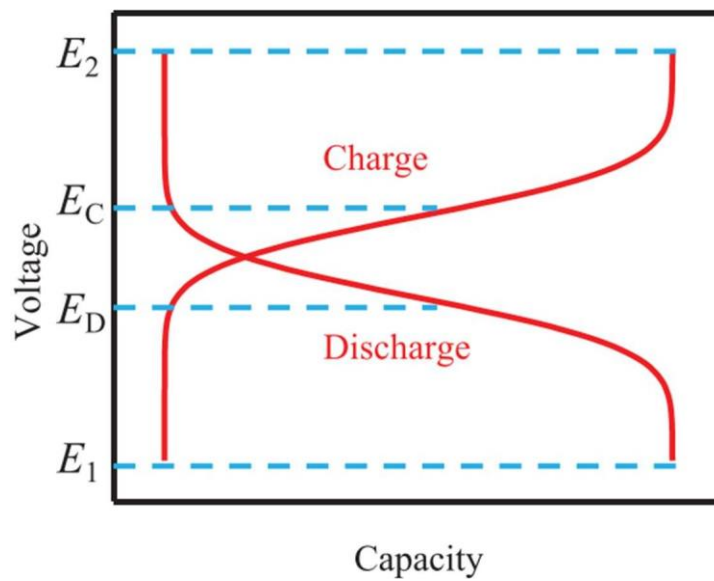
Figure 4-8. Typical charge-discharge profile versus capacity[143].

First, the specific capacity ($Q_{specific}$) in mAh g^{-1}, is the product of the apply current (I) with the charge/discharge time (t), divided by the mass of the active material ($m_{active\ material}$). The current divided by the mass of active material can also be designated as the specific current ($I_{specific}$):

$$Q_{specific} = \frac{I*t}{m_{active\ material}} = I_{specific} * t$$

The specific energy (in Wh kg^{-1}) can then be calculated from the specific current by integrating the product of specific current with the cell voltage over time:

$$E = \textit{f}\, I_{\text{specific}} * V_{\text{cell}}(t) dt$$

The study of the long-term cycling stability of a cell can be made by repeating charge and discharge cycles and evaluating the Coulombic efficiency. This corresponds to the ratio between the discharge and charge capacity for each cycle:

$$CE = \frac{Q_{\text{discharge}}}{Q_{\text{charg}}} * 100\%$$

For potential battery materials, excellent reversibility is needed which means close to 100% Coulombic efficiency. Furthermore, the discharge capacity of each cycle has to be compared to the initial discharge capacity to calculate the capacity retention (CR):

$$CR = \frac{Q_{\text{specific cycle n}}}{Q_{\text{specific cycle 1}}} * 100\%$$

The lifespan of a battery is commonly defined by the cycle at which the capacity retention is equal to 80% or less. This is the key parameter for a potential commercial implementation of the studied materials.

5. Experimental Part: Materials & Methods

5.1 Chemicals

4,4'-difluorodiphenyl sulfonee (($C_6H_4F_2$)$_2SO_2$, DFDPS), bromine (Br$_2$, 99.5%), lithium hydroxide monohydrate (LiOH, battery grade), para-terphenyl (99%) were purchased from Thermo Scientific Chemicals. Decafluorbiphenyl ((C_6F_5)$_2$, DFBP) was purchased from ABCR GmbH. 4,4'-dihidroxidiphenyl sulfone ((C_6H_4OH)$_2SO_2$, DHDPS) was purchased from Alfa Aesar. Tetrafluoro-2-(tetrafluoro-2-iodoethoxy)ethanesulfonylfluorid (ICF$_2$CF$_2$OCF$_2$CF$_2$SO$_2$F, 95%) and trifluoromethanesulfonamide (CF$_3$SO$_2$NH$_2$, 98%) were purchased from Matrix Scientific. 4'-brom-2,2,2-trifluoracetophenone (Br(C_6H_4)COCF$_3$, 99%) was purchased from Fluorochem. Trifluoromethanesulfonic acid (CF$_3$SO$_3$H, 99%), poly(ethylene glycol) dimethyl ether (CH$_3$O(CH$_2$CH$_2$O)$_n$CH$_3$, PEG), propylene carbonate (PC, 99%), acetic acid (CH$_3$CO$_2$H, 99%) were purchased from Sigma Aldrich. 4,4'-biphenol ((C_6H_4OH)$_2$, BP), potassium carbonate (K$_2$CO$_3$, 98%), triethylamide ((CH$_3$CH$_2$)$_3$N, TEA, 99.7%), copper powder (Cu), dimethyl sulfoxide ((CH$_3$)$_2$SO, DMSO, 99.8%), toluene (C_6H_5CH$_3$, 99.8%), hydrochloric acid (HCl, 37%), dichloromethane (CH$_2$Cl$_2$, 99.8%), methanol (CH$_3$OH, 99.8%), acetonitrile (CH$_3$CN, 99.8%), ethyl acetate (CH$_3$COOC$_2$H$_5$, 99.5%), dimethylacetamide (CH$_3$CON(CH$_3$)$_2$, DMAc, 99.8%), 1-methyl-2-pyrrolidon anhydrous (C_5H_9NO, NMP, 99.5%) were purchased from VWR.

4,4'-biphenol was repurified by recrystallization in isopropanol. In a round-bottom flask, a mixture of biphenol in isopropanol (~15 mL g^{-1}) was heated at 60 °C until the solid was dissolved. The solution was slowly cooled down at room temperature and the crystals were recovered by filtration under vacuum with a Büchner funnel. The same procedure was applied to 4,4'-difluorodiphenyl sulfone for purification.

For 4,4'-dihydroxidiphenyl sulfone, the mixture with isopropanol (~15 mL g^{-1}) was heated at 70 °C, and after the mixture was cooled down to room temperature. Subsequently, the solvent was removed on a rotary evaporator, and crystals were obtained.

For decaflurorobiphenyl, the purification was made by sublimation using the glassware[144] shown in **Figure 5-1**. The four chemicals were then dried at 60 °C overnight.
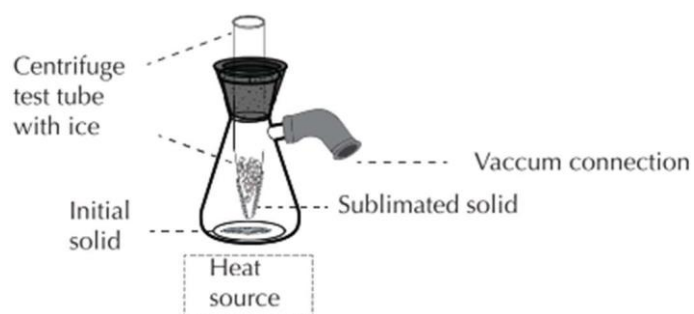
Figure 5-1. Scheme of a glass vacuum sublimator[144].

5.2 Synthesis of the Block Copolymer SIPE

5.2.1 Synthesis of the PES-FPES Backbone
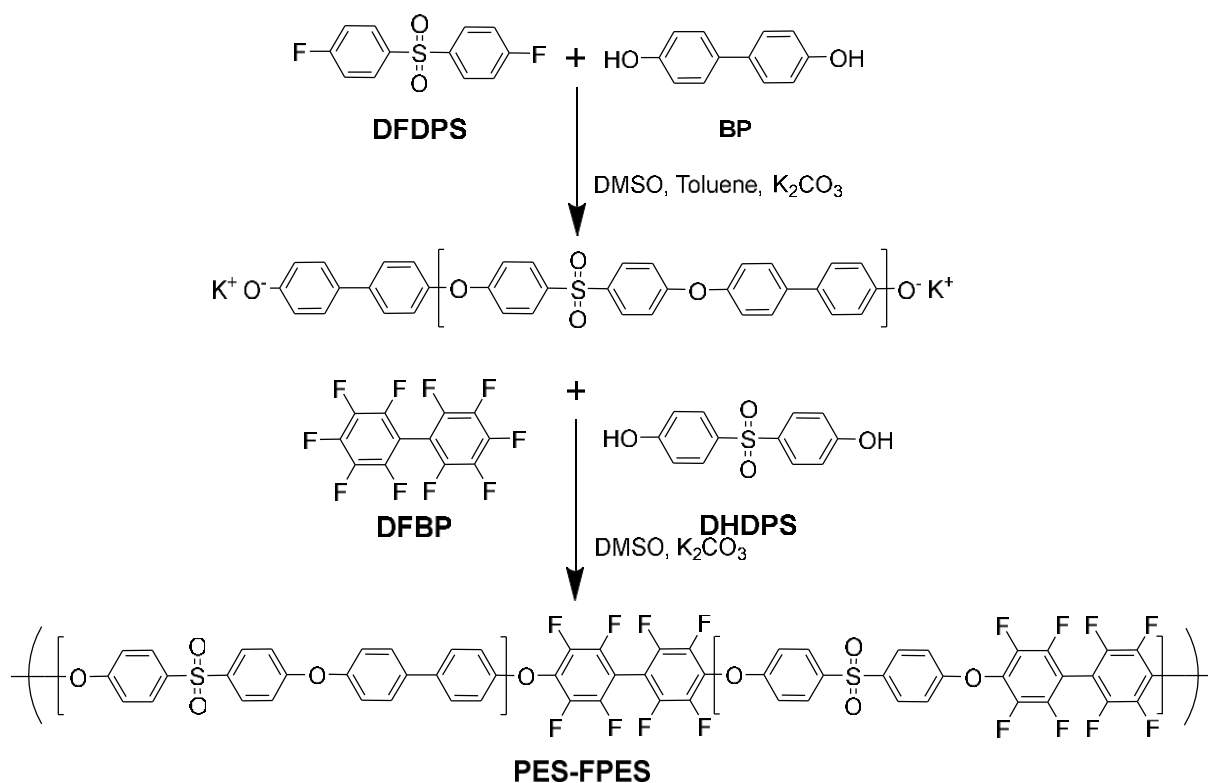
Figure 5-2. Synthesis scheme of PES-FPES block copolymer.

The PES-FPES block copolymer backbone was synthesized via one-pot-two-reaction synthesis. In a typical procedure, a polymer with a chain length of 15000 g mol^{-1} for the non-fluorinated block and 5000 g mol^{-1} for the fluorinated block was synthesized. In a three-necked flask equipped with an argon inlet, a mechanical stirrer, and a Dean-Stark trap, 3.01 g (16.2 mmol) of 4,4'-biphenol (BP), 4 g (15.7 mmol) of 4,4'-difluorodiphenyl sulfone (DFDPS) were introduced and dissolved in 30 mL of dimethyl sulfoxide (DMSO). Then 6.7 g (48.5 mmol) of potassium carbonate (K$_2$CO$_3$) and 15 mL of toluene as azeotropic agent were added. The reaction mixture was heated at reflux at 160 °C for 4 h to dehydrate the system. The temperature was then raised to 180 °C to distill off the toluene for 4 h. The temperature was then cooled

down to 125 °C, the reaction mixture was allowed to proceed at this temperature for 24 h. After 24 h, the temperature was decreased to 70 °C, and a solution of 0.87 g (3.49 mmol) 4.4'-dihydroxidiphenyl sulfone (DHDPS) in 20 mL DMSO was added. 1.45 g (10.5 mmol) of K_2CO_3 and 1.31 g (3.93 mmol) of decafluorobiphenyl (DFBP) were then successively added. The reaction mixture was allowed to proceed at this temperature for 2 h. Finally, the polymer was precipitated in an aqueous solution of hydrochloric acid (HCl) at 1 M and stirred for 24 h. A white solid was obtained after filtration.

5.2.2 Synthesis of the Brominated Intermediate
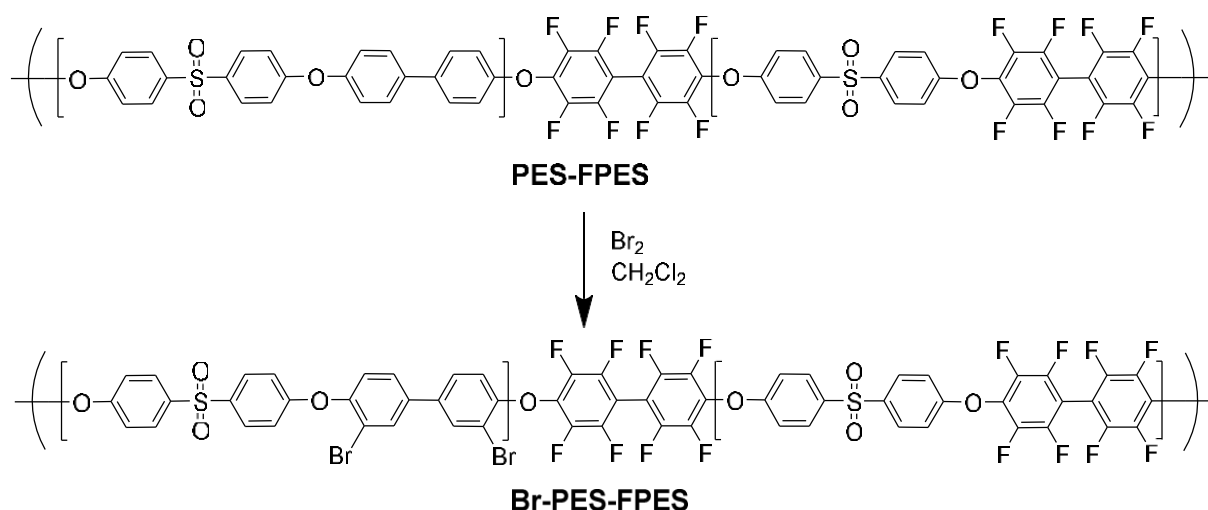
Figure 5-3. Bromination of the PES-FPES backbone.

The bromination of PES-FPES was carried out in a solution of dichloromethane and acetic acid (10% v/v) by the addition of a large excess of bromine (Br_2) at room temperature. In a typical procedure, 5 g (9.3 mmol of non-fluorinated block) of PES-FPES was introduced in a three-necked flask equipped with an argon inlet, refrigerant, and magnetic stirrer and dissolved in 100 mL of distillated dichloromethane. 10 mL of distilled acetic acid was added and after the precipitation of the polymer, 7.3 mL (140.9 mmol) of Br_2 were added drop by drop in two steps (3.7 and 3.6 mL per step). After 24 h of reaction, the mixture was poured in methanol. A white powder was obtained after filtration and dried at 60 °C under vacuum for 12 h.

5.2.3 Synthesis of the Anionic Side Chain
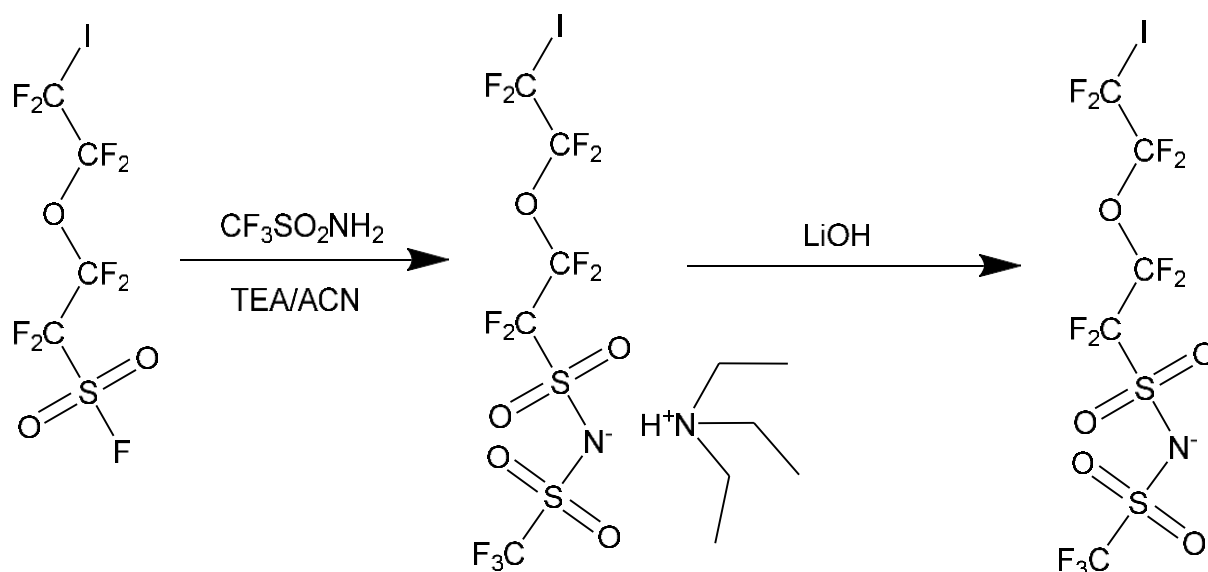
Figure 5-4. Synthesis of the LiTFSI-like anionic side chain.

In a typical procedure, 8.40 g (0.0563 mol) of $CF_3SO_2NH_2$ was introduced in a 100 mL two-neck round bottom flask equipped with an air condenser and a magnetic stirrer. Then, 10.43 g (0.103 mol) of triethylamine (TEA) and 20 mL of acetonitrile were added. The mixture was stirred to dissolve $CF_3SO_2NH_2$ and 20 g (0.0469 mol) of $ICF_2CF_2OCF_2CF_2SO_2F$ was added. The mixture was heated at 40 °C and the reaction was allowed to proceed at this temperature for 36 h. After 36 h, the resulting red mixture was concentrated on the rotary evaporator at 40 °C. The residue was dissolved in 250 mL of dichloromethane, washed four times with 250 mL of distilled water, and dried over magnesium sulfate. Finally, the dichloromethane was evaporated at 40 °C and a red oil was obtained. The oil was stirred with 200 mL of a LiOH aqueous solution (~0.2 M i.e. 5% molar excess of LiOH) for 1h. The water was removed by freeze-drying for 24 h, the resulting oil was dissolved in 250 mL of ethyl acetate, dried over magnesium sulfate and the solvent was evaporated using a rotary evaporator at 60 °C.

5.2.4   Addition of the Anionic Side Chain
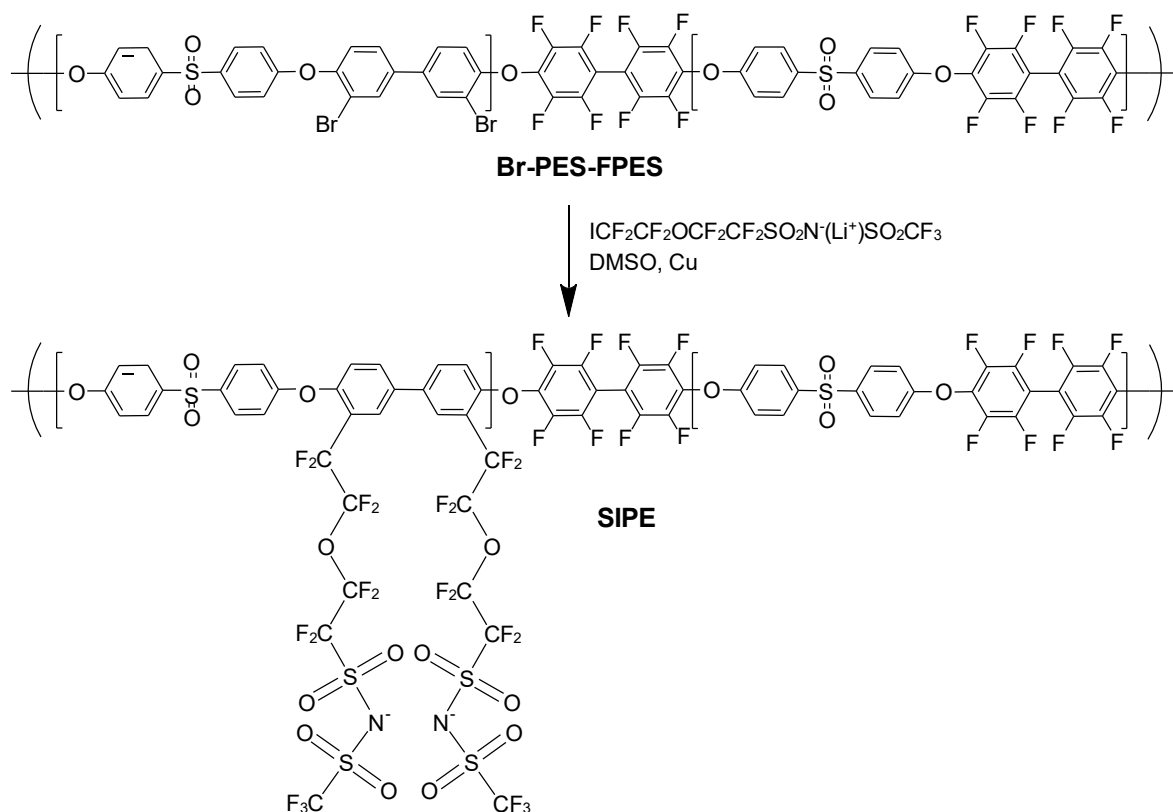
Figure 5-5. Addition of the I-psLi side chain by Ullman's coupling reaction.

The anionic side chain was added by Ullman coupling reaction using copper as a catalyst. In a typical procedure, 3 g (4.35 mmol) of BrPES-FPES was dissolved in 30 mL of DMSO, under stirring at 60 °C, in a three-neck 100 mL round-bottom flask, equipped with a mechanical stirrer, a condenser, an argon inlet, and a dropping funnel. After dissolution, 4 g (62.9 mmol) of copper powder was added, the temperature was raised to 120 °C and the stirring was set at a fast speed (400 rpm) for 3h. The stirring speed was slowed down to 100 rpm and 14 g (24.9 mmol) of ionic side chain was dissolved in 25 mL of DMSO and added drop by drop with the dropping funnel. The temperature was set to 140 °C (200 rpm) and the reaction was allowed to proceed at this temperature for 48 h. The mixture was then poured into a 600 mL aqueous solution of HCl (1 M) and a slightly orange solid was obtained after filtration, washed several times with

distilled water, and dried at 40 °C under vacuum for 4 h. The obtained polymer was designated as SIPE.

The IEC of SIPE was measured by acid–base titration in an organic solvent. The titrant solution was prepared by dissolving 0.05 g of anhydrous NaOH in 100 mL of diethylene glycol (DEG). The analyte solution was prepared by dissolving 0.1 g of ionomer powder in the acidic form in 5 mL of DGME. The acidic form of the ionomer was obtained by stirring the powder in a 2 M HCl solution for 24 h; the powder was then dried at 60 °C *in vacuo* for 12 h. Methyl orange was used as a pH indicator for the titration

5.3 Synthesis of the Ether-free SIPE

5.3.1 Synthesis of the TFPBr-TP Backbone
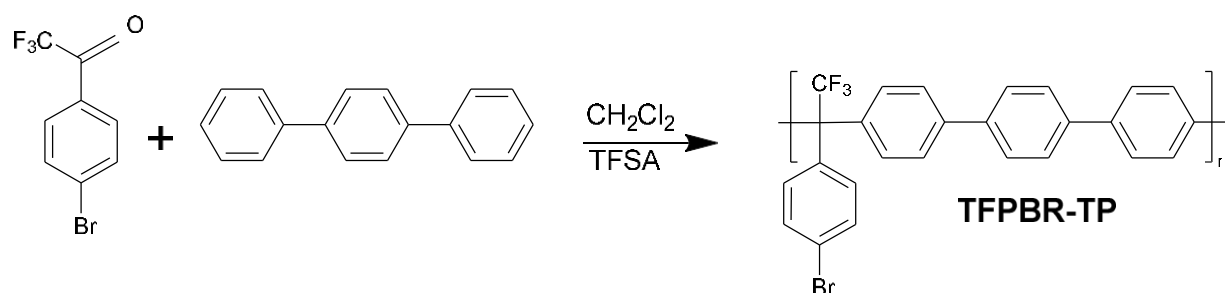
Figure 5-6. Synthesis scheme of TFPBr-TP backbone.

In an argon-filled glove box, 2 g (7.9 mmol) of 4'-brom-2,2,2-trifluoracetophenone and 1.818 g (7.9 mmol) of para-terphenyl were introduced in a one-neck 50 mL round-bottom flask equipped with a magnetic stirrer. Subsequently, 20 mL of dichloromethane were added as the reaction solvent. Once both compounds were dissolved, 4.2 mL (47 mmol) of trifluoromethanesulfonic acid were added drop by drop to avoid rapid heating, and the reaction was allowed to proceed at room temperature. After 8 h, the mixture was poured drop by drop

into 500 mL of methanol. After 4 h under strong stirring, a white solid was obtained by filtration and dried at 40 °C under vacuum. No further bromination step was needed.

5.3.2 Addition of the Anionic Side Chain
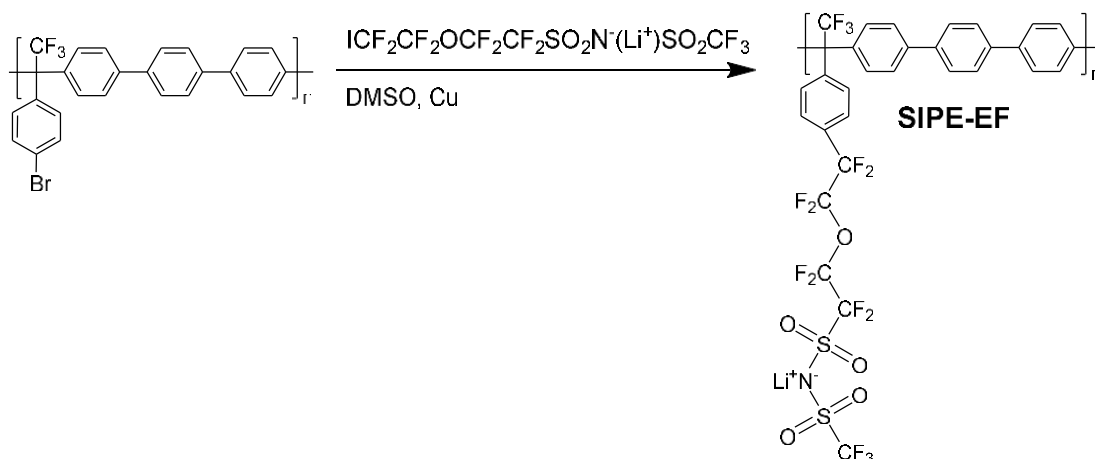
Figure 5-7. Addition of the I-psLi side chain to TFPBr-TP by Ullman's coupling reaction.

In a typical procedure, 1g (2.6 mmol) of TFPBr-TP was dissolved in 5 mL of dimethylacetamide (DMAc) in a three-neck 100 mL round-bottom flask equipped with a mechanical stirrer, a condenser, an argon inlet, and a dropping funnel and heated at 60 °C. Once the polymer was completely dissolved, 2.5 g (39.6 mmol) of copper powder was added under strong stirring with the temperature raised to 120 °C. After 3 h, 2.89 g (5.2 mmol) of the anionic side chain, dissolved in 5 mL of DMAc, was added drop by drop via the dropping funnel. The temperature was raised to 140 °C and the reaction was allowed to proceed at this temperature. After 24 h, another 3.6 g (6.4 mmol) of anionic side chain was added and the reaction proceeded for another 24 h. The mixture was poured drop by drop in 500 mL of aqueous solution of HCl (1 M). After 24 h under stirring, the solid was filtrated and dried at 40 °C under vacuum for 12 h. The obtained polymer was designated as SIPE-EF

5.4   Membrane Preparation

5.4.1 Single-Ion Conducting Polymer Electrolyte in Li form

To prepare the polymer electrolyte membrane of SIPE and SIPE-EF, 500 mg of polymer powder was dissolved in DMSO (~5% w/v) at 60 °C for 4 h via magnetic stirring. The solution was then cast in a petri dish. The solvent was evaporated in an oven at 60 °C for 24 h. The obtained solid membrane was cut into discs with a diameter of 14 mm. The ion exchange in the membrane was performed by immersing the discs in a 1 M LiOH aqueous solution and stirring for 4 h. The discs were then washed with deionized water many times, and subsequently dried at 80 °C in a Büchi oven for 24 h. After drying, the membranes were soaked with propylene carbonate in a dry room with a dew point below -70 °C. The solvent content (SC) was calculated as follows:

$$SC = \frac{w_s - w_d}{w_s} * 100\%$$

With w_s the weight of the soaked membrane and w_d the weight of the dry membrane.

5.4.2 "True" Solid-state Electrolyte

The SIPE powder (250 mg) and polyethylene glycol (1000 g mol^{-1}) (250 mg) were dissolved in DMSO (~25% w/v) at 60 °C for 4 h via magnetic stirring. The solution was then cast in a Petri dish. The solvent was evaporated in an oven at 60 °C for 24 h. A gummy membrane was obtained, this membrane was then hot pressed between two Mylar foils for 3 min at 60 °C under 30 µm. The membranes had a thickness of ~50 µm, were cut into discs (Ø=14 mm), and dried in a Büchi oven at 60 °C for 24 h. This material was designated as SIPE+PEG.

5.4.3 "True" Solid-state Hybrid Electrolyte

The SIPE powder (250 mg) and polyethylene glycol (1000 g mol^{-1}) (250 mg) were dissolved in DMSO (~25% w/v) at 60 °C for 2 h via magnetic stirring. A predetermined amount of LATP particles (300 nm with d=2.92 g cm^{-3}) was then added (20, 30, or 40% w_{LATP}/w_{blend}). The mixture was placed in an ultrasonic bath for 15 min to ensure good dispersion of the LATP particles. The solution was then cast in a Petri dish. The solvent was evaporated in an oven at 60 °C for 12 h. A gummy membrane was obtained, this membrane was then hot pressed for 3 min between two Mylar foils at 60 °C under 30 tons. White membranes were obtained with a thickness of ~50 μm, cut into discs (Ø=14 mm), and dried in a Büchi oven at 60 °C for 48 h. The obtained membranes were designated as SIPE-HE20, SIPE-HE30 and SIPE-HE40.

5.4.4 Multi-layer Polymer Electrolyte

In a dry room with a dew point well below -70 °C, 500 mg of PEO, 326 mg of LiTFSI (EO:salt ratio of 10:1), and 25 mg of benzophenone were mixed in a vial without any solvent. The resulting solid mixture was annealed at 100 °C for 36 h. A transparent and slightly yellow solid was obtained. This solid was hot-pressed between two mylar foils at 100 °C under 50 tons. The resulting transparent membranes were crosslinked under UV-light irradiation for 3 min on each side and finally, a polymer electrolyte with a thickness of ~20 μm was obtained. In parallel SIPE-E membranes were prepared as described earlier and soaked with 55% of propylene carbonate. These membranes were then sandwiched between two PEO membranes, or a PEO membrane was put in contact with only one side of the SIPE-EF membrane for the electrochemical characterization. The membrane was designated as SIPE-EF+PEO-L.

5.5 Electrode Preparation

LiFePO$_4$ (LFP) electrodes were prepared by mixing 80 wt.% of LFP, 10 wt.% of C65 black carbon, 5 wt.% of poly(vinylidene difluoride) (PVdF), and 5 wt.% of the single-ion conducting

polymers (SIPE or SIPE-EF) in an appropriate amount of N-methyl-2-pyrrolidone (NMP) to obtain a homogeneously dispersed slurry which was then placed in ultrasonic bath for 15 min to ensure the dispersion of the LFP and C65 particles. This slurry was then cast on battery-grade aluminum foil using a doctor-blade technique with a wet-film thickness of 100 μm. The sheet was dried in an oven at 70 °C for 12 hours, and afterward cut into discs with a diameter of 12 mm. Subsequently, the discs were dried for 24 h in a Büchi oven at 100 °C under vacuum. The electrodes were then pressed at 10 tons for 10 seconds to increase the electrode's density.

The $LiNi_{0.8}Mn_{0.1}Co_{0.1}O_2$ (NMC_{811}) electrodes were prepared by mixing 90 wt.% of NMC_{811} powder, 5 wt.% of C65 conducting carbon, 2.5 wt.% of PVdF and 2.5 wt.% of single-ion conducting polymer (SIPE or SIPE-EF) in an appropriate amount of NMP to obtain a homogeneously dispersed slurry. The subsequent steps are the same as the previously described for the LFP electrodes. The complete process of electrode preparation was performed in a dry room with a dew point well below -70 °C.

5.6   Physicochemical Characterization

NMR spectroscopy (^1H NMR and ^{19}F NMR) was performed using a Bruker Advance at room temperature. The data analysis was performed with Bruker's TopSpin software. The NMR tubes were prepared by dissolving ~5 mg of the material in ~0.5 mL of deuterated DMSO or deuterated chloroform.

TGA was performed between 20 °C and 600 °C with a heating ramp of 5 °C min^{-1} under a nitrogen atmosphere (flow of mL min^{-1}) using a thermogravimetric analyzer (NETZSCH). In an aluminum crucible, 2.5 mg to 5 mg of sample were sealed in an argon-filled glove box or a dry room with a dewpoint well below -70 °C.

DSC was performed on a Mettler Toledo DSC analyzer in a temperature range from -50 °C to 275 °C with a heating ramp of 5 °C min^{-1}. In an argon-filled glovebox or a dry room, about 5 mg of sample were sealed in an aluminum crucible before measurement under a nitrogen flow of 50 mL min^{-1}.

SEM images were recorded using a Zeiss Crossbeam 340 field-emission electron microscope equipped with a Capella-focused ion beam (FIB, gallium ion source). Samples were fixed on an aluminum sample holder with conductive carbon tape (Plano G3347) and transferred from the argon-filled glove box, or dry room, to the microscope using a Transfer chamber.

5.7 Cell Assembly and Electrochemical Characterization

All the coin cells for electrochemical characterization were assembled in an argon-filled glovebox with O_2 and H_2O contents well below 2 ppm.

The ionic conductivity was measured with stainless steel‖stainless steel cells in a climatic chamber (Vötsch VTM 4004) between 20 °C and 90 °C via EIS using a Hewlett Packard Impedance Analyzer in a frequency range from 1 MHz to 10 mHz with an AC amplitude of 10 mV. The cells were allowed to relax at each testing temperature for 3 h before the next measurement.

The conductivity was calculated as follows:

$$\sigma = \frac{L}{R * A}$$

where L is the thickness of the membrane, A is the electrode area, R is the bulk membrane resistance and σ the ionic conductivity.

The limiting current density was measured using symmetric Li‖Li cells and a VMP Biologic electrochemical workstation. Linear sweep voltammetry was conducted with a constant sweep rate of 0.01 mV s^{-1} from open circuit voltage (OCV) to 6.0 V.

The electrochemical stability window was determined in stainless steel‖Li cells via linear sweep voltammetry at a constant sweep rate of 1 mV s^{-1}. The anodic sweep was performed from OCV to 6 V and the cathodic sweep from OCV to -0.5 V using a VMP Biologic electrochemical workstation.

The lithium-ion transference number (t_{Li}^+) was measured in Li‖Li cells via chronoamperometry (CA) and EIS. The constant voltage for CA was 10 mV and the EIS was measured in a frequency

range from 200 kHz to 100 mHz with an AC amplitude of 10 mV before and after polarization. The transference number was calculated as follows [141]:

$$t_{Li}^{+} = \frac{I_S(\Delta V - I_0 R_0)}{I_0(\Delta V - I_S R_S)}$$

where I_0 and I_S are the initial and steady-state current, R_0 and R_S are the initial and steady-state resistance, and ΔV the polarization potential.

The stripping-plating experiments were conducted in symmetric Li∥Li cells using a Maccor S4000 battery tester and a VMP Biologic electrochemical workstation; the latter was used to combine stripping-plating with EIS measurements (from 200 kHz to 100 mHz with AC amplitude equal to 10 mV). One cycle is composed of a 30 min stripping step, followed by a 5 min rest, and a 30 min plating step, followed by 5 min rest.

Galvanostatic cycling was performed using a Maccor S4000 battery tester. The charge/discharge behavior of Li∥LFP cells was studied with a dis-/charge rate of 1C corresponding to a specific current of 170 mA g^{-1} and in the case of Li∥NMC$_{811}$ cells 1C corresponds to a specific current of 190 mA g^{-1}.

For each characterization, 3 cells were prepared and tested for reproducibility. The results presented in the following are an average of these three tests.

6. Results and Discussions

6.1 Replacing the Doping Solvent to Obtain a "True" Solid-State Single-Ion Conducting Polymer Electrolyte.

This section presents the study of the blend of poly(ethylene glycol) dimethyl ether (1000 g mol^{-1}) with the partially fluorinated multi-block co-poly (arylene ether sulfone) with lithium perfluorosulfonimide side chains. These copolymers have been already studied in our group doped with PC or EC. In this study, we maintained the general structure of the single-ion conducting polymer but opted to modify the average length of the different blocks compared to previous studies[129,145]. Herein, a polymer with average backbone block lengths of 15 kg mol^{-1} for the PES block, bearing the lithium perfluorinated sulfonimide function (called ionophilic block), and an average block length of 5 kg mol^{-1} for the FPES block (ionophobic block) was prepared. This design was chosen to obtain a higher lithium concentration but also a better flexibility of the polymer to ensure good lithium mobility even with PEG molecules being much more viscous than the usual PC or EC molecules.

6.1.1 Synthesis

The block length and the grafted side chains was confirmed by ^{1}H NMR analysis (**Figure 6-1** to **Figure 6-3**).

Figure 6-1 shows the NMR spectra recorded after the synthesis of PES-FPES. The ratio between the hydrophilic block (PES) and the hydrophobic block can be calculated from the integral of the H_2 or H_4 peaks and the integral of the H_6 peak. The experimental ratio is 5 which is a bit higher than the theoretical ratio calculated for this polymer (4.2 [146]) this means the hydrophobic part is longer than expected one, i.e. if we consider PES block 1500 g/mol (n=37), the FPES will be about 5950 g/mol (m=11).
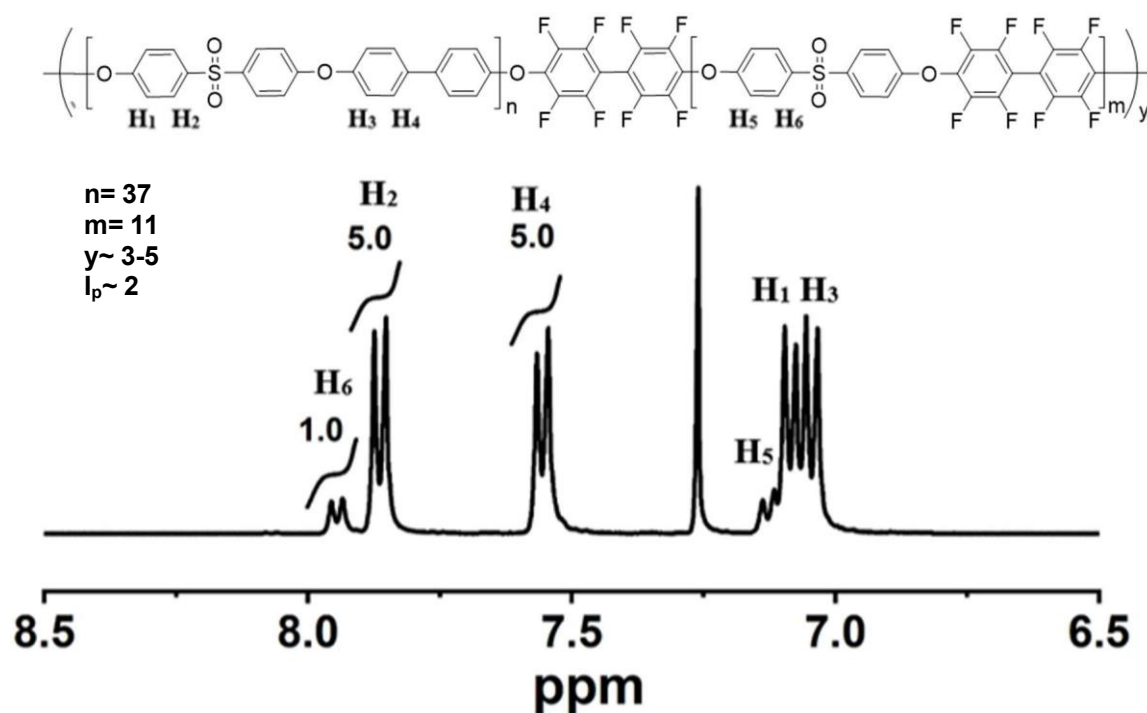
Figure 6-1. H NMR spectrum recorded for PES-FPES recorded in chloroform.

Figure **6-2** presents the NMR spectra recorded after the bromination of the PES-FPES backbone. The apparition of a singlet at 7.85 ppm confirms the substitution of a hydrogen atom by a bromine atom. The ratio of the integral for H_2 and H_7 allows us to determine that the substitution yield is 90 %, which is in good accordance with previous results on this polymer [146].
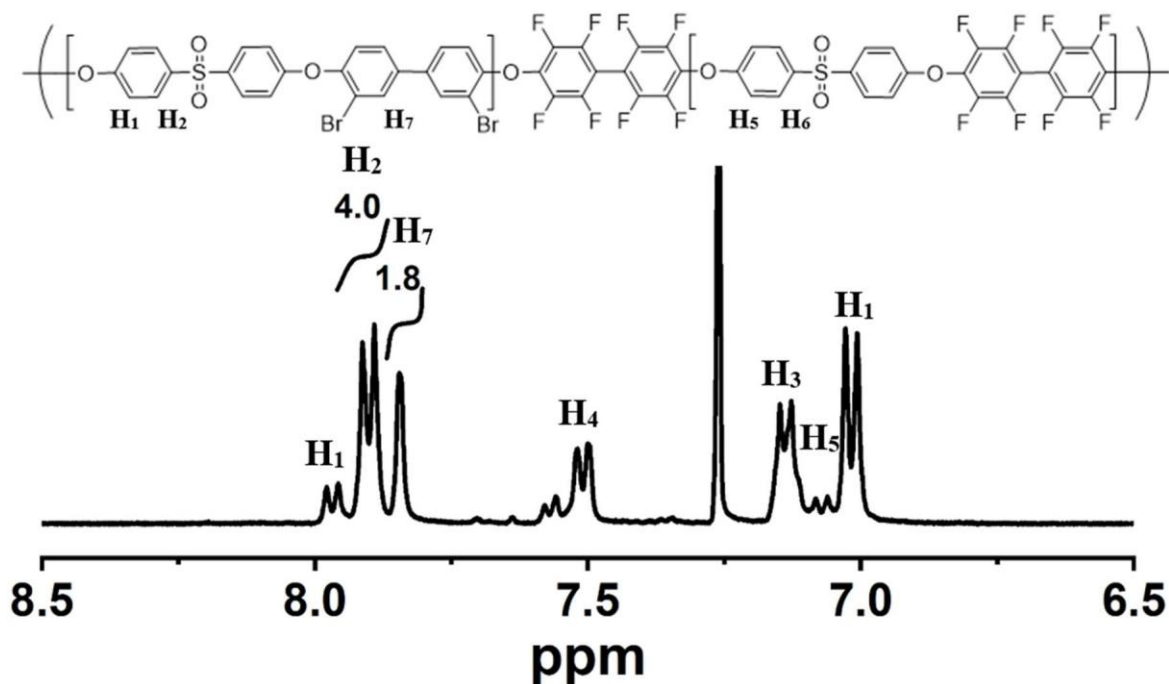
Figure 6-2. ^{1}H NMR spectrum recorded for Br-PES-FPES recorded in chloroform.

After the coupling reaction, the ^{19}F-NMR spectra of the single-ion conducting multiblock copolymer was recorded (**Figure 6-3**). This spectrum allow us to calculate the grafting degree of perfluoroalkyl sulfonimide groups with the following equation:

$$N_{NMR} = \frac{2 * I_1}{I_7 * R_{exp}}$$

where N_{NMR} is the number of ionic function per PES repeating unit, I_1 is the peak integral of F_1 (-110.69 ppm), I_7 is peak integral of fluorine atoms of the FPES block F_7 (-137.72 ppm) + peak integral of fluorine atoms at the end of the FPES block ($F_{7'}$) and R_{exp} the experimental ratio between the PES and FPES blocks (measured to be 5). With the integral values on the spectra, we determined that there are 0.86 ionic functions per PES repeating unit. This value can then be used to determine the Ionic Exchange Capacity (IEC) of the polymer with the following equation:

$$IEC_{NMR} = N_{NMR} * IEC_{theo} = N_{NMR} * \frac{2 * \chi n_{PES}}{M n_{psi-PES} + Mn_{FPES}} * 1000$$

where $\chi n_{PES} = 37$ is the average repeating unit number in PES blocks, Mn_{FPES} (5950 g mol^{-1}) is the molar mass of the FPES block. $Mn_{psi-PES}$ is the molar mass of psi-PES block = ($M_{PES} + N$ x M_{psi}) x χn_{PES} (where M_{PES} is molar mass of structural unit of PES and M_{psi} is molar mass of psi side chain). This calculation results in an IEC of 1.22 meq Li$^+$ g^{-1}, which is once again in excellent accordance with previous results [146]. To confirm this value, the IEC was also measured by acid–base titration in an organic solvent. After titration, a value of 1.37 meq H$^+$ g^{-1}. This value is close to the theoretical and NMR values, once again confirming the successful synthesis of this single-ion conducting polymer.
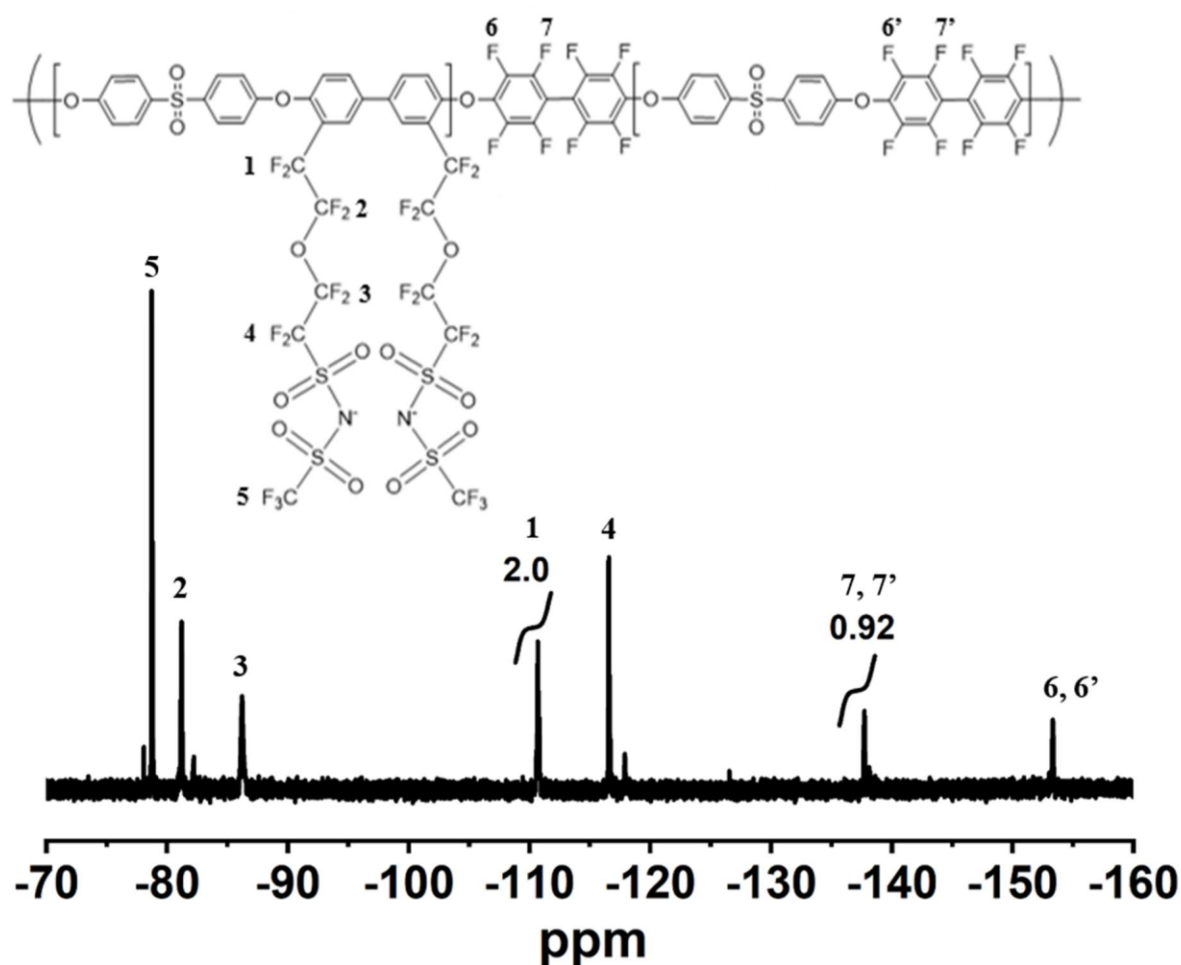
Figure 6-3. ^{19}F NMR spectrum recorded for SIPE recorded in DMSO.

The thermal properties, ionic conductivity, and electrochemical properties were compared to those of the single-ion membranes doped with propylene carbonate.

6.1.2 Membrane Preparation and Thermal Characterization
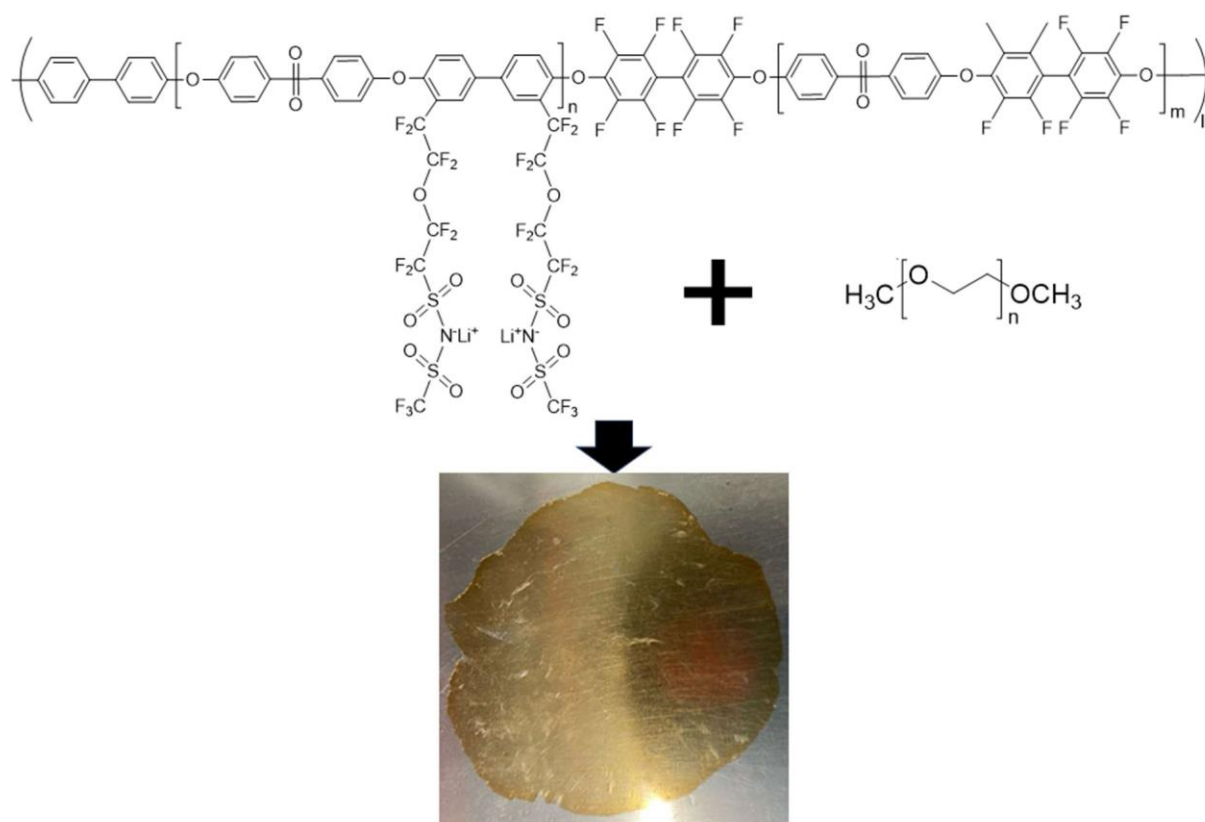
Figure 6-4. Molecular structure of the single-ion polymer and the preparation of "true" solid-state single-ion conducting polymer electrolyte.

SIPE/PEG in mass ratio 1/1 was blended and after the hot-pressing process, an orange translucent membrane with a thickness of about 50 µm was obtained. T membrane displays suitable mechanical stability even when stretched. However, the membrane is sticky and needs to be manipulated carefully.

Regarding the thermal properties, the SIPE, before doping with PC, is stable until 250 °C before a linear weight loss was observed in the TGA data (**Figures 6-5**). The small weight loss starting around 100 °C is due to residual water. The SIPE as well as the casting solvent are very hydrophilic and, due to the high Tg of the SIPE and the strong interaction between the SIPE and water, the drying step was probably not enough to completely remove the water.

The TGA profile for SIPE+PEG reveals a weight loss starting around 220 °C, which accounts for about 50% of the total weight and is attributed to the PEG incorporated in the blend. Interestingly, this weight loss starts at a higher temperature than the degradation of pure PEG, suggesting that the PEG is in interaction with the SIPE. The blend SIPE +PEG shows a higher onset temperature for weight loss compared to SIPE+PC, with more than 100°C, indicating excellent thermal stability. Furthermore, the introduction of solvent, either PEG or PC, does not affect the thermal stability of SIPE.
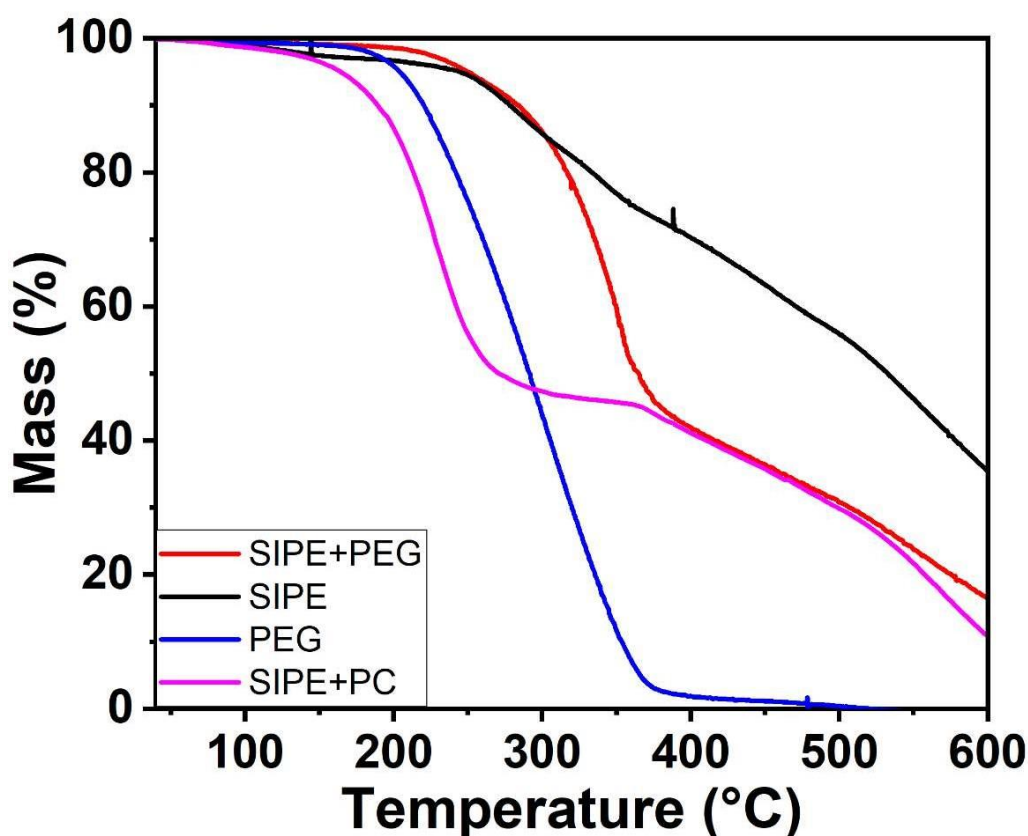
Figure 6-5. TGA curve of the SIPE+PEG (red) compared to the TGA curves of PEO (blue) and "after casting" SIPE (black).

The DSC diagram of the SIPE (**Figure 6-6**) is typical of an amorphous polymer exhibiting two glass transition temperatures, one at about 130 °C (T_g^{SIPE1}) assigned to the ionophilic block and one at about 240 °C (T_g^{SIPE2}) assigned to the ionophobic block. The lower Tg of ionophilic bloc

is due to both the non-fluorinated backbone and the presence of the side chains. In the DSC diagram of SIPE+PEG, $T_g^{SIPE+PEG1} = -30\ ^\circ C$ and $T_g^{SIPE+PEG2} = 255\ ^\circ C$ were measured. The second value is a little higher than the one for the ionophobic block of SIPE, probably indicating a better separation and organization of the ionophobic part in the blend, due to the higher mobility of ionophilic block. On the other hand, the first value is well above the reported T_g for PEG (-80 $^\circ C$ for 1000 g mol^{-1} [147]) and well below the measured T_g^{SIPE1} meaning that the PEG is mainly incorporated in the ionophilic domain by interaction probably with the Li cation. The theoretical Tg can be calculated by applying the Flory Fox equation [148]:

$$\frac{1}{T_g} = \frac{w_1}{T_{g1}} + \frac{w_2}{T_{g2}}$$

We consider the system to be composed only of the hydrophilic block of the single-ion conducting polymer and the poly(ethylene glycol) dimethyl ether since the T_g of the hydrophobic block is not highly impacted by the blending with poly(ethylene glycol).

  w_1 is the weight fraction of ionophilic block

  w_2 is the weight fraction of poly (ethylene glycol)

  T_{g1} is the transition glass temperature of the hydrophilic block (130 $^\circ C$ = 403.15 K)

  T_{g2} is the transition glass temperature of poly (ethylene glycol) (-76.5 $^\circ C$ = 196.65 K

  (see appendix A.2))

The calculated value is -18 $^\circ C$, higher than the measured one. This difference can be related to the imprecision in the calculation of the ionophilic block % in the total polymer as well as the T_g value measured with a crystalline PEG (see Figure S2 in appendix) while in the SIPE it is completely amorphous.
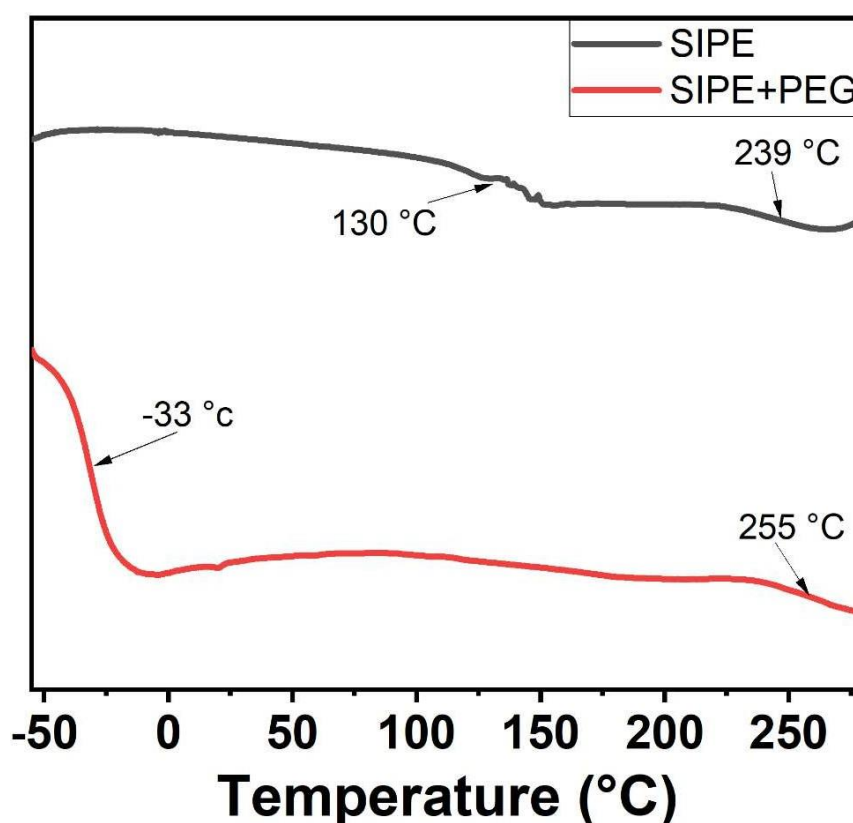
Figure 6-6. DSC diagrams of the SIPE after casting with DMSO (black) and of the SIPE+PEG after hot-pressing (red)

6.1.3 Electrochemical Properties

Figure 6-7 presents the ionic conductivity of the SIPE+PEG electrolyte compared to the SIPE doped with 55% PC in a temperature range of 20 °C to 90 °C. The 55% PC content was selected because at this concentration it was shown in previous publications to be the best compromise between conductivity, mechanical, and thermal properties. The conductivity data reveal a typical Vogel-Tramman-Fulcher (VTF) behavior, indicating in booth case the lithium cation transport is related to the coordination of the cation with the solvent, e.g. with PC in the case of SIPE+PC or with PEG in the case of SIPE+PEG. The solvent molecules coordinate the Li^+ cations and act as transporters for lithium. Nevertheless, a huge difference is observed between SIPE+PC and SIPE+PEG. The much lower conductivity of SIPE+PEG can be explained by

the nature of two solvents. The PC has a lower viscosity (2,54 mPa s^{-1} at 25 °C [149]) and much higher dielectric constant (64.92 at 25 °C [148]) that can affect positively both lithium mobility and dissociation (lithium cation concentration), while with the higher viscosity (~110 mPa s^{-1} for PEG with 600 g mol-1 at 30 °C [150]), lower dielectric constant (11.55 at 40°C [151]) and high donor number PEG, the transport is slown down resulting in lower conductivity. Also, the change from an ion hopping mechanism (in the case of PC) to a complexation/decomplexation mechanism (similar to the one in PEO:LiTFSI electrolytes) for the lithium cation transport could explain the lower Li cation mobility.

Nonetheless, the SIPE+PEG conductivity was measured to be 10^{-5} S cm^{-1} at 40 °C, a high value for a single-ion conducting polymer electrolyte with no volatile organic liquid plasticizers.
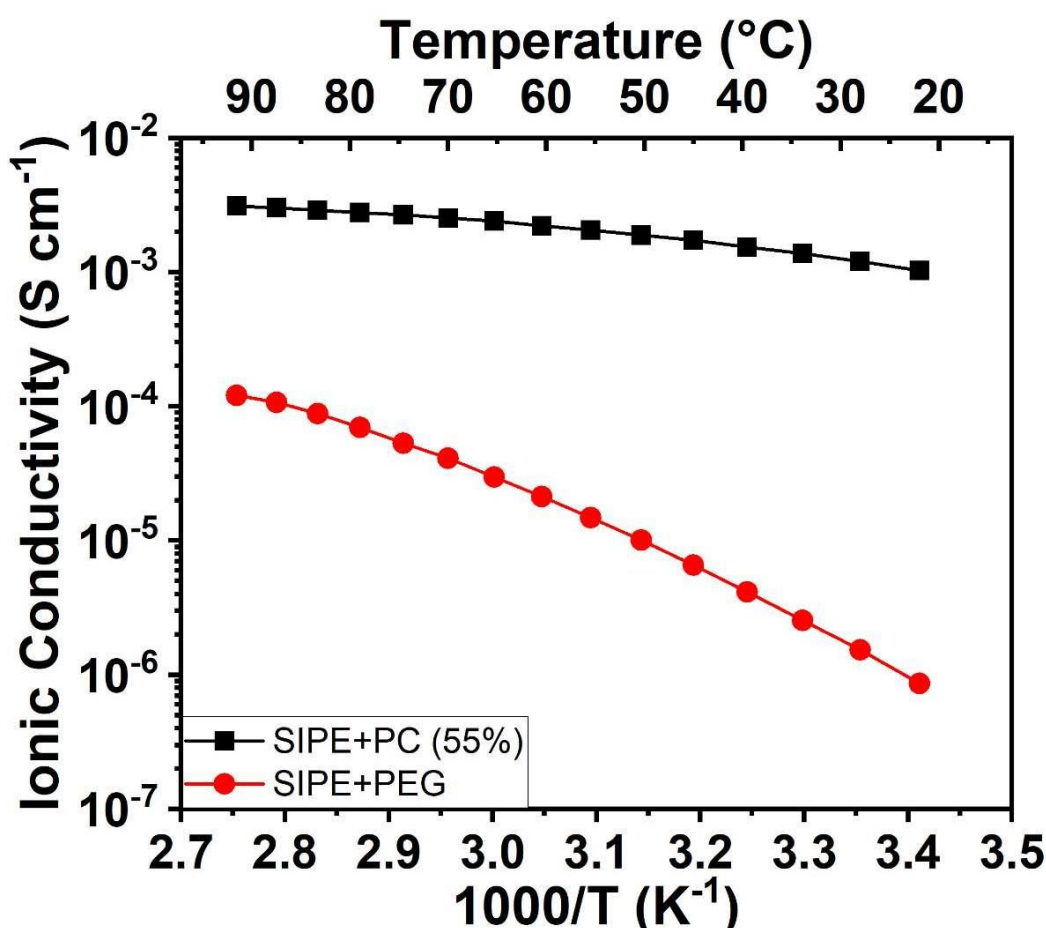
Figure 6-7. Conductivity, as a function of temperature, of the SIPE+PEG electrolyte compared to the conductivity of the SIPE+PC electrolyte with 55wt% PC.

To determine the t+ of SIPE+PEG, we employed the Bruce and Vincent potentiostatic polarization method (**Figure 6-8**). The current measured in **Figure 6-8.a** went through a quick drop at the very beginning of the polarization with stabilization at a constant current after about 20 minutes. The impedance spectra before and after 115 minutes of polarization gave nearly identical results, indicating the achievement of a stable SIPE+PEG‖lithium interface. For the equation used in the Bruce-Vincent method, we do not need to separate the bulk resistance from the interfacial resistance and therefore the total resistance was used for the calculation (**Figure 6-8.c**). Through this method, we obtained a lithium transference number of 0.99. The single-ion conducting nature of the solvent-free electrolyte was well addressed by this high lithium transference number.

R_0 (Ohm)	R_{ss} (Ohm)	I_0 (mA)	I_{ss} (mA)	t^+
942.16	947.84	0.0101	0.0086	0.99
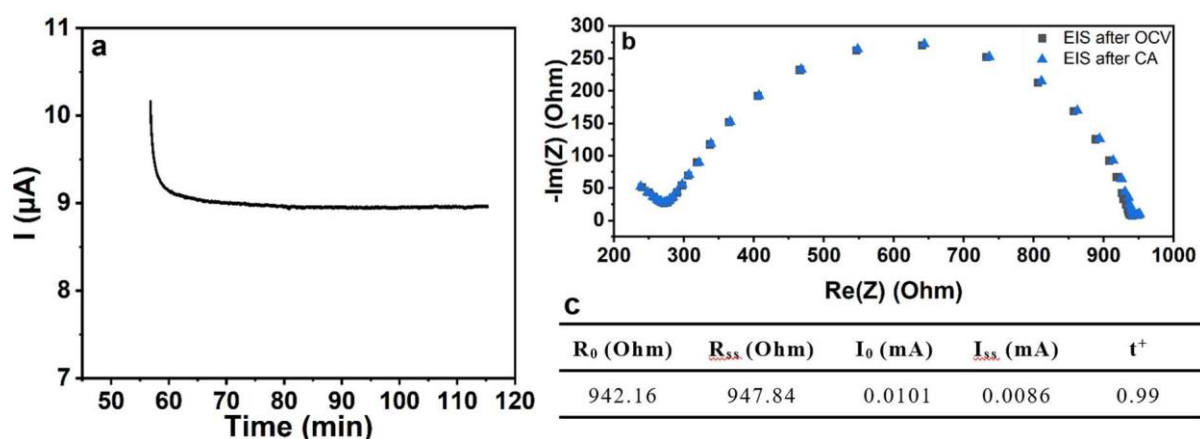
Figure 6-8. Determination of the transference Number by Bruce and Vincent potentiostatic method. a) chronoamperometry data obtained when applying a constant voltage of 10 mV to a symmetric Li/Li cell containing the SIPE as electrolyte. b) Impedance measurement before (black) and after (blue) the chronoamperometry measurement. c) Values used in the Bruce and Vincent equation to determine the transference number.

The limiting current density was also measured at 40 °C (**Figure 6-9**). The obtained value was 0.2 mA cm^{-2} which is lower than the previously reported value for this polymer structure[145]. The limiting current density is related to the mobility of the cation in the electrolyte; this lower

value is then not surprising taking into account the significant difference in conductivity reported previously for SIPE+PC and SIPE+PEG.
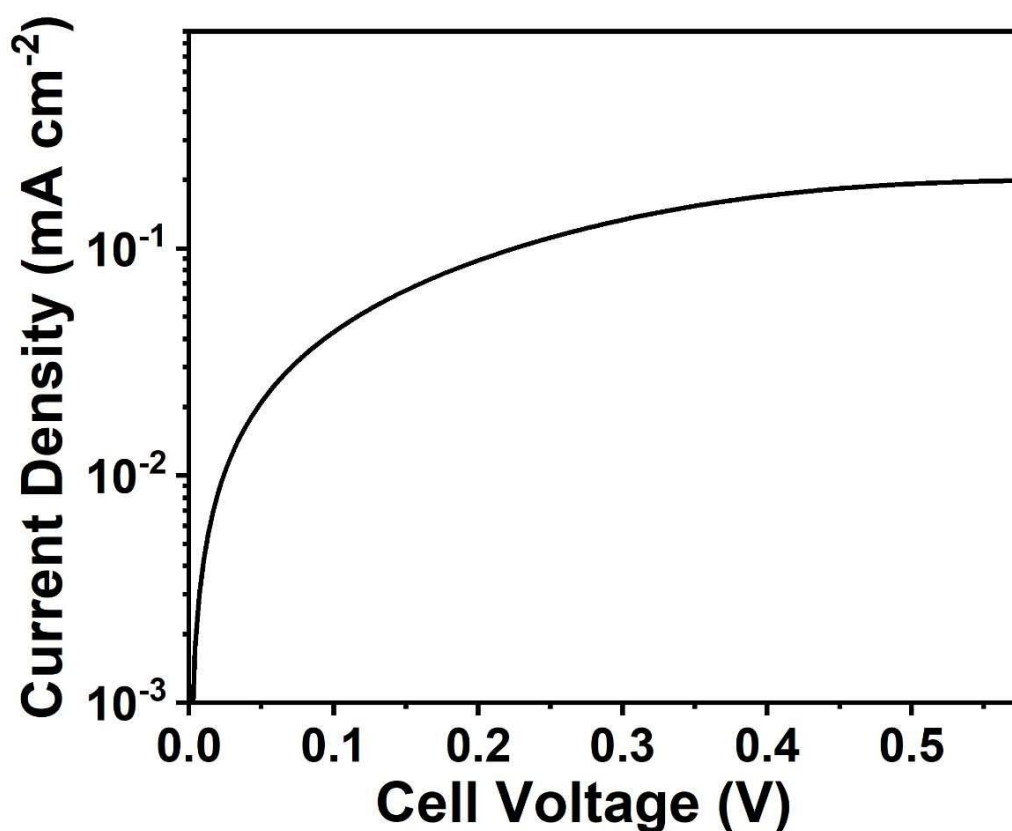
Figure 6-9. Determination of the limiting current density of SIPE+PEG by linear sweep voltammetry at 40 °C (sweep rate= 0.01 mV s^{-1}).

The determination of the electrochemical stability window of the SIPE+PEG system is presented in **Figures 6-10 and 6-11**. On the cathodic sweep from LSV (**Figure 6-10** (red)), the current density increase at 0 V is assigned to the metallic lithium deposition, and the small increase at 0.8 V can be attributed to the reductive decomposition of the remaining trace of DMSO from the casting process[152]. Another small increase is observed at 1.6V, which was also observed in a previous study dealing with polyethylene oxide based electrolytes and was assigned to water and oxygen reduction[153]. On the anodic sweep (**Figure 6-10** (black)) no oxidative peak was observed until a sharp increase at 4.6 V. This corresponds to the oxidative

decomposition of the bulk electrolyte. The stability almost matches SIPE+PC reported in another study[129] and overcomes the usually reported values for polyethylene oxide-based electrolytes[154].
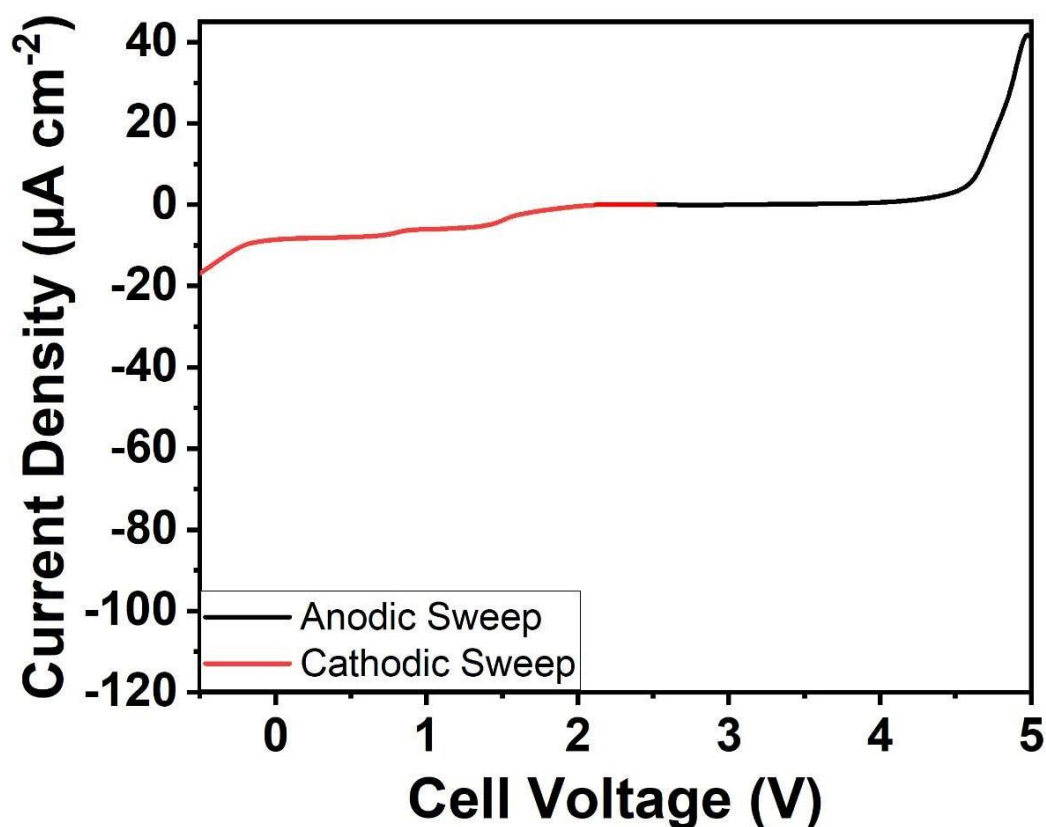
Figure 6-10. Determination of the electrochemical stability window of SIPE+PEG by linear sweep voltammetry at 40 °C using Li/Stainless steel cells (sweep rate = 1 mV s^{-1}).

To analyze this behavior in more details, the electrochemical stability was then further investigated also by cyclic voltammetry (**Figure 6-11**). Starting from OCV, the cell was polarized up to 4.6 V and an oxidation peak appeared at around 4.4-4.5 V. The intensity of this peak decreases, indicating stabilization of the electrode‖electrolyte interface during cycling. Two reductive peaks at close value to thus in LSV, i.e. at 1.5 V and 0.9 V are observed. However, these peaks are irreversible, agreeing with previous observation, the reaction of DMSO, or water traces.   Whereas some other peaks appear between 1.1-1.2 V, and the intensity of these

peaks tends to decrease and stabilize after the first cycle, indicating the formation of a stable SEI at the lithium surface. For the first cycle, a strong reduction peak was observed between 0 to -0.3 V, which is ascribed to lithium plating on the stainless-steel surface[155]. Surprisingly, this sharp current decrease was suppressed after the first cycle. This could suggest that the lithium metal plated in the stainless steel during the first cycle reacted with the electrolyte to form dead lithium. This is even more probable considering that the amount of lithium plated is very low (0.0095 mAh cm^{-2} in the first cycle) and can easily be consumed by side reaction.
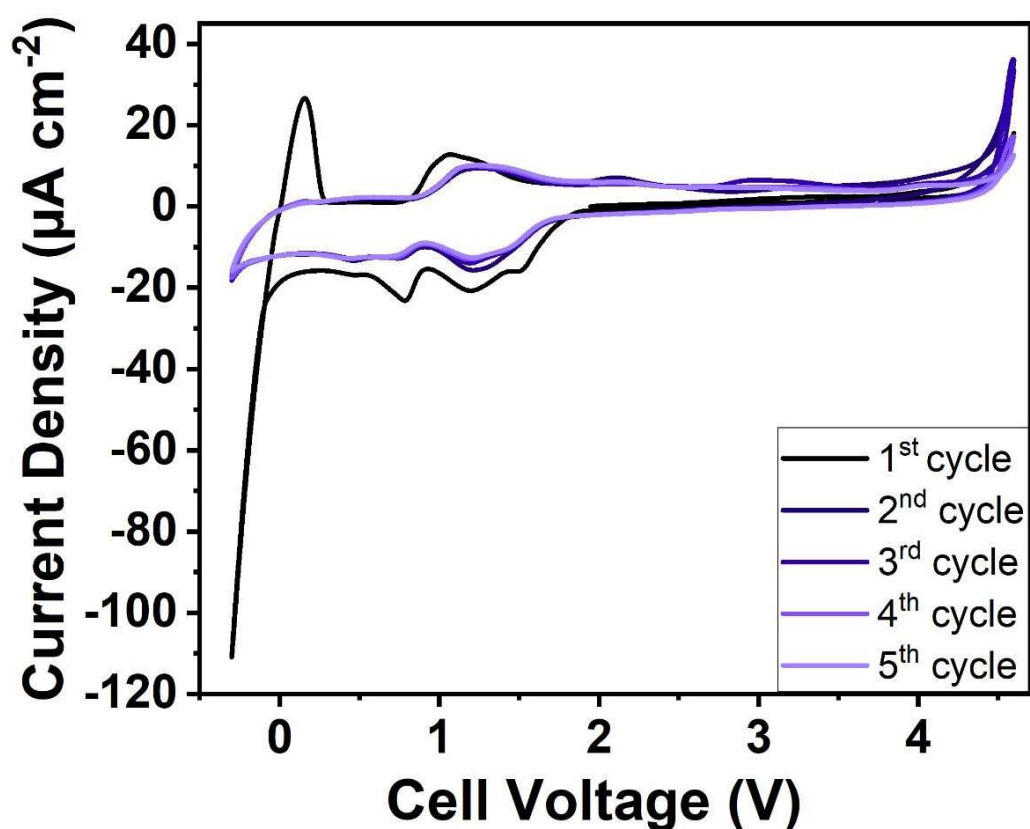
Figure 6-11. Cyclic voltammetry for electrochemical stability determination by using freshly built Li/stainless steel cells between -0.3 V and 4.6V vs. Li^{+}/Li (sweep rate = 1 mV s^{-1}).

To conduct a more in-depth examination of the electrochemical stability, separate cathodic and anodic cyclic voltammetry tests were performed. This should avoid the influence of oxidative degradation in the following reduction process and vice versa. The anodic scan was performed

between OCV and 4.6V with a scan rate of 1 mV s^{-1} for 6 cycles and is presented in **Figure 6-12**. The first scan showed some minor current evolving after 3.9 V, the maximum current density was 2.8 μA cm^{-2}, indicating some reaction upon oxidation, which is much lower than 10 μA cm^{-2} generally considered as lower value for an oxidation process. Upon cycling an increase in oxidation voltage and a decrease in current density was observed. Their values become closer after 3 cycles, which indicates a stabilization of the interface with the electrode.
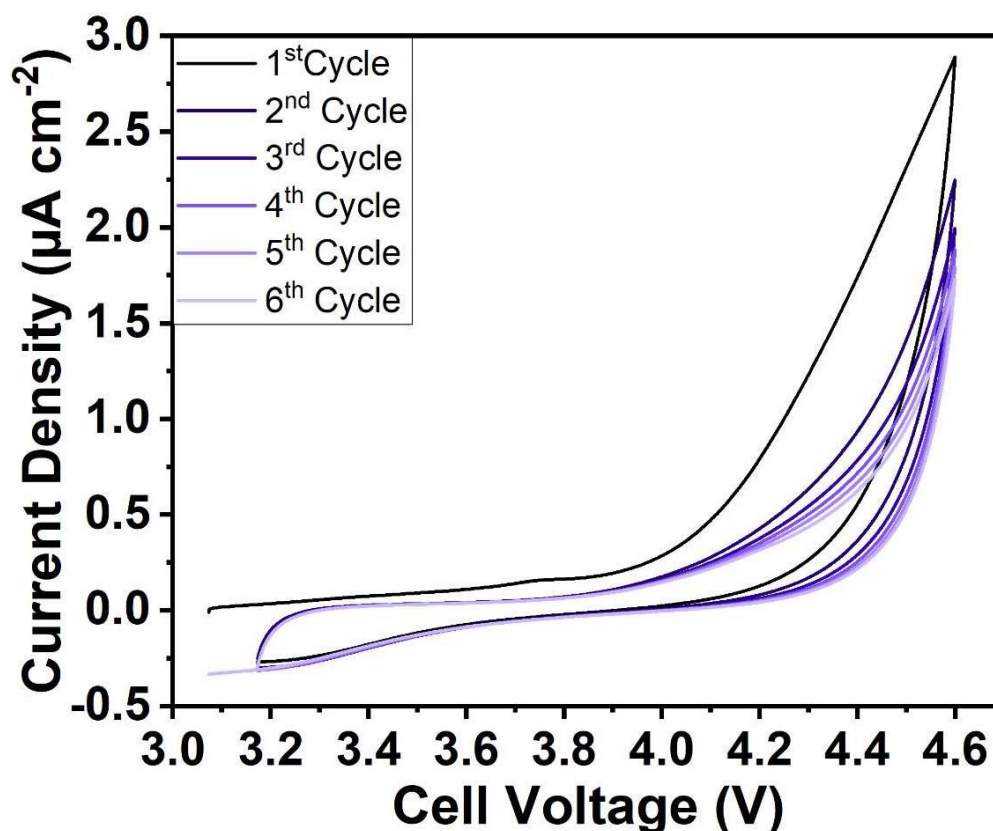
Figure 6-12. Anodic cyclic voltammetry for further investigation of electrochemical stability by using freshly built Li/stainless steel cells between OCV and 4.6V vs. Li$^+$/Li (sweep rate= 1 mV s^{-1}).

Similarly, the cathodic scans were conducted from OCV to 0V with a scan rate of 1 mV s^{-1} and are presented in **Figure 6-13.** We decided to stop at 0V to avoid the lithium plating on the stainless steel and investigate only the potential side reactions. The first cycle showed a strong

reaction between 0 -1.7 V which could be associated with the formation of a passivation layer, and then the intensity of the reaction decreased in the following cycles. Additionally, a pair of small peaks could be observed at 0.7 V and 1.1 V, which appear to be reversible. These tiny peaks could be associated with the presence of oxides on the surface of the working electrode and the intercalation of lithium ions in these metal oxides[156].
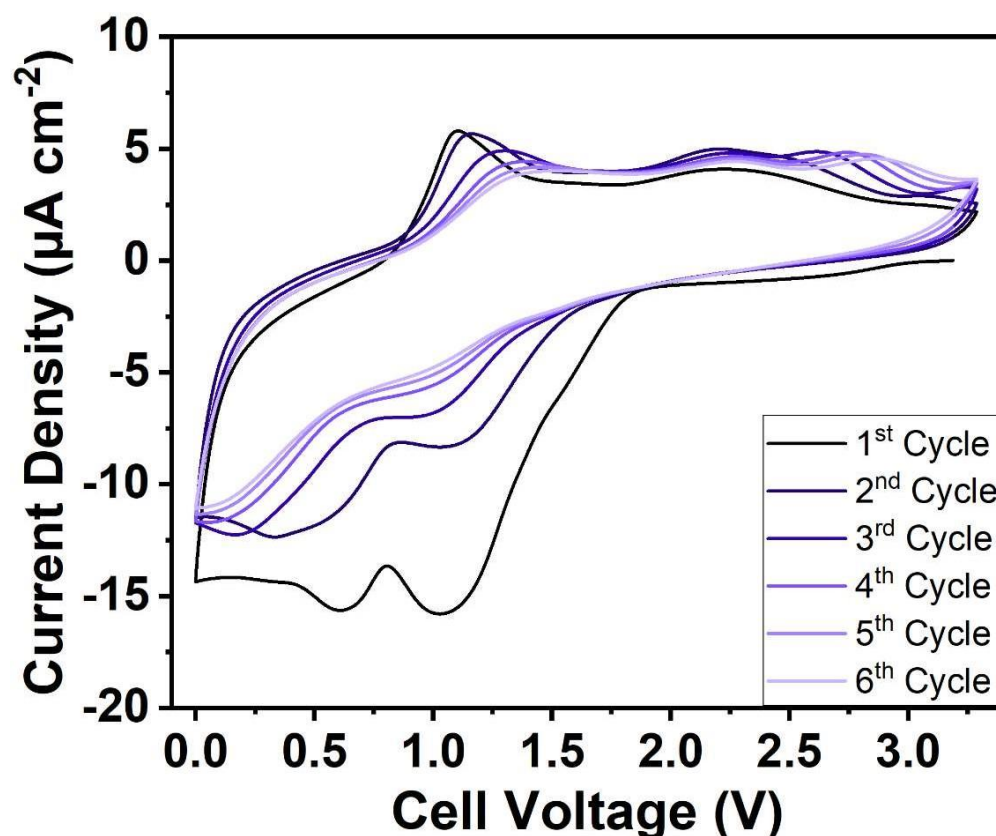
Figure 6-13. Cathodic cyclic voltammetry for further investigation of electrochemical stability by using freshly built Li/stainless steel cells between OCV and 4.6V vs. Li^+/Li (sweep rate= 1 mV s^{-1}).

In the end, the electrochemical stability until 4.6 V, obtained on the LSV and CV measurements, allows for the implementation of the SIPE+PEG electrolyte in batteries using high-energy density cathode material such as Nickel-Manganese-Cobalt electrodes (NMC). The irreversible

observed reactions between 1.7 V and 0.5 V should not affect since the full-cell investigations with NMC are conducted between 3 and 4.2 V.

6.1.4 Lithium Stripping/Plating

To assess the potential use of a new electrolyte material in lithium metal batteries, it is crucial to determine its capacity to facilitate the transfer of lithium cations between electrodes and its ability to inhibit or minimize the formation of lithium dendrites. Therefore, lithium stripping/plating tests were conducted in symmetrical Li/Li cells with the SIPE+PEG electrolyte sandwiched between the two Li electrodes at different current densities. The resulting data are presented in **Figure 6-14** to **Figure 6-14**. First, we conducted this test at very low current densities (**Figure 6-14**). The results revealed a rather low overpotential for the lowest current density (0.002 V for 0.002 mA cm^{-2}) followed by an increase when applying higher current density until 0.037 V for a current density of 0.027 mA cm^{-2}. These overpotential values are higher than the one observed for the same polymer structure swollen with PC[129], this can be explained by the higher ionic conductivity for the PC-doped electrolyte compared to the SIPE+PEG electrolyte. However, it can be noted that the increase in overpotential is lower (one order of magnitude) than the difference in conductivity which is much higher (about two orders of magnitude). Also, important to notice, that the voltage response at all current densities is stable upon cycling with a steady state reach almost immediately, after applying the current, indicating that lithium cations are the only charge carrier and once again, confirming the single-ion conducting behavior of the membrane (**Figure 6-11** insert).
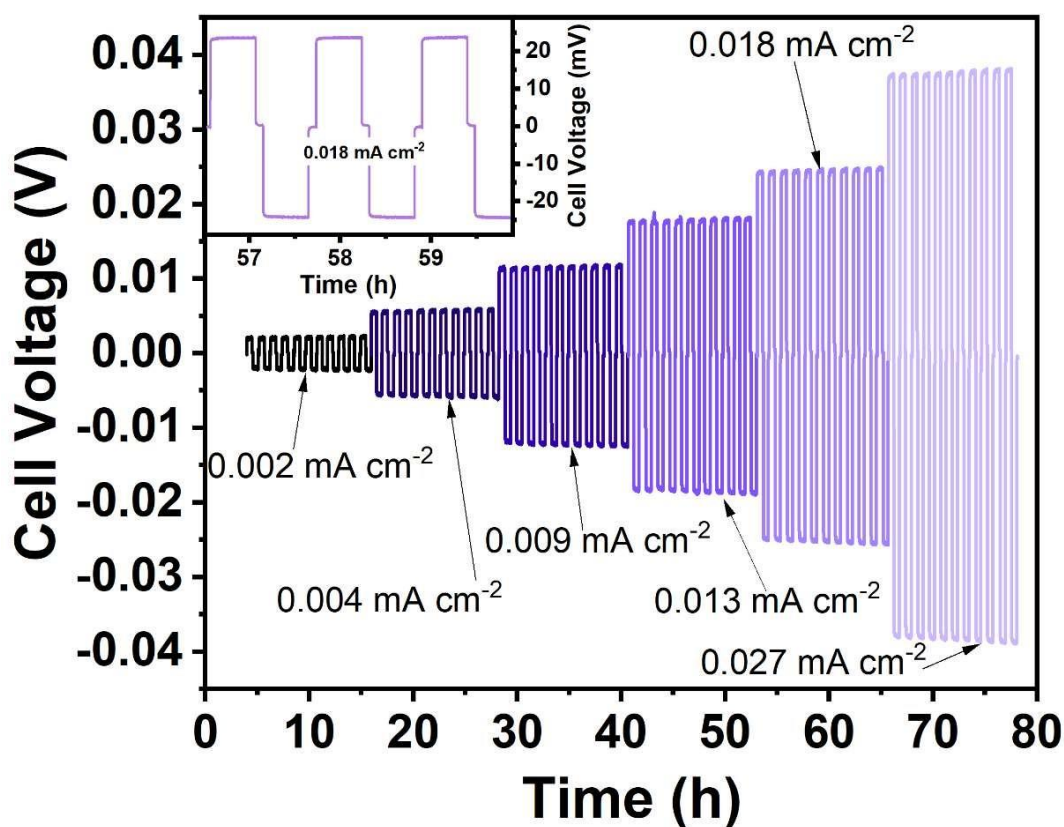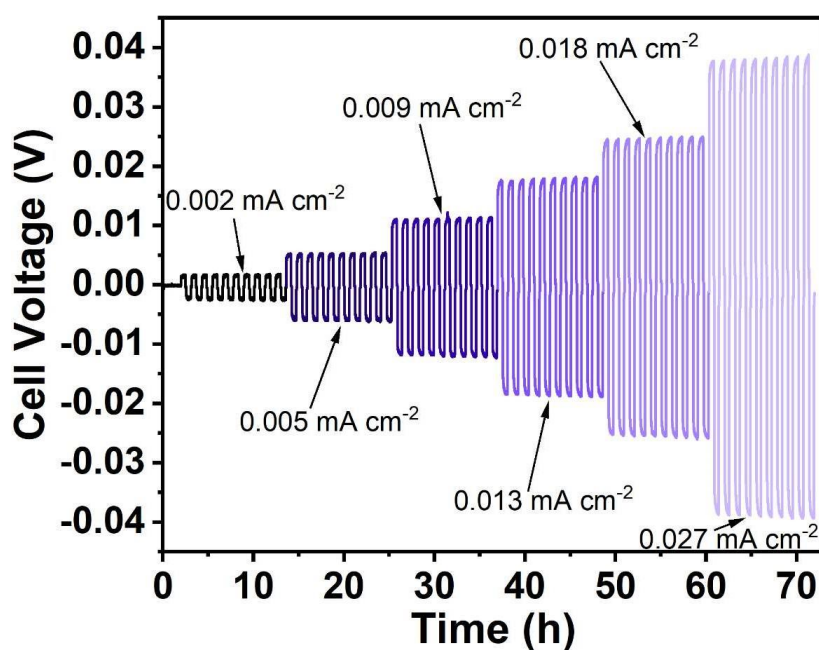
Figure 6-14. Investigation of the stripping/plating behavior of the SIPE+PEG electrolyte in Li/Li symmetrical cells at 40 °C subjected to elevated current 0.002, 0.005, 0.01, 0.015, 0.02, 0.03 mA, *i.e.*, 0.002, 0.004, 0.009, 0.013, 0.017, 0.027 mA cm^{-2}, respectively (Ø=12mm and electrode surface area = 1.131 cm^{-2}).

Further investigation of the behavior was conducted with higher current density (**Figure 6-15**). When applying 0.044 mA cm^{-2}, lithium stripping/plating was still observed but, in this case, the overpotential is increasing during one stripping or one plating step. However, the same potential is reached at the end of each cycle. This last observation tends to indicate that the increase in potential is not due to the decomposition of the electrolyte. The increase in polarization indicates a sluggish charge transfer at the interface, potentially owing to the depletion of Li^{+} in the interphase[157]. Higher current densities were then applied (more than 0.18 mA cm^{-2}) and huge increases in the overpotential were observed (**Figure 6-15**). The increase was so important that the cut-off voltage of 2 V was reached in a few minutes or even seconds for the highest

current density. This is not surprising since these current density values are very close (0.18 mA cm^{-2}) or higher (0.44, 0.66, 0.88 mA cm^{-2}) than the limiting current density measured earlier (0.2 mA cm^{-2}). However, these high voltages do not result in any degradation of the electrolyte, as a similar lithium stripping/plating behavior was observed when reducing the current density back to 0.018 and 0.044 mA cm^{-2}.
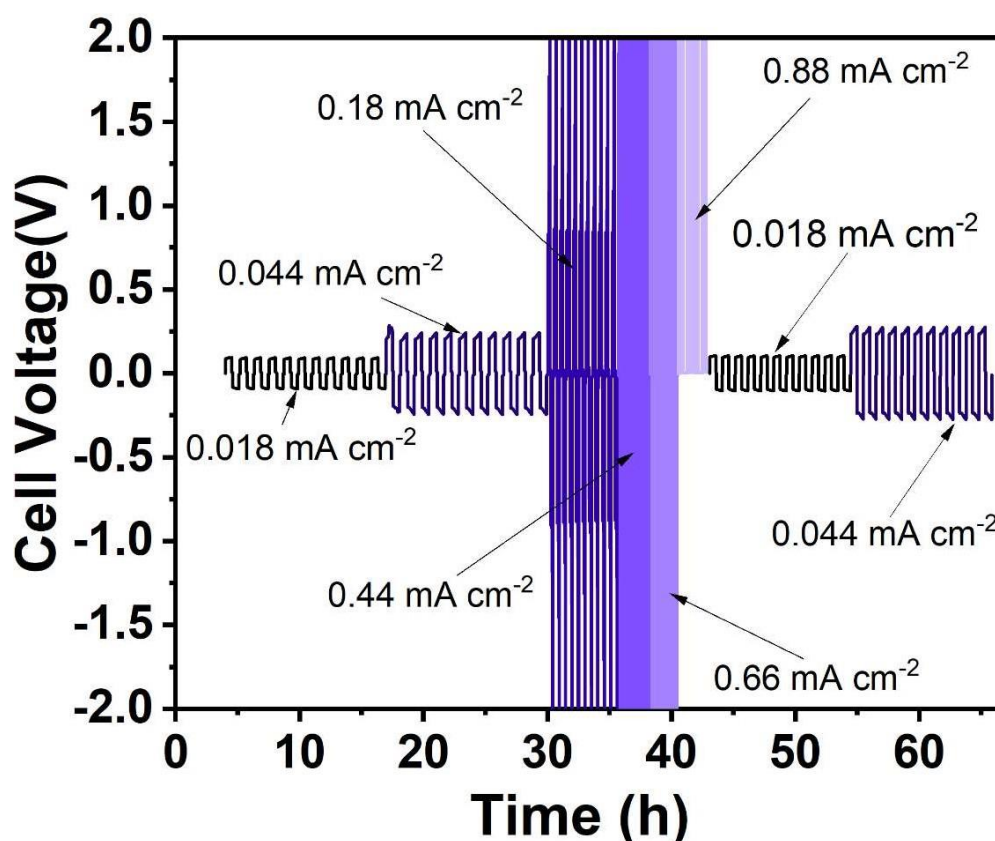
Figure 6-15. Li/Li cell subjected to elevated current 0.02, 0.05, 0.2, 0.5, 0.75, 1 mA, *i.e.*, 0.017, 0.044, 0.18, 0.44, 0.66, 0.88 mA cm^{-2}, respectively (Ø = 12mm and electrode surface area = 1.131 cm^{-2}) followed by lowering the current back to 0.017 and 0.044 mA cm^{-2} for subsequent stripping/plating cycles.

To confirm the non-degradation of the electrolyte, we performed impedance spectroscopy after each full stripping/plating cycle, and the EIS data were fitted with an equivalent circuit composed of two constant phase elements (CPE) (**Figure 6-16**). The resistance of the high-

frequency semi-circle corresponded to the resistance obtained during the ionic conductivity measurement with blocking electrodes, therefore this first semi-circle is related to the resistance of the polymer electrolyte. At low-frequency, the semi-circle is associated with the charge transfer at the electrode $\parallel$ electrolyte interface[158]. We can see that the first semi-circle before and after the high polarizations observed at 0.18, 0.44, 0.66, and 0.88 mA cm^{-2} are perfectly superposing indicating no change in the bulk electrolyte, confirming the non-degradation. Nevertheless, after the high polarization, the interfacial resistance has decreased, which remains unclear to us. The impedance results after decreasing the current back to 0.018 and 0.044 mA cm^{-2} are almost superposing the impedance results before the high polarization, showing that the interfacial resistance decrease was reversible and that overall the electrolyte is not degraded by the polarization at the highest current densities tested here.
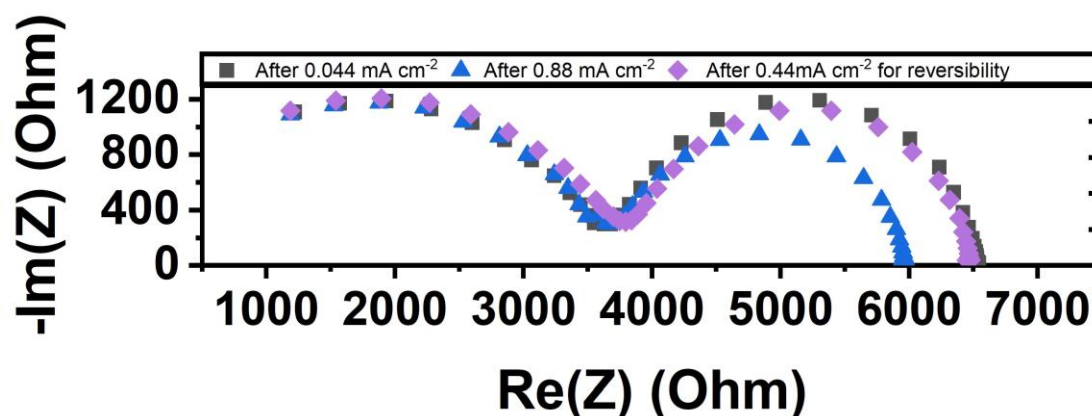
Figure 6-16. Nyquist plots of the EIS data recorded after the last stripping/plating cycles for different current densities.

Post-mortem SEM images were recorded after the cycling at different current densities and compared to the pristine lithium metal foil directly taken from the glovebox (**Figure 6-17**). **Figure 6-17.a** shows the surface of the pristine lithium is flat and homogeneous. A rather smooth and flat lithium surface with no indication of lithium dendrite growth was observed in **Figure 6-17.b** recorded after stripping plating at 0.018 mA cm^{-2} and 0.044 mA cm^{-2} for 10 cycles each (capacity= 0.225 mAh cm^{-2}), and **Figure 6-17.c** recorded after the full

stripping/plating procedure presented in **Figure 6-17** (capacity= 0.675 mAh cm^{-2}). This demonstrates homogeneous lithium deposition throughout cycling, confirming the excellent compatibility of the SIPE+PEG electrolyte with lithium metal.
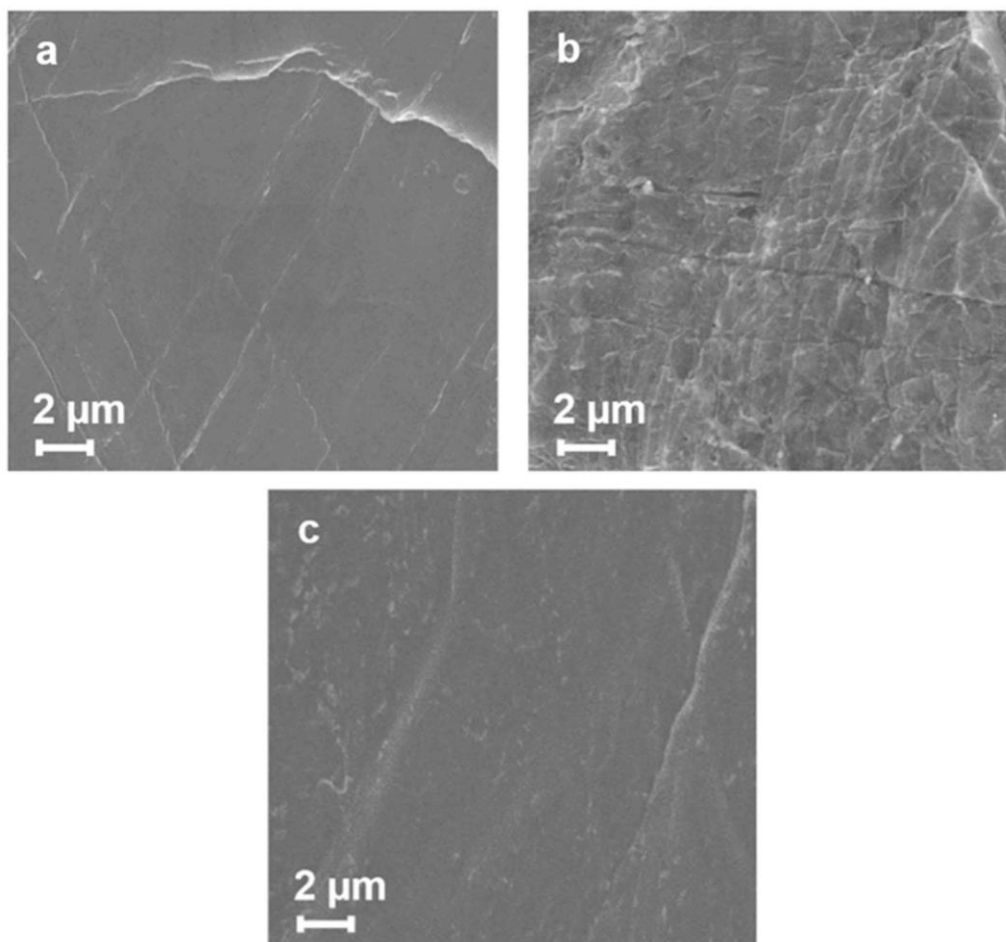
Figure 6-17. Comparative SEM images of the pristine lithium surface (a), the lithium surface after stripping/plating at 0.018 and 0.044 mA cm^{-2} (b) and after lowering the current back to 0.018 and 0.044 mA cm^{-2} (c)

At this stage, as the SIPE+PEG was found to be very stable against lithium metal, we evaluated its long-term behavior by subjecting a symmetrical Li/Li to long-term lithium stripping/plating cycling at 0.018 mA cm^{-2} for more than 2000 h (**Figure 6-18**). A slight increase of the overpotential during this long-term cycling was observed, with stabilization occurring after 1700 hours. This variation is commonly related to the formation and organization of the

electrode‖electrolyte interface during the lithium stripping/plating before reaching a steady state corresponding to the stabilization of the overpotential. The magnifications of the stripping/plating cycles at 510 hours and 1700 hours indicate a stable overvoltage during both the stripping and plating steps. Furthermore, no indication of degradation of the SIPE+PEG electrolyte was observed even after more than 2000 h, once again showing the stability and compatibility of this polymer electrolyte with lithium metal. Unfortunately, after long cycling test, it was not possible to remove properly the lithium metal from the electrolyte and analyze by SEM its surface.
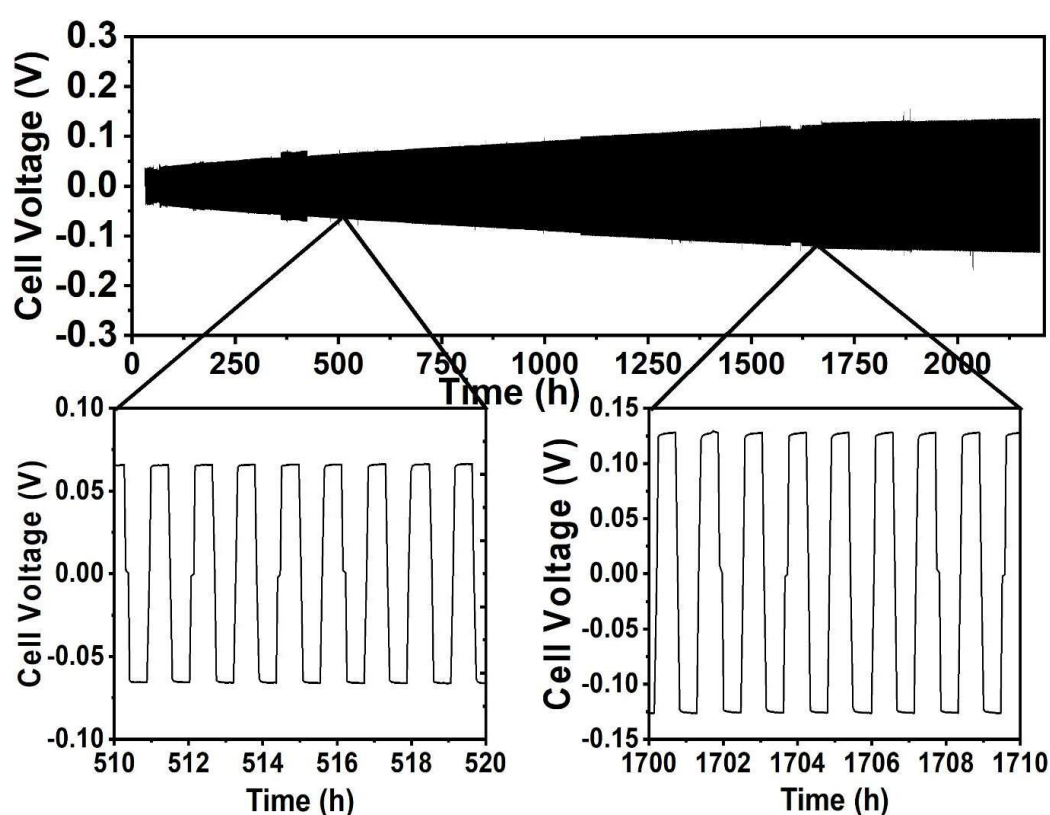
Figure 6-18. Li/Li cell subjected to a constant current of 0.02 mA, *i.e.*, 0.018 mA cm^{-2} for than 2000 h (each cycle is composed of a 30-minute stripping step followed by a 5 minutes rest and a 30-minute plating step and another 5 minutes rest).

To further investigate the compatibility of our SIPE+PEG electrolyte and to see how the temperature impact the interface behavior, we conduct the same stripping/plating test as

previously presented but at 60 °C. The results obtained with the lower current density (**Figure 6-19**) are very similar to the ones obtained at 40 °C. The voltage response at all current densities is stable upon cycling with a steady state reached almost immediately after applying the current, which was already observed at 40°C. It was surprising to see, that despite an increase in conductivity by a factor 4, the overpotentials at all current densities remain very close (**Figure 6-20**). The overpotential vs. current plot are linear in accordance with the Ohm's law:

$$U = R * i$$

The linear fit of these data allows us to calculate $R_{40 °C}$= 1264 Ω and $R_{60 °C}$= 1296 Ω. For 40 °C. The conductivity being higher at 60°C, this value can only correspond to the interfacial resistance. These results show that, within this low range of applied current densities, interfacial resistance is probably the driving factor and temperature does not have a significant impact on this resistance.

Figure 6-19. Investigation of the stripping/plating behavior of the SIPE+PEG electrolyte in Li/Li symmetrical cells at 60 °C subjected to elevated current 0.002, 0.005, 0.01, 0.015, 0.02, 0.03 mA, *i.e.*, 0.002, 0.004, 0.009, 0.013, 0.018, 0.027 mA cm^{-2}, respectively (Ø =12mm and electrode surface area= 1.131 cm^{-2}).
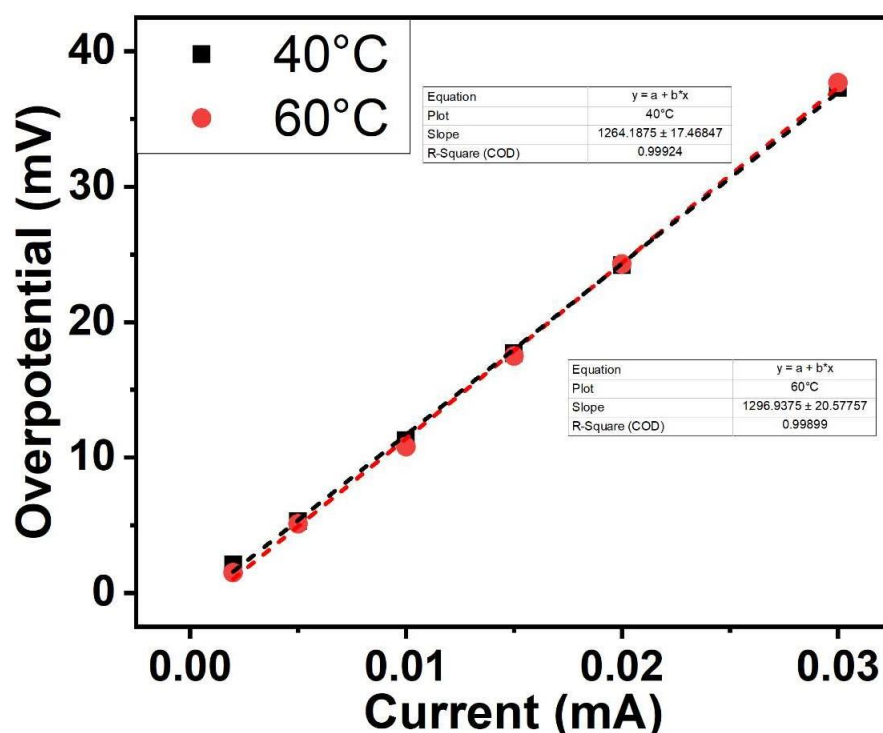
Figure 6-20. Overpotential as a function of current for the stripping-plating at 40 °C and 60 °C and linear fit.

At higher current density (**Figure 6-21**), a big improvement was observed compared to the same test at 40 °C. First, for 0.018 and 0.044 mA cm^{-2} a more rectangular shape was observed, indicating a better and faster charge transfer at the interface[157]. When using 0.18 mA cm^{-2} at 40 °C, the polarization of the cell was extremely fast, and no stripping plating was observed. At 60 °C, on the contrary, a really good stripping/plating was obtained at this current density. It can also be seen that the steady state is not immediately reached meaning the polarization of the cell starts to limit the charge transfer at the interface. At more than 0.44 mA cm^{-2}, huge increases in the overpotential were observed. The increases were so important that the cut-off voltage of 2 V was reached in a few minutes or even seconds meaning no stripping/plating at these current density values. But, as previously observed, this does not result in electrolyte degradation since a good reversibility was observed when lowering the current back to 0.018 and 0.044 mA cm^{-2}.
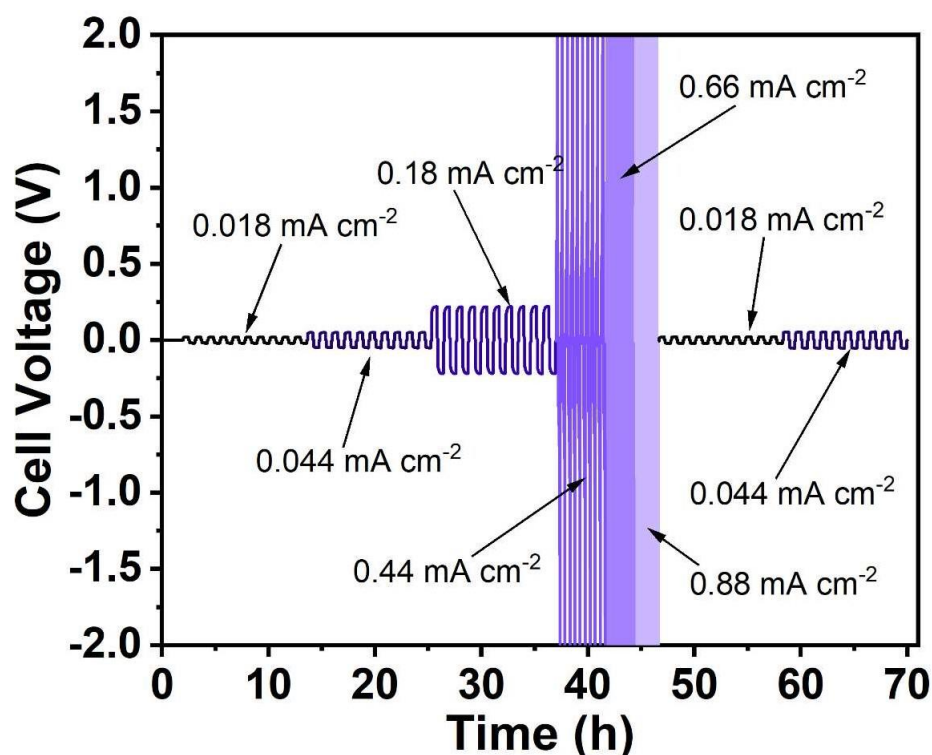
Figure 6-21. Li/Li cell at 60°C subjected to elevated current 0.02, 0.05, 0.2, 0.5, 0.75, 1 mA, *i.e.*, 0.018, 0.044, 0.18, 0.44, 0.66, 0.88 mA cm^{-2}, respectively (Ø = 12mm and electrode surface area = 1.131 cm^{-2}) followed by lowering the current back to 0.018 and 0.044 mA cm^{-2} for subsequent stripping/plating cycles.

Overall, these results at 40 and 60 °C indicate excellent compatibility of the SIPE+PEG with lithium metal and the ability to form a very stable electrode∥electrolyte interface at different current densities. The increase in the temperature from 40 to 60°C allows platting/stripping at higher current density without any SIPE degradation and with a stable interface.

6.1.5 Evaluation of Li∥NMC$_{811}$ Cells

To further investigate the implementation of this polymer electrolyte with a high-energy density cathode, we assembled Li/NMC$_{811}$ cells and subjected them, in the first time, to galvanostatic cycling at 40 °C (**Figure 6-22**). Considering the rather low limiting current density measured

earlier and the electrode mass loading (~1.8 mg cm^{-2}) we decided to cycle the cells only at 0.05C to stay at a rather low current density. The cell exhibited a specific discharge capacity of 127 mAh g^{-1} in the first cycle with an initial Coulombic efficiency of 99% with an average 99.6% Coulombic efficiency for the subsequent cycles. After 40 cycles, a capacity retention of 80% was obtained with no indication of electrolyte degradation, meaning that this fade mostly comes from the cathode material. The rather fast capacity decay for NMC811 is a well-known phenomenon that was already observed at 25 °C. It is assumed that this decrease results from the formation of stable phases upon cycling, leading to an increase in the interfacial resistance[26].
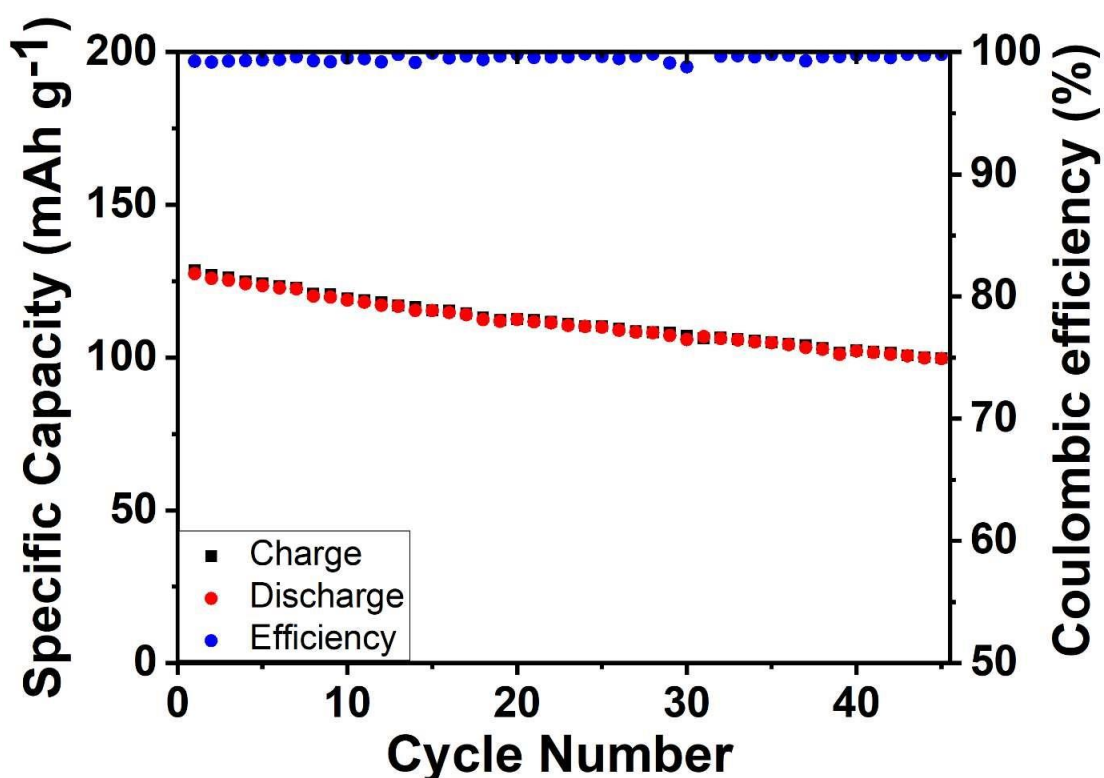
Figure 6-22. Investigation of SIPE+PEG electrolyte in Li/NMC$_{811}$ cells at 40 °C. Charge and discharge capacity and Coulombic efficiency as a function of cycle number.

The voltage profiles at different cycles (**Figure 6-23**) do not show any voltage fluctuation that could indicate dendrites growth or degradation of the SIPE+PEG electrolyte. This tends to confirm a chemically stable electrolyte material toward NMC. Despite the noticeable capacity

loss, all the voltage profiles exhibit a similar shape, indicating a consistent electrochemical process throughout the cycle (**Figure 6-23**). This indicates a general good compatibility of the SIPE+PEG electrolyte with positive and negative electrode materials. Concerning the capacity decay, we assume that this is not (or only to a very small extent) related to the electrolyte degradation. It is known that the decay/aging of the cells is a very complex process and should be connected to many parameters including electrode morphology, quality of the lithium, temperature, pressure on the cell, current density, compatibility between the binder and polymer electrolyte, and so on. We assume this phenomenon is linked to the incomplete de-/lithiation of the active material caused by sluggish kinetics at the lower temperature (40 °C) as well as to the loss of the ionic and electronic percolation.
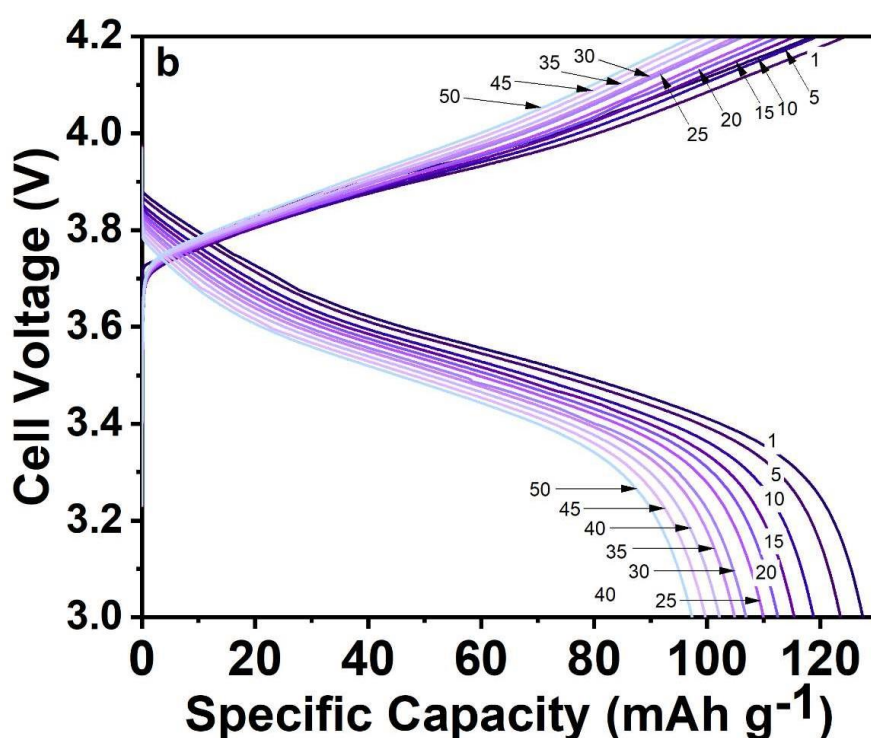
Figure 6-23. Investigation of SIPE+PEG electrolyte in Li/NMC$_{811}$ cells at 40 °C. Voltage profiles for selected cycles, all cycles were conducted at 0.05C with 1C= 190 mA g^{-1} and cut-off voltage set to 3.0 and 4.2 V vs. Li$^+$/Li.

At 60 °C, the Li│SIPE+PEG│NMC811 cell was then subjected to a C rates capability test at 0.05C, 0.1C, 0.2C, 0.5C and 1C (1C not represented here since the specific capacity was 0 mAh g^{-1}) followed by a long-term constant current cycling stability test at 0.05C with (**Figure 6-24**). The cell exhibited a reversible discharge capacity of about 180 mAh g^{-1} during the first cycles at 0.05C with a Coulombic efficiency (CE) of 90%. This low CE indicates that some side reaction occurs during the first cycle. We can suppose the formation of the SEI but also some degradations, i.e. of electrolyte, SIPE+PEG, at the interface with NMC811 at 4.2 V. In the next four cycles at 0.05C, the coulombic efficiency reaches an average value of 95% with a rather high decrease of specific capacity, proving still some side reactions. At 0.1 and 0.2C, a higher coulombic efficiency with a more stable specific capacity was obtained (CE= 98% with C= 140 mAh g^{-1} and CE= 99% with C= 100 mAh g^{-1} respectively), only the first cycle does not exhibit these values of C. This means that during the first cycle, the higher current density induces changes at the interface to support the higher current. With the C rates capability increase a decrease of the capacity was observed (144 mAh g^{-1} at 0.1C, 103 mAh g^{-1} at 0.2C, and 40 mAh g^{-1} at 0.5C). This decline of capacity is due to kinetic and mass transport limitation and increased polarization which leads to incomplete lithiation/delithiation of the active NMC material and also to the more sluggish charge transfer at the interface that we already observed at higher current density during stripping/plating test. At last, the test was carried out at 0.05C again to check if the capacity decline was reversible or not. The 21st cycle yielded a capacity of 138 mAh g^{-1}, which is relatively close to the capacity of the 5th cycle (155 mAh g^{-1}), showing an acceptable reversibility of the capacity decline during the C rates capability test.

At 60 °C, the capacity decay from cycles 1 to 5 was measured to be 88% and 0.91% from cycles 21 to 25. This decay is faster than the one at 40 °C (96%) and is probably related to the rather low thermal stability of NMC$_{811}$ or side reaction with the polymer electrolyte. Indeed, it has been shown that increasing the temperature increases de capacity lost for this cathode material[26].
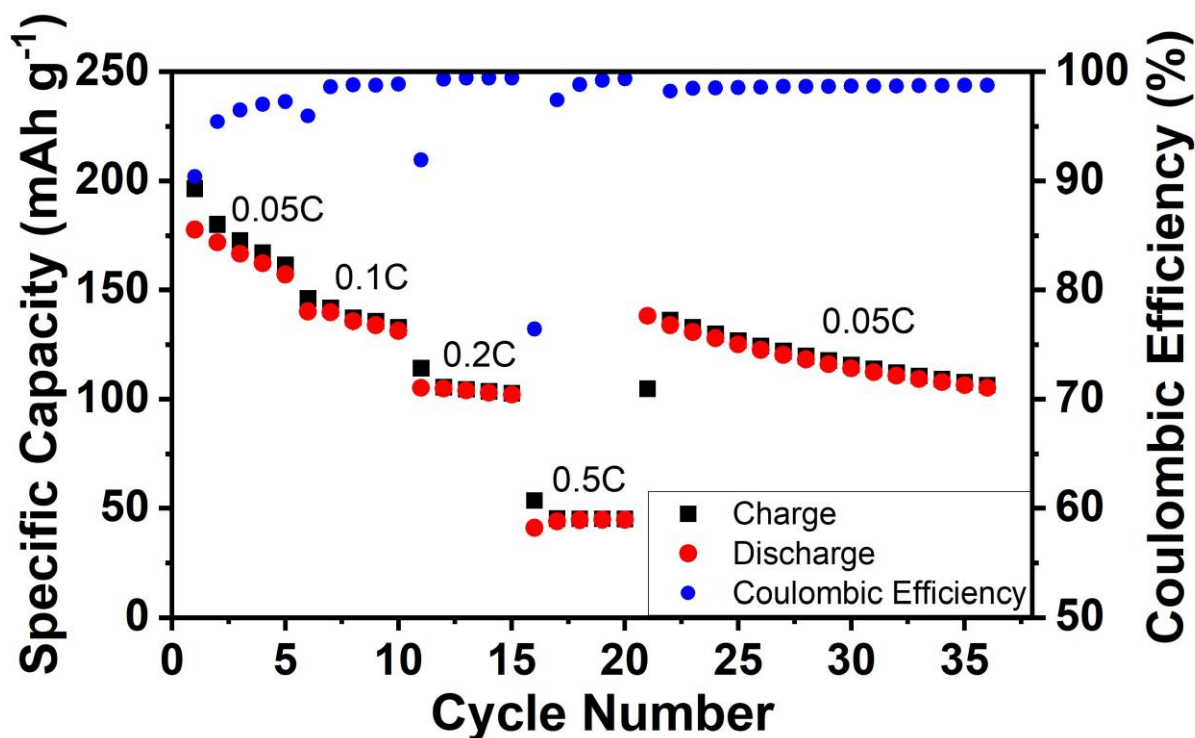
Figure 6-24. Investigation of SIPE+PEG electrolyte in Li/NMC$_{811}$ cells at 60 °C. Charge and discharge capacity and Coulombic efficiency as a function of cycle number.

However, the voltage profiles at different C rates (**Figure 6-25**) do not show any voltage fluctuation that could indicate dendrites growth or degradation of the SIPE+PEG electrolyte, which confirms the good compatibility of the electrolyte material toward NMC, even at 60 °C. The polarization of the cell can be estimated by the dis-/charge hysteresis, i.e., the voltage difference between charge and discharge at the point of 50% capacity. The differences at 0.05C, 0.1C, 0.2C, and 0.5C were 81, 171, 359, and 763 mV respectively. These polarization voltages follow a linear trend with the corresponding current densities (**Figure 6-26**), which suggests the impedance of the cell at 50% of the state of charge (SOC) was stable also at the increased current densities.
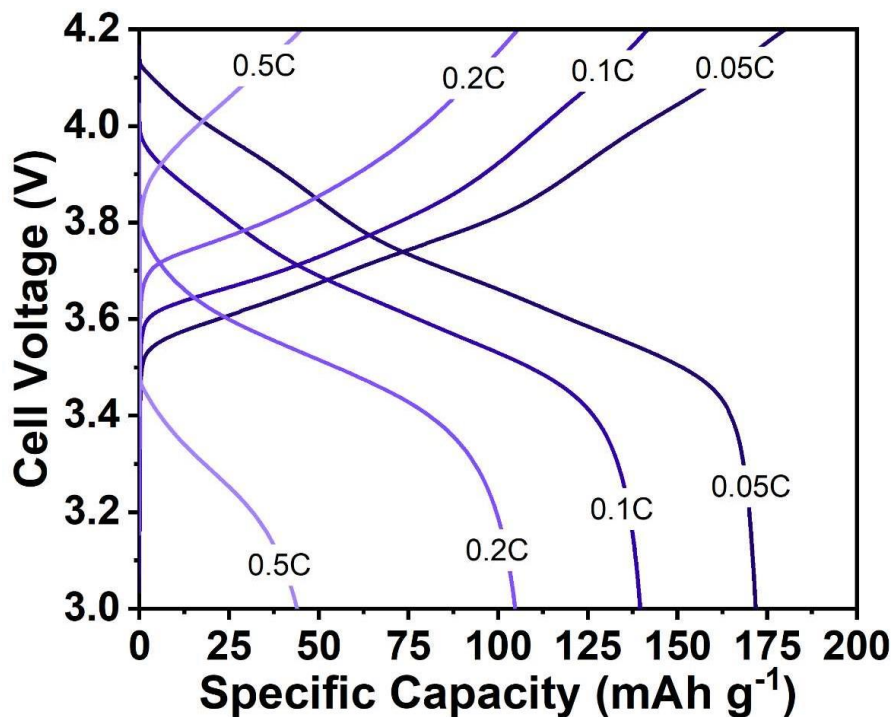
Figure 6-25. Investigation of SIPE+PEG electrolyte in Li/NMC$_{811}$ cells at 60 °C. Voltage profiles for selected cycles during the C rates capability test with cut-off voltage set to 3 and 4.2 V vs. Li$^+$/Li.

Equation	y = a + b*x
Slope	0.00786 ± 4.32694E-
R-Square (COD)	0.99398
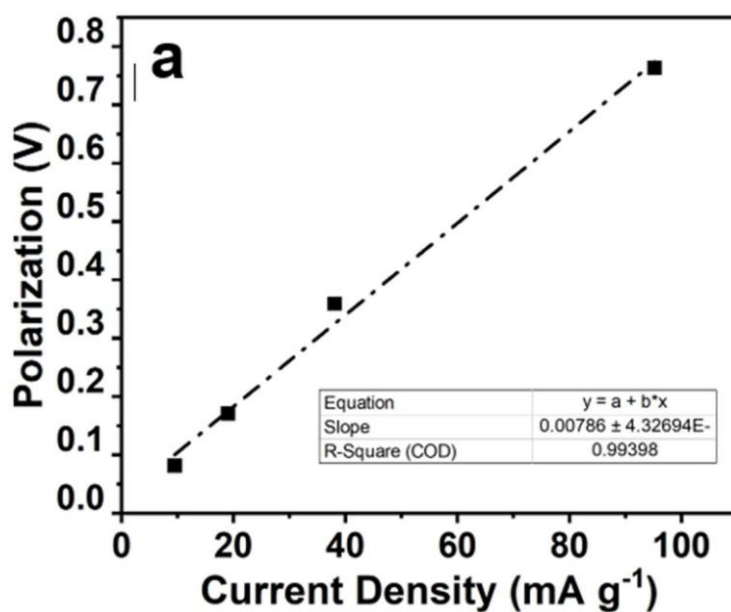
Figure 6-26. (a) Polarization *vs*. current density and (b) Specific capacity *vs*. polarization of Li∥NMC$_{811}$ cell subjected to a C rate test at 60 °C.

The C rate test has fully demonstrated that the Li∥NMC$_{811}$ cell has good capacity retention at different current densities. The capacity loss from increased C rate is rather high, probably due to rather low ionic conductivity and lithium-ion transport, but was also demonstrated to be reversible.

Several works have already been reporting the use of full solid-state polymer electrolytes with NMC$_{811}$ cathodes. But they are all using the usual polymer matrix + lithium salt approach with a polymer matrix based on PEO (133.7 mAh g^{-1} at 40 °C with a capacity retention of 85.7% after 200 cycles at 0.2C) [159], poly(ethylene glycol) dimethylether (PEGDME) (101.4 mAh g^{-1} at 45 °C with a capacity retention of 82% after 200 cycles at 0.1C) [160], poly(diallyldimethylammonium) bis(fluorosulfonyl) imide (PDADMAFSI) (161 mAh g^{-1} at 25 °C with 92% capacity retention after 120 cycles at 0.1 mA cm^{-2}) [161] and poly-oxalate (190.5 mAh g^{-1} at 45 °C with a capacity retention of 82% after 100 cycles at 0.15C) [162]. All these electrolytes exhibit good cyclability with NMC but none are actual single-ion conducting polymers which means they can present the polarization problem presented in the motivation part of this work. On another hand, single-ion polymer electrolytes have shown good results with NMC811 at 40 and 60 °C [163,164,165] but these membranes were all swollen with at least 50% of carbonate solvent. This means that to the best of our knowledge, this is the first work reporting good battery performance at 40 °C and 60 °C with NMC 811 and a solvent-free SIPE.

6.1.6 Conclusions

In this section, we have shown that the already reported partially fluorinated multi-block co-poly (arylene ether sulfone) with lithium perfluorosulfonimide side chains can be blended with low molecular weight poly(ethylene glycol) dimethyl ether instead of volatile organic solvent such as propylene or ethylene carbonate. The film fabrication was found to be relatively easy; the obtained membrane was self-standing and provided sufficient mechanical stability with a

remarkable conductivity of 10^{-5} S cm^{-1} at 45 °C, which is among the highest reported conductivity for a polymer electrolyte containing no volatile molecules. In addition, a good electrochemical stability window until 4.6 V was reported with an excellent electrolyte‖lithium metal compatibility during stripping/plating test at 40 °C and different current densities but also for long-term cycling with a constant current density. These stripping/plating at 60 °C highlighted the good results already obtained at 40°C. Nevertheless, the polymer electrolyte demonstrated at 40°C rather low limiting current density of 0.2 mA cm^{-2}, which hindered fast charging and discharging in a full-cell setup using NMC$_{811}$ as the cathode material. The cycling test at 40°C and a current of 0.05C exhibited a good initial discharge capacity and, despite the rather fast loss of capacity retention, the cell exhibited an excellent Coulombic efficiency upon cycling. The use of higher temperatures allows us to conduct a C rates capability test, which demonstrates a good capacity retention at different current densities but a rather high capacity loss when increasing the current density. These results make this polymer electrolyte an interesting candidate for further development.

Improving the cyclability versus NCM8111 should be the focus for future work for example by working on the mass loading of the electrode or optimizing the electrode and the cycling procedure.

6.2 Solvent-Free Hybrid Solid-State Single-Ion Conducting Polymer Electrolyte

To address the challenge presented by lithium metal anodes, researchers have preferred solid-state electrolytes as the material of choice. However, neither the solid polymer electrolytes (SPEs) nor the solid ceramic electrolytes (SCEs) have been successful for commercial implementation. To combine the advantages of each while reducing their drawbacks, hybrid electrolytes have been a new promising approach.

This technique has already largely been used with the common polymer electrolyte using a polymer matrix and a lithium salt. For example with poly(ethylene oxide) (PEO)[166,167,168,169], poly(vinylidene fluoride-hexa-fluoropropylene) (PVDF-HFP)[170], PEO/PVDF-HFP[171], PEO/ Poly(methyl methacrylate) (PMMA)[172], polyacrylonitrile (PAN)[173], poly(vinylidene fluoride) (PVDF)[174], poly(vinyl carbonate) (PVCA)[175] or poly(propylene carbonate) (PPC)[176]. However, the number of studies on hybrid electrolytes containing single-ion conducting polymer is very limited[177,178,179,180]. These studies show that the addition of inorganic filler has a beneficial effect on the electrochemical stability window, the stripping/plating cyclability, and the cycling stability of the full-cells. They also show that generally, the addition of particles increases the ionic conductivity but the trend is not as obvious as for the other electrochemical properties since a high dependence on temperature and filler content is reported. However, none of these studies investigate the hybrid electrolyte containing single-ion conducting polymer with NMC materials and most of them are using organic solvents as plasticizers. Moreover, to the best of our knowledge, no studies about the multiblock copolymer in hybrid electrolytes have been published yet.

Therefore, this section investigated the combination of the previously studied blend and different amounts of NASICON-type LATP particles ($Li_{1+x}Al_xTi_{2-x}(PO_4)_3$) to form HEs.

6.2.1 Membrane Preparation and Thermal Characterization

Three Solvent-Free Hybrid SIPE were prepared starting from 50/50 in weight SIPE/PEG at which 20, 30 and 40 % of LATP was added.
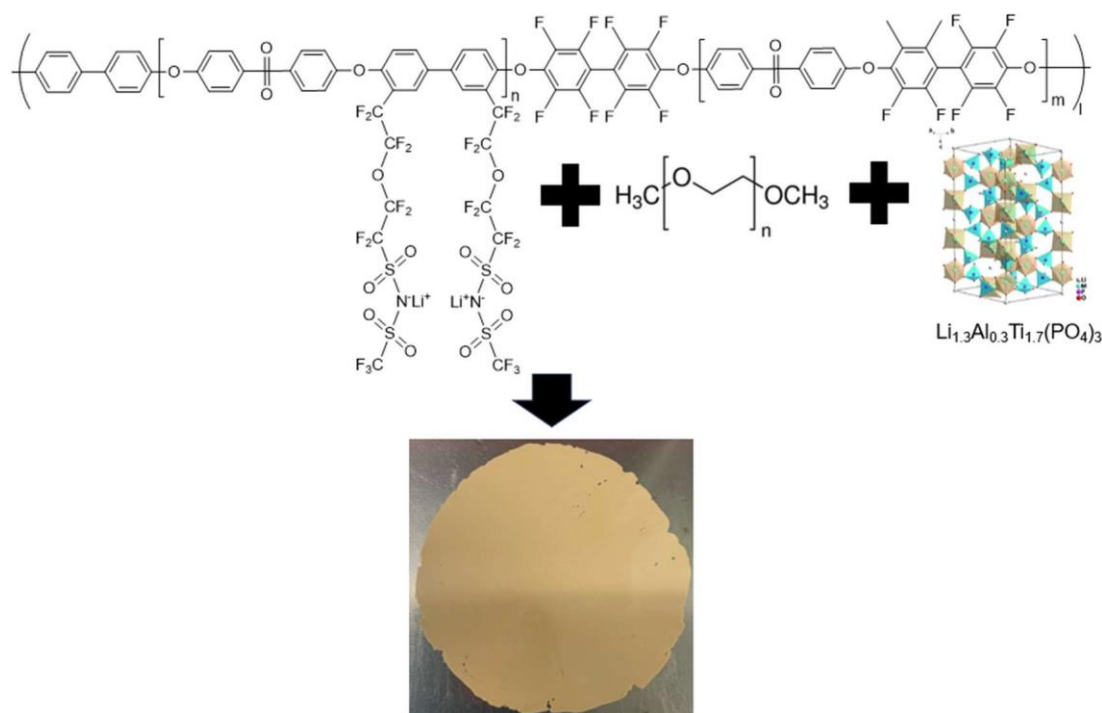
Figure 6-27. Molecular structure of the single-ion conducting polymer and the preparation of the hybrid solid-state electrolyte.

After the hot-pressing process of the SIPE-HE blend at 60 °C and 50 bar, a slightly colored and non-translucent membrane was obtained with a thickness of about 50 µm (**Figure 6-27**). The first consequence of LATP particle addition is to improve mechanical stability compared to the SIPE membrane when reasonably stretched. This test is qualitative, but the observations appear obvious. Another aspect is that the SIPE-HE membranes are less sticky than the SIPE membranes making them much easier to manipulate but also meaning that the membrane is more "rigid" than SIPE+PEG alone. We find that the composite membranes are homogeneous after preparation with an homogeneous dispersion of LATP particles. Indeed, as seen in the SEM images of the three membrane surfaces (**Figure 6-28**) no aggregation of LATP was

observable and the particles appear to have a rather homogeneous size and repartition in the membrane, which should ensure homogeneous conductivity and lithium transport along the electrolyte in a battery application. The cross-section allows for the same conclusion in the thickness of the membrane and shows that no sedimentation happened during membrane preparation.
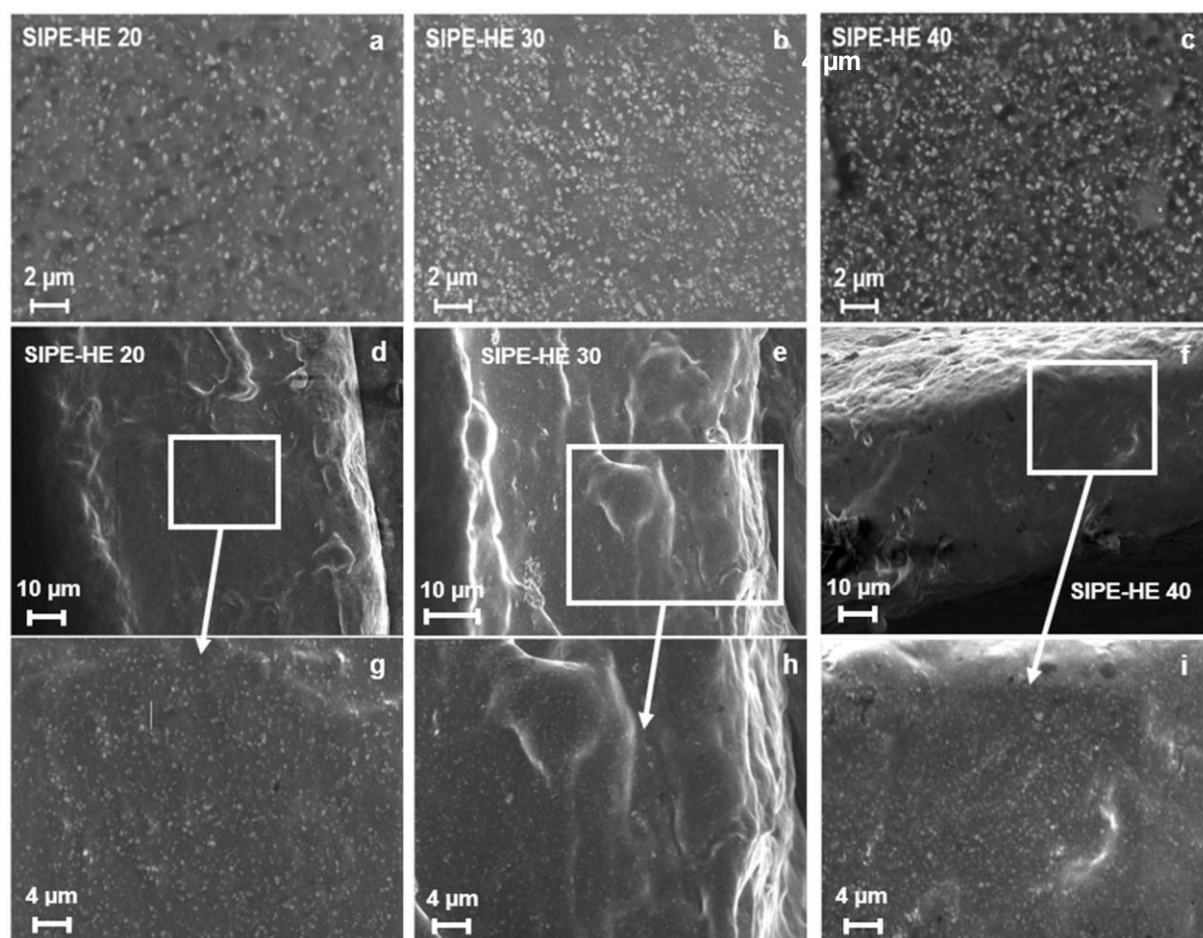
Figure 6-28. SEM images of the different SIPE-HE after membrane preparation. (a), (b), (c) surface of the hybrid electrolyte; (d), (e), (f), (g), (h), (i) cross-section and zoom from the hybrid electrolytes.

The thermal properties of the partially fluorinated multi-block co-poly (arylene ether sulfone) with lithium perfluorosulfonimide side chains were already reported elsewhere[129]. We also reported the thermal properties of the SIPE in the previous chapter. From the TGA

measurements (**Figure 6-29**), all the SIPE-HE (20, 30, 40) show a stability higher than 200 °C followed by a linear weight loss due to the degradation of PEG contained in the membrane. The different percentages of mass loss observable are due to the increase in LATP weight percent in the membrane that logically reduced the PEG weight percentage. It can be observed that the weight loss of PEG is faster for SIPE-HE as compared to the SIPE-PEG, which could be due to the impurities that may be present at the surface of the ceramic particles (e.g., the precursor of the LATP synthesis) and may catalyze the decomposition of the polymer chain, in this case of the PEG[166]. The second weight loss starting around 360 °C corresponds to the degradation of the single-ion conducting polymer, in accordance with previous results. Overall, the addition of LATP particles does not affect the degradation temperature of the electrolyte.
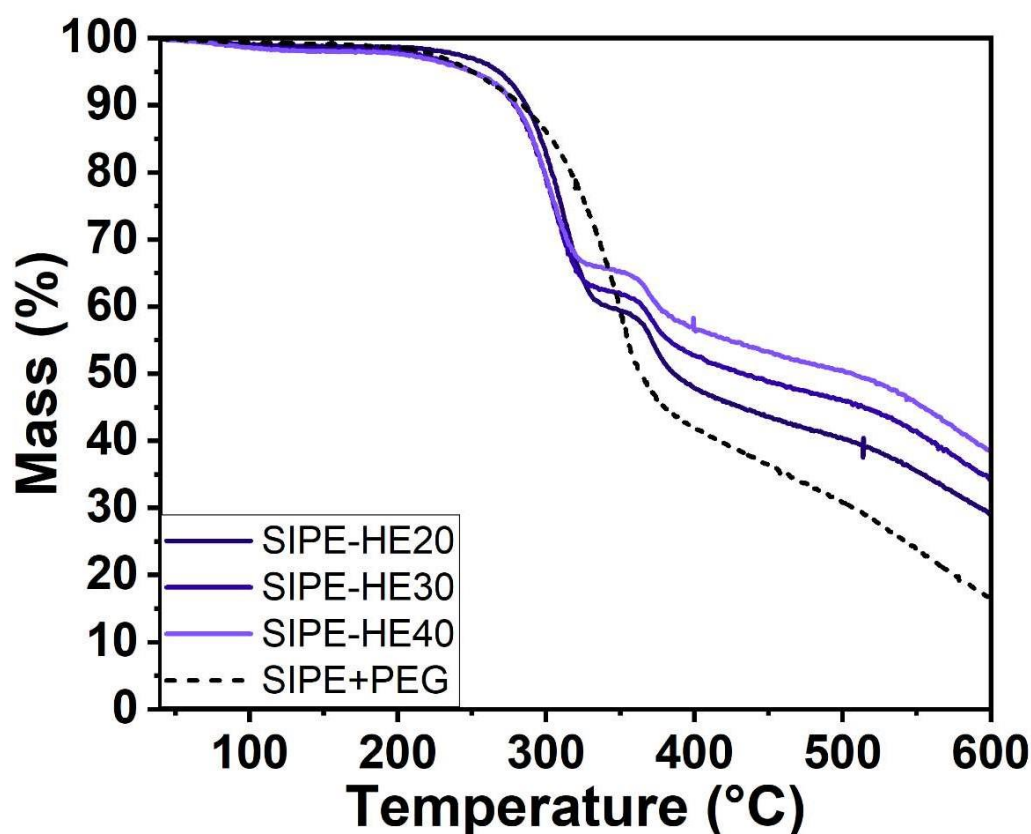
Figure 6-29. TGA curve of the SIPE-HE compared to the TGA curves of SIPE+PEG.

The addition of inorganic particles in PEO-based polymer electrolytes is known to typically decrease the T_g of the membrane, as these particles reduce the crystallinity of the polymer matrix[181]. In our work, an opposite behavior was observed with the addition of LATP particles tending to increase the T_g from -35 °C for SIPE-HE20 to -20 °C for SIPE-HE40 (**Figure 6-30**). This results indicate a strong interaction between the polymer blend and the inorganic particles.
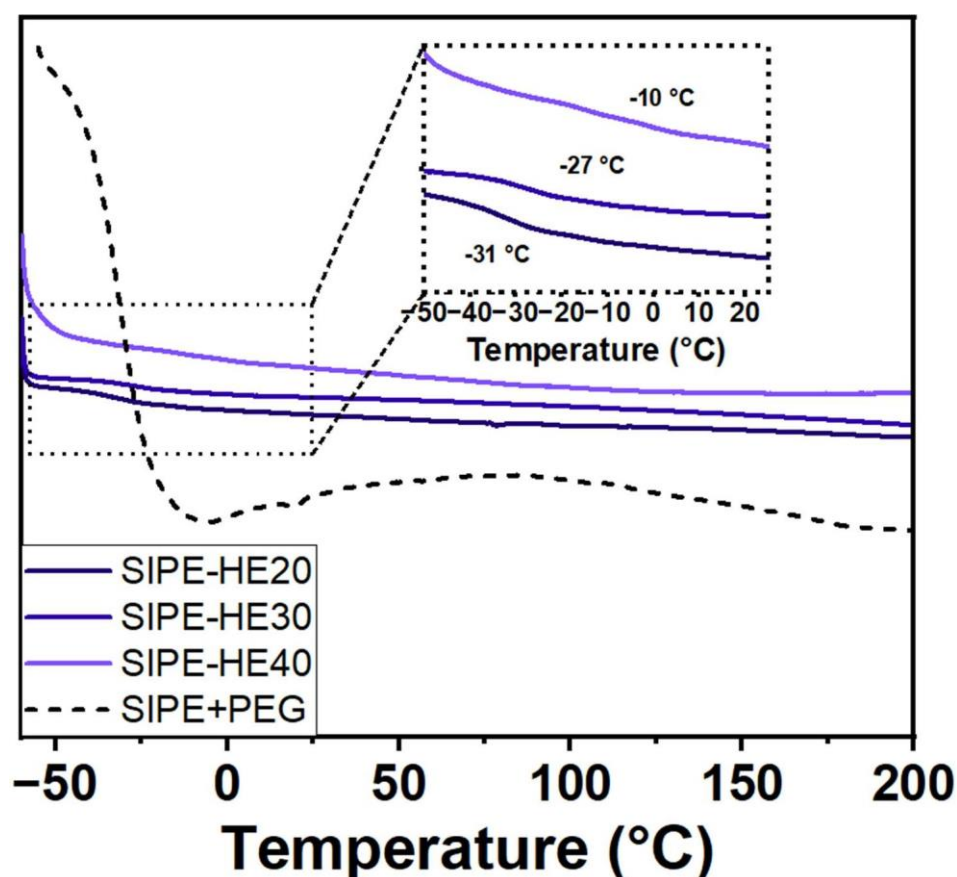
Figure 6-30. DSC diagrams of the SIPE-HE and SIPE after hot-pressing.

6.2.2 Electrochemical Properties

The ionic conductivity (**Figure 6-31**) was determined in a temperature range from 20 °C to 90 °C and the conductivities of the hybrid electrolyte at 40 °C for SIPE-HE20, SIPE-HE30 are 1.86×10^{-6} S cm^{-1}, 3.9×10^{-6} S cm^{-1}, for respectively, which are lower than of SIPE-PEG (6.6×10^{-6} S cm^{-1}). The conductivity of SIPE-HE40 at 40°C is 8.4×10^{-6} S cm^{-1} which is slightly

higher than the one of SIPE+PEG. In the SIPE+PEG the transport occurs through the domains formed by the ionic block and the PEG whereas in the hybrid electrolyte, different ionic conduction pathways can be supposed: i) through the domain formed by the ionophilic block of the polymer and PEG, ii) though the polymer-filler interfaces, iii) through the fillers particles [181]. However, the decrease in conductivity in the case of SIPE-HE20 and SIPE-HE30 as compared with SIPE-PEG proves that the presence of LATP affects negatively the conductivity of the host polymer. In the SIPE+PEG the ionophilic and ionophobic domains are phase separated and in the previous publication it was shown that the sizes of these domains are about 20-40 nm [129]. The size of LATP particles is about 300 nm, meaning that the inorganic filler can block the ionic domains and therefore reduce the conductivity compared to SIPE+PEG, by increasing the tortuosity.

On the other hand, the conductivity of the hybrid electrolyte increases with the filler content to reach more or less the same conductivity as SIPE+PEG with SIPE-HE40. For polymers, the conductivity is dependent on chain mobility, and we showed previously that the Tg values measured also constantly increase with the increase of LATP content. This means that the mobility of the polymer chains in the ionophilic domains decreases while the LATP content increases allthough an increase in ionic conductivity was observed. Considering the three pathways presented earlier, we therefore assume that the conductivity through the polymer-filler interface and the conductivity through the filler particles are predominant over the conductivity through the hydrophilic domains when increasing the LATP content beyond certain concentration threshold. Nonetheless, these conductivity values are good considering that no organic solvent plasticizer was added and, for SIPE-HE40, even almost achieved 10^{-5} S cm^{-1} at 40°C.
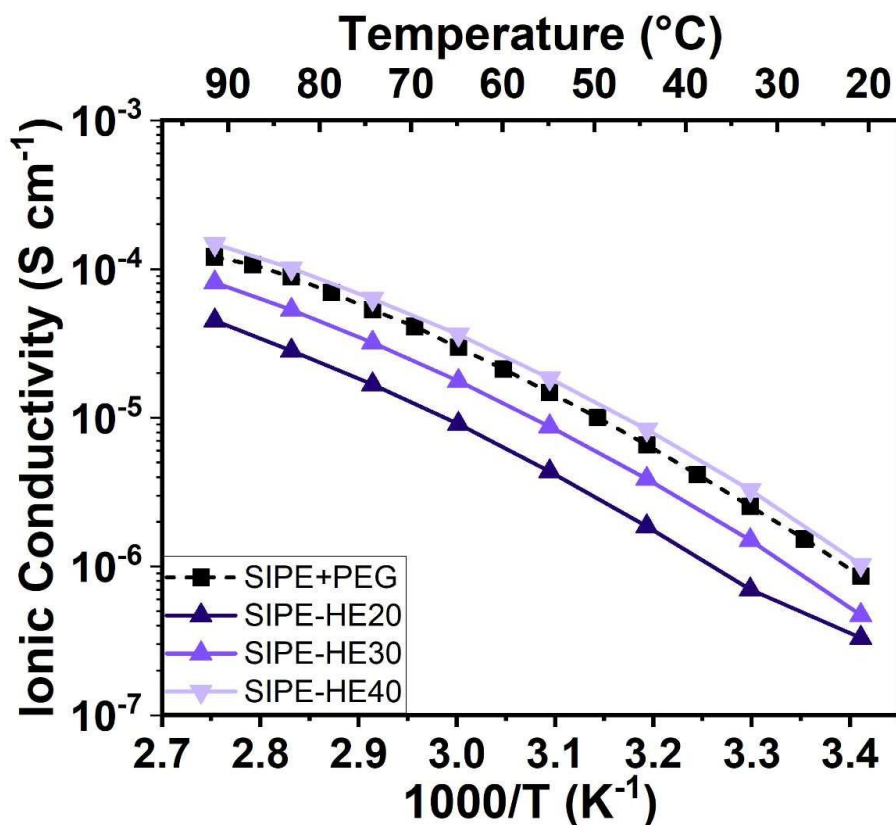
Figure 6-31. Conductivity, as a function of temperature, of the SIPE-HE electrolyte compared to the conductivity of the SIPE+PEG electrolyte

To further investigate the transport properties of this hybrid electrolyte, the limiting current density and transference number were measured at 40 °C. The Bruce and Vincent potentiostatic polarization method was used for the determination of t^+ and values of 0.89, 0.88, and 0.91 were obtained for respectively SIPE-HE20, SIPE-HE30, and SIPE-HE40 (**Figure 6-32**). They are lower than the 0.99 measured for the SIPE and lower than the theoretical $t^+=1$ for single-ion conducting polymer. The current measured in **Figure 6-32.a** went through a quick drop at the very beginning of the polarization with stabilization at a constant current after about 1000 minutes. The impedance spectra before and after 1400 minutes of polarization reveal that the first semi-circle, assigned to the resistance of the bulk electrolyte and therefore the ionic conductivity, are almost identical, indicating that the electrolyte is stable during the polarization. On another hand, the second semi-circle is assigned to the SIPE-HE∥lithium

interfacial resistance and this interfacial resistance shows an increase after polarization. This is due to side reactions between LATP and lithium metal which results in change in the oxidation state of the LATP compounds and eventually formation of mixed conducting interphase which results in a more resistive interface[182]. The modification of the oxidation state can also be follow by the release of ionic species which could explain the t^+ values lower than 1.

R_0 (Ohm)	R_{ss} (Ohm)	I_0 (mA)	I_{ss} (mA)	t^+
3826	4358	0.00245	0.00189	0.88
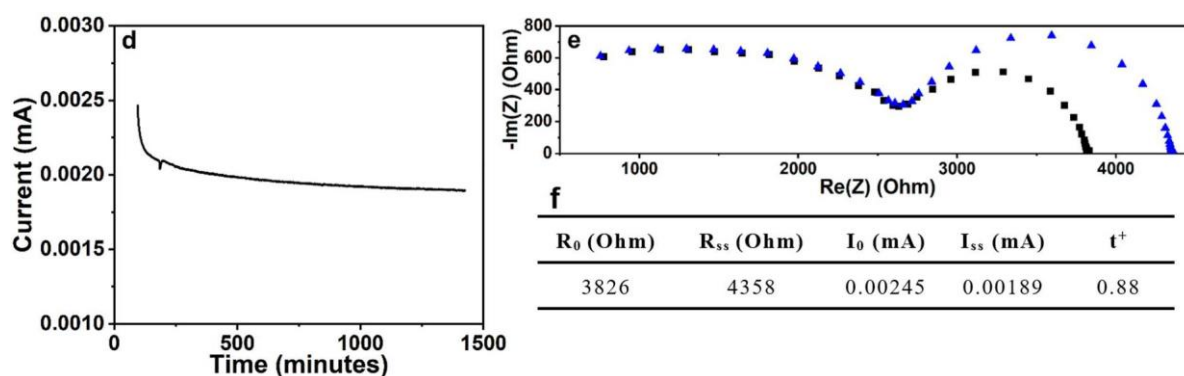
Figure 6-32. Determination of the transference Number of SIPE-HE30 by Bruce and Vincent potentiostatic method. a) Chronoamperometry data obtained when applying a constant voltage of 10 mV to a symmetrical lithium/lithium cell containing the SIPE as electrolyte. b) Impedance measurement before (black) and after (blue) the chronoamperometry measurement. c) Values used in the Bruce and Vincent equation to determine the transference number. (Figures for SIPE-HE20 and 40 can be found in the Appendix).

The limiting current densities are shown in **Figure 6-33**, with values of 0.035, 0.041, and 0.058 mA cm^{-2} for SIPE-HE20, SIPE-HE30, and SIPE-HE40, respectively. These results follow the same trend observed in the ionic conductivity but are almost one order of magnitude lower than the previous 0.2 mA cm^{-2} measured for SIPE+PEG. For SIPE-HE20 and SIPE-HE30, it can be explained by a lower ionic conductivity since the two properties are linked. But SIPE-HE40 also exhibited a lower limiting current density even with a slightly higher ionic conductivity than SIPE+PEG. Therefore, these lower limiting current densities mainly result from the instability of LATP with lithium metal as already reported in the literature[183], but we should also take into account that the SIPE-HE are more "rigid" and therefore suppose that the

lithium‖SIPE-HE interfaces are not as good as for SIPE+PEG. These low values will reduce the accessible C rates for this electrolyte in full-cell tests.
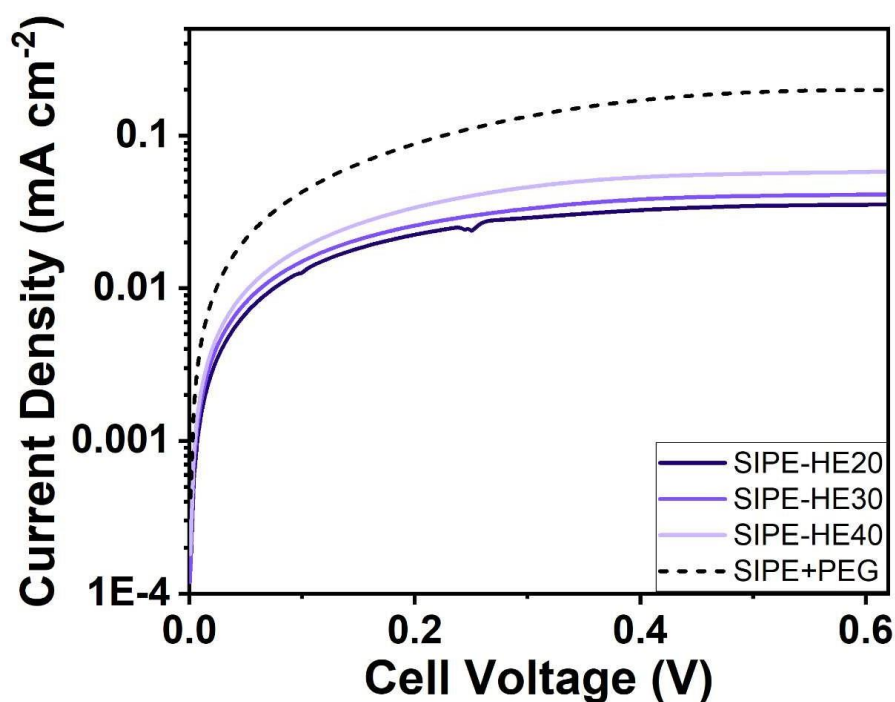
Figure 6-33. Determination of the limiting current density of the SIPE-HE by linear sweep voltammetry at 40 °C (sweep rate = 0.01 mV s^{-1}).

The determination of the electrochemical stability window of the three hybrid electrolytes by linear sweep voltammetry is presented in **Figure 6-34**. For the three SIPE-HE, decomposition can be observed on the cathodic sweep (between OCV and -0.5 V) starting around 2.5 V and particularly around 1.5 V. This corresponds to the lower potential value of the electrochemical stability window reported in the literature for LATP [184]. A small contribution from the remaining solvent from the casting process was previously observed for SIPE, but it is negligible here compared to the reductive degradation of LATP. Surprisingly, no sharp decrease of the current density was observed at 0 V for SIPE-HE20 and SIPE-HE40 compared to the results for SIPE+PEG. However, a decrease was still observed and could correspond to lithium plating. The characteristic sharp decrease is present for SIPE-HE30 indicating lithium plating on the stainless steel for this material. We assume this non-obvious lithium plating indication for SIPE-

HE20 and SIPE-HE40 is due to the degradation of the LATP. The amount of lithium that should theoretically be plated during one cycle is very low and the lithium may instantly react with LATP and passivate the stainless-steel electrode. During the anodic sweep (from OCV to 6V) no particular oxidative peak was observed until about 5,2 V for the three hybrid electrolytes (value at which 10 μA cm^{-2} was reached). This sharp increase is assigned to the oxidative degradation of the bulk electrolyte. It corresponds to a higher electrochemical stability window compared to the SIPE+PEG without LATP particles and the previously reported single-ion conducting multiblock copolymer doped with propylene carbonate[130]. This high stability value versus oxidation allows for the use of these hybrid electrolytes with high-voltage cathode materials such as Nickel-Manganese-Cobalt electrodes (NMC). Usually, the cut-off voltage of these materials during discharge is 3 V which means that the reductive degradation observed during LSV measurement will not be reached and therefore these hybrid electrolytes are a potential candidate for further battery investigation.
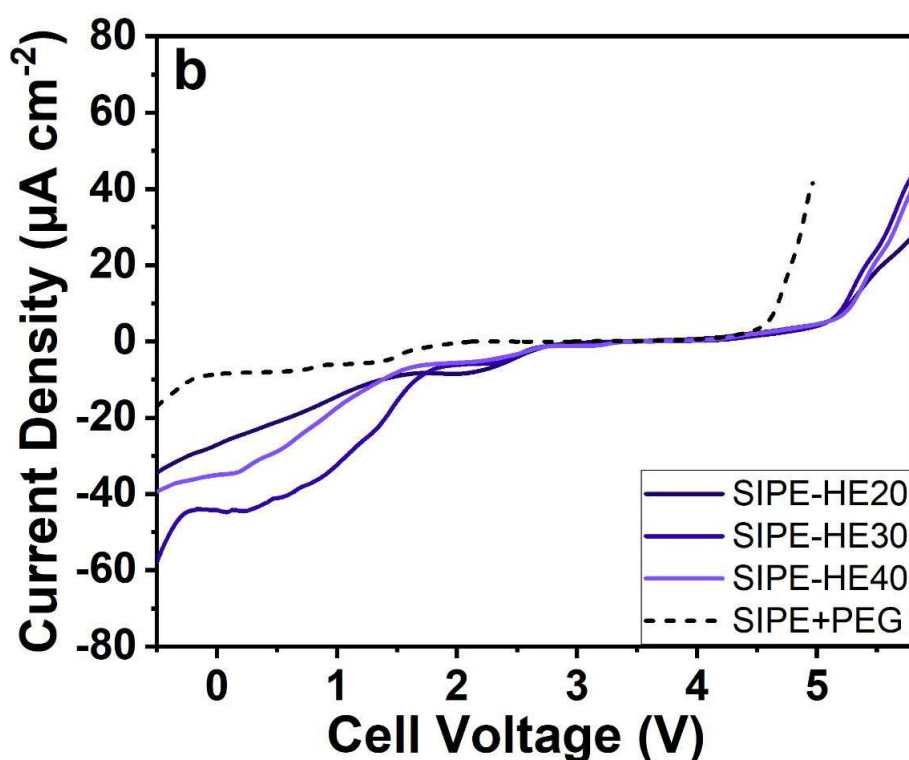
Figure 6-34. Determination of the electrochemical stability window of SIPE-HE by linear sweep voltammetry at 40 °C using Li/stainless steel cells (sweep rate = 1 mV s^{-1}).

A more in-depth examination of the electrochemical stability was conducted by performing separate cathodic and anodic cyclic voltammetry tests. This helps to avoid the influence of oxidative degradation in the following reduction process and vice versa. The anodic scan was performed between OCV and 5 V with a scan rate of 1 mV s^{-1} for 6 cycles and is presented in **Figure 6-35**. For the three-hybrid electrolyte, the first scan showed some minor current evolving between 3.8 and 5 V, indicating some side reaction upon oxidation. Nevertheless, the current density never exceeds the commonly used value to determine the anodic stability (10 μA cm^{-2}). The following cycles showed a much more stable behavior with the intensity of the current decreasing upon cycling, which indicates a stabilization of the electrode/electrolyte interface. All three electrolytes exhibited a similar behavior with excellent stability until 5 V which allows for the use of high energy density cathode material.
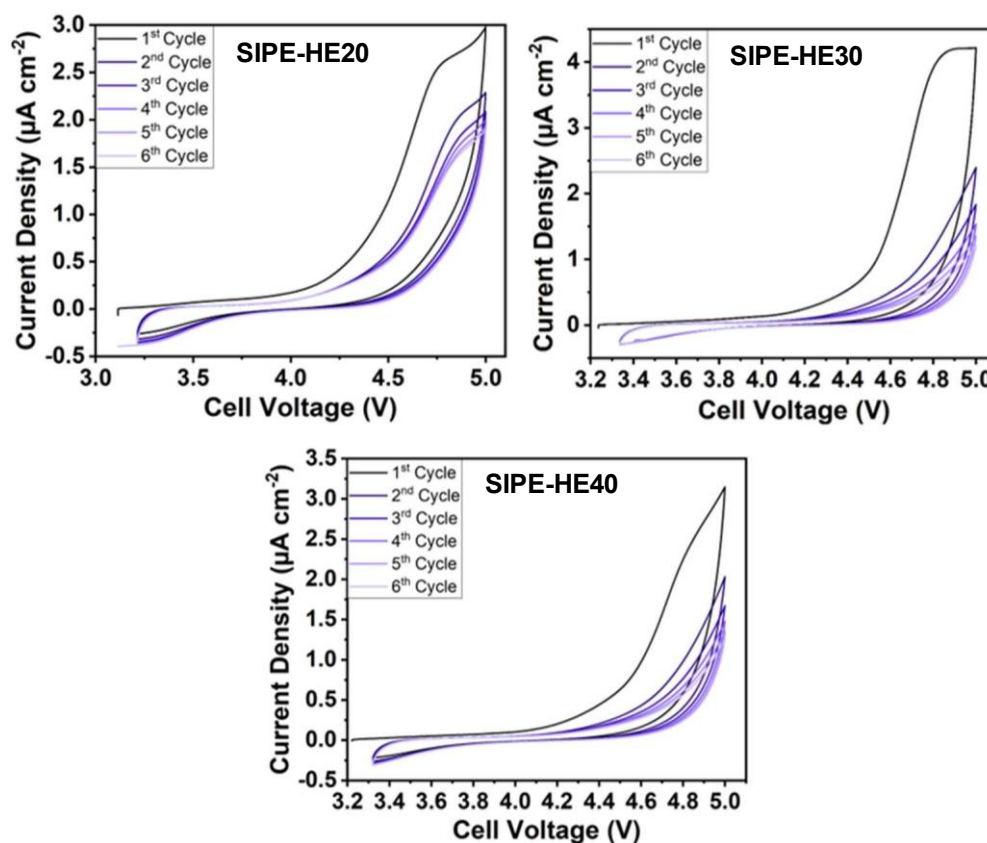
Figure 6-35. Anodic cyclic voltammetry for further investigation of electrochemical stability by using freshly built Li/stainless steel cells between OCV and 0 V vs. Li$^+$/Li (sweep rate = 1 mV s^{-1}) for the three SIPE-HE hybrid electrolytes.

Similarly, the cathodic scans were conducted from OCV to 0V with a scan rate of 1 mV s^{-1} and are presented in **Figure 6-36**. For all the hybrid electrolytes, the first cycle showed a strong reaction between 0 -1.7 V which could be associated with the formation of a passivation layer on the electrode and/or the reductive degradation of LATP. The intensity of the reaction decreased in the following cycles which tends to validate the passivation layer formation. Additionally, a pair of small peaks could be observed between 0.6 and 0.7 V and between 1.1 and 1.25 V for the three hybrid electrolytes studied. These peaks appear to be reversible when sweeping from 0V to OCV. These tiny peaks could be associated with the intercalation of lithium ions in the metal oxide at the stainless steel electrode surface[156].

In the end, the electrochemical stability until 5V, obtained on the LSV and CV measurements is a great improvement compared to the electrolyte without inorganic particles and should allow for the implementation of the SIPE-HE electrolyte in batteries using high-energy density cathode material. Moreover, the irreversible side reaction between 1.7 V and 0.5 V should not be a problem since the full-cell investigations with NMC are conducted between 3 and 4.2 V.
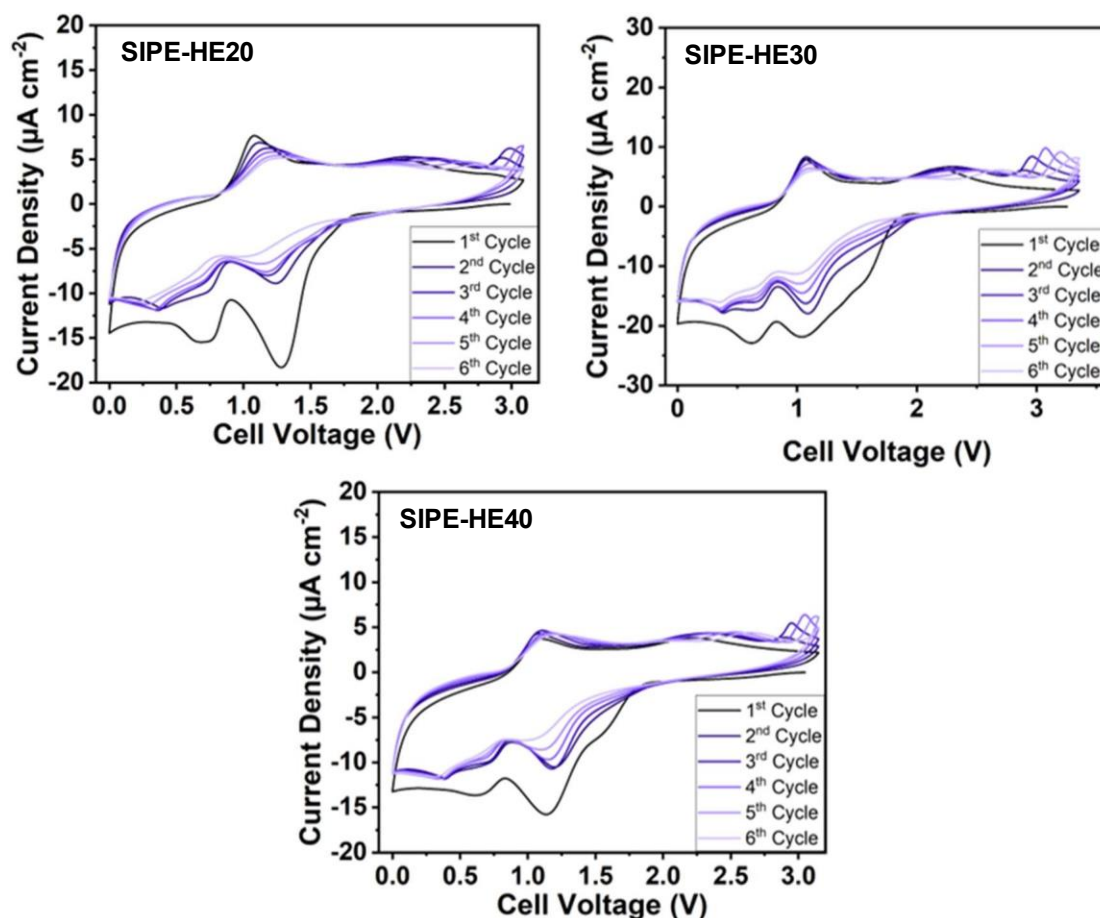
Figure 6-36. Cathodic cyclic voltammetry for further investigation of electrochemical stability by using freshly built Li/stainless steel cells between OCV and 0 V vs. Li^+/Li (sweep rate = 1 mV s^{-1}) for the three SIPE-HE hybrid electrolytes.

6.2.3 Lithium Stripping/Plating

The ability of the hybrid electrolyte to transfer lithium cation from one electrode to the other is the next key factor that needs to be investigated via lithium stripping-plating tests. These tests were conducted in symmetrical lithium/lithium cells where the SIPE-HE were sandwiched between two electrodes and subjected to different current densities. The resulting data are presented in **Figure 6-37**. First, we subjected the cells to very low current densities (**Figure 6-37.a, 6-37.c, and 6-37.e** for respectively SIPE-HE20, SIPE-HE30, and SIPE-HE40). The data for stripping /plating at low current densities exhibited similar overpotential values for the three

electrolytes and identical overpotential behavior at 0.002, 0.005, and 0.009 mA cm^{-2}. For 0.013, 0.018, and 0.027 mA cm^{-2}, the overpotential is slightly decreasing upon cycling, this could indicate a change in the interfacial resistance which could be due to a better organization of the interface or some degradations of the electrolyte resulting in a change in the interface. However, the slight decrease and the absence of short circuits suggest that better organization is more likely. The stripping/plating at higher current densities (**Figure 6-37.b, 6-37.d, and 6-37.f**) confirms this assumption since no short-circuit or dendrites growth indication appears at these higher current densities. The SIPE-HE30 electrolyte also exhibits excellent reversibility since similar overpotential, and behavior can be observed after lowering the current density back to 0.018 mA cm^{-2} even if the high cut-off voltage was achieved when trying to have a stripping plating at high current density. For the SIPE-HE40 electrolyte, no changes in overpotential upon cycling were obtained at the lower current densities, indicating a stable electrode/electrolyte interface from the beginning. When increasing the current densities (**Figure 6-37.f**), the same behavior as for SIPE-HE30 was observed with also excellent reversibility when lowering the current back. Overall, these results show the ability of this solid-state electrolyte to transport lithium cations from one electrode to the other. Nevertheless, the current density values should not exceed the limiting current density value otherwise the lithium transport abilities are lost. For i = 0.044 mA cm^{-2} (slightly exceeding the limiting current density), the overpotential during the stripping or the plating step is not reaching a steady state but is continuously increasing. We assume that it comes from an accumulation of electrons at the interface due to a slow transfer of the cations compared to the transfer of the electrons to the interface. Overall, a trend can be observed with the overpotential being lower when increasing the inorganic particles percentage. This means that the interface formed by SIPE-HE40 is better than for SIPE-HE30 and SIPE-HE20.
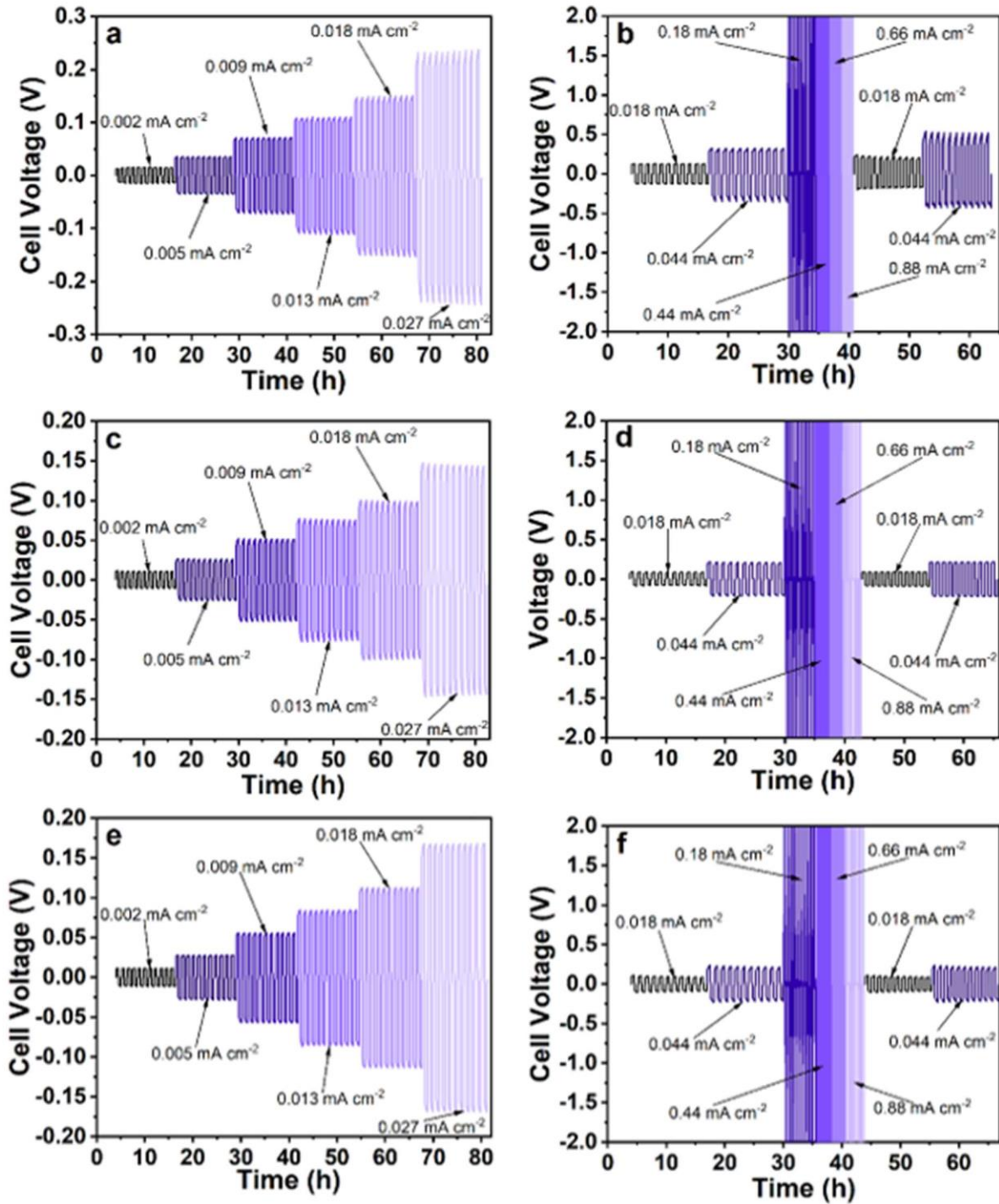
Figure 6-37. Investigation of the stripping/plating behavior of hybrid electrolyte in Li/Li symmetrical cells at 40 °C: (a), (d) and (g), respectively SIPE-HE20, SIPE-HE30 and SIPE-HE40, Li/Li cell subjected to elevated current 0.002, 0.005, 0.01, 0.015, 0.02, 0.03 mA, *i.e.*, 0.002, 0.004, 0.009, 0.013, 0.018, 0.027 mA cm^{-2}, respectively (Ø=12mm and electrode surface

area= 1.131 cm^{-2}); (b), (e) and (h), SIPE-HE20, SIPE-HE30 and SIPE-HE40, Li/Li cell subjected to elevated current 0.02, 0.05, 0.2, 0.5, 0.75, 1 mA, *i.e.*, 0.018, 0.044, 0.18, 0.44, 0.66, 0.88 mA cm^{-2}, respectively (Ø=12mm and electrode surface area= 1.131 cm^{-2}) followed by lowering the current back to 0.017 and 0.044 mA cm^{-2} for subsequent stripping/plating cycles (each cycle is composed of 30 minutes stripping step followed by a 5 minutes rest, a 30 minutes plating step and another 5 minutes rest).

The long-term stripping/plating tests are presented in **Figures 6-38.a, 6-38.b, and 6-38.c**, for respectively SIPE-HE20, SIPE-HE30, and SIPE-HE40. They show that the three hybrid electrolytes can support lithium stripping/plating without any indication of electrolyte degradation and/or dendrites growth even after more than 600 hours. Nevertheless, a few differences can be observed. SIPE-HE20 (**Figure 6-38.a**) exhibits the highest overpotential among the three hybrid electrolytes with a slight increase upon cycling and no particular stabilization after 600H. SIPE-HE30 (**Figure 6-38.b**) exhibits a lower overpotential which is slightly increasing upon cycling, which indicates changes in the electrode/electrolyte interface. On the other hand (**Figure 6-38.c**), the overpotential for SIPE-HE40 is lower, which is probably due to a better electrode‖electrolyte interface. A slight decrease can be observed until about 150 hours followed by a slow increase before eventually stabilizing after 450 hours. This is usually attributed to a reorganization of the interface. Those results confirm the trend observed earlier: the higher the inorganic particle content, the lower the overpotential and the better the electrolyte‖lithium interface.
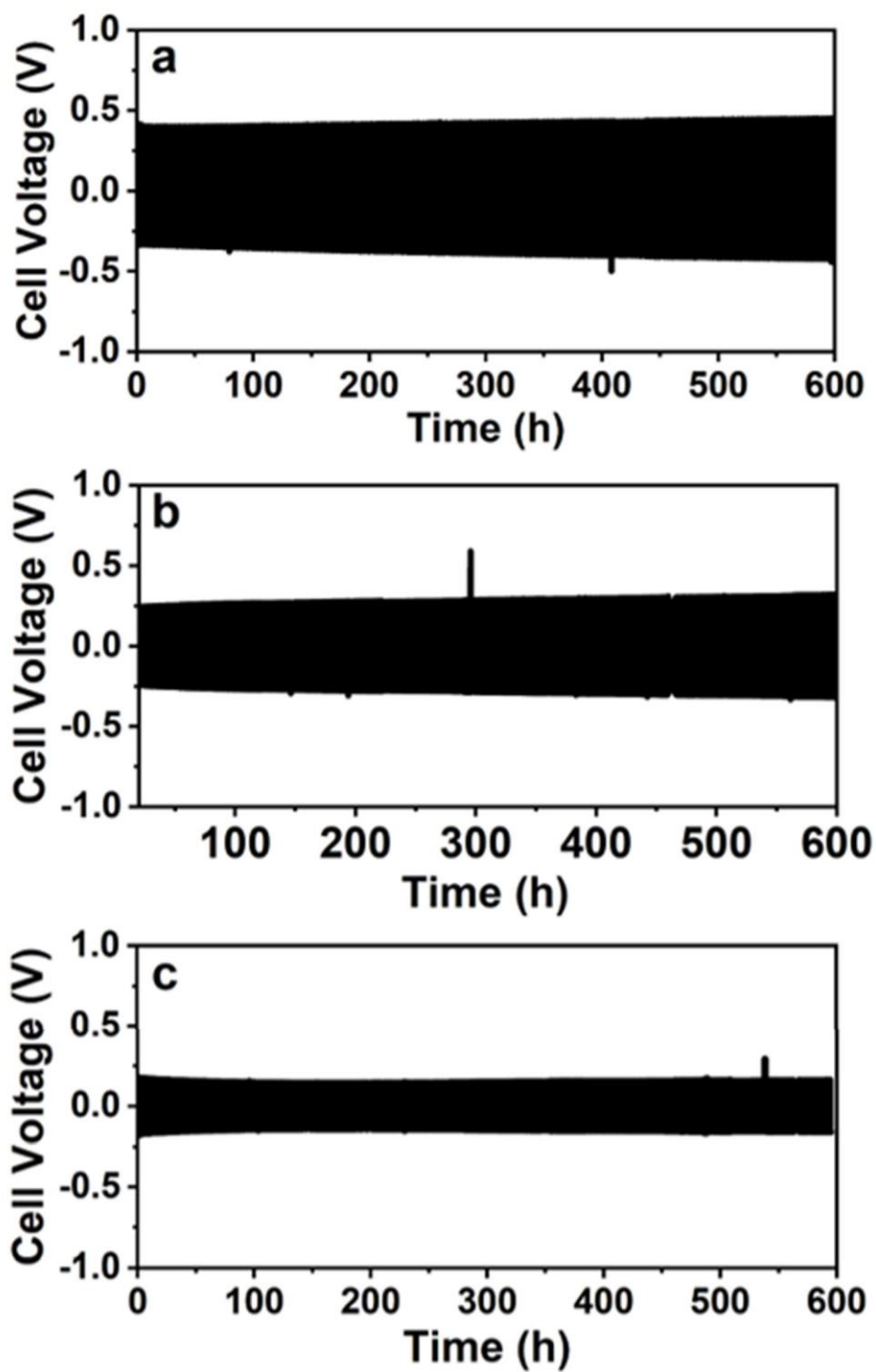
Figure 6-38. Long-term stripping/plating investigation for SIPE-HE20 (a), SIPE-HE30 (b), and SIPE-HE40 (c), Li/Li cell subjected to a constant current of 0.03 mA, *i.e.*, 0.027 mA cm^{-2} for more than 600 hours.

Than To confirm these different assumptions about interfacial changes, impedance spectroscopy measurements were performed after each stripping/plating cycle and are presented in **Figure 6-39**. These EIS spectra consist of two semi-circles: a high-frequency one corresponding to the electrolyte conductivity, and a low-frequency one assigned to the electrode∥electrolyte interfacial process. This interfacial resistance is much lower for SIPE-HE40 (**Figure 6-39.c**) than for SIPE-HE30 (**Figure 6-39.b**) and SIPE-HE20 (**Figure 6-39.a**), explaining the lower overpotential during stripping-plating. In **Figure 6-39.a** and **Figure 6-39.b**, changes in the first semi-circles upon cycling can be seen but these changes are rather small compared to the increase of the interfacial resistance observable on the low frequencies semi-circles. This continuous increase corresponds to the rising overpotential observed on the stripping/plating data. The reason for this resistance increase is not clear to us and needs further investigation. For SIPE-HE40 (**Figure 6-39.c**), the high-frequency semi-circles are all similar, and the main changes are related to the low-frequency semi-circle (the big change from the first to the fiftieth cycle is related to the formation of the SEI during the first lithium deposition). The evolution of the interfacial resistances follows the trend observed for the overpotential during the long-term stripping plating with a decrease until 100 cycles followed by an increase until 400 cycles and a stabilization of the interfacial resistance values, confirming the reorganization of the interface to be the most stable possible. Overall, these long-term stripping/plating and EIS results show the abilities of the hybrid electrolyte SIPE-HE40 to form a better interface, than SIPE-HE20 and SIPE-HE30, with lithium metal for battery application.
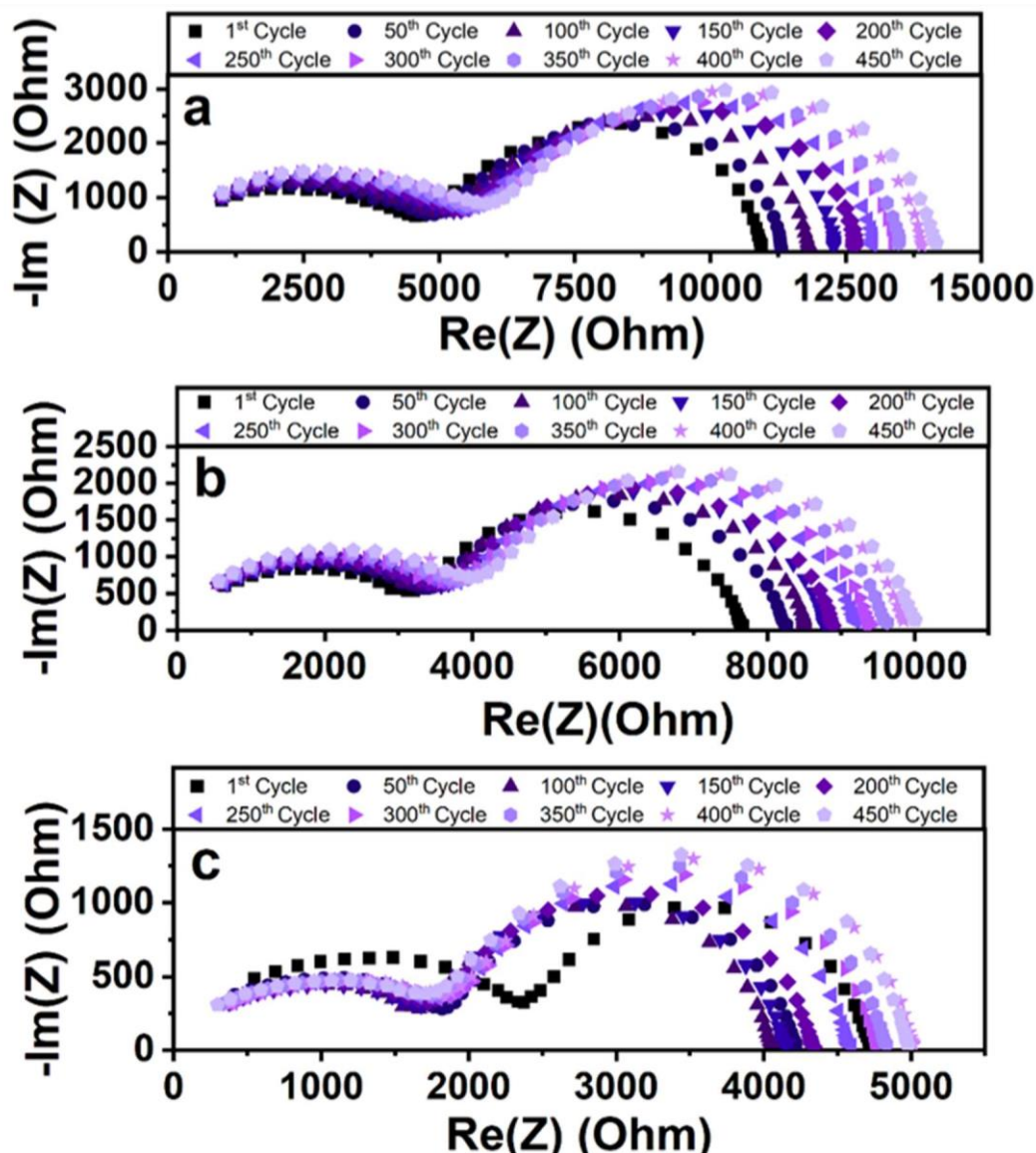
Figure 6-39. Nyquist plots of the EIS data, recorded after certain stripping/plating cycles during the long-term cycling at 0.027 mA cm^{-2} and 40 °C, for respectively SIPE-HE20 (a), SIPE-HE30 (b) and SIPE-HE40 (c).

To further investigate the compatibility of our SIPE-HE electrolyte, we conduct the same stripping/plating test as previously presented but at 60 °C. The results obtained with the lower current density (**Figure 6-40.a, c, e**) are very similar to the one obtained at 40 °C. The voltage response at all current densities is stable upon cycling with a steady state reach almost immediately after applying the current which is expected for a single-ion conducting polymer

electrolyte especially when this behavior was already observed at lower temperatures. But for the SIPE-HE, compared to SIPE+PEG, the overpotential at each current density is much lower than the one measured at 40 °C. This means that increasing the temperature has a bigger impact on the SIPE-HE∥lithium interface than the SIPE+PEG∥lithium.

When going to higher current density (**Figure 6-40.b, d, f**), a big improvement was observed compared to the same test at 40 °C. First, for 0.018 and 0.044 mA cm^{-2}, we can see that a more rectangular shape was observed with a lower overvoltage, indicating a better and faster charge transfer at the interface[157] and a better electrolyte∥lithium interface. When using 0.18 mA cm^{-2} at 40 °C, the polarization of the cell was extremely fast, and no stripping plating was observed. At 60 °C, on the contrary, a really good stripping/plating was obtained at this current density. It can also be seen that the steady state is not immediately reached meaning the polarization of the cell starts to limit the charge transfer at the interface. This shows that a higher limiting current density is obtained at 60°C. For 0.44 mA cm^{-2} and higher, huge increases in the overpotential were observed, the increases were so important that the cut-off voltage of 2 V was reached in a few minutes or even seconds meaning no stripping/plating at these current density values. But, as previously observed, this does not result in electrolyte degradation since a good reversibility was observed when lowering the current back to 0.018 and 0.044 mA cm^{-2}. Once again, the trend previously described is observable in these stripping/plating results.
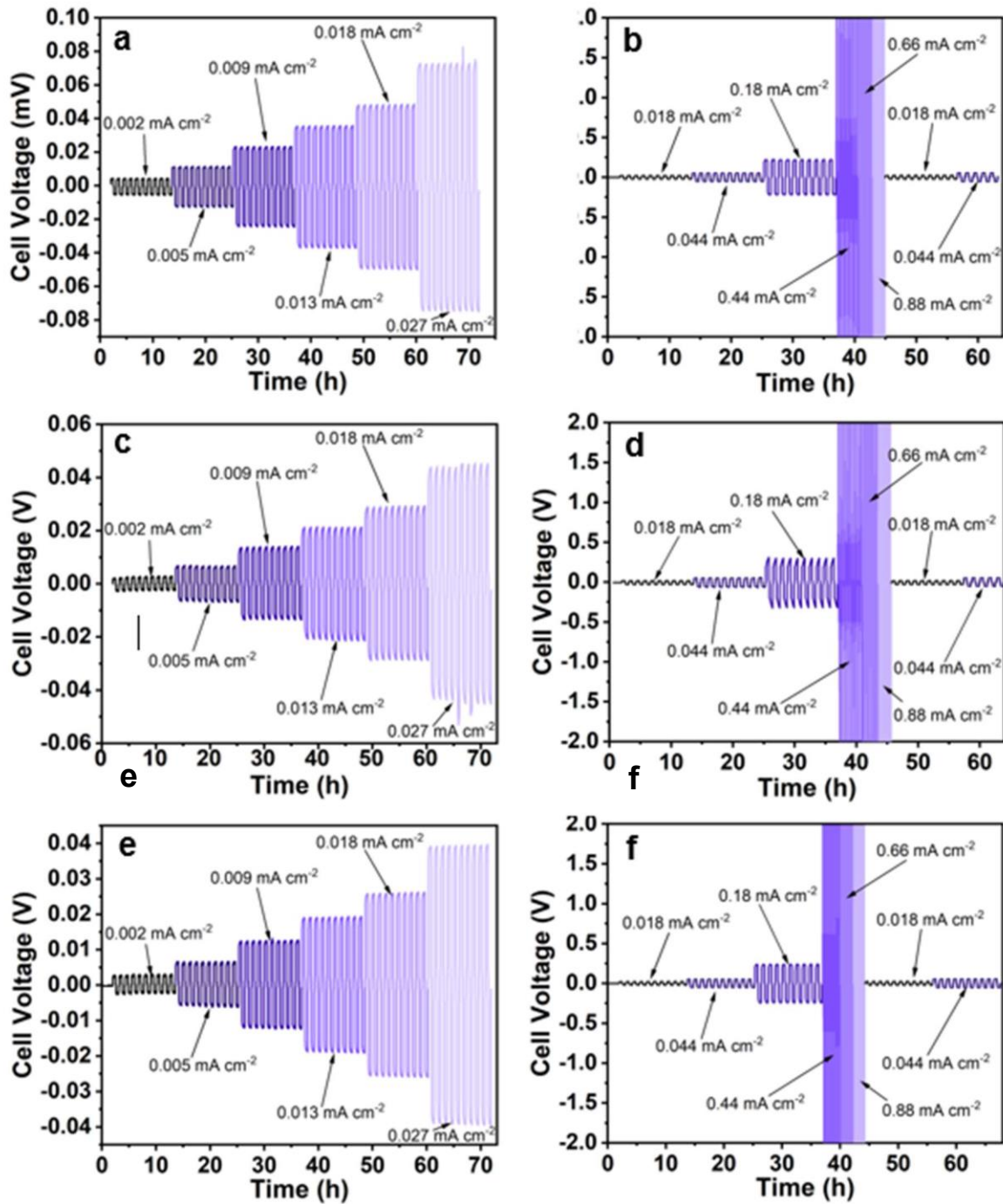
Figure 6-40. Investigation of the stripping/plating behavior of hybrid electrolyte in Li/Li symmetrical cells at 60 °C: (a), (d) and (g), respectively SIPE-HE20, SIPE-HE30 and SIPE-HE40, Li/Li cell subjected to elevated current 0.002, 0.005, 0.01, 0.015, 0.02, 0.03 mA, *i.e.*, 0.002, 0.004, 0.009, 0.013, 0.018, 0.027 mA cm^{-2}, respectively (Ø=12mm and electrode surface

area= 1.131 cm^{-2}); (b), (e) and (h), respectively SIPE-HE20, SIPE-HE30 and SIPE-HE40, Li/Li cell subjected to elevated current 0.02, 0.05, 0.2, 0.5, 0.75, 1 mA, *i.e.*, 0.018, 0.044, 0.18, 0.44, 0.66, 0.88 mA cm^{-2}, respectively (Ø=12mm and electrode surface area= 1.131 cm^{-2}) followed by lowering the current back to 0.018 and 0.044 mA cm^{-2} for subsequent stripping/plating cycles (each cycle is composed of 30 minutes stripping step followed by a 5 minutes rest, a 30 minutes plating step and another 5 minutes rest).

The long-term stripping/plating tests at 60 °C are presented in **Figures 6-41.a, 6-41.b, and 6-41.c**, for respectively SIPE-HE20, SIPE-HE30, and SIPE-HE40. They confirm that the higher temperature allows us to use higher current density and that the three electrolytes can support lithium stripping/plating at this higher current density without any indication of electrolyte degradation and/or dendrites growth even after more than 450 hours. Overall, these results at higher temperature for long-term stripping plating once again highlight the trend observed earlier, e.g. the higher the inorganic particle content, the lower the overpotential and the better the electrolyte‖lithium interface.
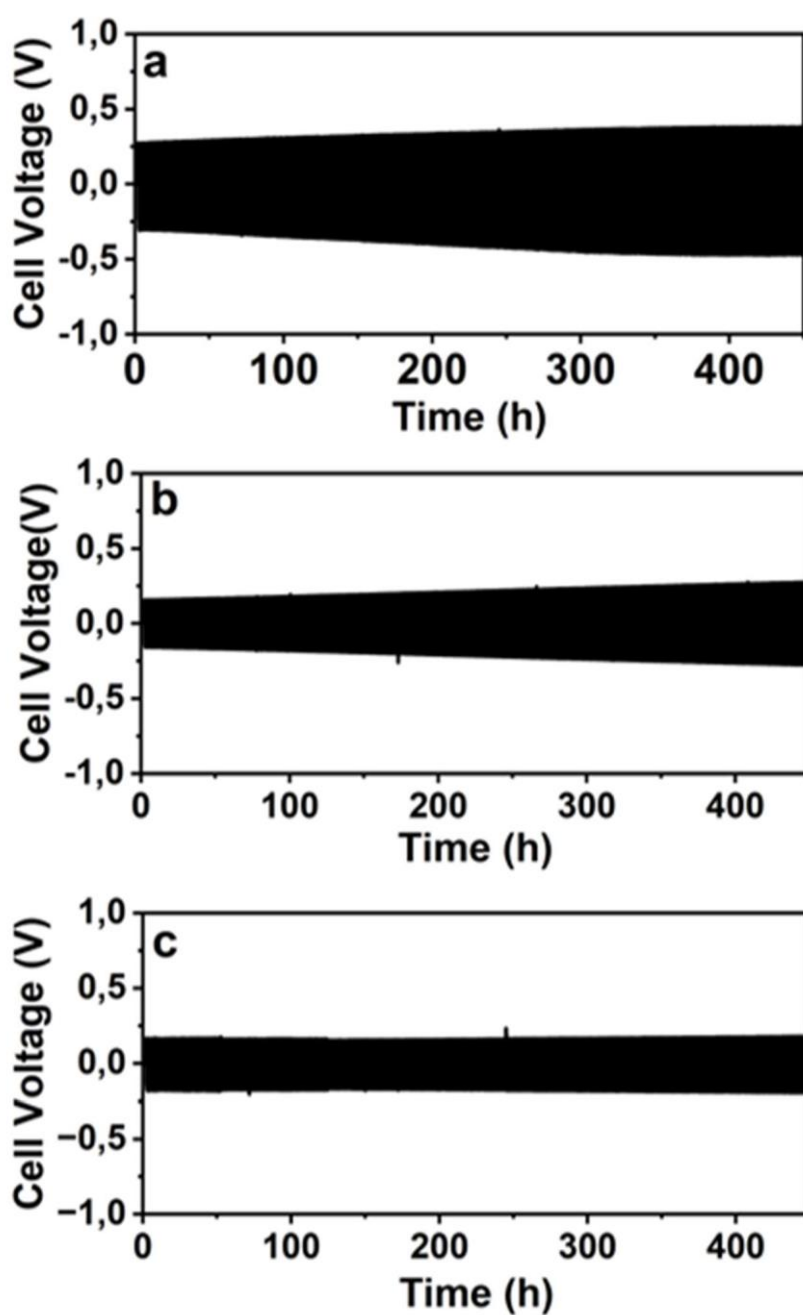
Figure 6-41. Long-term stripping/plating investigation for SIPE-HE20 (a), SIPE-HE30 (b), and SIPE-HE40 (c) at 60°C, Li/Li cell subjected to a constant current of 0.1 mA, *i.e.*, 0.088 mA cm^{-2} for more than 450 hours.

Overall, these stripping/plating results at different temperatures and different current densities reveal the good compatibility of the hybrid electrolyte with lithium metal even though we

observed LATP degradation in the electrochemical stability window, transference number, and limiting current density measurements presented earlier. This renders these electrolytes good candidates for further investigations.

6.2.4 Evaluation of Li∥NMC811 Cells

The next step was to test the different hybrid electrolytes with high-voltage cathodes. We assembled Li/SIPE-HE/NMC$_{811}$ cells and subjected them to galvanostatic cycling at 40 °C (**Figure 6-42**) using a C-rate of 0.05C. This C rate was chosen because of the low limiting current density measured earlier and the previous stripping plating results. Indeed, the prepared electrodes have a mass loading of approximately 1.5 mg cm^{-2}. Therefore, 0.05C corresponds to I ≈ 0.015 mA for the standard 1C = 190 mAh g-1 for NMC$_{811}$ electrodes.

Figure 6-42.a presents the results for SIPE-HE20. The cell exhibited a specific discharge capacity of 117 mAh g^{-1} in the first cycle with an initial Coulombic efficiency of more than 100%. This value is probably related to side reactions occurring during the first cycle, the formation of the SEI, and a possible small prelithiation of the active material from the synthesis process. Afterward, an average 99.6% Coulombic efficiency for the subsequent cycles was obtained. After 40 cycles, a capacity retention of 80% was obtained without any indication of polymer degradation. For SIPE-HE30 (**Figure 6-42.b**), the cell exhibits the same behavior with a slightly higher initial specific discharge capacity of 122 mAh g^{-1}, a coulombic efficiency higher than 100% in the first cycle which averages 99.7% in the subsequent cycles, and a capacity retention of 80% after 40 cycles. In the case of SIPE-HE40 (**Figure 6-42.c**), the cell exhibited a specific discharge capacity of 88 mAh g^{-1} in the first cycle with an initial Coulombic efficiency of more than 100%. After these initial cycles, an average Coulombic efficiency of 99.8% for the subsequent cycles. After 55 cycles, a capacity retention of 80% was obtained.
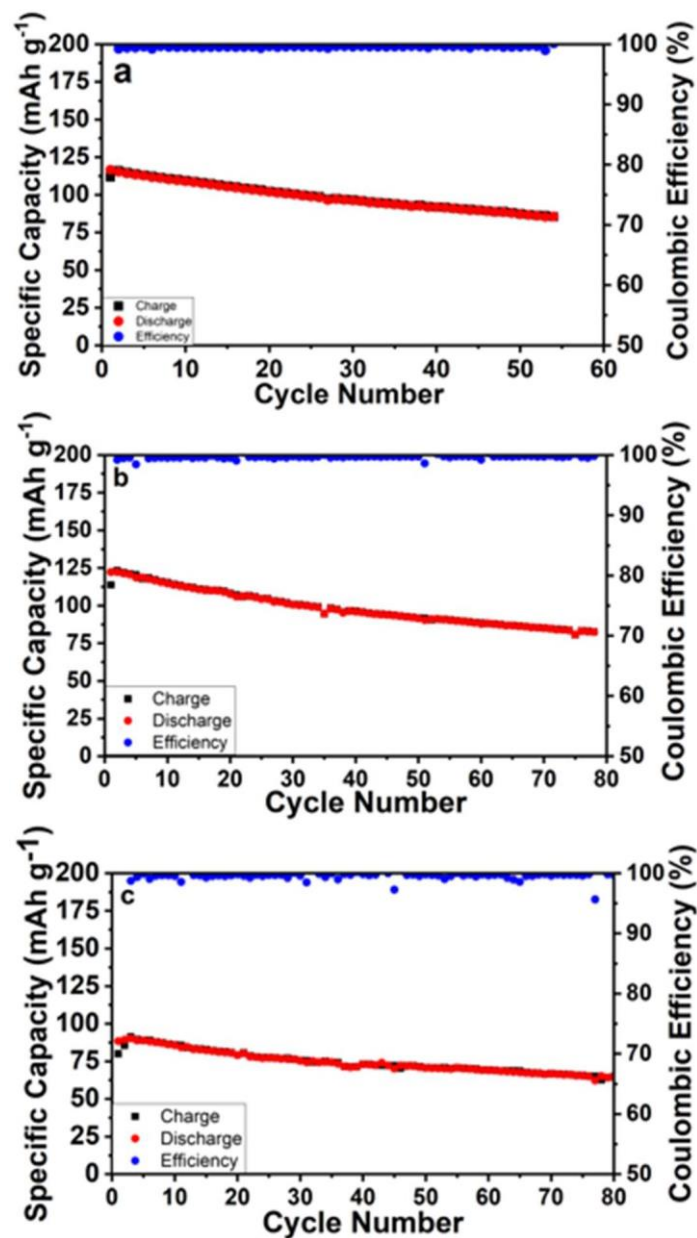
Figure 6-42. Investigation of SIPE-HE electrolyte in Li/NMC$_{811}$ cells at 40 °C: charge and discharge capacity and Coulombic efficiency as a function of cycle number for SIPE-HE20 (a), SIPE-HE30 (b) and SIPE-HE40 (c); all cycles were conducted at 0.05C with 1C= 190 mA g^{-1} and cut-off voltage set to 3.0 and 4.2 V vs. Li$^+$/Li.

For the three hybrid electrolytes, the voltage profiles at different cycles (**Figure 6-43**) do not show any voltage fluctuation that could indicate dendrites growth or degradation of the SIPE-

HE electrolyte. This confirms the chemical stability of the electrolyte material towards NMC. Despite the noticeable capacity loss, these profiles all exhibit a similar shape, indicating a consistent electrochemical process throughout the cycle. The loss of capacity is here probably related to the current density which is close to or higher than the limiting current density, even at 0.05C. These results at 40 °C tend to show an opposite trend to the one observed from the stripping/plating test with the electrode‖electrolyte interface being better with the lower inorganic particle content.
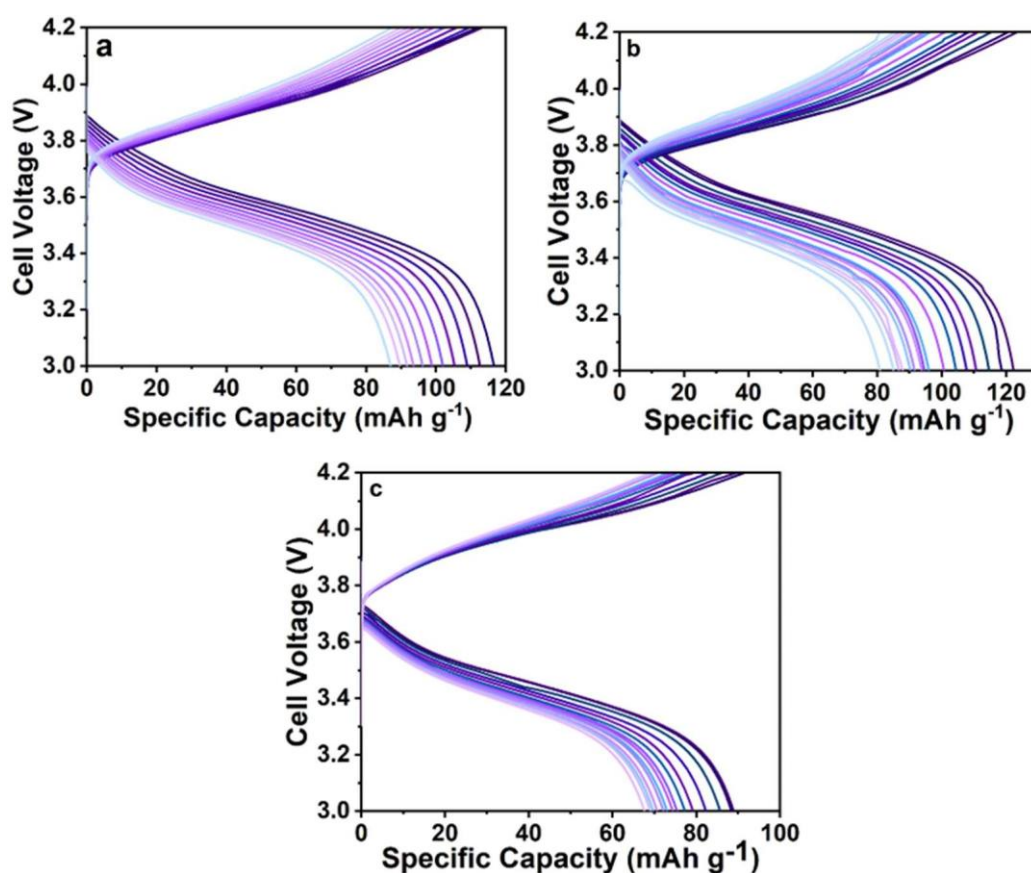
Figure 6-43. Investigation of SIPE-HE electrolyte in Li/NMC$_{811}$ cells at 40 °C: voltage profiles for selected cycles for SIPE-HE20 (a), SIPE-HE30 (b), and SIPE-HE40 (c); all cycles were conducted at 0.05C with 1C= 190 mA g^{-1} and cut-off voltage set to 3.0 and 4.2 V vs. Li$^+$/Li.

At 60 °C, the Li│SIPE-HE│NMC811 cell was then subjected to a C rates capability test (**Figure 6-44)** at 0.05C, 0.1C, 0.2C, 0.5C and 1C (1C not represented here since the specific

capacity was 0 mAh g^{-1}) followed by a long-term constant current cycling stability test at 0.05C with 1C= 190 mAh g^{-1}.

For SIPE-HE20 (**Figure 6-44.a**), the cell exhibited a reversible discharge capacity of about 175 mAh g^{-1} during the first cycles at 0.05C with a Coulombic efficiency of 93%. In the next four cycles at 0.05C, the coulombic efficiency increases from 96% to 99% with a decrease of specific capacity. At 0.1 and 0.2C, a higher coulombic efficiency with a more stable specific capacity was obtained, except for each first cycle. The C rates capability test also highlighted a decrease of the capacity with higher C rates (140 mAh g^{-1} at 0.1C, 106 mAh g^{-1} at 0.2C and 20 mAh g^{-1} at 0.5C).

In the case of SIPE-HE30 (**Figure 6-44.b**), we observed an initial discharge capacity of 160 mAh g^{-1} with a coulombic efficiency of 95%. In the next four cycles at 0.05C, the coulombic efficiency increases from 96% to 98% with a decrease of specific capacity. The same observations as previously can be made at 0.1, 0.2 and 0.5C with the more stable specific capacity and higher coulombic efficiency. The lower specific capacity with higher C rates (115 mAh g^{-1} at 0.1C, 80 mAh g^{-1} at 0.2C and 15 mAh g^{-1} at 0.5C) can also clearly be seen.

Finally for SIPE-HE40 (**Figure 6-44.c**), the initial specific capacity was 140 mAh g^{-1} with the same behavior as SIPE-HE20 and SIPE-HE30 with lower specific capacity (103 mAh g^{-1} at 0.1C, 75 mAh g^{-1} at 0.2C and 10 mAh g^{-1} at 0.5C).

For all three hybrid electrolytes, similar behavior at 0.05C can be observed like the low coulombic efficiency of the first cycle. This is due to the formation of the different SEI during the first cycles but maybe also to the reaction of the incorporated PEG that may react with NMC at 4.2 V. Also, when increasing the C rates, the coulombic efficiency reaches 99% except for each first cycle, showing that side reactions still occur when increasing the currents to enhance the electrode∥electrolyte interface. This decline of capacity that can be observed for the three electrolytes when increasing the C rate, is due to kinetic and mass transport limitation and increased polarization from the increased current density which leads to incomplete lithiation/delithiation of the active NMC material and also to the more sluggish charge transfer at the interface that we already observed at higher current density during stripping/plating test.
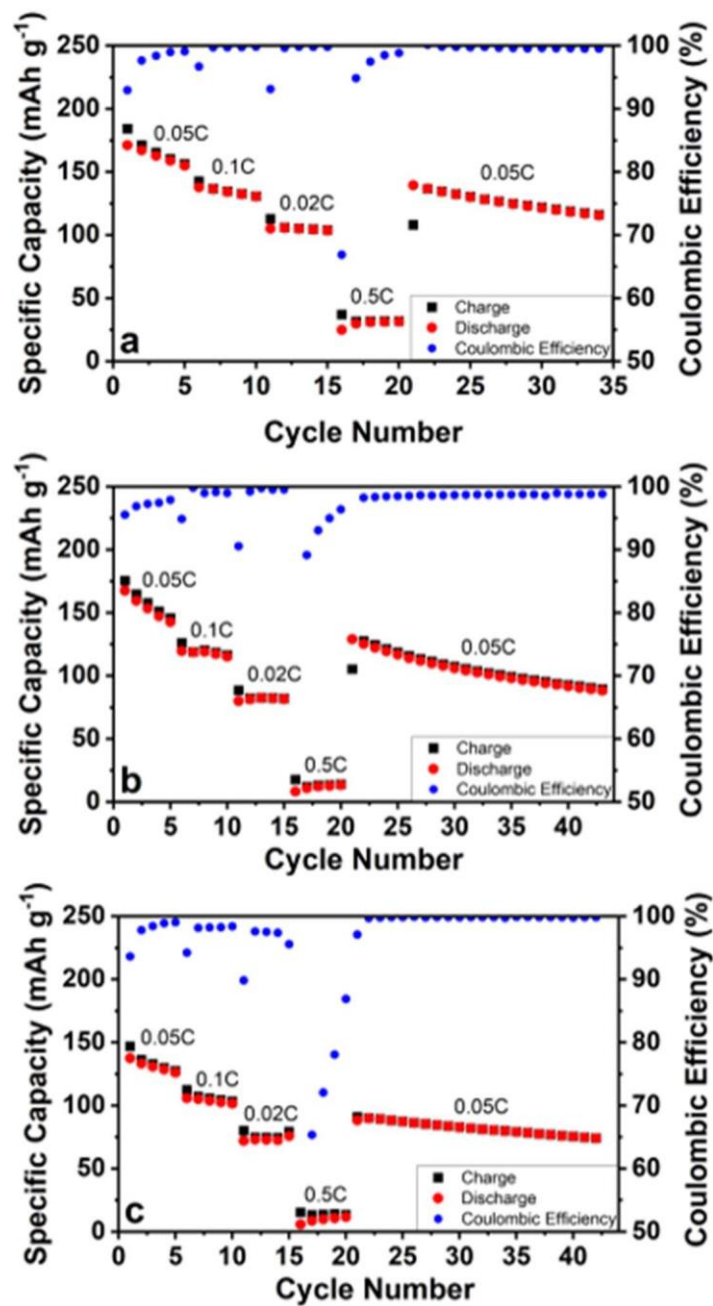
Figure 6-44. Investigation of SIPE-HE electrolyte in Li/NMC$_{811}$ cells at 60 °C: charge and discharge capacity and Coulombic efficiency as a function of cycle number for SIPE-HE20 (a), SIPE-HE30 (b) and SIPE-HE40 (c); C rates test and long term cycling were conducted with 1C= 190 mAh g^{-1} and cut-off voltage set to 3 and 4.2 V vs. Li$^+$/Li.

The voltage profiles at different C rates (**Figure 6-45**) do not show any voltage fluctuation that could indicate dendrites growth or degradation of the SIPE-HE electrolyte, which once again confirm the good compatibility of the electrolyte material toward NMC, even at 60 °C.

Same as we did in the previous chapter, the polarization of the cell was be estimated by the voltage difference between charge and discharge at the point of 50% capacity. These polarization voltages as function of the current density, for the three SIPE-HE electrolytes, are presented in **Figure 6-45.d**. For SIPE-HE20, the polarization follows a linear trend with the corresponding current densities which suggests that the impedance of the cell at 50% of state of charge (SOC) was stable also at the increased current densities. For the other two (SIPE-HE30 and SIPE-HE40), the linear trend was less obvious which is confirmed by the lower r^2 values. This most probably indicates a less stable impedance at 50% of SOC. These results, the C rates capability test, and the long-term cycling at 0.05C all tend to confirm the opposite trend to the one observed from the stripping/plating test with the electrode‖electrolyte interface being better with the lower inorganic particle content. This is probably due to the "rigidity" of the membrane being higher with 40% LATP than 20%, and rendering the formation of the electrode‖electrolyte harder to achieve.
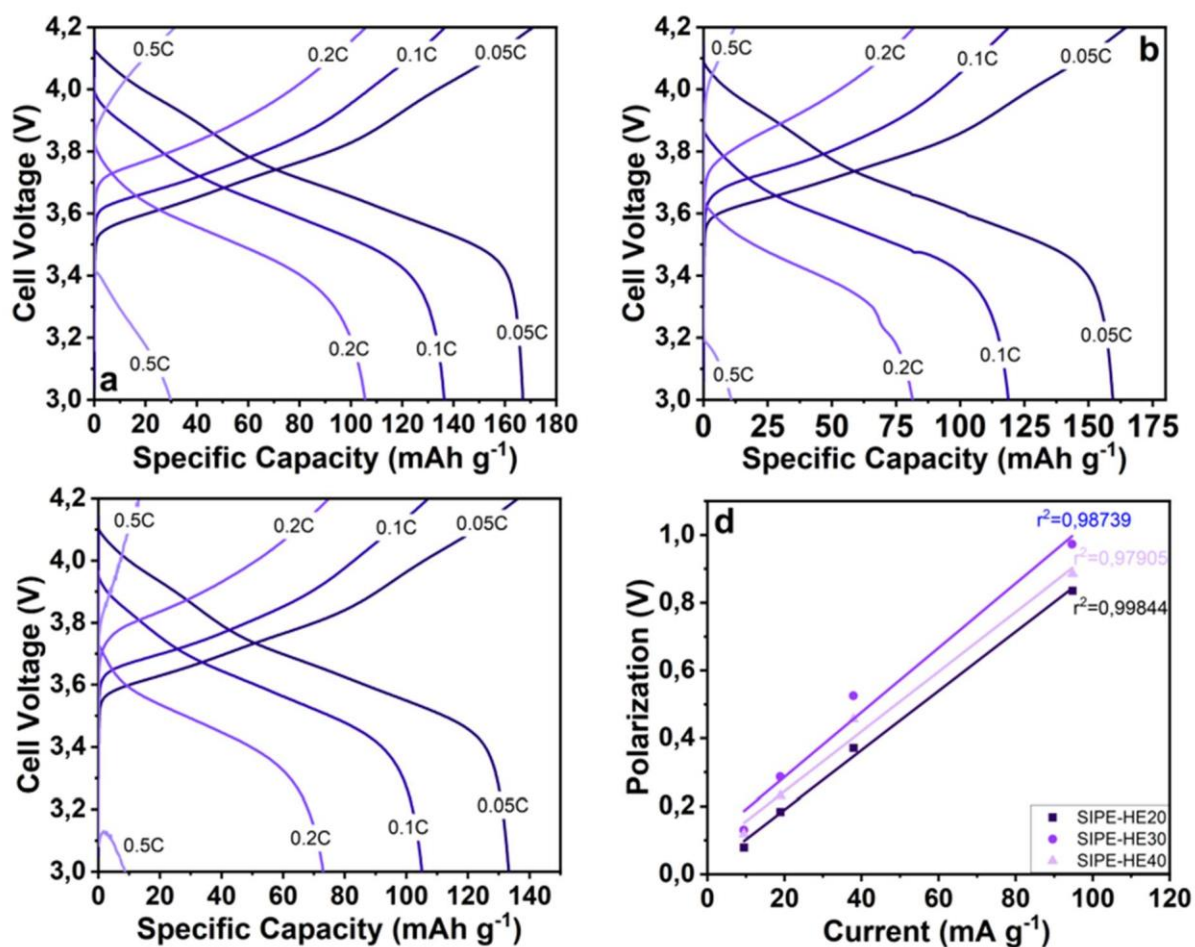
Figure 6-45. Investigation of SIPE-HE electrolyte in Li/NMC$_{811}$ cells at 40 °C: voltage profiles for selected cycles for SIPE-HE20 (a), SIPE-HE30 (b) and SIPE-HE40 (c); all cycles were conducted with 1C = 190 mAh g^{-1} and cut-off voltage set to 3 and 4.2 V vs. Li$^+$/Li. (d) polarization *vs.* current density for Li‖SIPE-HE20‖NMC$_{811}$, Li‖SIPE-HE30‖NMC$_{811}$ and Li‖SIPE-HE40‖NMC$_{811}$ cells subjected to a C rate test at 60 °C.

These results at 40 and 60°C indicate a generally good compatibility of the SIPE-HE electrolyte with positive and negative electrode materials. The good compatibility of hybrid electrolyte with lithium metal has already been reported in many studies [177,178,180]. The results with NMC are hard to compare since no studies on this type of material *vs.* NMC has been published yet. But the experiment with other cathode materials tends to show a better capacity retention with hybrid electrolyte which is not really the case in this work.

6.2.5 Conclusions

In this section, we show that the previously studied blend of a partially fluorinated multi-block co-poly (arylene ether sulfone) with lithium perfluorosulfonimide side chains with low molecular weight poly(ethylene glycol)dimethyl ether can be improved by adding LATP particles to form a fully solid hybrid electrolyte. The preparation of the membrane by solvent casting followed by a hot-pressing step was demonstrated to be rather easy and allowed for the formation of a self-standing and mechanically stable film for all LATP percentages. Concerning the ionic conductivity, a decrease compared to the blend was obtained with 20% LATP, the conductivity then increases with the filler percentage to reach similar values as for the blend when 40% of particles were added (8.4×10^{-6} at 40°C). An enhancement of the electrochemical stability window until about 5 V was measured. The cathodic linear and cyclic voltammetry, the transference number measurement, and the limiting current density determination tend to show a degradation of the LATP when in contact with lithium but on the other hand, the hybrid electrolyte also exhibited excellent cyclability with lithium metal electrodes during stripping/plating tests at different current densities but also at a constant current density during long-term test. This means that the reaction of LATP with lithium metal helps to form a stable SEI at the lithium electrode surface. From the low limiting current densities measurement, we can say that the ability of the hybrid electrolyte for fast charge and discharge is limited. Therefore, cycling tests with NMC_{811} as cathode material at 40°C were conducted only at 0.05C and the cells exhibited acceptable initial discharge capacity but a similar capacity retention as the blend without LATP particles. A good Coulombic efficiency upon cycling and no indication of degradation of the electrolyte upon cycling were also reported. The use of a higher temperature (60°C) allows use to conduct C rates capability tests for all HEs. These tests demonstrate a rather fast capacity decline in the first cycles at 0.05C before stabilization and good capacity retention at other current densities. A rather high-capacity loss when increasing the current density was also observed but this capacity loss has been shown to be reversible when decreasing the C rate. These results make this composite electrolyte an interesting

candidate for further development. Work on improving the electrode/electrolyte interface is the next key step to obtain better cyclability for this solid hybrid electrolyte.

6.3 New Ether-Free Single-Ion Conducting Polymer Electrolyte and Multilayer Electrolyte System for Lithium Metal Batteries

For single-ion conducting polymer, it has been demonstrated that despite the different possible structures, the presence of ether bound can limit the oxidation potential, particularly when these bound are not substituted with electron-withdrawing groups[185].

Therefore, in this section, we design a new ether-free single-ion conducting polymer (labeled SIPE-EF), and we study its performance when dopped with different amounts of PC.

6.3.1 Synthesis

This ether-free copolymer was synthesized by Fridel Crafts hydroxy alkylation reaction using Brønsted superacid trifluoromethanesulfonic acid as a catalyzer. **Figure 6-46** presents the reaction mechanism for the first step of the polymerization. The intermediate (**6**) can then react with the remaining 4'-brom-2,2,2-trifluoracetophenone and so on to form a high molecular weight polymer. This synthesis between deactivated ketones and an electron-rich arenes can occur because of the trifluoromethyl group which activates the carboxonium ion intermediate (**2**), leading to enhanced electrophilic reactivity [186]. To combine high mechanical properties and conductivity we select among the aromatic monomers the p-terphenyl structures, which, due to their high rigidity can assure a certain mechanical stability by limiting the movement in the backbone. The utilization of 4'-brom-2,2,2-trifluoracetophenone allows the grafting of perfluorosulfonimide function by coupling reaction. The synthesis of the backbone occurs in a short reaction time (~8 hours) without the use of high temperature and no further purification step, rendering this ether-free backbone a quite simple polymer to prepare at the lab scale.
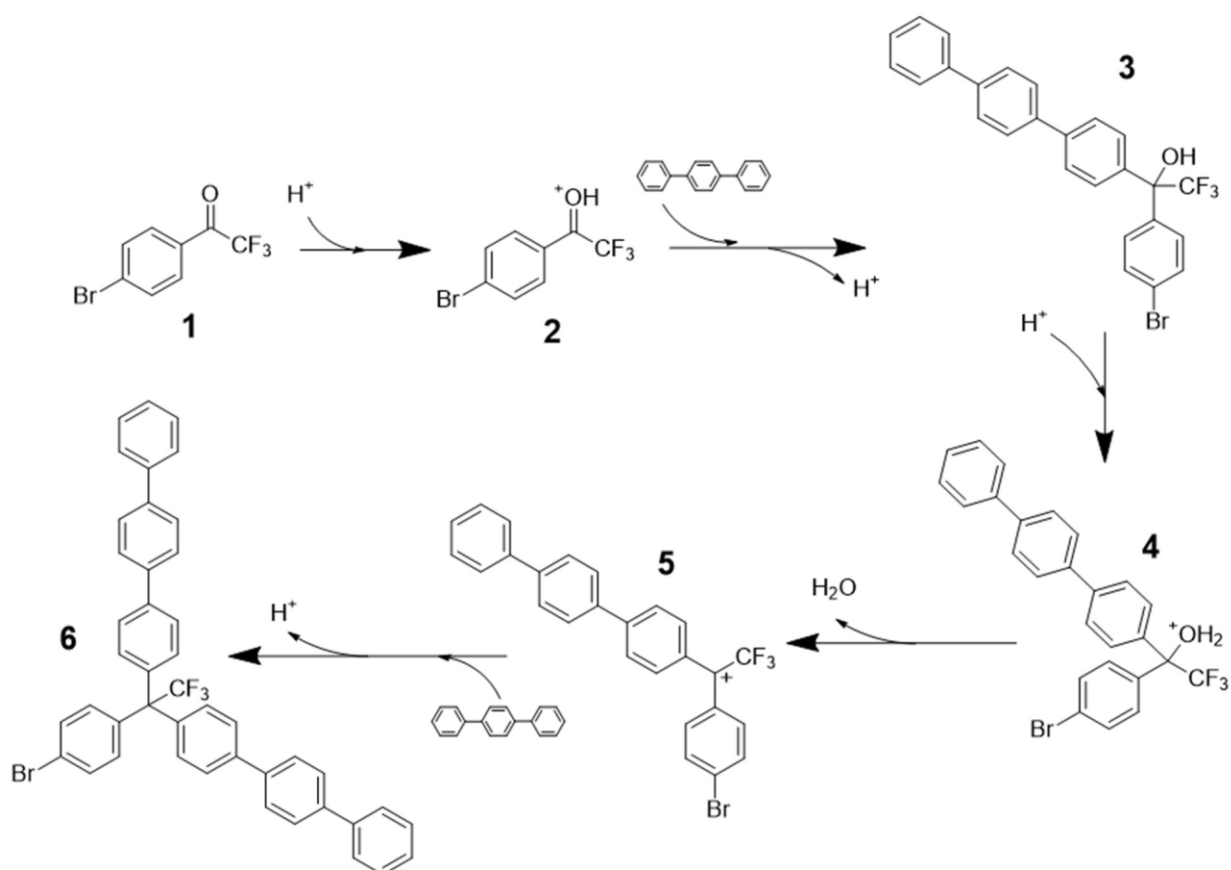
Figure 6-46. Reaction scheme for the ether-free backbone.

Figure 6-47 shows the NMR spectra of the backbone after precipitation in methanol and the drying step. The integral of each peak is in perfect accordance with the expected one and no further peak was observed, meaning that the purity of our ether-free backbone is excellent.
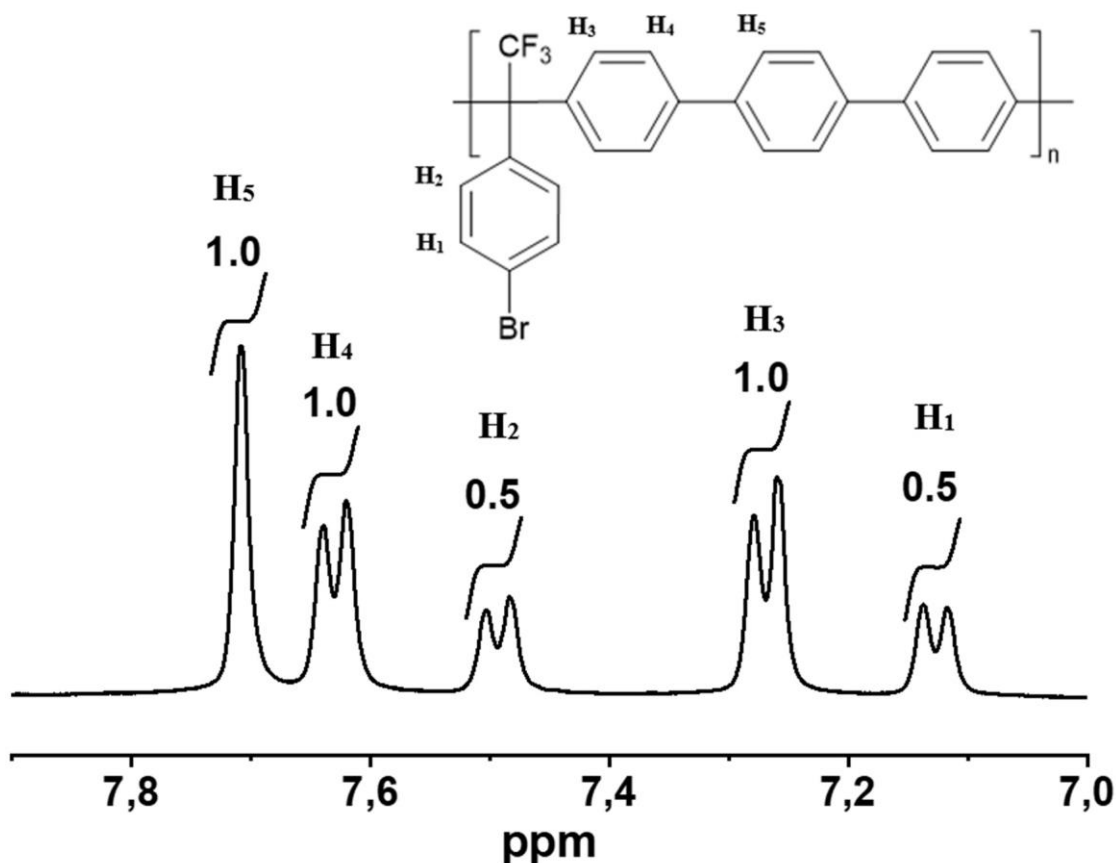
Figure 6-47. ^{1}H NMR spectrum recorded for the ether-free backbone.

The molecular weight, Mn, of the obtained polymer, was measured by GPC, and a value of about 500 000 g mol^{-1} with a polydispersity index of 1.67 was obtained, which is higher than the previous work using this hydroxyalkylation reaction[187].

The use of an already brominated monomer (4'-brom-2,2,2-trifluoracetophenone) allows us to obtain directly the brominated polymer and thus suppress the step that was used in our group to prepare other single-ion conducting polymer[188,189,190] rendering again this synthesis easier and safer at the lab scale. The chemical bonding of the anionic side chain to the backbone via a copper-catalyzed Ullmann-type coupling reaction was already used for other single-ion conducting polymers and allowed for good yield with sufficient substation percentage.

141

After the coupling reaction, the NMR spectrum of the ether-free single-ion conducting polymer was recorded (**Figure 6-48**). This spectrum allows us to calculate the grafting degree of perfluoroalkyl sulfonimide groups with the following equation:

$$N_{NMR} = \frac{3 * I_2}{2 * I_1}$$

where N_{NMR} is the number of ionic functions per repeating unit, where I_1 is the peak integral of fluorine from the ether-free backbone (-113.52 ppm) I_2 is the peak integral of F_2 (-57.81 ppm). With the integral values on the spectra, we determined that there are 0.80 ionic functions per repeating unit. This value can then be used to determine the Ionic Exchange Capacity (IEC) of the polymer with the following equation:

$$IEC_{NMR} = N_{NMR} \times IEC_{th} = N_{NMR} \times \frac{n}{M_{SIPE\,th}}$$

Where n is the number of repetition units, and $M_{SIPE\,th}$ the molar mass of the polymer considering one ionic side chain per repetition unit. The calculated IEC_{NMR} is 0.98 meq Li^+ g^{-1}. This value is slightly lower than for the polymer previously presented.
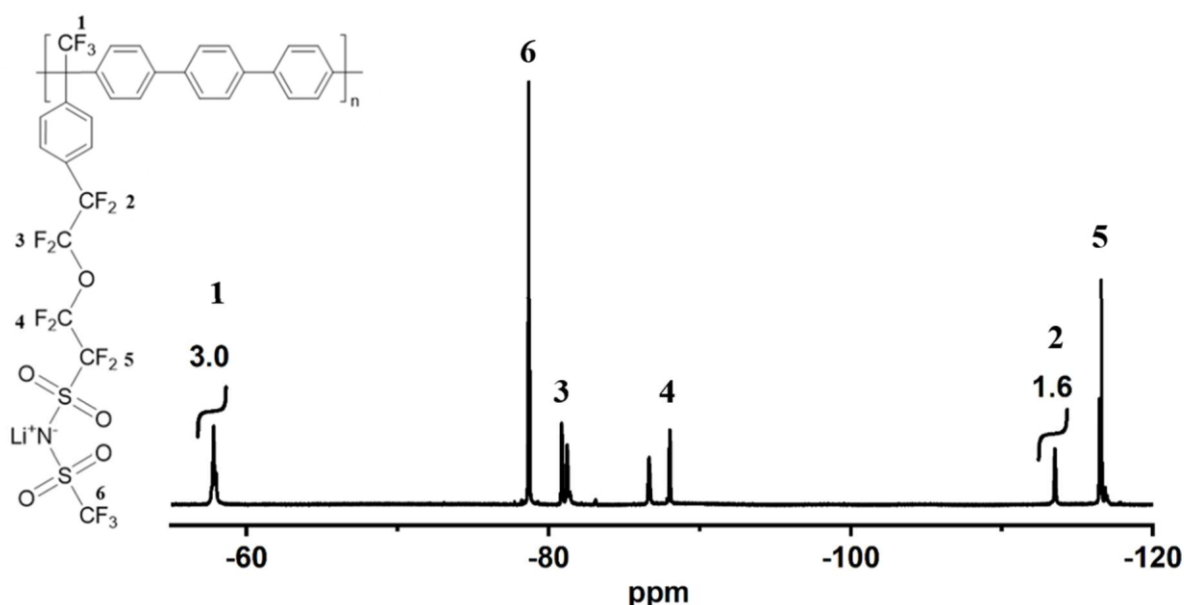
Figure 6-48. ^{19}F NMR spectrum recorded for SIPE-EF recorded in DMSO.

6.3.2 Membrane Preparation and Thermal Characterization

The membrane obtained by casting were doped with different amounts of PC (**Table 6-1**). The lithium concentration can be calculated from the IEC and the solvent uptake (SU) as follow:

$$C_{\mathrm{Li}} = \frac{IEC}{1 + 0.01 \times SU} \quad with \quad SU = \frac{w_\mathrm{s} - w_\mathrm{d}}{w_\mathrm{d}} * 100$$

where w_s is the mass of the swollen membrane and w_d the mass of the dry membrane.

By adding different amounts of solvent, the Li concentration in the membrane will decrease from 0.63 to 0.34 mol kg^{-1}. Even when 55% of solvent was added, a self-standing membrane was obtained with a thickness of about 100µm with rather good mechanical stability when reasonably stretched making this solvent-doped membrane easy to manipulate.

Sample name	C_{Li} (mol kg^{-1})
SIPE-EF dry	0.98
SIPE-EF+PC (35%)	0.63
SIPE-EF +PC (45%)	0.53
SIPE-EF +PC (55%)	0.44
SIPE-EF +PC (65%)	0.34

Table 6-1. Lithium concentration (C_{Li}) from the single-ion conducting polymer membrane doped with different amounts of propylene carbonate.

The thermal stability of the polymers and doped membranes were evaluated by the TGA data (**Figure 6-49**). The degradation of dry polymer starts at a temperature higher than 300°C. For SIPE-EF+PC, the mass losses occur in two main steps. The first one corresponds to the evaporation of the PC from the membrane and starts around 160 °C. This mass loss can also be used to confirm the solvent uptake calculated from the dry and swollen weight of the membrane. In this case, the calculated solvent contents were 35, 45, 55, and 65 % and the TGA data give a value of 37, 42, 57, and 62% of solvent uptake, showing that the swelling process

is quite accurate for the polymer electrolyte preparation. The second weight loss, starting at about 350 °C corresponds to the thermal degradation of the polymer that can be observed on the TGA data for the dry polymer power. This proves that the PC does not impact the thermal degradation of the polymer. The comparison with the TGA data for PC demonstrates that the incorporation of PC in the polymer retard the evaporation by about 15 °C, indicating a good interaction between the polymer and the doping solvent. In the end, these results show that this new ether-free single-ion conducting polymer exhibits good thermal properties even when swollen with carbonated solvent and can be further investigated for battery applications.
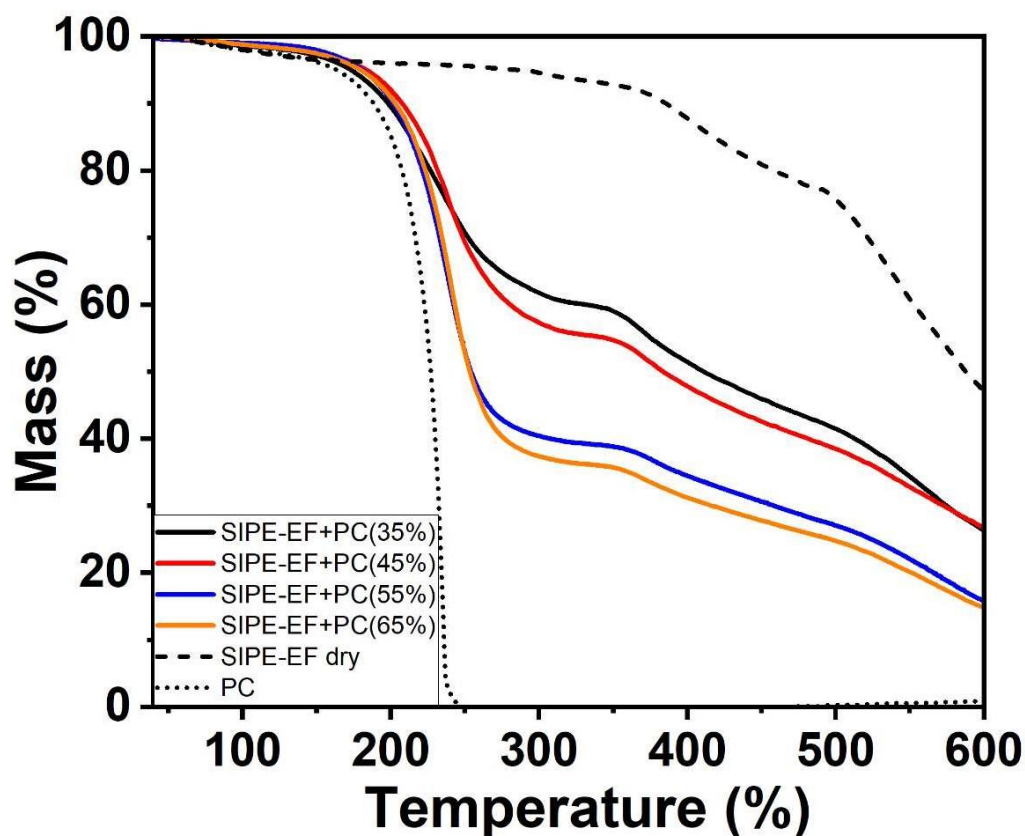
Figure 6-49. TGA curve of the SIPE-EF after casting and after swelling with propylene carbonate.

The thermal behavior was analyzed by DSC. Regarding the dry polymer (**Figure 6-50**) it shows only a glass transition temperature (T_g) of about 165 °C. When the PC is added a very curious

behavior can be observed. Firstly, a new Tg appears at -33 ±2°C and seems to be dependent on the amount of added PC. The T_g from 165 °C first decreases to 146°C (for 35% PC content) and then with adding more and more PC, a slight increase in T_g is observed (up to 150 °C for 65% PC content), as if the chain would become more rigid despite adding more solvent. To understand this behavior, we can suppose that PC is not compatible with the backbone and that, when we add it, it interacts only with the ionic functions creating the phase separation between the ionophobic domains (backbone) and ionophilic domains (ionic functions). The flexibility of the ionic clusters help in better organization of the polymer backbone. The T_g of the ionophilic domain remains more or less constant, probably because at 35% PC content, it is already saturated in solvent. More added solvent will be probably located between the domains and have no impact on the flexibility of ionophobic or ionophilic domains.
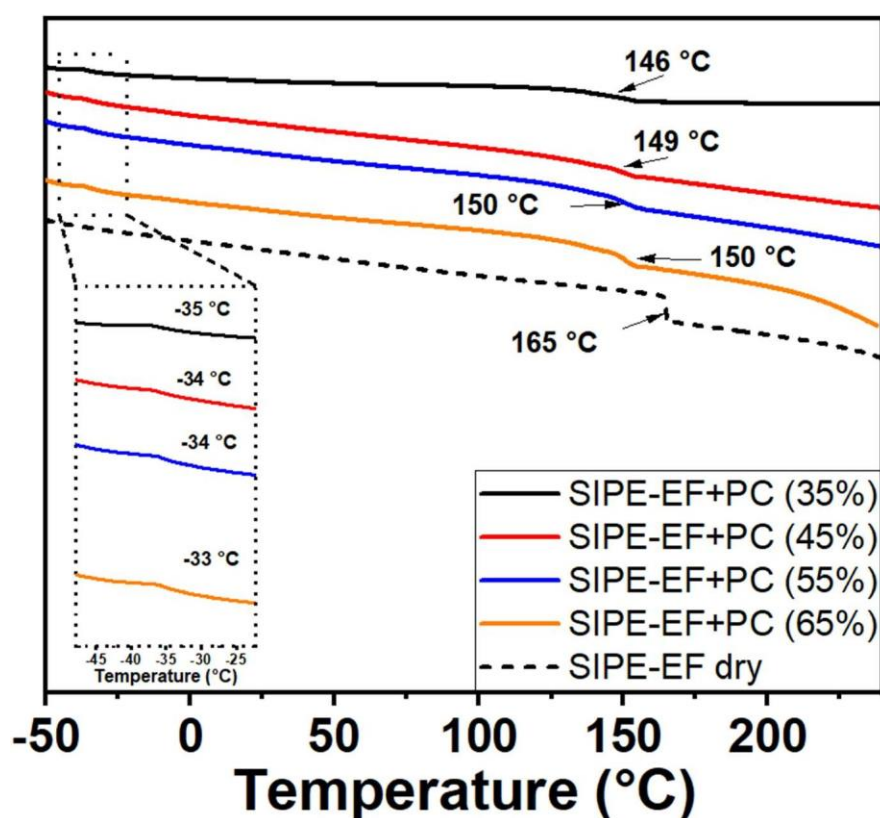
Figure 6-50. DSC diagrams of the SIPE-EF after casting with DMSO and after swelling with different propylene carbonate weight percentages.

145

6.3.3 Electrochemical Properties

In the case of new material for battery, it is usually admitted that the ionic conductivity must exceed 10^{-4} S cm^{-1} at room temperature for a potential industrial implementation. In the case of PEO-based polymer electrolytes, the key factor is the lithium salt concentration that commonly has an optimal value to obtain the best conductivity[191]. With our SIPE-EF, the Li peflurosulfonimide is grafted on a rigid and non-solvating polymer chain. Thus, to dissociate and transport the Li cation, the PC solvent was added, and therefore, the key factor for conductivity is the solvent content (SC). The conductivities as a function of the temperature for different SC are presented in **Figure 6-51**. The conductivity increases with the SC and all the membranes exhibit a typical Vogel-Tramman-Fulcher (VTF) behavior which indicates that the lithium cations transport is related to the coordination of the cations with the solvent molecules and therefore, the higher the number of solvents molecules, the higher the cations transport and the higher the ionic conductivity. In this particular case, the higher amount of solvent does not correspond to higher T_g and therefore not to higher mobility of the side chain. This means that the increase in conductivity is probably mainly due to the enhancement of the ion pair dissociation, a better percolation, and lower tortuosity of ionic domains, which consequently increase the ionic conductivity of the electrolyte despite the decrease of the lithium concentration with the increase of solvent content (**Table 6-1**). The ionic conductivity of the SIPE-EF+PC with an SC of 65% gives no reproducible results because the membrane becomes too sticky and difficult to manipulate. The data plot in **Figure 6-51** exhibited ionic conductivities higher than 10^{-4} S cm^{-1} for all electrolytes at a temperature of 20 °C or higher which are excellent results exceeding the criteria for potential commercial implementation ($>10^{-4}$ S cm^{-1} at 25 °C). For the rest of the study, we selected the SIPE+PC electrolyte with a solvent content of 55% to ensure the best ionic conductivity and the most suitable mechanical properties.

.
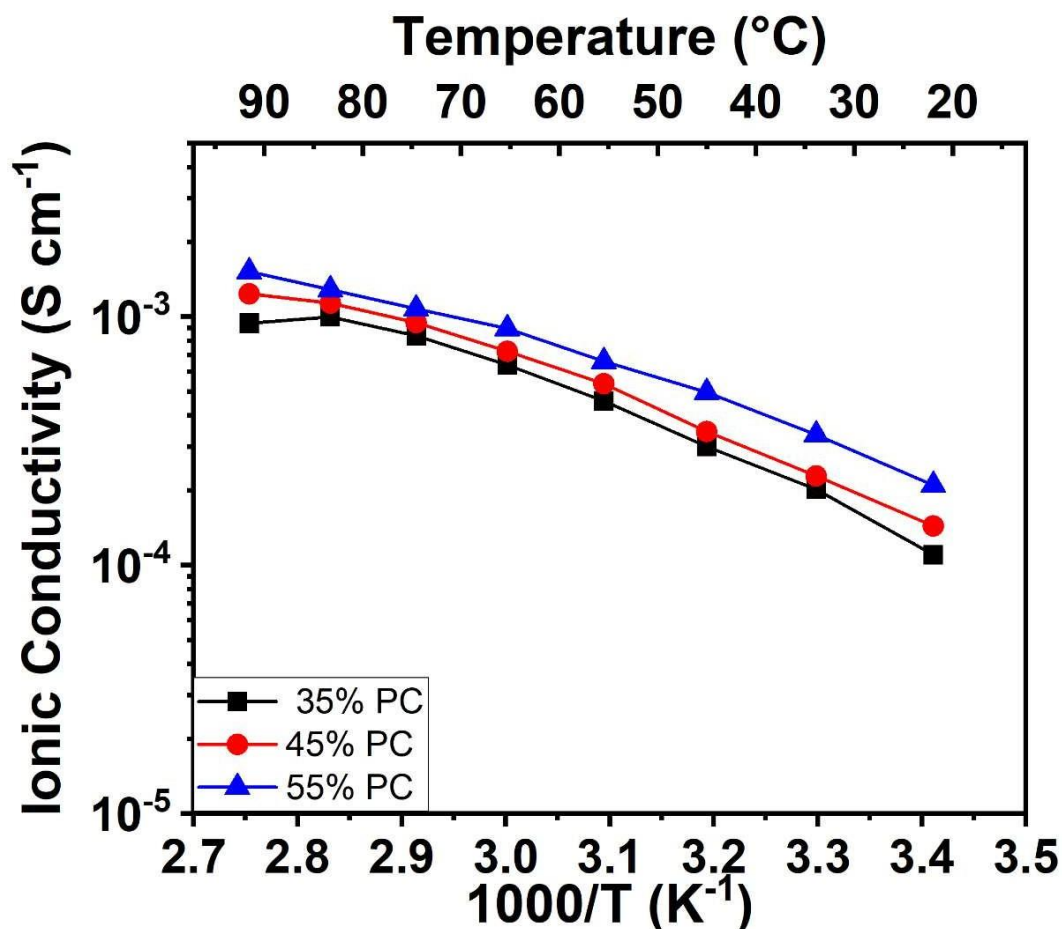
Figure 6-51. Conductivity, as a function of temperature, of the SIPE-EF swollen with different weight percentages of propylene carbonate.

For further information about the transport properties of polymer electrolytes, the Bruce and Vincent potentiostatic polarization method was used (**Figure 6-52**). The current measured in **Figure 6-52.a** went through a quick drop at the very beginning of the polarization with stabilization at a constant current after about 10 minutes. The impedance spectra before and after 27 minutes of polarization gave slightly different results with a higher interfacial resistance, indicating changes of the SIPE-EF+PC‖lithium interface i.e., formation of a SEI. Nevertheless, a lithium transference number of 0.94 was obtained. This value is slightly lower than one and may be explained by the presence of free anions resulting from the SEI formation that will reduce the transference number value.
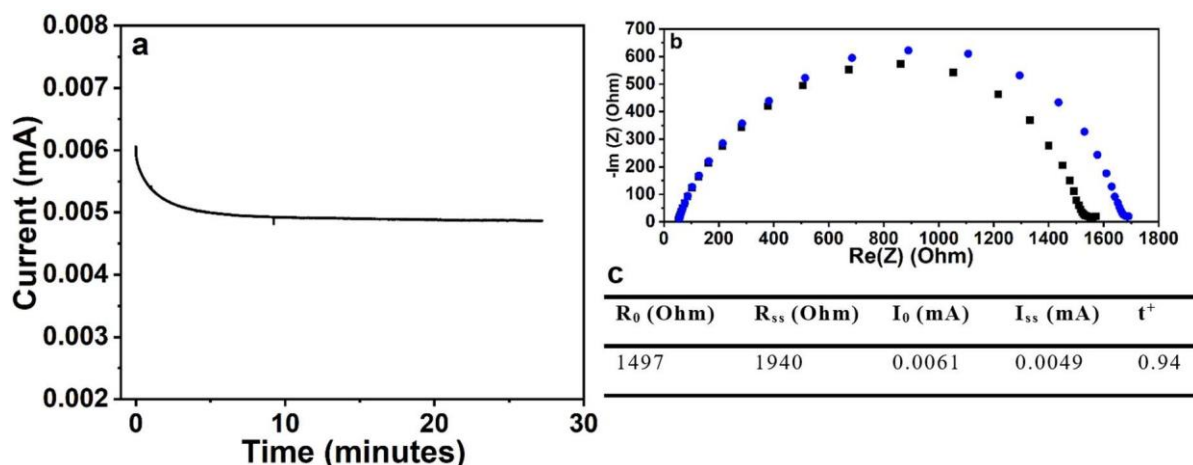
Figure 6-52. Determination of the transference Number by Bruce and Vincent potentiostatic method. a) chronoamperometry data obtained when applying a constant voltage of 10 mV to a symmetrical lithium/lithium cell containing the SIPE as electrolyte. b) Impedance measurement before (black) and after (blue) the chronoamperometry measurement. c) Values used in the Bruce and Vincent equation to determine the transference number

The limiting current density was also measured at 20 °C (**Figure 6-53**) and the obtained value was 0.4 mA cm^{-2}. The limiting current density being related to the mobility of the cation, a higher value was expected considering the excellent ionic conductivity and the close to one value of the transference number. This is probably related to the interfacial change already observed in the transference number determination. The polarization of the cell seems to create a more resistive interface, which could explain the rather low limiting current density.
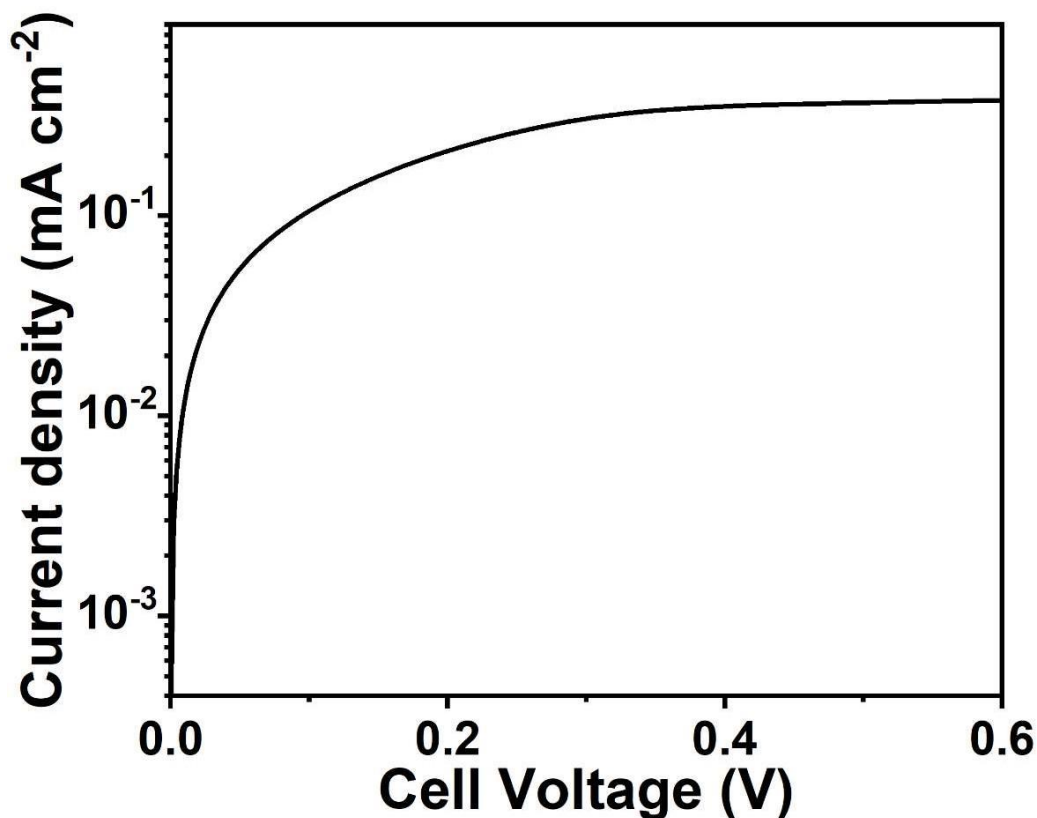
Figure 6-53. Determination of the limiting current density of SIPE-EF swollen with 55 wt.% of PC by linear sweep voltammetry at 20 °C (sweep rate = 0.01 mV s^{-1}).

The determination of the electrochemical stability window of the new ether-free SIPE-EF+PC is presented in **Figure 6-54**. The anodic scan (**Figure 6-54** (black)) reveals no particular peak before a sharp increase starting around 4.3 V corresponding to the decomposition of the polymer electrolyte. The current density reached 10 μA cm^{-2} (commonly used value to determine the anodic stability) at 4.5 V which can be considered as the anodic stability of our new ether-free single-ion conducting polymer electrolyte.
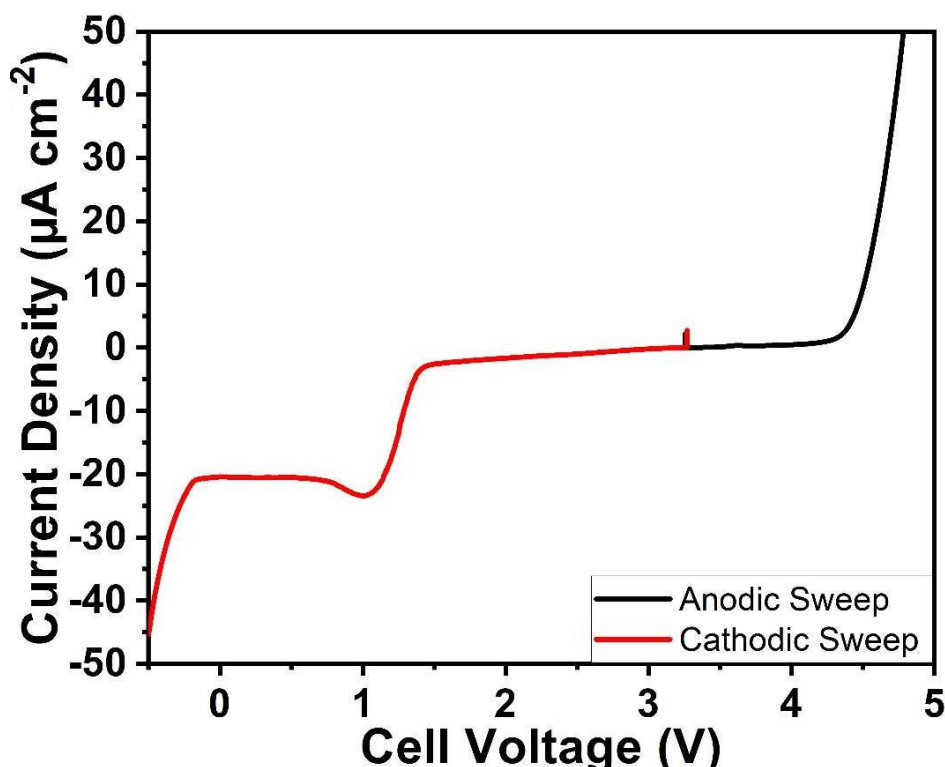
Figure 6-54. Determination of the electrochemical stability window of SIPE-EF swollen with 55 wt.% PC by linear sweep voltammetry at 20 °C using Li/stainless steel cells (sweep rate = 1 mV s^{-1}).

On the cathodic scan of the linear sweep voltammetry (**Figure 6-54** (red)), the sharp increase in the current density below 0 V is assigned to the metallic lithium deposition, the other increase at about 1.2 V was already observed in a previous study and can be attributed to the reductive decomposition of propylene carbonate[192] superposed with the reductive decomposition of remaining traces of DMSO from the casting process[145]. Furthermore, the cyclic voltammetry conducted on this SIPE-EF+PC (**Figure 6-55**) indicates that this peak disappears after the initial cathodic scan, suggesting a stabilization of the lithium∥electrolyte interphase. For the first cycle, a strong reduction peak was observed between 0 to -0.3 V, which is ascribed to lithium plating on the stainless-steel surface[155]. Surprisingly, this sharp current decrease was suppressed after the first cycle. This could suggest that very low amount of lithium metal plated on the stainless steel during the first cycle (0.0083 mAh cm^{-2}) can reacted with the electrolyte to form

dead lithium and/or passivate the stainless-steel electrode, which will block the lithium plating in the next cycles.
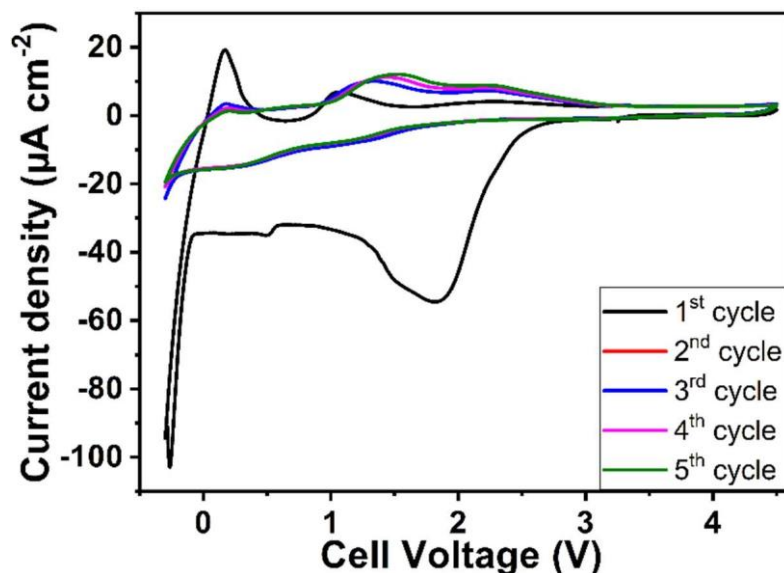
Figure 6-55. Cyclic voltammetry study of the SIPE swollen with 55 wt.% propylene carbonate at 20°C using Li/Stainless steel (sweep rate, 1 mV s^{-1}).

Such value must be handled carefully due to the sweep rate dependence of most electrochemical phenomena in LSV measurement. Overall, both electrochemical characterization methods confirm an anodic stability up to 4,5 V.

6.3.4 SIPE in Symmetrical lithium‖lithium Cells

The ability of our ether-free single-ion conducting polymer to transfer lithium cation from one electrode to the other is an important factor for further battery application. This was evaluated by lithium stripping-plating tests conducted in symmetrical Li/Li cells comprising the SIPE-EF+PC as the electrolyte; subjected to different current densities. The resulting data are presented in **Figure 6-56**. For the low current densities, i.e. 0.018 and 0.044 mA cm^{-2}, rather high overpotentials (respectively 0.1 and 0.2 V) are observed with an increase of the

overpotential during a stripping or plating step which was a bit surprising. Indeed, it is well known that the overpotential during stripping or plating for single-ion conducting polymer electrolyte; has a rectangular shape with a constant overvoltage. This is due to the immobility of the anions and the absence of charge gradient in the electrolyte[193]. In our case, this increase is closer to the behavior of the common salt in polymer electrolyte[194] with the difference that a steady state still can be obtained with longer stripping time, corresponding to a single-ion conducting polymer behavior. This non-immediate steady state is not completely clear to us but might be due to a high charge transfer resistance at the SEI, which would be in accordance with the increase of the interfacial resistance observed during the transference number measurement.
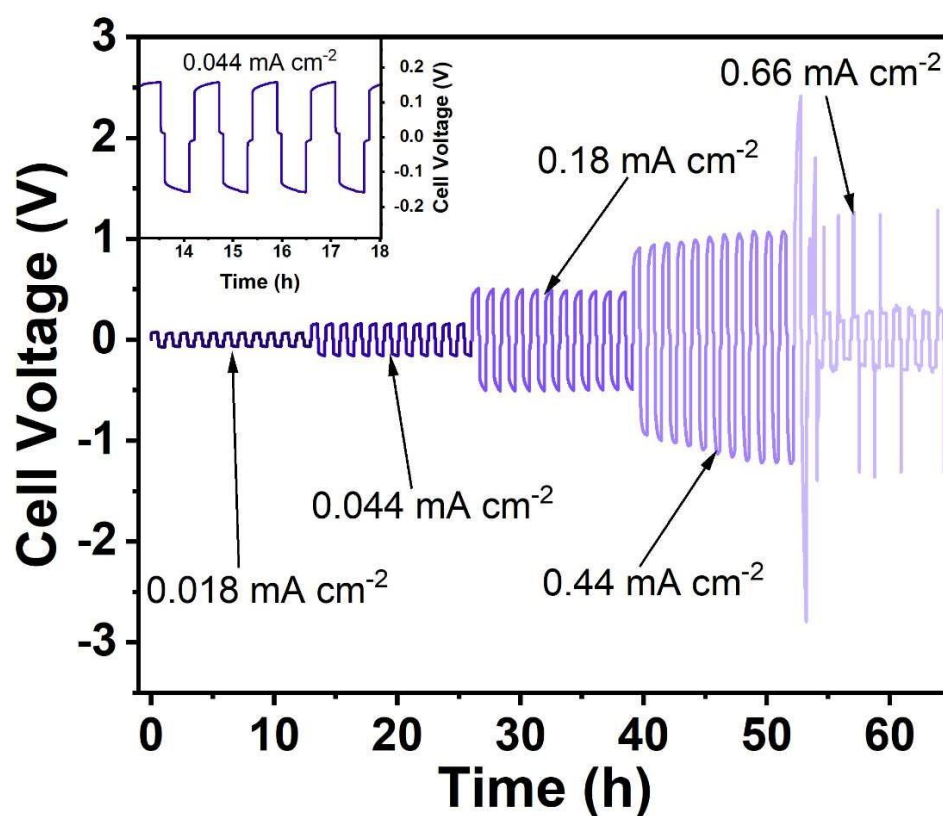
Figure 6-56. Investigation of the stripping/plating behavior of the SIPE-EF swollen with 55 wt.% of propylene carbonate in Li/Li symmetrical cells at 20 °C: (a) Li/Li cell subjected to elevated currents of 0.02, 0.05, 0.2, 0.5, 0.75 mA, *i.e.*, 0.017, 0.044, 0.18, 0.44, 0.66 mA cm^{-2}, respectively (Ø = 12mm and electrode surface area = 1.131 cm^{-2}) (each cycle is composed of

30 minutes stripping step followed by a 5 minutes rest, a 30 minutes plating step and another 5 minutes rest).

Another idea was to relate this increase to a degradation of the polymer forming anionic species and creating a charge gradient. This hypothesis was discarded by the overpotential reached at the end of each stripping or plating step. It is constant upon cycling, indicating no degradation of the polymer, at least at the lowest current density. It was also confirmed by the impedance spectroscopy and post-mortem SEM analysis made after cycling at 0.044 mA cm^{-2}. **Figure 6-57.a** shows the EIS data after the first (black) and the last (blue) full stripping plating cycle (i.e. after 30 minutes of plating, 5 minutes rest, 30 minutes of stripping, and 5 minutes rest). The observed semi-circles correspond to the electrode/electrolyte interfacial resistance. They are perfectly superposing demonstrating a stable electrode‖electrolyte interface and consequently confirming the non-degradation of the polymer. **Figure 6-57.b** shows the lithium surface after 10 stripping plating cycles at 0.044 mA cm^{-2}. A rather flat and homogeneous surface can be observed with no evidence of surface degradation or lithium dendrite growth, again confirming the previous conclusion. Generally speaking, the rather good stripping/plating behavior at low current density is considered as encouraging for further battery application.
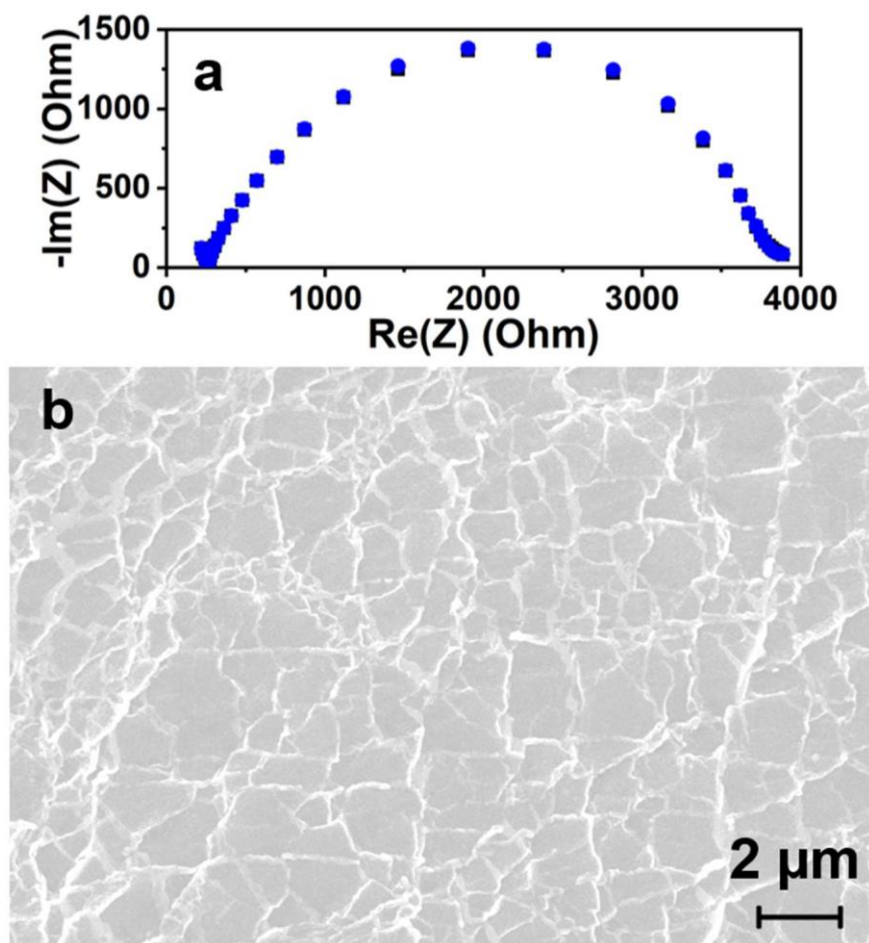
Figure 6-57. Nyquist plot of the EIS data of the Li/Li cell recorded after the first cycle (black) and after the last cycle (blue) and post-mortem SEM images of the lithium surface after the last cycles at 0.044 mA cm^{-2}.

But with an applied current density of 0.44 mA cm^{-2}, it can be seen that the overall overpotential is increasing upon cycling which indicates a degradation of the SIPE-EF+PC. This current density value is similar to the previously determined limiting current density, so it is not surprising to observe a degradation during striping/plating. This is even more significant at 0.66 mA cm^{-2} where the highly fluctuating current corresponds to the formation of dendrites and short circuits in the cell. The impedance spectroscopy data (**Figure 6-58.a**) and post-mortem SEM analysis (**Figure 6-58.b**) after cycling at 0.44 mA cm^{-2} confirm these previous observations. On the EIS data, the semi-circle after the ten stripping/plating cycles reveals a

much lower interfacial resistance indicating a change at the electrode/electrolyte interface. This kind of decrease in the interfacial resistance has already been reported. This is attributed to the higher amount of lithium being non-homogeneously deposited and creating a porous surface that allows for dendrite growth when applying a higher current[195]. The post-mortem SEM images (**Figure 6-59.b**) confirmed this assumption since a rather porous and non-homogenous lithium surface can be easily observed.
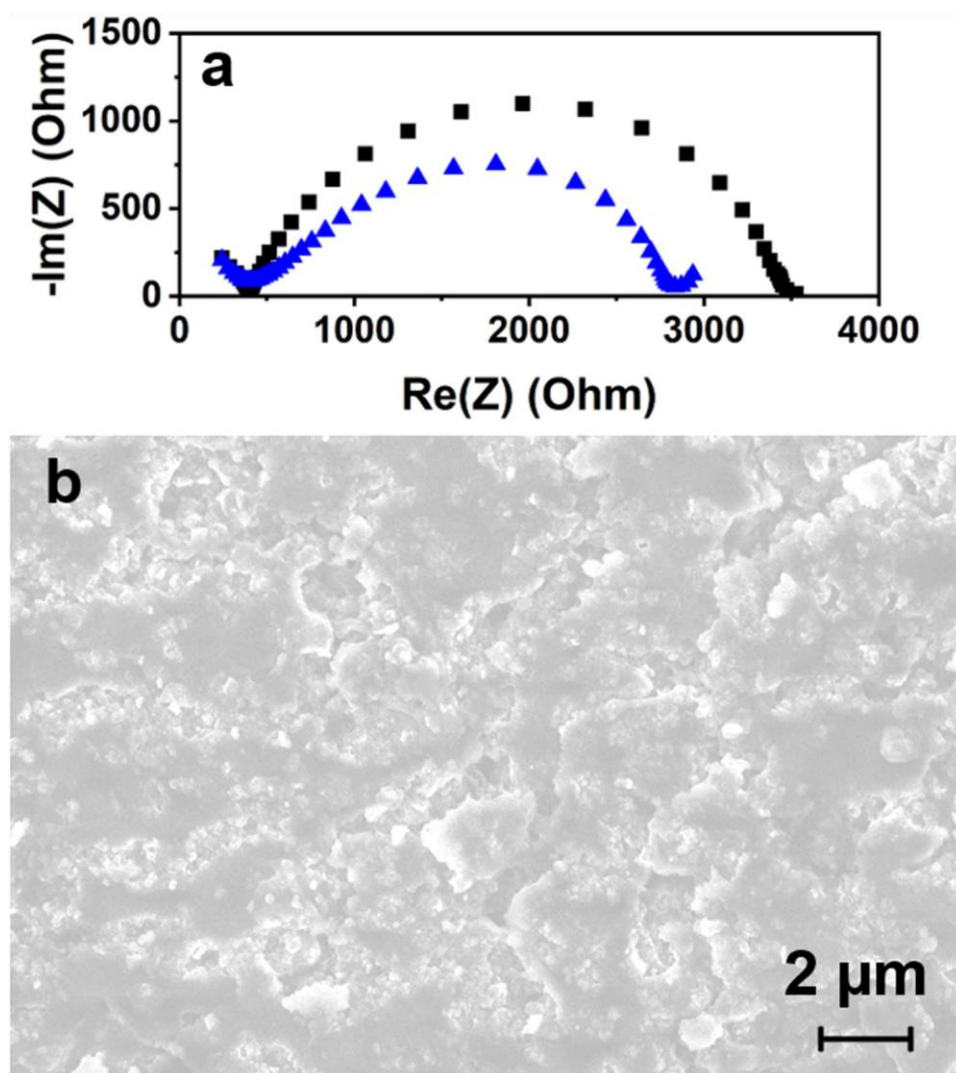
Figure 6-58. Nyquist plot of the EIS data of the Li/Li cell recorded after the first cycle (black) and after the last cycle (blue) and post-mortem SEM images of the lithium surface after the last cycles at 0.44 mA cm^{-2}.

Nevertheless, this threshold value for the growth of lithium dendrite is in good accordance with the limiting current density measured earlier. In a work by Jiang et al.[196], it has been shown that the potential at which a -CF$_3$ group can be reduced highly depends on the surrounding groups. The authors utilize quantum chemical calculations to predict the reduction and oxidation potential of various trifluoromethyl-containing compounds. In the case of a trifluoromethyl group surrounded by 3 phenyl groups (CF$_3$-C(Ph)$_3$), they obtained a potential of 0.63 V vs Li$^+$/Li (-2.41 V vs SHE) for the anionic reduction. It means that the -CF$_3$ group is reduced to a -CF$_3^-$ and the rest to a radical form ($^\cdot$C(Ph)$_3$)) (**Figure 6-59**). During the stripping/plating test, the overpotential reaches this value when a higher current density than the limiting current density is applied, meaning that this degradation could happen to the polymer backbone degradation.
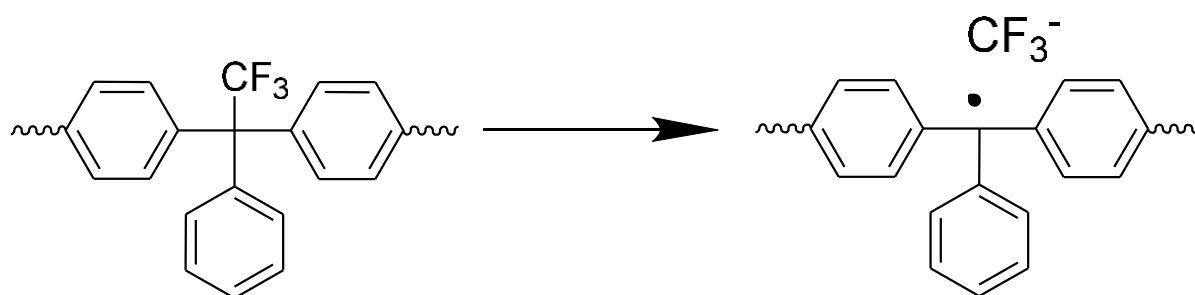
Figure 6-59. Polymer backbone degradation mechanism by anionic reduction.

In this case, the radical is extremely stable due to the high electron delocalization. On another hand, the -CF$_3$ anion will react with lithium and form a layer on top of the lithium metal electrodes. This resistive layer can explain the high overpotential observed at 0.44 and 0.66 mA cm^{-2} and the polymer degradation by anionic reduction of the CF$_3$ groups explains the highly fluctuating current observed at 0.66 mA cm^{-2}. This assumption is generally supported by the results of the EDX mapping (**Table 6-2**). The results show that fluorine and carbon are the two prominent elements at the lithium surface after 10 stripping/plating cycles at 0.44 mA cm^{-2} compared to the pristine lithium metal. This confirms that the degradation of the polymer is mainly due to a reaction between lithium metal and a fluorinated group, most probably the

trifluoromethyl from the backbone. This degradation mechanism is highlighted when using high current density but is most probably also happening at low current density even if the SEM and impedance data do not show any evidence. Indeed, the rather high overpotential at 0.018 and 0.44 mA cm^{-2} indicates that the formation of a resistive SEI, most probably by the reaction discussed before. Overall, these stripping/plating results and linear/cyclic voltammetry data show that our ether-free electrolyte is unstable toward lithium.

	Pristine	until 0.44mA cm^{-2}	until 0.44 mA cm^{-2} with PEO interlayer
Element	wt.%	wt.%	wt.%
C	14.6	40.5	20.0
F	0.0	40.7	8.7
O	85.4	18.8	71.3

Table 6-2. Weight percentage, determined by EDX mapping, of carbon, fluorine, and oxygen measured at the lithium surface for the pristine lithium and after 10 stripping/plating cycles at 0.44 mA cm^{-2} for the polymer electrolyte without and with the PEO interlayer protection.

6.3.5 Improving the Lithium Compatibility with a PEO-Based Protective Interlayer

To overcome the poor compatibility observed between our ether-free single-ion conducting polymer electrolyte and Li metal we decided to try a multilayer system with a protective layer made of a PEO:LiTFSI (EO:salt ratio of 10:1) polymer electrolyte. After preparation by a hot-pressing process, a thickness of about 15 μm was obtained for the PEO:LiTFSI membrane. The SIPE-EF+PC membrane was placed between two PEO membranes to create the SIPE-EF+PEO-L multilayer electrolyte, which had a thickness of approximately 130 μm and exhibited excellent mechanical stability when stretched multiple times. The SIPE-EF+PEO-L

shows similar thermal stability as the SIPE+PC, as indicated by TGA analysis in the Appendix
. The transference number was measured to be $t^+= 0.56$ (Appendix), which is comprised
between the transference number of PEO:LiTFSI electrolyte with O:Li ratio of 10:1 ($t^+ \approx 0.2$
[197]) and the value measured for SIPE-EF+PC ($t^+=0.94$). It shows that, despite the introduction
of a dual-ion electrolyte, our system exhibited a high transference number which should reduce
the concern about charge gradient in the electrolyte. The main idea of the PEO:LiTFSI
protective membrane was to improve the compatibility with lithium, therefore we conducted
the same test as for the SIPE-EF+PC on the SIPE-EF+PEO-L electrolyte but at a temperature
of 40 °C. The stripping/plating behavior when subjecting the cell to 0.018, 0.044, and 0.18 mA
cm^{-2} (**Figure 6-60**) is similar to the one from SIP-EF+PC with a slightly lower overpotential,
probably due to better contact and better electrode/electrolyte interface. The interesting point
starts at 0.44 mA cm^{-2} where the increase in overpotential observed earlier has disappeared and
a slightly decreasing overpotential is now observed. This shows the good compatibility between
the multilayer system and the lithium metal, and the decrease is assigned to a better organization
of the electrode/electrolyte interface upon cycling. The results at 0.66 and 0.88 mA cm^{-2}
confirmed good compatibility with lithium metal and the suppression of lithium dendrite
growth. This improvement of the electrode/electrolyte interface is also shown by the results
when lowering the current back to 0.18 mA cm^{-2} since a lower overpotential can be observed
compared to the first cycling at the same current density. It also shows that our multilayer
polymer electrolyte is highly reversible in terms of lithium cation transport.
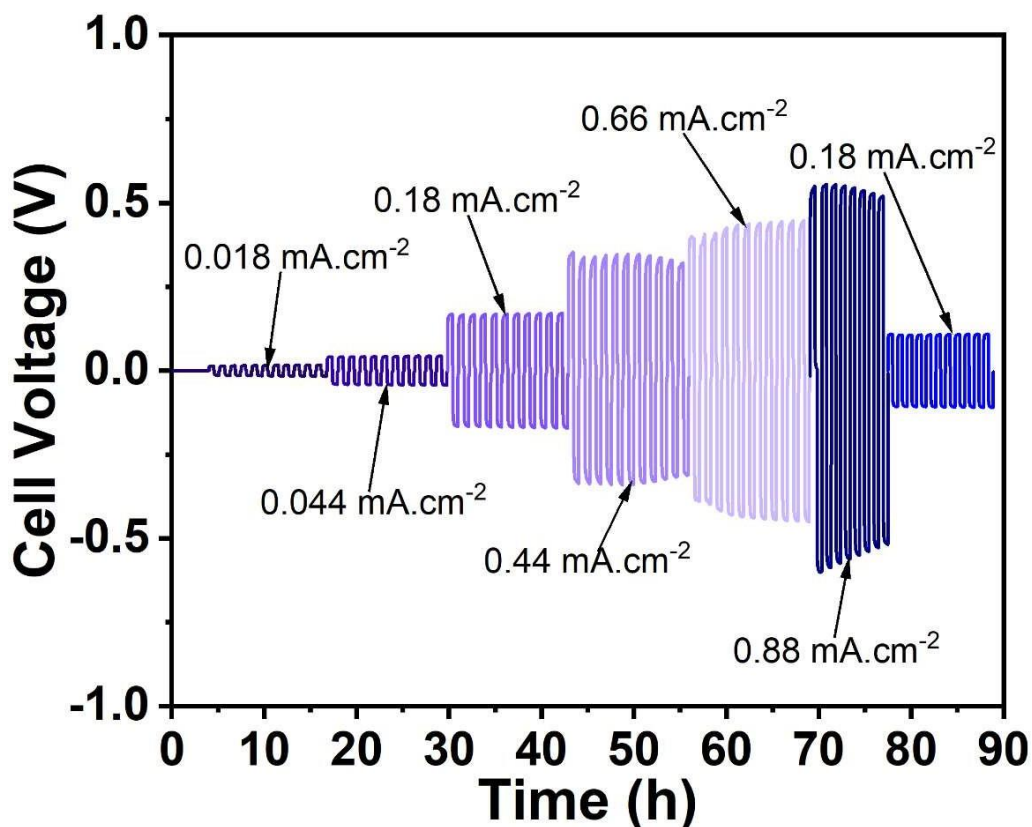
Figure 6-60. Investigation of the stripping/plating behavior of the SIPE-EF+PEO-L electrolyte in Li/Li symmetrical cells at 40 °C: (a) Li/Li cell subjected to elevated current 0.02, 0.05, 0.2, 0.5, 0.75, 1 mA, *i.e.*, 0.017, 0.044, 0.18, 0.44, 0.66, 0.88 mA cm^{-2}, respectively (Ø=12mm and electrode surface area= 1.131 cm^{-2}) followed by lowering current back to 0.18 mA cm^{-2} for subsequent stripping/plating cycles (each cycle is composed of 30 minutes stripping step followed by a 5 minutes rest, a 30 minutes plating step and another 5 minutes rest).

Subsequently, a long-term stripping/plating test was conducted with a symmetrical Li/Li cell subjected to 0.18 mA cm^{-2} for 500 hours (**Figure 6-61**). A constant overpotential was observed for the entire test and no indication of polymer degradation or lithium dendrite growth was observed, confirming the excellent compatibility of our SIPE-EF+PEO-L system with lithium metal.
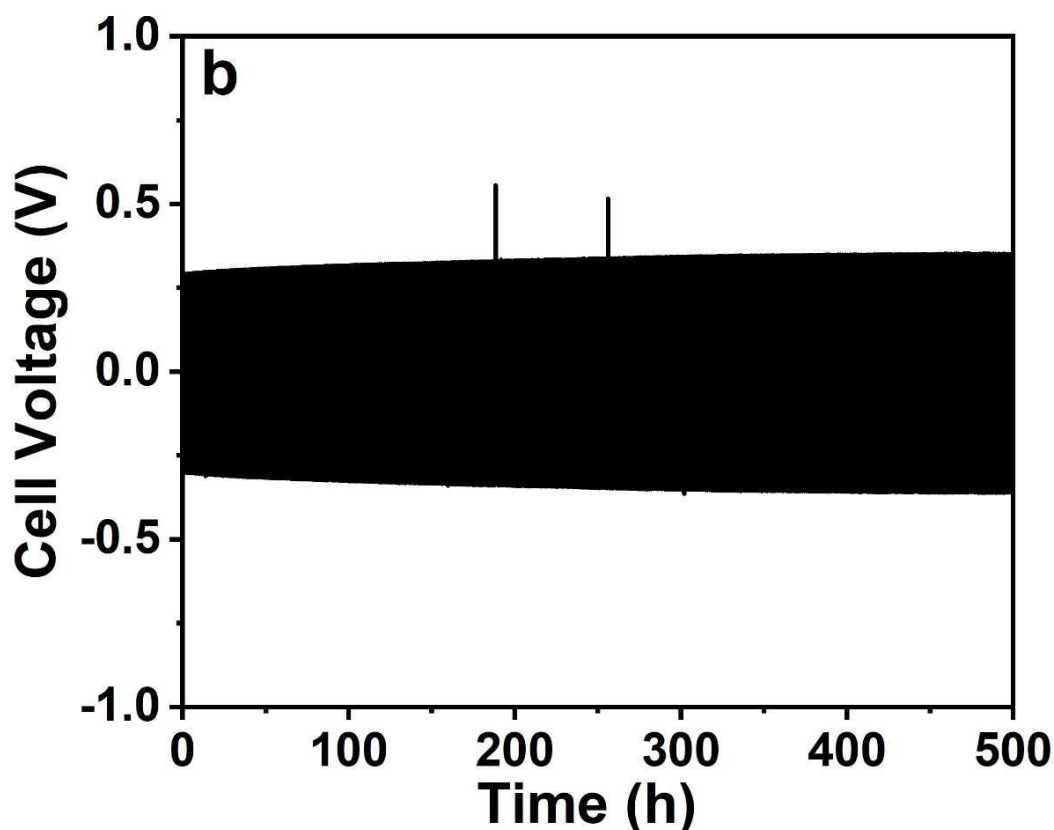
Figure 6-61. Investigation of the long-term stripping/plating behavior of the SIPE-EF+PEO-L electrolyte in Li/Li cell subjected to a constant current of 0.2 mA, *i.e.*, 0.18 mA cm^{-2} for 500 h with a similar cycling procedure as before.

Figures 6-62 show the comparison of the stripping/plating for the SIPE-EF+PEO-L (black) and the PEO:LiTFSI electrolyte alone (red) at two different current densities, i.e. 0.044 mA cm^{-2} (**Figure 6-62.a**) and 0.66 mA cm^{-2} (**Figure 6-62.b**). The data indicates that the behavior of the two systems is highly similar at low current density, exhibiting the same overpotential and a closely aligned potential evolution during a single stripping or plating step. However, the most notable observation is the significantly improved behavior at higher current density. In this case, the multilayer system exhibited a lower overpotential and a lower potential increase during one stripping or plating step, rendering this multilayer system an excellent candidate for potential battery applications. In the end, it seems that the SIPE-EF+PC benefits from the PEO:LiTFSI layer to achieve excellent compatibility with lithium metal but that the PEO:LiTFSI layer also

benefits from the SIPE-EF+PC membrane to ensure better lithium cation transport in the electrolyte.
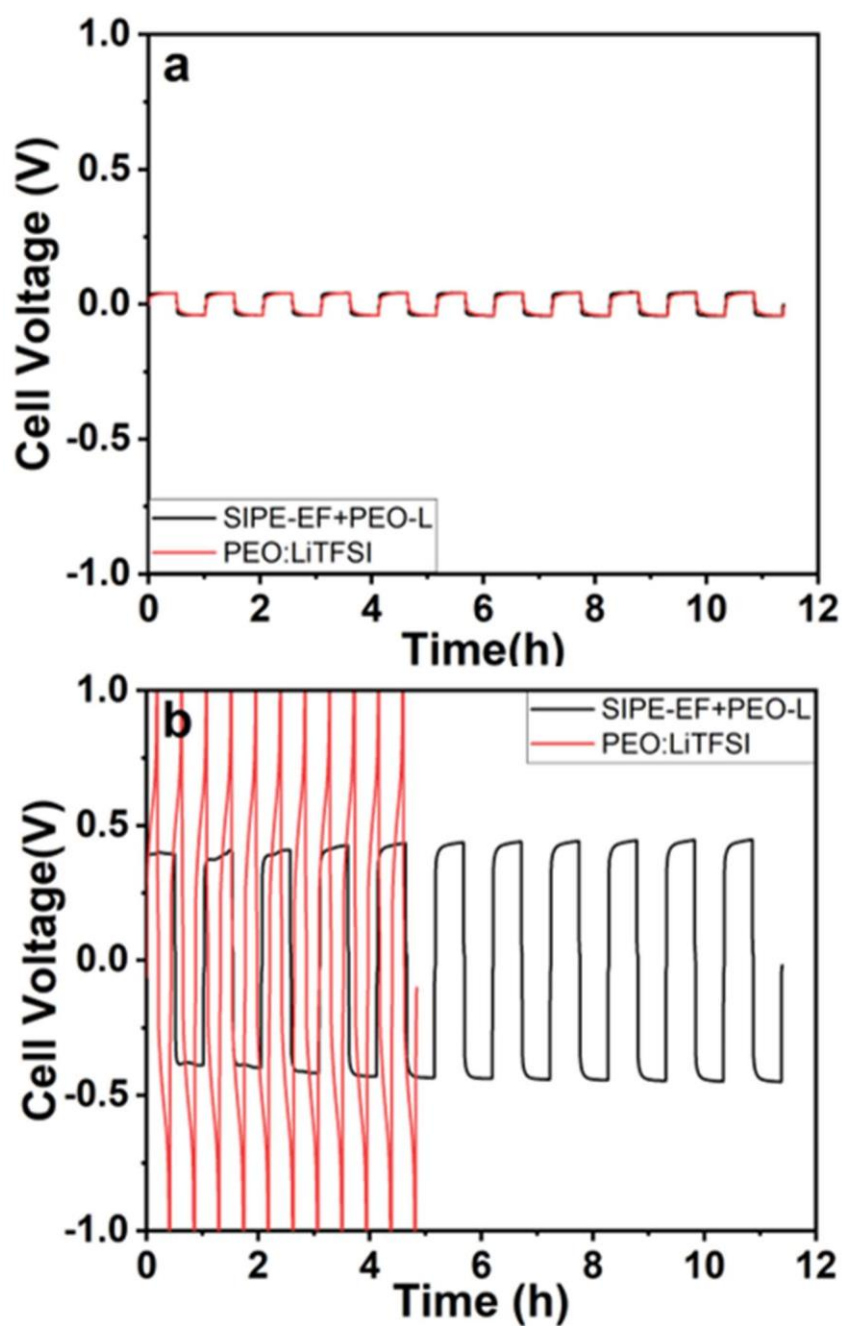
Figure 6-62. Comparison of the Li/Li stripping-plating cycling results of SIPE-EF+PEO-L (black) and PEO:LiTFSI polymer electrolyte when cycled at respectively 0.044 mA cm^{-2} (a) and 0.66 mA cm^{-2} (b).

6.3.6 Evaluation of the Multilayer System in Li║LFP Cells

To demonstrate the effectiveness of this multilayer electrolyte, we constructed Li/LFP cells, as shown in **Figure 6-63**. The PEO interlayer was positioned next to the lithium metal anode, and the ether-free single-ion conducting polymer was in direct contact with the LFP cathode.
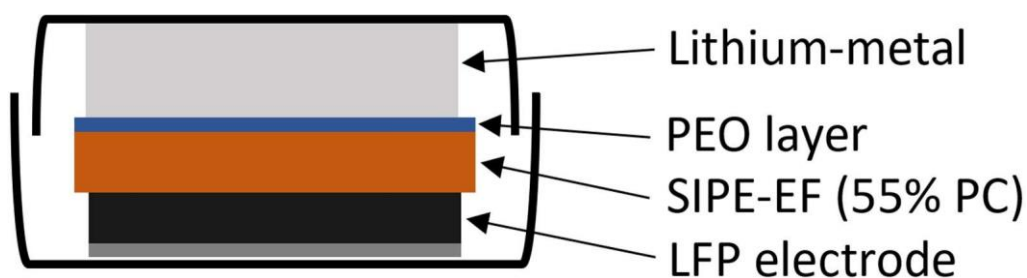
Figure 6-63. Scheme of the cell with the interlayer protecting the single-ion conducting electrolyte from lithium metal.

This cell was then subjected to a C rates capability test at 0.05C, 0.1C, 0.2C, 0.3C, 0.5C, and 1C followed by a long-term constant current cycling stability test at 0.1C with 1C= 170 mAh g^{-1} (**Figure 6-64**). The cell exhibited a reversible discharge capacity of about 160 mAh g^{-1} during the first cycles at 0.05C with a Coulombic efficiency of 90%. This indicates that some side reaction occurs during the first cycle but not in the subsequent ones since the Coulombic efficiency reaches 98% in the second cycle and is then higher than 99%. The C rates capability test exhibited a stable specific discharge capacity at all currents with a high Coulombic efficiency except for each first cycle, showing that side reactions still occur at higher currents, most probably to form a stable electrode/electrolyte interface. The C rates capability test also highlighted a decrease in the capacity with higher C rates (154 mAh g^{-1} at 0.1C, 152 mAh g^{-1} at 0.2C, 151 mAh g^{-1} at 0.3C, 150 mAh g^{-1} at 0.5C and 145 mAh g^{-1} at 1C). This decline in capacity is due to kinetic and mass transport limitation and increased polarization from the increased current density which leads to incomplete lithiation/delithiation of the active LFP material. Nevertheless, the value of 145 mAh g^{-1} at 1C and 40°C is an excellent result compared

to PEO versus LFP cells reported in the literature where much lower discharge capacity where obtained at all current densities[198,199,200].

The subsequent long-term cycling stability test at 0.1C shows an "initial" discharge capacity of 151 mAh g^{-1} with a Coulombic efficiency of 97% which will increase to reach >99% in the next cycle showing that the capacity decline observed during the C rates capability test is reversible. A good capacity retention of 84% after 200 cycles was observed with no indications of electrolyte degradation or lithium dendrite growth.
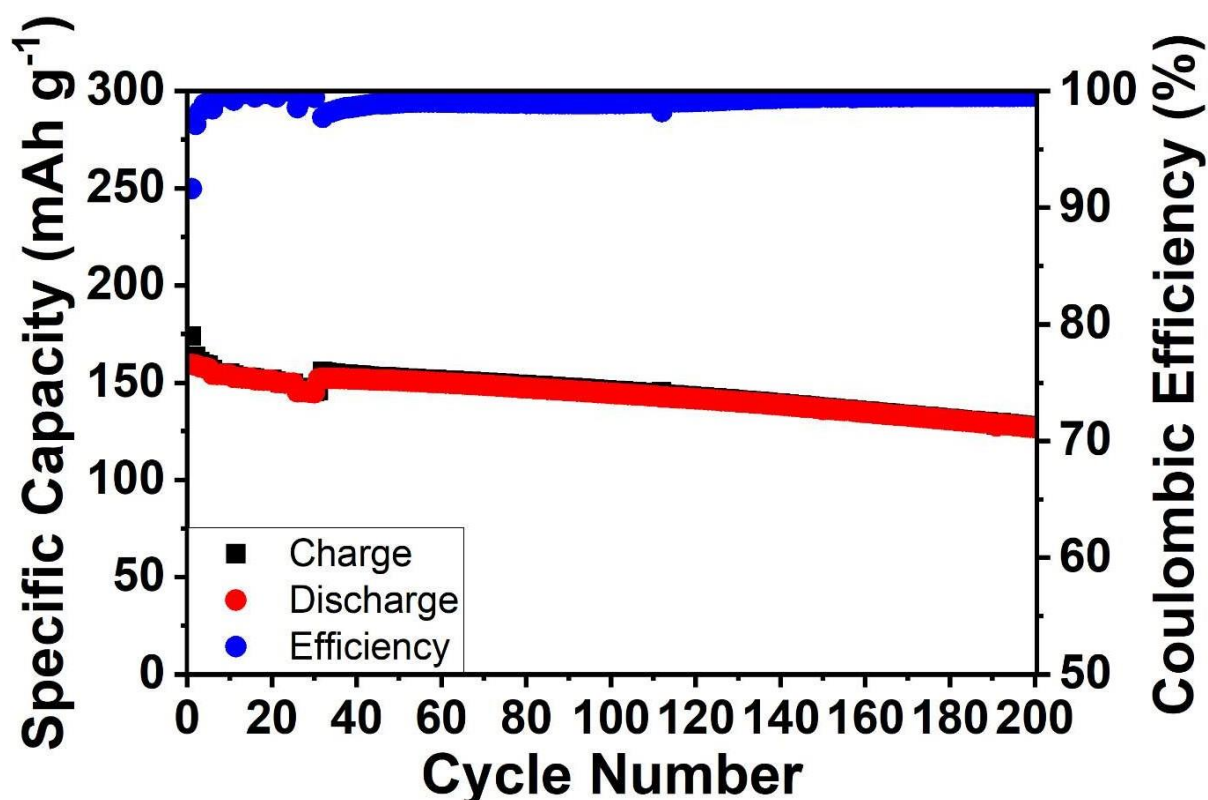
Figure 6-64. Investigation of SIPE-EF+PEO-L electrolyte in Li/LFP cells at 40 °C, charge, and discharge C rates capability (cycle 1 to 29) and long-term cycling capacity (cycle 30 to 200) and Coulombic efficiency of the Li/LFP cell.

The voltage profiles for the C rates capability test (**Figure 6-65**) highlight these excellent cycling results. The decrease of the plateau voltage at a higher current is an already reported result and is related to the low electric conductivity and/or lithium diffusivity in the LFP

electrodes[201]. The sharp end of the plateau at 0.05C suggests a complete lithiation/delithiation reaction. For the higher C rates, a slope was observed for the charge and discharge profile, which indicates that a part of the lithium from the active material is not easily accessible. This explains the capacity decline identified earlier in the cycling data.
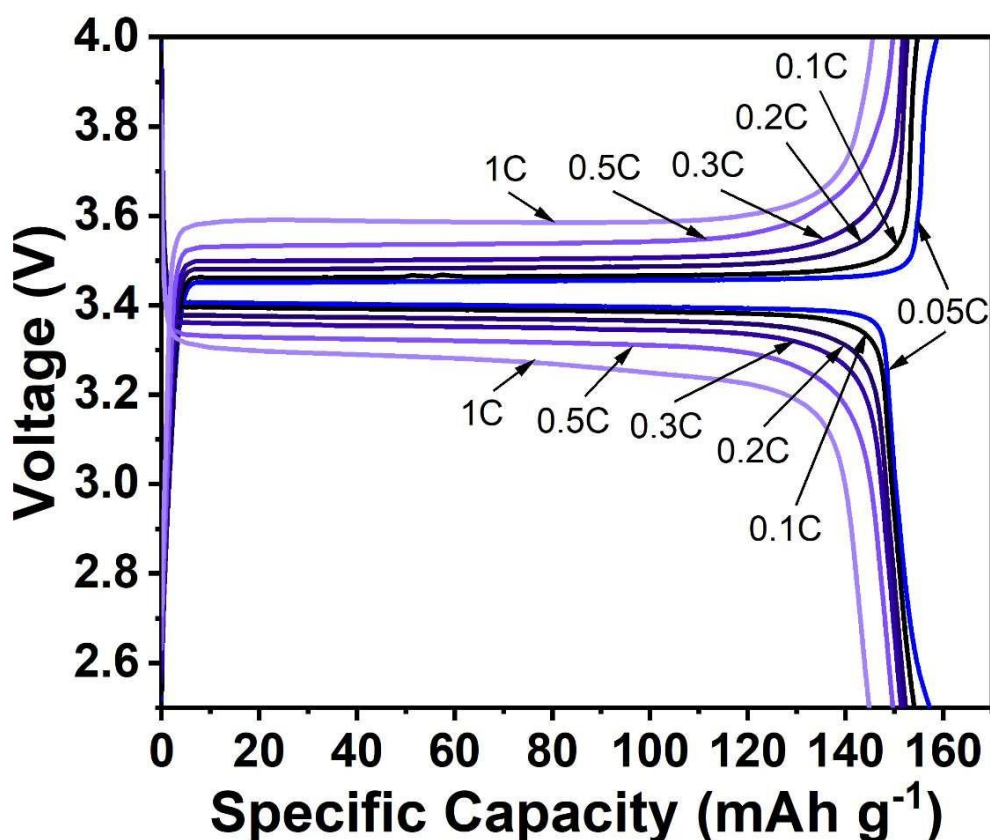
Figure 6-65. Potential profiles for the C rates capability at 0.05C, 0.1C, 0.2C, 0.3C, 0.5C, 1C with 1C= 170 mA g^{-1} and cut-off voltage set to 2.5 and 4.0 V vs. Li$^+$/Li.

 During the long-term cycling stability test (**Figure 6-66**), the discharge voltage is extremely stable, indicating no degradation of the electrode material during cycling. As observed on the cycling data, the capacity lost from the fiftieth to the two-hundredth cycles appears almost linear and could be due to multiple factors such as the contact loss between the LFP and the current collector, the degradation of the lithium‖SIPE-EF+PEO-L interphase, reaction of propylene carbonate with lithium. To the best of your knowledge, these good cycling results are the first

reported for a multilayer electrolyte comprising a single-ion conducting polymer electrolyte and open a large field for further research.
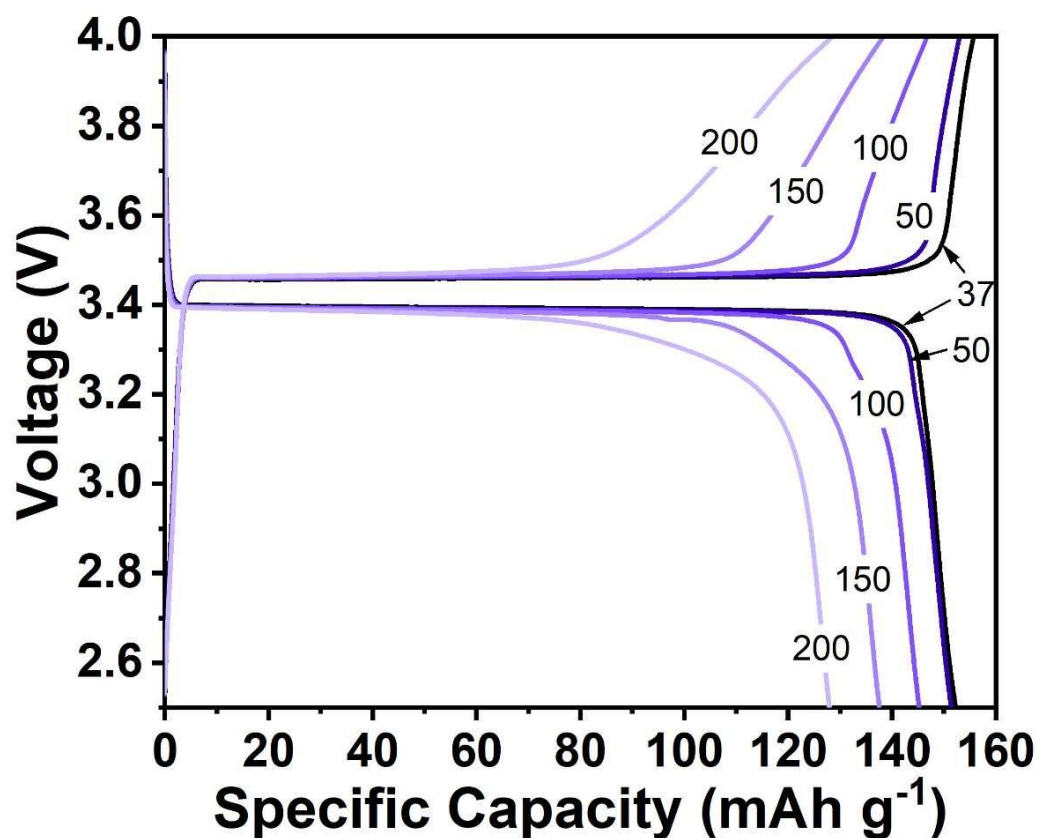
Figure 6-66. Potential profile at different selected cycles during the long-term cycling of the Li/LFP cell, all cycles were conducted at 0.1C with 1C= 170 mA g^{-1} and cut-off voltage set to 2.5 and 4.0 V vs. Li^{+}/Li.

6.3.7 Conclusions

To summarize, in this work, we developed a new ether-free high molecular weight polymer backbone, and we managed to couple it with an anionic side chain to obtain a new ether-free single-ion conducting polymer. When doped with an optimal 55% solvent content of propylene carbonate, we achieved excellent ionic conductivity at room temperature (>10^{-4} S cm^{-1}). Additionally, the electrochemical stability window was suitable for battery application (4.5 V). However, the lithium stripping/plating test with a symmetrical Li/Li cell revealed poor compatibility between lithium metal and our electrolyte when subjected to high current density.

To solve this problem, we prepared a conventional PEO:LiTFSI polymer electrolyte and used it as a thin protective layer between lithium metal and our ether-free single-ion conducting electrolyte. A thin trilayer system shows excellent cyclability and reversibility in symmetrical Li/Li cells at various current densities. The first tests of the multilayer system in a full-cell with lithium metal as anode and $LiFePO_4$ cathode also exhibit good results in C rates capability with high specific discharge capacity and a rather low capacity loss when increasing the C-rate. The long-term cycling stability shows an excellent Coulombic efficiency upon cycling with a good capacity retention of 84% after 200 cycles.

The next step would be to test and optimize this system to cycle it with high-voltage cathode material like NMC. Nevertheless, to the best of our knowledge, this is the first reported multilayer system comprising a single-ion conducting polymer layer, and this opens a new field of research for the potential implementation of lithium metal batteries.

7. Summary & Conclusion

Through the literature review, we realized that our actual battery technologies are not sufficient to answer the demand for batteries for a successful substitution of the combustion engine by the electrical engine and for the storage of the energy produced by renewable resources. Indeed, batteries with higher energy density and power are needed but, despite their excellent ionic conductivity and their ease of preparation, the actual commercial liquid electrolytes are not stable at high voltage, are corrosive, flammable, and cannot be used with lithium metal. The development of suitable solid electrolytes, i.e. with high electrochemical stability, high ionic conductivity, and good mechanical stability, could be a solution for commercialization of high-energy-density batteries. In this matter, salts in polymer solid electrolytes have been largely investigated over the last 20 years but still present drawbacks, especially with high-voltage cathode materials. More recently, some research groups are focusing on SIPEs, due to their t_{Li}^+ being close to unity, their good mechanical stability, and their easy film fabrication, Nevertheless, these polymers need to be doped with organic solvent to achieve acceptable ionic conductivity, raising again concerns about flammability. On another hand, most of the SIPEs reported in the literature have backbones containing ether bound that are known to be unstable toward oxidation and could limit their use with high-voltage cathodes.

In chapter 6.1, we address the issue of doping the SIPEs with organic solvents, by preparing a blend of an already reported multi-blocks copolymer SIPE with low molecular and non-volatile weight poly(ethylene glycol) dimethyl ether. The obtained membrane was self-standing and provided sufficient mechanical stability with a remarkable conductivity of 10^{-5} S cm^{-1} at 45 °C, a good electrochemical stability window until 4.6 V, a transference number of 0.99 and an excellent electrolyte ‖ lithium metal compatibility during stripping/plating test at different temperatures and current densities. Nevertheless, the polymer electrolyte demonstrated at 40°C rather low limiting current density of 0.2 mA cm^{-2}, which hindered fast charging and discharging in a full-cell setup using NMC$_{811}$ as the cathode material. The cycling tests at 40°C

were limited to 0.05C but exhibited a good initial discharge capacity and, despite the rather fast loss of capacity retention, an excellent Coulombic efficiency upon cycling was obtained. The use of higher temperatures (60 °C) allows us to conduct C rates capability tests, which demonstrate good capacity retention at different current densities but a rather high but reversible capacity loss when increasing the current density.

In Chapter 6.2, we focus on improving the previous blend by addition of LATP particles to obtain a solvent-free hybrid electrolyte. The preparation of the membrane by solvent casting followed by a hot-pressing step was easy and allowed for the formation of a self-standing, homogeneous, and mechanically stable film at all LATP percentages. Concerning the ionic conductivity, a decrease compared to the blend was observed with 20% LATP. When increasing the filler content to 30 and 40% an increase of conductivity was observed compared to the 20% composition and the values for 40% reached a similar value as for the blend (8.4×10^{-6} at 40°C). An enhancement of the electrochemical stability window until about 5 V and a transference number of ~0.9 was measured for all compositions. However, all electrochemical characterization tends to show a degradation of LATP when in contact with lithium but, on the other hand, the hybrid electrolyte exhibited excellent cyclability with lithium metal electrodes during stripping/plating tests, meaning that this degradation helps to form a stable SEI. Cycling tests with NMC_{811} at 40°C were conducted at 0.05C and the cells exhibited acceptable initial discharge capacity but a similar capacity retention as the previous blend. A good Coulombic efficiency upon cycling and no indication of degradation of the electrolyte was also reported. The C rates capability tests at 60 °C demonstrate a rather fast capacity decline in the first cycles at 0.05C before stabilization and a good capacity retention at other current densities. A high but reversible capacity loss was observed when increasing the current density.

Finally, in chapter 6.3 we synthesized a new ether-free high molecular weight polymer backbone, and we managed to couple it with an anionic side chain to obtain a single-ion conducting polymer. When doped with an optimal 55% solvent content of propylene carbonate, we achieved good mechanical stability, excellent ionic conductivity at room temperature ($>10^{-4}$ S cm^{-1}), and suitable electrochemical stability window (4.6 V). However, the lithium

stripping/plating tests revealed poor compatibility with lithium metal. Therefore, we introduced a thin protective PEO:LiTFSI layer and the so obtained multi-layer system showed excellent cyclability and reversibility in symmetrical Li/Li cells but also in Li/SIPE/LFP with high specific discharge capacity, excellent Coulombic efficiency, and a capacity retention of 84% after 200 cycles.

All these results open several perspectives for further work.

Concerning the blend, improving the cyclability versus NCM8111 should be the main focus for example by working on the mass loading of the electrode or optimizing the electrode and the cycling procedure. Testing this blend versus other cathode materials and particularly other NMC compositions could also be considered.

The same work perspective applies to the solvent-free hybrid electrolyte, but the improvement of the electrode/electrolyte interface is the next key step to obtain better cyclability with NMC_{811}.

For the ether-free single-ion conducting polymer, two main paths open to us. First, work on the backbone design to replace the $-CF_3$ with a more stable group could be interesting. On the other hand, the optimization of the multilayer system to achieve good cyclability versus high-voltage cathode material is the next step.

Appendix

A.1   Supplementary Information for Chapter 5.2
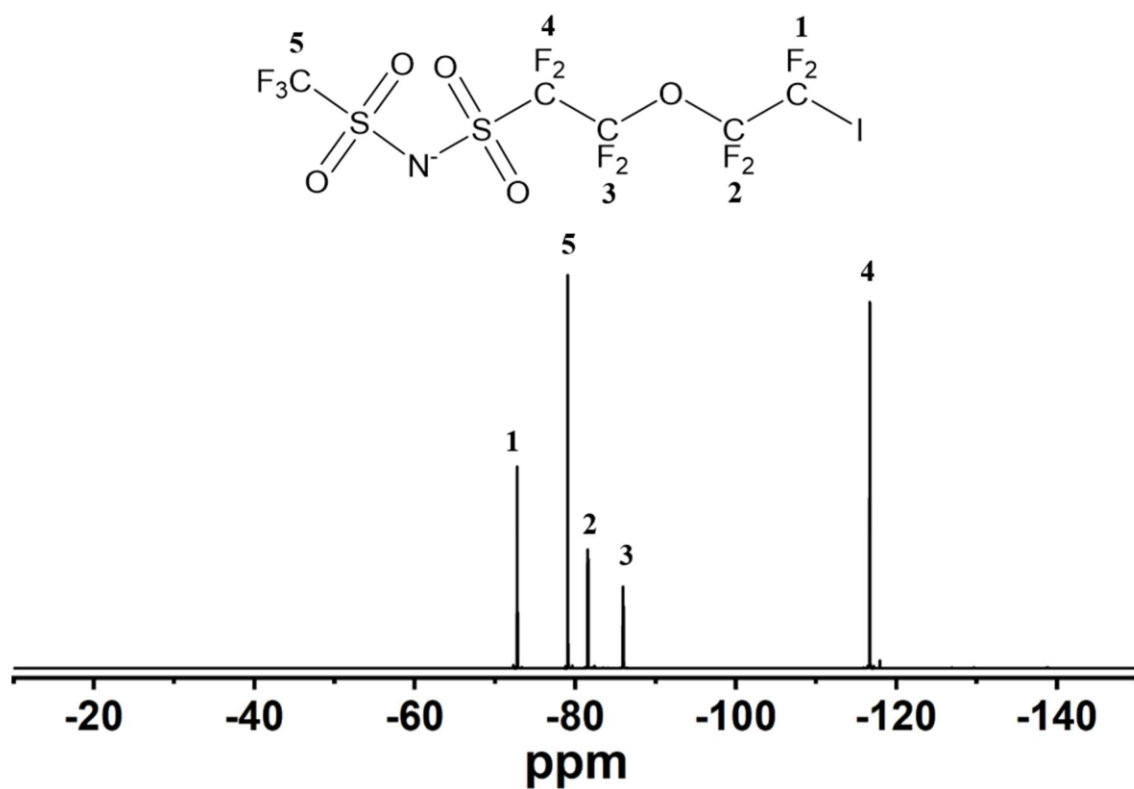
Figure S1. ^{19}F NMR spectrum recorded for the LiTFSI-like anionic side chain.

A.2   Supplementary Information for Chapter 6.1
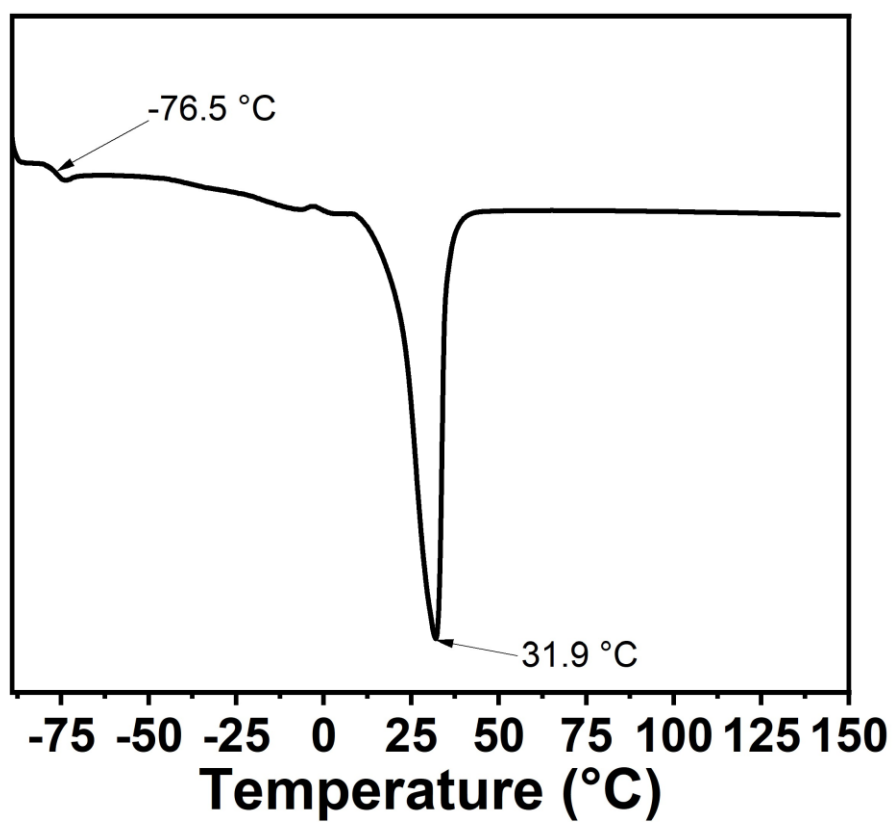
Figure S2. DSC analysis of poly(ethylene glycol) dimethyl ether

A.3 Supplementary Information for Chapter 6.2
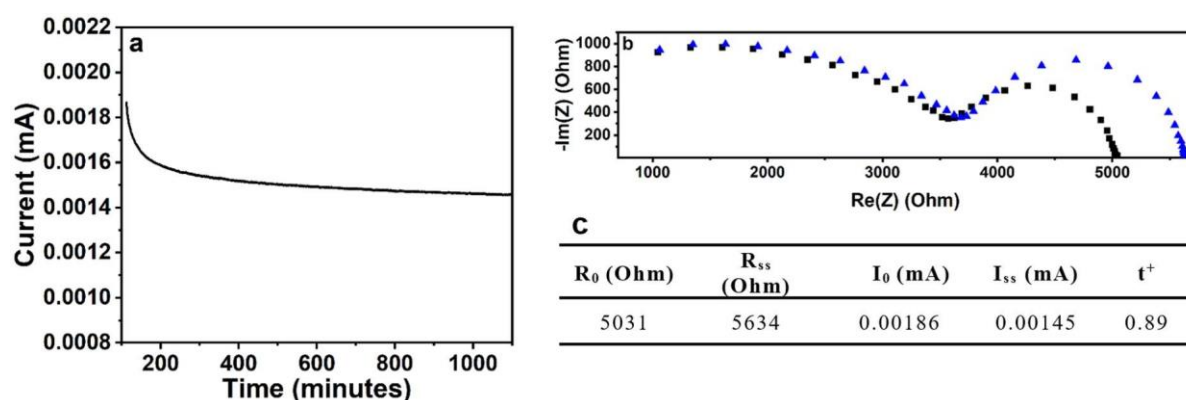
Figure S3. Determination of the transference Number of SIPE-HE20 by Bruce and Vincent potentiostatic method. a) chronoamperometry data obtained when applying a constant voltage of 10 mV to a symmetrical lithium/lithium cell containing the SIPE as electrolyte. b) Impedance measurement before (black) and after (blue) the chronoamperometry measurement. c) Values used in the Bruce and Vincent equation to determine the transference number.
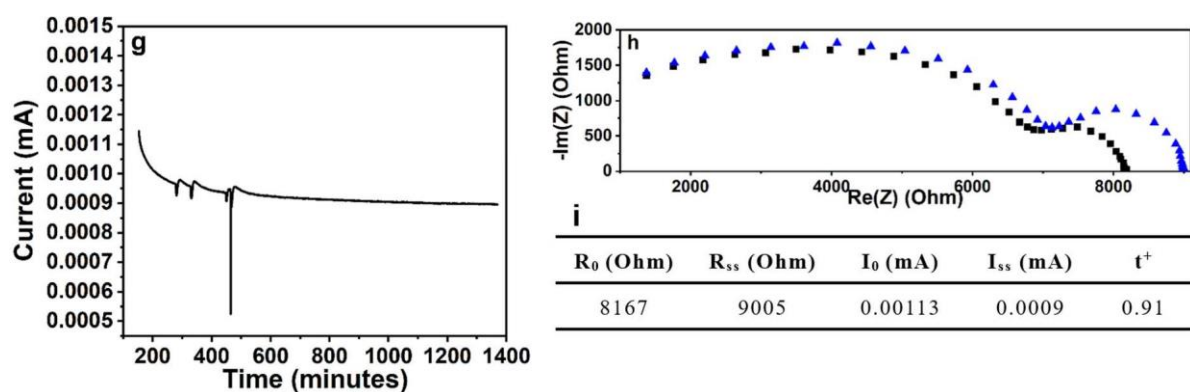
Figure S4. Determination of the transference Number of SIPE-HE40 by Bruce and Vincent potentiostatic method. a) chronoamperometry data obtained when applying a constant voltage of 10 mV to a symmetrical lithium/lithium cell containing the SIPE as electrolyte. b) Impedance measurement before (black) and after (blue) the chronoamperometry measurement. c) Values used in the Bruce and Vincent equation to determine the transference number.

A.4 Supplementary Information for Chapter 6.3

R_0 (Ohm)	R_{ss} (Ohm)	I_0 (mA)	I_{ss} (mA)	t^+
570.9	1026.4	0.017	0.0063	0.56
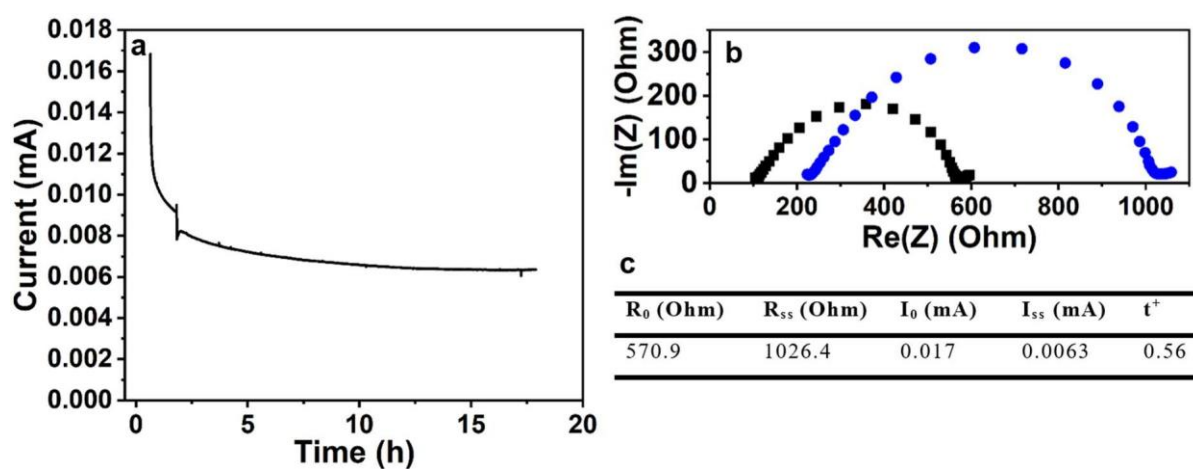
Figure S5. Determination of the transference Number by Bruce and Vincent potentiostatic method. a) chronoamperometry data obtained when applying a constant voltage of 10 mV to a symmetrical lithium/lithium cell containing the SIPE as electrolyte. b) Impedance measurement before (black) and after (blue) the chronoamperometry measurement. c) Values used in the Bruce and Vincent equation to determine the transference number
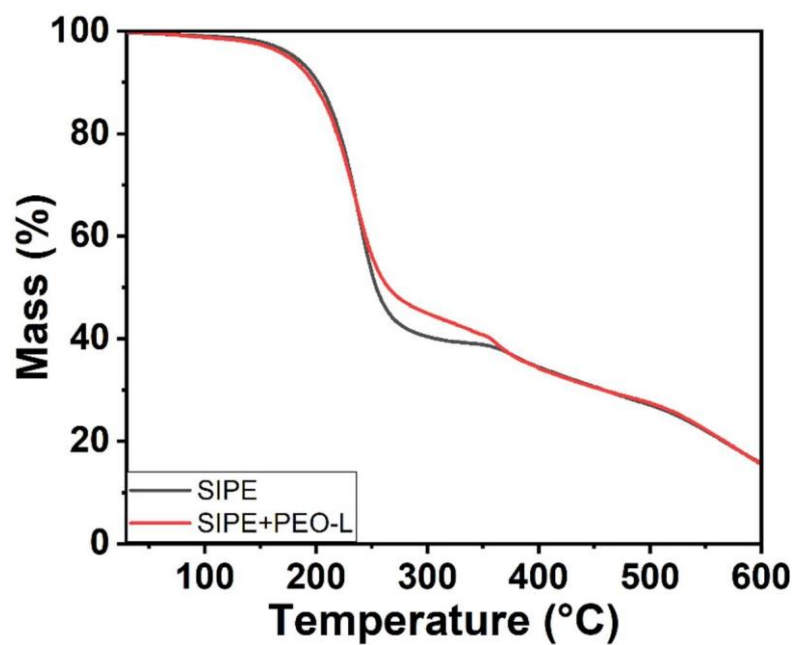
Figure S6. TGA curve of the SIPE swollen with 55 wt.% propylene carbonate (black) compared to the TGA curve of the multilayer system made of SIPE+PC and a PEO protective layer (red)

Acknowledgments

Firstly, I would like to express my deep appreciation to my supervisors Prof. Dr. Dominic Bresser, Dr. Cristina Iojoiu, and Dr. Sandrine Lyonnard with the sincerest heart. I am grateful to them for giving me the chance for this international PhD experience in their different groups and providing me with all the experimental conditions, instruments as well as precious experimental guidance. Thanks to Dr. Cristina Iojoiu for her full support during my time at the LEPMI, her precious advice for the preparation and synthesis of the different materials but also her help for the analysis of the experimental data. Thanks to Prof. Dr. Dominic Bresser for his support during my time at HIU, the implementation of the electrochemical characterization, and his help in understanding the experimental data. Thanks to Dr. Sandrine Lyonnard for offering me opportunities to perform experiments at ILL. Even if these experiments have not been really successful for the thesis, they are still valuable for my research career. Additionally, I would like to thank the reporters and all the members of my jury. Prof. Elie Paillard and Prof. Christel Laberty, for taking the time to read and comment carefully on my manuscript. I appreciated all the comments and the interesting discussion we had during the defense. I would like to thank Prof. Patrick Théato, Dr. Thi Khanh Ly Nguyen and Prof. Jean-Claude Lepretre for taking the time to attend my defense and their interesting thoughts and comments on my work.

Then, I would like to thank my colleagues from the FestBatt project: Dr. Xu Dong, Wenbo Wang, Ran Dong, Leo Gräber, and Medina Jasarevic. All of them are so friendly and provided me with quite a lot of help and useful discussion about experiments and data analysis, particularly during our polymer subgroup meetings.

Meanwhile, I would like to thank all my office mates, Dr. Justine Solier, Dr. Tanguy Picard, Dr. Yunfan Shao, Dr. Benjamin Mercier-Guyon, Adriana Capozzi, and all the other who had to

spend some time with us in the officet at LEPMI; Anja Lenzer, Dr. Mintao Wan and Dr. Qi Li at HIU for their help and great office hours over the past four years.

Furthermore, I would like to sincerely thank all the other colleagues I met during my PhD, thank you Dominik Steinle for all the useful discussions, his experience on PEO electrolytes, and his help in implementing the experiments, thank you Clemens Wunder for the help and discussion to analyze experimental data, thank to Dr. Dominik Stepien for the help with the SEM instruments. Thank you to everyone who made the last four years at LEPMI and HIU such a good experience: Dr. Thomas Basso-bert, Dr. Regis Porhiel, Dr. Léa Mangani, Dr. Timothée Fabre, Dr. Po-Hua Su, Dr. Markus Binder, Timo Böhler and so on. I cannot imagine how my PhD would have been without you, and I am grateful to have found such colleagues.

Additionally, I would like to express a huge thanks to all my friends. Without you, this thesis would not have been possible. Thank you to my Parisian friends (Benjamin, Axel, and Robin) for hosting me way too many times when I needed to escape the academic world. Thank you to all the other for their endless support and amazing times whenever we could meet. Thanks you to all the skaters I met in Grenoble and Ulm (too many to name them all), all the sessions, trips, and fun times we shared were essential for me to keep a good life/work balance.

Finally, I would like to show my deepest gratitude to my family, thank you to my mom and dad for giving me endless support during the good but also the bad times, I love you more than I can express here. Thank you to my brother, I cannot wait to share more amazing times with you at home or around the globe and I wish you the best for your PhD!

List of Figures

List of Tables

References

1.   Our World in Data. Energy consumption by sources, Word. Published 2024. https://ourworldindata.org/grapher/energy-consumption-by-source-and-country

2.   Kirsch S. Running out? Rethinking resource depletion. *Extr Ind Soc*. 2020;7(3):838-840. doi:10.1016/j.exis.2020.06.002

3.   Calvin K, Dasgupta D, Krinner G, et al. *IPCC, 2023: Climate Change 2023: Synthesis Report. Contribution of Working Groups I, II and III to the Sixth Assessment Report of the Intergovernmental Panel on Climate Change [Core Writing Team, H. Lee and J. Romero (Eds.)]. IPCC, Geneva, Switzerland.* (Arias P, Bustamante M, Elgizouli I, et al., eds.).; 2023. doi:10.59327/IPCC/AR6-9789291691647

4.   Nations Un. Treaty Series. 2016;3156:79. https://treaties.un.org/Pages/ViewDetails.aspx?src=IND&mtdsg_no=XXVII-7-d&chapter=27&clang=_en

5.   Trout K, Muttitt G, Lafleur D, et al. Existing fossil fuel extraction would warm the world beyond 1.5 °C. *Environ Res Lett*. 2022;17(6):064010. doi:10.1088/1748-9326/ac6228

6.   Liu J, Wang J, Xu C, et al. Advanced Energy Storage Devices: Basic Principles, Analytical Methods, and Rational Materials Design. *Adv Sci*. 2018;5(1). doi:10.1002/advs.201700322

7.   Eurostat. Energy statistics - an overview. Published 2023. https://ec.europa.eu/eurostat/statistics-explained/index.php?title=Energy_statistics_-_an_overview#Energy_dependency

8.   Singh R. Biofuels in Transport Sector. In: *Green Energy and Technology*. ; 2018:113-122. doi:10.1007/978-981-10-7326-7_7

9.   Zhao Y, Pohl O, Bhatt AI, et al. A Review on Battery Market Trends , Second-Life Reuse , and Recycling hybrid. Published online 2021:167-205.

10.   List of Nobel prizes. Published online 2023. https://www.nobelprize.org/prizes/

11.   Ziemann S, Grunwald A, Schebek L, Müller DB, Weil M. The future of mobility and its critical raw materials. 2013;54:47-54. doi:10.1051/metal/2013052

12.   Xu K. Nonaqueous liquid electrolytes for lithium-based rechargeable batteries. *Chem Rev*. 2004;104(10):4303-4417. doi:10.1021/cr030203g

13.   Whittingham MS. Electrical Energy Storage and Intercaltion. *Science (80-)*. 1976;192(4244):1126-1127.

14.   Besenhard JO, Schöllhorn R. The discharge reaction mechaniscm of the MoO3 electrode in organic electrolyte. *J Power Sources*. 1976;1:267-276.

15.   April R, Goodenough CJB. A NEW CATHODE MATERIAL FOR BATTERIES OF HIGH ENERGY DENSITY. 1980;15(c):783-789.

16.   Yazami R, Ozawa Y, Gabrisch H, Fultz B. New Trends in Intercalation Compounds for Energy Storage and Conversion. In: *Journal of the Electrochemical Society*. Vol 2003. ; 2003:317.

17.   Daniel C, Mohanty D, Li J, Wood DL. Cathode Materials Review. 2014;43:26-43. doi:10.1063/1.4878478

18.   Guan T, Sun S, Yu F, et al. Electrochimica Acta The degradation of LiCoO 2 / graphite

batteries at different rates. *Electrochim Acta*. 2018;279:204-212. doi:10.1016/j.electacta.2018.04.197

19. Doughty D, Roth EP. A General Discussion of Li Ion Battery Safety. *J. Electrochem Soc*. 2012;21:37.

20. Milan Grohol, Veeh C. *Study on the Critical Raw Material for the EU - Final Report*.; 2023.

21. Arai H, Okada S, Sakurai Y, Yamaki J ichi. Thermal behavior of Li 1 2 y NiO 2 and the decomposition mechanism. 1998;109(October 1997):295-302.

22. Tanner CW, Virkar A V. Optimization of the Composition of the Li 1 − z Ni 1 + z O 2 Electrode Materials : Structural , Magnetic , and Electrochemical Studies Optimization of the Composition of the Li1 _ Ni1 + O2 Electrode Materials : Structural , Magnetic , and Electrochemical . Published online 1996.

23. Sleigh AK, Murray JJ, Mckinnon WR. MEMORY EFFECTS DUE TO PHASE CONVERSION HYSTERESIS IN Li / Li , MnO , CELLS. 1991;36.

24. Vogler C, Garche J. Aging mechanisms of lithium cathode materials. 2004;127:58-64. doi:10.1016/j.jpowsour.2003.09.034

25. Bloom I, Jones SA, Battaglia VS, et al. Effect of cathode composition on capacity fade , impedance rise and power fade in high-power , lithium-ion cells. 2003;124:538-550. doi:10.1016/S0378-7753(03)00806-1

26. Noh H joo, Youn S, Seung C, Sun Y kook. Comparison of the structural and electrochemical properties cathode material for lithium-ion batteries. 2013;233:2-11. doi:10.1016/j.jpowsour.2013.01.063

27. Nanjundaswamya KS, Araib H, Yamakib J, Okadab S, Ohtsukab H. SOLID Synthesis , redox potential evaluation and electrochemical characteristics of NASICON-related-3D framework compounds. 1996;92.

28. Goodenough JB. Lithium Insertion into Fe2 (# O & M = W with M = MO * Frameworks : Comparison of. 1987;360:349-360.

29. Manthiram A, Goodenough JB. vice versa. 1989;26:403-408.

30. Behavior E, Theuwis A, Gomes WP, et al. L ' fJ. 1997;(I).

31. Tesla made $1.6 billion in Q3, is switching to LFP batteries globally | Ars Technica. Accessed January 17, 2024. https://arstechnica.com/cars/2021/10/tesla-made-1-6-billion-in-q3-is-switching-to-lfp-batteries-globally/

32. Xia Y, Yoshio M, Noguchi H. Improved electrochemical performance of LiFePO4 by increasing its specific surface area. *Electrochim Acta*. 2006;52(1):240-245. doi:10.1016/j.electacta.2006.05.002

33. Zaghib K, Mauger A, Gendron F, Julien CM. Surface effects on the physical and electrochemical properties of thin LiFePO4 particles. *Chem Mater*. 2008;20(2):462-469. doi:10.1021/cm7027993

34. Tolganbek N, Yerkinbekova Y, Kalybekkyzy S, Bakenov Z, Mentbayeva A. Current state of high voltage olivine structured LiMPO4 cathode materials for energy storage applications: A review. *J Alloys Compd*. 2021;882:160774. doi:10.1016/j.jallcom.2021.160774

35. Huang H, Yin SC, Kerr T, Taylor N, Nazar LF. Nanostructured Composite: A High Capacity, Fast Rate Li3V2(PO4)3 /Carbon Cathode for Rechargeable Lithium Batteries.

Adv Mater. 2002;14(21):1525-1528.

36. Barker J, Gover RKB, Burns P, Bryan A, Saidi MY, Swoyer JL. Structural and electrochemical properties of lithium vanadium fluorophosphate, LiVPO4F. *J Power Sources*. 2005;146(1-2):516-520. doi:10.1016/j.jpowsour.2005.03.126

37. Hérold A. Recherches sur les composés d'insertion du graphite. *Bull Soc Chim Fr*. 1955;(187):999-1012.

38. Kaskhedikar NA, Maier J. Lithium storage in carbon nanostructures. *Adv Mater*. 2009;21(25-26):2664-2680. doi:10.1002/adma.200901079

39. Manthiram A, Tsang C. Electrode materials for rechargeable lithium batteries. *An des la Asoc Quim Argentina*. 1996;84(3):265-270. doi:10.3390/books978-3-0365-8781-3

40. Persson K, Sethuraman VA, Hardwick LJ, et al. Lithium diffusion in graphitic carbon. *J Phys Chem Lett*. 2010;1(8):1176-1180. doi:10.1021/jz100188d

41. Schweidler S, De Biasi L, Schiele A, Hartmann P, Brezesinski T, Janek J. Volume Changes of Graphite Anodes Revisited: A Combined Operando X-ray Diffraction and in Situ Pressure Analysis Study. *J Phys Chem C*. 2018;122(16):8829-8835. doi:10.1021/acs.jpcc.8b01873

42. Gross SJ, Hsieh MT, Mumm DR, Valdevit L, Mohraz A. Alleviating expansion-induced mechanical degradation in lithium-ion battery silicon anodes via morphological design. *Extrem Mech Lett*. 2022;54:101746. doi:10.1016/j.eml.2022.101746

43. Aurbach D, Markovsky B, Weissman I, Levi E, Ein-Eli Y. On the correlation between surface chemistry and performance of graphite negative electrodes for Li ion batteries. *Electrochim Acta*. 1999;45(1):67-86. doi:10.1016/S0013-4686(99)00194-2

44.   Zhang SS. The effect of the charging protocol on the cycle life of a Li-ion battery. *J Power Sources*. 2006;161(2):1385-1391. doi:10.1016/j.jpowsour.2006.06.040

45.   Xu W, Wang J, Ding F, et al. Lithium metal anodes for rechargeable batteries. *Energy Environ Sci*. 2014;7(2):513-537. doi:10.1039/c3ee40795k

46.   Wang Q, Liu B, Shen Y, et al. Confronting the Challenges in Lithium Anodes for Lithium Metal Batteries. *Adv Sci*. 2021;8(17):1-25. doi:10.1002/advs.202101111

47.   Koch VR, Goldman JL, Mattos CJ, Mulvaney M. Specular Lithium Deposits from Lithium Hexafluoroarsenate/Diethyl Ether Electrolytes. *J Electrochem Soc*. 1982;129(1):1-4. doi:10.1149/1.2123756

48.   Abraham KM, Goldman JL, Natwig DL. Characterization of Ether Electrolytes for Rechargeable Lithium Cells. *J Electrochem Soc*. 1982;129(11):2404-2409. doi:10.1149/1.2123556

49.   Campbell SA, Bowes C, McMillan RS. The electrochemical behaviour of tetrahydrofuran and propylene carbonate without added electrolyte. *J Electroanal Chem*. 1990;284(1):195-204. doi:10.1016/0022-0728(90)87072-R

50.   Harris WS. *Electrochemical Studies in Cyclic Esters*. University of Californie, Berkley, CA;   1958. https://books.google.com/books?hl=en&lr=&id=tP00GZiyMNMC&oi=fnd&pg=PA2& dq=Harris,+W.S.+Electrochemical+Studies+in+Cyclic+Esters.+Ph.D.+Thesis,+Univ.+ California,+Berkeley,+CA,+USA,+1958.&ots=PYXMpoQmf9&sig=6hG9fTnWkms67 aNYTNYiWnNrw5Y#v=onepage&q&f=false%0A

51.   Li X, Guo L, Li J, et al. Reversible Cycling of Graphite Electrodes in Propylene

Carbonate Electrolytes Enabled by Ethyl Isothiocyanate. *ACS Appl Mater Interfaces*. 2021;13(22):26023-26033. doi:10.1021/acsami.1c04607

52.   Jiang J, Dahn JR. Effects of solvents and salts on the thermal stability of LiC6. *Electrochim Acta*. 2004;49(26):4599-4604. doi:10.1016/j.electacta.2004.05.014

53.   Zhang SS, Jow TR, Amine K, Henriksen GL. LiPF6-EC-EMC electrolyte for Li-ion battery. *J Power Sources*. 2002;107(1):18-23. doi:10.1016/S0378-7753(01)00968-5

54.   Liu YK, Zhao CZ, Du J, Zhang XQ, Chen AB, Zhang Q. Research Progresses of Liquid Electrolytes in Lithium-Ion Batteries. *Small*. 2023;19(8):1-14. doi:10.1002/smll.202205315

55.   Berhaut CL, Lemordant D, Porion P, Timperman L, Schmidt G, Anouti M. Ionic association analysis of LiTDI, LiFSI and LiPF 6 in EC/DMC for better Li-ion battery performances. *RSC Adv*. 2019;9(8):4599-4608. doi:10.1039/c8ra08430k

56.   Abouimrane A, Ding J, Davidson IJ. Liquid electrolyte based on lithium bis-fluorosulfonyl imide salt: Aluminum corrosion studies and lithium ion battery investigations. *J Power Sources*. 2009;189(1):693-696. doi:10.1016/j.jpowsour.2008.08.077

57.   He X, Bresser D, Passerini S, et al. The passivity of lithium electrodes in liquid electrolytes for secondary batteries. *Nat Rev Mater*. 2021;6(11):1036-1052. doi:10.1038/s41578-021-00345-5

58.   Murayama M, Kanno R, Irie M, et al. Synthesis of new lithium ionic conductor thio-LISICON - Lithium silicon sulfides system. *J Solid State Chem*. 2002;168(1):140-148. doi:10.1006/jssc.2002.9701

59. Tatsumisago M, Yamashita H, Hayashi A, Morimoto H, Minami T. Preparation and structure of amorphous solid electrolytes based on lithium sulfide. *J Non Cryst Solids*. 2000;274(1):30-38. doi:10.1016/S0022-3093(00)00180-0

60. Stramare S, Thangadurai V, Weppner W. Lithium Lanthanum Titanates: A Review. *Chem Mater*. 2003;15(21):3974-3990. doi:10.1021/cm0300516

61. Letchworth AT, Chard T. Human Placental Lactogen Levels in Pre-Eclampsia. *BJOG An Int J Obstet Gynaecol*. 1972;79(8):680-683. doi:10.1111/j.1471-0528.1972.tb12900.x

62. Yu X, Bates JB, Jellison GE, Hart FX. A Stable Thin-Film Lithium Electrolyte: Lithium Phosphorus Oxynitride. *J Electrochem Soc*. 1997;144(2):524-532. doi:10.1149/1.1837443

63. Thangadurai V, Kaack H, Weppner WJF. Novel fast lithium ion conduction in garnet-type Li5La3M2O12 (M = Nb, Ta). *J Am Ceram Soc*. 2003;86(3):437-440. doi:10.1111/j.1151-2916.2003.tb03318.x

64. Shin YK, Sengul MY, Jonayat ASM, et al. Development of a ReaxFF reactive force field for lithium ion conducting solid electrolyte Li1+: xAlxTi2- x(PO4)3 (LATP). *Phys Chem Chem Phys*. 2018;20(34):22134-22147. doi:10.1039/c8cp03586e

65. Zhou W, Wang S, Li Y, Xin S, Manthiram A, Goodenough JB. Plating a Dendrite-Free Lithium Anode with a Polymer/Ceramic/Polymer Sandwich Electrolyte. *J Am Chem Soc*. 2016;138(30):9385-9388. doi:10.1021/jacs.6b05341

66. Wakasugi J, Munakata H, Kanamura K. Effect of Gold Layer on Interface Resistance between Lithium Metal Anode and Li 6.25 Al 0.25 La 3 Zr 2 O 12 Solid Electrolyte . *J*

Electrochem Soc. 2017;164(6):A1022-A1025. doi:10.1149/2.0471706jes

67.   Zhao N, Fang R, He MH, et al. Cycle stability of lithium/garnet/lithium cells with different intermediate layers. *Rare Met.* 2018;37(6):473-479. doi:10.1007/s12598-018-1057-3

68.   Wang C, Gong Y, Liu B, et al. Conformal, Nanoscale ZnO Surface Modification of Garnet-Based Solid-State Electrolyte for Lithium Metal Anodes. *Nano Lett.* 2017;17(1):565-571. doi:10.1021/acs.nanolett.6b04695

69.   Armand M, Chabagno J, Duclot M. Poly-ethers as solid electrolytes. *Fast ion Transp solids.* 1979;(131).

70.   Zhou D, Shanmukaraj D, Tkacheva A, Armand M, Wang G. Polymer Electrolytes for Lithium-Based Batteries: Advances and Prospects. *Chem.* 2019;5(9):2326-2352. doi:10.1016/j.chempr.2019.05.009

71.   Xue Z, He D, Xie X. Poly(ethylene oxide)-based electrolytes for lithium-ion batteries. *J Mater Chem A.* 2015;3(38):19218-19253. doi:10.1039/c5ta03471j

72.   Fenton DE, Parker JM, Wright P V. Complexes of alkali metal ions with poly(ethylene oxide). *Polymer (Guildf).* 1973;14(11):589. doi:10.1016/0032-3861(73)90146-8

73.   Sequeira C, Santos D. *Polymer Electrolytes: Fundamentals and Applications.*; 2010.

74.   Berthier C, Gorecki W, Minier M, Armand MB, Chabagno JM, Rigaud P. Microscopic investigation of ionic conductivity in alkali metal salts-poly(ethylene oxide) adducts. *Solid State Ionics.* 1983;11(1):91-95. doi:10.1016/0167-2738(83)90068-1

75.   Zhang H, Liu C, Zheng L, et al. Lithium bis(fluorosulfonyl)imide/poly(ethylene oxide) polymer   electrolyte.   *Electrochim   Acta.*   2014;133:529-538.

doi:10.1016/j.electacta.2014.04.099

76. Chintapalli S, Frech R. Effect of plasticizers on ionic association and conductivity in the (PEO)9LiCF3SO3 system. *Macromolecules*. 1996;29(10):3499-3506. doi:10.1021/ma9515644

77. Frech R, Chintapalli S. Effect of propylene carbonate as a plasticizer in high molecular weight PEO-LiCF3SO3 electrolytes. *Solid State Ionics*. 1996;85(1-4):61-66. doi:10.1016/0167-2738(96)00041-0

78. Fan L, Dang Z, Nan CW, Li M. Thermal, electrical and mechanical properties of plasticized polymer electrolytes based on PEO/P(VDF-HFP) blends. *Electrochim Acta*. 2002;48(2):205-209. doi:10.1016/S0013-4686(02)00603-5

79. Lang-sheng Y, Zhong-qiang S, Pei-min H, Wei-xiang C, Li L. Polyaniline used as a positive in solid-state lithium battery. *J Power Sources*. 1993;44(1-3):499-503. doi:10.1016/0378-7753(93)80195-U

80. Wang C, Liu Q, Cao Q, Meng Q, Yang L. Investigation on the structure and the conductivity of plasticized polymer electrolytes. *Solid State Ionics*. 1992;53-56(PART 2):1106-1110. doi:10.1016/0167-2738(92)90298-4

81. Wang H, Im D, Lee DJ, et al. A Composite Polymer Electrolyte Protect Layer between Lithium and Water Stable Ceramics for Aqueous Lithium-Air Batteries. *J Electrochem Soc*. 2013;160(4):A728-A733. doi:10.1149/2.020306jes

82. Watanabe M, Endo T, Nishimoto A, Miura K, Yanagida M. High ionic conductivity and electrode interface properties of polymer electrolytes based on high molecular weight branched polyether. *J Power Sources*. 1999;81-82:786-789. doi:10.1016/S0378-

7753(99)00250-5

83. Hong H, Liquan C, Xuejie H, Rongjian X. Studies on PAN-based lithium salt complex. *Electrochim Acta*. 1992;37(9):1671-1673. doi:10.1016/0013-4686(92)80135-9

84. Yuan F, Chen HZ, Yang HY, Li HY, Wang M. PAN-PRO solid polymer electrolytes with high ionic conductivity. *Mater Chem Phys*. 2005;89(2-3):390-394. doi:10.1016/j.matchemphys.2004.09.032

85. Sadoway DR. Block and graft copolymer electrolytes for high-performance, solid-state, lithium batteries. *J Power Sources*. 2004;129(1 SPEC. ISS.):1-3. doi:10.1016/j.jpowsour.2003.11.016

86. Niitani T, Shimada M, Kawamura K, Dokko K, Rho YH, Kanamura K. Synthesis of Li+ ion conductive PEO-PSt block copolymer electrolyte with microphase separation structure. *Electrochem Solid-State Lett*. 2005;8(8). doi:10.1149/1.1940491

87. Tanaka R, Sakurai M, Sekiguchi H, Mori H, Murayama T, Ooyama T. Lithium ion conductivity in polyoxyethylene/polyethylenimine blends. *Electrochim Acta*. 2001;46(10-11):1709-1715. doi:10.1016/S0013-4686(00)00775-1

88. Jacob MME, Prabaharan SRS, Radhakrishna S. Effect of PEO addition on the electrolytic and thermal properties of PVDF-LiClO4 polymer electrolytes. *Solid State Ionics*. 1997;104(3-4):267-276. doi:10.1016/s0167-2738(97)00422-0

89. Lizundia E, Costa CM, Alves R, Lanceros-Méndez S. Cellulose and its derivatives for lithium ion battery separators: A review on the processing methods and properties. *Carbohydr Polym Technol Appl*. 2020;1(July):100001. doi:10.1016/j.carpta.2020.100001

90. Samad YA, Asghar A, Lalia BS, Hashaikeh R. Networked cellulose entrapped and reinforced PEO-based solid polymer electrolyte for moderate temperature applications. *J Appl Polym Sci*. 2013;129(5):2998-3006. doi:10.1002/app.39033

91. Brissot C, Rosso M, Chazalviel J -N., Lascaud S. In Situ Concentration Cartography in the Neighborhood of Dendrites Growing in Lithium/Polymer-Electrolyte/Lithium Cells. *J Electrochem Soc*. 1999;146(12):4393-4400. doi:10.1149/1.1392649

92. Chazalviel JN. Electrochemical aspects of the generation of ramified metallic electrodeposits. *Phys Rev A*. 1990;42(12):7355-7367. doi:10.1103/PhysRevA.42.7355

93. Sun XG, Kerr JB, Reeder CL, Liu G, Han Y. Network single ion conductors based on comb-branched polyepoxide ethers and lithium bis(allylmalonato)borate. *Macromolecules*. 2004;37(14):5133-5135. doi:10.1021/ma049331c

94. Doyle M, Fuller TF, Newman J. The importance of the lithium ion transference number in lithium/polymer cells. *Electrochim Acta*. 1994;39(13):2073-2081. doi:10.1016/0013-4686(94)85091-7

95. Tikekar MD, Archer LA, Koch DL. Stability Analysis of Electrodeposition across a Structured Electrolyte with Immobilized Anions. *J Electrochem Soc*. 2014;161(6):A847-A855. doi:10.1149/2.085405jes

96. Diederichsen KM, McShane EJ, McCloskey BD. Promising Routes to a High Li+ Transference Number Electrolyte for Lithium Ion Batteries. *ACS Energy Lett*. 2017;2(11):2563-2575. doi:10.1021/acsenergylett.7b00792

97. Mogurampelly S, Borodin O, Ganesan V. Computer Simulations of Ion Transport in Polymer Electrolyte Membranes. *Annu Rev Chem Biomol Eng*. 2016;7:349-371.

doi:10.1146/annurev-chembioeng-080615-034655

98. Blazejczyk A, Szczupak M, Wieczorek W, et al. Anion-binding calixarene receptors: Synthesis, microstructure, and effect on properties of polyether electrolytes. *Chem Mater*. 2005;17(6):1535-1547. doi:10.1021/cm048679j

99. Abe T, Gu N, Iriyama Y, Ogumi Z. Lithium-ion-conductive polyethylene oxide based polymer electrolytes containing tris(pentafluorophyenyl)borane. *J Fluor Chem*. 2003;123(2):279-282. doi:10.1016/S0022-1139(03)00143-X

100. Matsumi N, Sugai K, Ohno H. Selective ion transport in organoboron polymer electrolytes bearing a mesitylboron unit. *Macromolecules*. 2002;35(15):5731-5733. doi:10.1021/ma0121666

101. Herath MB, Creager SE, Rajagopal R V., Geiculescu OE, DesMarteau DD. Ionic conduction in polyether-based lithium arylfluorosulfonimide ionic melt electrolytes. *Electrochim Acta*. 2009;54(24):5877-5883. doi:10.1016/j.electacta.2009.05.050

102. Cao C, Li Y, Feng Y, et al. A sulfonimide-based alternating copolymer as a single-ion polymer electrolyte for high-performance lithium-ion batteries. *J Mater Chem A*. 2017;5(43):22519-22526. doi:10.1039/c7ta05787c

103. Transport I. of Polymeric Solid Electrolyte for Alkali-Metal Ion Transport. 1989;1775(4):1771-1775.

104. Kim HT, Park JK. Effects of cations on ionic states of poly(oligo-oxyethylene methacrylate-co-alkali metal acrylamidocaproate) single-ion conductor. *Solid State Ionics*. 1997;98(3-4):237-244. doi:10.1016/s0167-2738(97)00099-4

105. Huang X, Chen L, Huang H, et al. Electrical properties of a single lithium-ion conductor

PMSEO-PLPMS. *Solid State Ionics*. 1992;51(1-2):69-73. doi:10.1016/0167-2738(92)90345-P

106. Tsuchida E, Kobayashi N. Single-Ion Conduction in Poly [(oligo (oxyethylene). 1988;(c):96-100.

107. Park CH, Sun YK, Kim DW. Blended polymer electrolytes based on poly(lithium 4-styrene sulfonate) for the rechargeable lithium polymer batteries. *Electrochim Acta*. 2004;50(2-3 SPEC. ISS.):375-378. doi:10.1016/j.electacta.2004.01.110

108. Sun XG, Hou J, Kerr JB. Comb-shaped single ion conductors based on polyacrylate ethers and lithium alkyl sulfonate. *Electrochim Acta*. 2005;50(5):1139-1147. doi:10.1016/j.electacta.2004.08.011

109. Cowie JMG, Spence GH. Novel single ion, comb-branched polymer electrolytes. *Solid State Ionics*. 1999;123(1):233-242. doi:10.1016/S0167-2738(99)00080-6

110. Snyder JF, Ratner MA, Shriver DF. Ion Conductivity of Comb Polysiloxane Polyelectrolytes Containing Oligoether and Perfluoroether Sidechains. *J Electrochem Soc*. 2003;150(8):A1090. doi:10.1149/1.1589759

111. Feng S, Shi D, Liu F, et al. Single lithium-ion conducting polymer electrolytes based on poly[(4-styrenesulfonyl)(trifluoromethanesulfonyl)imide] anions. *Electrochim Acta*. 2013;93:254-263. doi:10.1016/j.electacta.2013.01.119

112. Siska DP, Shriver DF. Li+ conductivity of polysiloxane - Trifluoromethylsulfonamide polyelectrolytes. *Chem Mater*. 2001;13(12):4698-4700. doi:10.1021/cm000420n

113. Ma Q, Zhang H, Zhou C, et al. Single lithium-ion conducting polymer electrolytes based on a super-delocalized polyanion. *Angew Chemie - Int Ed*. 2016;55(7):2521-2525.

doi:10.1002/anie.201509299

114. Müller-Plathe F, Van Gunsteren WF. Computer simulation of a polymer electrolyte: Lithium iodide in amorphous poly(ethylene oxide). *J Chem Phys*. 1995;103(11):4745-4756. doi:10.1063/1.470611

115. Wen K, Xin C, Guan S, et al. Ion–Dipole Interaction Regulation Enables High-Performance Single-Ion Polymer Conductors for Solid-State Batteries. *Adv Mater*. 2022;34(32):1-12. doi:10.1002/adma.202202143

116. Meng N, Ye Y, Yang Z, Li H, Lian F. Developing Single-Ion Conductive Polymer Electrolytes for High-Energy-Density Solid State Batteries. *Adv Funct Mater*. 2023;33(43). doi:10.1002/adfm.202305072

117. Abbott LJ, Lawson JW. Effects of Side Chain Length on Ionic Aggregation and Dynamics in Polymer Single-Ion Conductors. *Macromolecules*. 2019;52(19):7456-7467. doi:10.1021/acs.macromol.9b00415

118. Devaux D, Liénafa L, Beaudoin E, et al. Comparison of single-ion-conductor block-copolymer electrolytes with Polystyrene-TFSI and Polymethacrylate-TFSI structural blocks. *Electrochim Acta*. 2018;269:250-261. doi:10.1016/j.electacta.2018.02.142

119. Chen Y, Xu G, Liu X, et al. A gel single ion conducting polymer electrolyte enables durable and safe lithium ion batteries via graft polymerization. *RSC Adv*. 2018;8(70):39967-39975. doi:10.1039/C8RA07557C

120. Du D, Li H, Xu H, et al. Lithium propanesulfonyl(trifluoromethylsulfonyl)imide grafted polybenzimidazole as a self-supporting single ion conducting polymer electrolyte membrane for lithium metal secondary batteries. *J Alloys Compd*. 2021;881.

doi:10.1016/j.jallcom.2021.160573

121.   Zhang J, Wang S, Han D, Xiao M, Sun L, Meng Y. Lithium (4-styrenesulfonyl) (trifluoromethanesulfonyl) imide based single-ion polymer electrolyte with superior battery performance. *Energy Storage Mater*. 2020;24(March 2019):579-587. doi:10.1016/j.ensm.2019.06.029

122.   Liang HP, Chen Z, Dong X, et al. Photo-Cross-Linked Single-Ion Conducting Polymer Electrolyte for Lithium-Metal Batteries. *Macromol Rapid Commun*. 2022;43(12):1-7. doi:10.1002/marc.202100820

123.   Förster S, Konrad M. From self-organizing polymers to nano- and biomaterials. *J Mater Chem*. 2003;13(11):2671-2688. doi:10.1039/b307512p

124.   Feng H, Lu X, Wang W, Kang NG, Mays JW. Block copolymers: Synthesis, self-assembly, and applications. *Polymers (Basel)*. 2017;9(10). doi:10.3390/polym9100494

125.   Bouchet R, Maria S, Meziane R, et al. Efficient electrolytes for lithium-metal batteries. *Nat Mater*. 2013;12(5):1-6. doi:10.1038/namt3602

126.   lingua-et-al-2021-unique-carbonate-based-single-ion-conducting-block-copolymers-enabling-high-voltage-all-solid-state.pdf.crdownload.

127.   Zhang Y, Lim CA, Cai W, et al. Design and synthesis of a single ion conducting block copolymer electrolyte with multifunctionality for lithium ion batteries. *RSC Adv*. 2014;4(83):43857-43864. doi:10.1039/c4ra08709g

128.   Bresser D, Lyonnard S, Iojoiu C, Picard L, Passerini S. Decoupling segmental relaxation and ionic conductivity for lithium-ion polymer electrolytes. *Mol Syst Des Eng*. 2019;4(4):779-792. doi:10.1039/c9me00038k

129. Nguyen HD, Kim GT, Shi J, et al. Nanostructured multi-block copolymer single-ion conductors for safer high-performance lithium batteries. *Energy Environ Sci*. 2018;11(11):3298-3309. doi:10.1039/c8ee02093k

130. Chen Z, Steinle D, Nguyen HD, et al. High-energy lithium batteries based on single-ion conducting polymer electrolytes and Li[Ni0.8Co0.1Mn0.1]O2 cathodes. *Nano Energy*. 2020;77(June):105129. doi:10.1016/j.nanoen.2020.105129

131. Steinle D, Chen Z, Nguyen HD, et al. Single-ion conducting polymer electrolyte for Li‖LiNi0.6Mn0.2Co0.2O2 batteries—impact of the anodic cutoff voltage and ambient temperature. *J Solid State Electrochem*. 2022;26(1):97-102. doi:10.1007/s10008-020-04895-6

132. Pecher O, Carretero-Gonzalez J, Griffith KJ, Grey CP. Materials' methods: NMR in battery research. *Chem Mater*. 2017;29(1):213-242. doi:10.1021/acs.chemmater.6b03183

133. Unkel A. *Basic Knowledge of Nuclear Magnetic Resonance Spectroscopy (NMR)*.; 2012.

134. Saadatkhah N, Carillo Garcia A, Ackermann S, et al. Experimental methods in chemical engineering: Thermogravimetric analysis—TGA. *Can J Chem Eng*. 2020;98(1):34-43. doi:10.1002/cjce.23673

135. Nawaz A, Kumar P. Impact of temperature severity on hydrothermal carbonization: Fuel properties, kinetic and thermodynamic parameters. *Fuel*. 2023;336(September 2022):127166. doi:10.1016/j.fuel.2022.127166

136. Elmanzalawy M, Innocenti A, Zarrabeitia M, et al. Mechanistic understanding of microstructure formation during synthesis of metal oxide/carbon nanocomposites. *J*

Mater Chem A. 2023;11(32):17125-17137. doi:10.1039/d3ta01230a

137. Caruso T, Capoleoni S, Cazzanelli E, Agostino RG, Villano P, Passerini S. Characterization of PEO-Lithium Triflate polymer electrolytes: Conductivity, DSC and Raman investigations. *Ionics (Kiel)*. 2002;8(1-2):36-43. doi:10.1007/BF02377751

138. Mohammed A, Abdullah A. Scanning Electron Microscopy (Sem): a Review. *Int Conf onHydraulics Pneum*. Published online 2018:77-85.

139. Microscopy : an introduction. 2000;13(4):40-44.

140. Kim T, Choi W, Shin HC, et al. Applications of voltammetry in lithium ion battery research. *J Electrochem Sci Technol*. 2020;11(1):14-25. doi:10.33961/jecst.2019.00619

141. Zugmann S, Fleischmann M, Amereller M, Gschwind RM, Wiemhöfer HD, Gores HJ. Measurement of transference numbers for lithium ion electrolytes via four different methods, a comparative study. *Electrochim Acta*. 2011;56(11):3926-3933. doi:10.1016/j.electacta.2011.02.025

142. Lazanas AC, Prodromidis MI. Electrochemical Impedance Spectroscopy─A Tutorial. *ACS Meas Sci Au*. 2023;3(3):162-193. doi:10.1021/acsmeasuresciau.2c00070

143. Yang X, Rogach AL. Electrochemical Techniques in Battery Research: A Tutorial for Nonelectrochemists. *Adv Energy Mater*. 2019;9(25):1-10. doi:10.1002/aenm.201900747

144. Isac-García J, Dobado JA, Calvo-Flores FG, Martínez-García H. Microscale. *Exp Org Chem*. Published online 2016:353-370. doi:10.1016/b978-0-12-803893-2.50010-3

145. Chen Z, Steinle D, Nguyen HD, et al. High-energy lithium batteries based on single-ion conducting polymer electrolytes and Li[Ni0.8Co0.1Mn0.1]O2 cathodes. *Nano Energy*. 2020;77(July):105129. doi:10.1016/j.nanoen.2020.105129

146.   Communaute DELA, Alpes G. f communauté Grenoble Alpes Electrolytes polymères aromatiq ues nanostructu rés pour PEMFC : Relation structu relm o rpho I og ie / pro priété E uxvERsrrÉ Grenoble Alpes Nanostructured Aromatic Polymer Electrolytes for PEMFC : Structure-Morphology-. Published online 2016.

147.   Costa LT, Lavall RL, Borges RS, Rieumont J, Silva GG, Ribeiro MCC. Polymer electrolytes based on poly(ethylene glycol) dimethyl ether and the ionic liquid 1-butyl-3-methylimidazolium hexafluorophosphate: Preparation, physico-chemical characterization, and theoretical study. *Electrochim Acta*. 2007;53(4):1568-1574. doi:10.1016/j.electacta.2007.03.061

148.   Polymer C. Compositional Variation of Glass-Transition. Published online 1978:1156-1161.

149.   Number P. Propylene carbonate for synthesis. 2024;(1907).

150.   Sequeira MCM, Avelino HMNT, Caetano FJP, Fareleira JMNA. Viscosity and Density Measurements of Poly(ethyleneglycol) 200 and Poly(ethyleneglycol) 600 at High Pressures. *J Chem Eng Data*. 2023;68(1):64-72. doi:10.1021/acs.jced.2c00578

151.   Koizumi, N., & Hanai T. Dielectric properties of polyethylene glycols: Dielectric relaxation in solid state. *Bull Inst Chem Res Kyoto Univ*. 1964;(42(2-3)):115-127.

152.   Yamada Y, Takazawa Y, Miyazaki K, Abe T. Electrochemical lithium intercalation into graphite in dimethyl sulfoxide-based electrolytes: Effect of solvation structure of lithium ion. *J Phys Chem C*. 2010;114(26):11680-11685. doi:10.1021/jp1037427

153.   Cheng H, Zhu C, Huang B, Lu M, Yang Y. Synthesis and electrochemical characterization of PEO-based polymer electrolytes with room temperature ionic liquids.

Electrochim Acta. 2007;52(19):5789-5794. doi:10.1016/j.electacta.2007.02.062

154. Yang X, Jiang M, Gao X, et al. Determining the limiting factor of the electrochemical stability window for PEO-based solid polymer electrolytes: Main chain or terminal -OH group? *Energy Environ Sci*. 2020;13(5):1318-1325. doi:10.1039/d0ee00342e

155. Lin X, Khosravinia K, Hu X, Li J, Lu W. Lithium Plating Mechanism, Detection, and Mitigation in Lithium-Ion Batteries. *Prog Energy Combust Sci*. 2021;87(July). doi:10.1016/j.pecs.2021.100953

156. Wetjen M, Kim GT, Joost M, Winter M, Passerini S. Temperature dependence of electrochemical properties of cross-linked poly(ethylene oxide)-lithium bis(trifluoromethanesulfonyl)imide-N-butyl-N-methylpyrrolidinium bis(trifluoromethanesulfonyl)imide solid polymer electrolytes for lithium batteries. *Electrochim Acta*. 2013;87:779-787. doi:10.1016/j.electacta.2012.09.034

157. Borzutzki K, Nair JR, Winter M, Brunklaus G. Does Cell Polarization Matter in Single-Ion Conducting Electrolytes? *ACS Appl Mater Interfaces*. 2022;14(4):5211-5222. doi:10.1021/acsami.1c19097

158. Keefe AS, Buteau S, Hill IG, Dahn JR. Temperature Dependent EIS Studies Separating Charge Transfer Impedance from Contact Impedance in Lithium-Ion Symmetric Cells. *J Electrochem Soc*. 2019;166(14):A3272-A3279. doi:10.1149/2.0541914jes

159. Liu L, Wang T, Sun L, et al. Stable Cycling of All-Solid-State Lithium Metal Batteries Enabled by Salt Engineering of PEO-Based Polymer Electrolytes. *Energy Environ Mater*. 2024;7(2):1-8. doi:10.1002/eem2.12580

160. Nguyen TM, Kim DW, Kim DY, Choi G, Suk J, Kang Y. Enhanced Performance of

Lithium Polymer Batteries Based on the Nickel-Rich LiNi0.8Mn0.1Co0.1O2Cathode Material and Dual Salts. *ACS Appl Energy Mater*. 2022;5(12):15768-15779. doi:10.1021/acsaem.2c03336

161. Fu C, Homann G, Grissa R, et al. A Polymerized-Ionic-Liquid-Based Polymer Electrolyte with High Oxidative Stability for 4 and 5 V Class Solid-State Lithium Metal Batteries. *Adv Energy Mater*. 2022;12(27):1-10. doi:10.1002/aenm.202200412

162. Sun H, Xie X, Huang Q, et al. Fluorinated Poly-oxalate Electrolytes Stabilizing both Anode and Cathode Interfaces for All-Solid-State Li/NMC811 Batteries. *Angew Chemie*. 2021;133(33):18483-18491. doi:10.1002/ange.202107667

163. Liang HP, Zarrabeitia M, Chen Z, et al. Polysiloxane-Based Single-Ion Conducting Polymer Blend Electrolyte Comprising Small-Molecule Organic Carbonates for High-Energy and High-Power Lithium-Metal Batteries. *Adv Energy Mater*. 2022;12(16). doi:10.1002/aenm.202200013

164. Nguyen TKL, Lopez G, Iojoiu C, Bouchet R, Ameduri B. Novel single-ion conducting electrolytes based on vinylidene fluoride copolymer for lithium metal batteries. *J Power Sources*. 2021;498:1-28. doi:10.1016/j.jpowsour.2021.229920

165. Electrolytes P, Ni L, Mn C. High-Energy Lithium Batteries based on Single-Ion Conducting. 2020;(Lm):1-30.

166. Piana G, Bella F, Geobaldo F, Meligrana G, Gerbaldi C. PEO/LAGP hybrid solid polymer electrolytes for ambient temperature lithium batteries by solvent-free, "one pot" preparation. *J Energy Storage*. 2019;26(August):100947. doi:10.1016/j.est.2019.100947

167. Angulakshmi N, Nahm KS, Nair JR, et al. Cycling profile of MgAl2O4-incorporated

composite electrolytes composed of PEO and LiPF6 for lithium polymer batteries. *Electrochim Acta*. 2013;90:179-185. doi:10.1016/j.electacta.2012.12.003

168. Weston JE, Steele BCH. Effects of preparation method on properties of lithium salt-poly(ethylene oxide) polymer electrolytes. *Solid State Ionics*. 1982;7(1):81-88. doi:10.1016/0167-2738(82)90073-X

169. Khan K, Hanif MB, Xin H, et al. PEO-Based Solid Composite Polymer Electrolyte for High Capacity Retention All-Solid-State Lithium Metal Battery. *Small*. 2024;20(4):1-9. doi:10.1002/smll.202305772

170. Zhang W, Nie J, Li F, Wang ZL, Sun C. A durable and safe solid-state lithium battery with a hybrid electrolyte membrane. *Nano Energy*. 2018;45(January):413-419. doi:10.1016/j.nanoen.2018.01.028

171. Liao YH, Li XP, Fu CH, et al. Polypropylene-supported and nano-Al2O3 doped poly(ethylene oxide)-poly(vinylidene fluoride-hexafluoropropylene)-based gel electrolyte for lithium ion batteries. *J Power Sources*. 2011;196(4):2115-2121. doi:10.1016/j.jpowsour.2010.10.062

172. Liang B, Tang S, Jiang Q, et al. Preparation and characterization of PEO-PMMA polymer composite electrolytes doped with nano-Al2O3. *Electrochim Acta*. 2015;169:334-341. doi:10.1016/j.electacta.2015.04.039

173. Liu W, Liu N, Sun J, et al. Ionic Conductivity Enhancement of Polymer Electrolytes with Ceramic Nanowire Fillers. *Nano Lett*. 2015;15(4):2740-2745. doi:10.1021/acs.nanolett.5b00600

174. Zhang X, Liu T, Zhang S, et al. Synergistic coupling between

Li6.75La3Zr175Ta0.25O12 and poly(vinylidene fluoride) induces high ionic conductivity, mechanical strength, and thermal stability of solid composite electrolytes. *J Am Chem Soc*. 2017;139(39):13779-13785. doi:10.1021/jacs.7b06364

175. Ju J, Wang Y, Chen B, et al. Integrated Interface Strategy toward Room Temperature Solid-State Lithium Batteries. *ACS Appl Mater Interfaces*. 2018;10(16):13588-13597. doi:10.1021/acsami.8b02240

176. Zhang J, Zang X, Wen H, et al. High-voltage and free-standing poly(propylene carbonate)/Li6.75La3Zr1.75Ta0.25O12 composite solid electrolyte for wide temperature range and flexible solid lithium ion battery. *J Mater Chem A*. 2017;5(10):4940-4948. doi:10.1039/c6ta10066j

177. Yu S, Xu Q, Lu X, et al. Single-Ion-Conducting "Polymer-in-Ceramic" Hybrid Electrolyte with an Intertwined NASICON-Type Nanofiber Skeleton. *ACS Appl Mater Interfaces*. 2021;13(51):61067-61077. doi:10.1021/acsami.1c17718

178. Chen Y, Li C, Ye D, Zhang Y, Bao H, Cheng H. Lithiated polyanion supported Li1.5Al0.5Ge1.5(PO4)3 composite membrane as single-ion conducting electrolyte for security and stability advancement in lithium metal batteries. *J Memb Sci*. 2021;620(July 2020). doi:10.1016/j.memsci.2020.118926

179. Merrill LC, Chen XC, Zhang Y, et al. Polymer-Ceramic Composite Electrolytes for Lithium Batteries: A Comparison between the Single-Ion-Conducting Polymer Matrix and Its Counterpart. *ACS Appl Energy Mater*. 2020;3(9):8871-8881. doi:10.1021/acsaem.0c01358

180. Wen K, Guan S, Liu S, et al. Single-Ion Conductive Polymer-Based Composite Electrolytes for High-Performance Solid-State Lithium Metal Batteries. *Small*.

2024;20(6):1-11. doi:10.1002/smll.202304164

181. Feng J, Wang L, Chen Y, Wang P, Zhang H, He X. PEO based polymer-ceramic hybrid solid electrolytes: a review. *Nano Converg*. 2021;8(1). doi:10.1186/s40580-020-00252-5

182. Hartmann P, Leichtweiss T, Busche MR, et al. Degradation of NASICON-type materials in contact with lithium metal: Formation of mixed conducting interphases (MCI) on solid electrolytes. *J Phys Chem C*. 2013;117(41):21064-21074. doi:10.1021/jp4051275

183. Liu Y, Sun Q, Zhao Y, et al. Stabilizing the Interface of NASICON Solid Electrolyte against Li Metal with Atomic Layer Deposition. *ACS Appl Mater Interfaces*. 2018;10(37):31240-31248. doi:10.1021/acsami.8b06366

184. Benabed Y, Rioux M, Rousselot S, Hautier G, Dollé M. Assessing the Electrochemical Stability Window of NASICON-Type Solid Electrolytes. *Front Energy Res*. 2021;9(May):1-13. doi:10.3389/fenrg.2021.682008

185. Mayer A, Nguyen HD, Mariani A, et al. Influence of Polymer Backbone Fluorination on the Electrochemical Behavior of Single-Ion Conducting Multiblock Copolymer Electrolytes. *ACS Macro Lett*. 2022;11(8):982-990. doi:10.1021/acsmacrolett.2c00292

186. Kray WD, Rosser RW. of Multifunctional Triarylfluoroethanes. 1977;42(7):1186-1189.

187. Olvera LI, Guzmán-Gutiérrez MT, Zolotukhin MG, et al. Novel high molecular weight aromatic fluorinated polymers from one-pot, metal-free step polymerizations. *Macromolecules*. 2013;46(18):7245-7256. doi:10.1021/ma401306s

188. Assumma L, Nguyen HD, Iojoiu C, Lyonnard S, Mercier R, Espuche E. Effects of Block Length and Membrane Processing Conditions on the Morphology and Properties of

Perfluorosulfonated Poly(arylene ether sulfone) Multiblock Copolymer Membranes for PEMFC. *ACS Appl Mater Interfaces*. 2015;7(25):13808-13820. doi:10.1021/acsami.5b01835

189. Assumma L, Iojoiu C, Mercier R, Lyonnard S, Nguyen HD, Planes E. Synthesis of partially fluorinated poly(arylene ether sulfone) multiblock copolymers bearing perfluorosulfonic functions. *J Polym Sci Part A Polym Chem*. 2015;53(16):1941-1956. doi:10.1002/pola.27650

190. Mayer A, Ates T, Varzi A, Passerini S, Bresser D. Novel sulfur-doped single-ion conducting multi-block copolymer electrolyte. *Front Chem*. 2022;10(August):1-9. doi:10.3389/fchem.2022.974202

191. Ibrahim S, Yassin MM, Ahmad R, Johan MR. Effects of various LiPF6 salt concentrations on PEO-based solid polymer electrolytes. *Ionics (Kiel)*. 2011;17(5):399-405. doi:10.1007/s11581-011-0524-8

192. Zhang X, Kostecki R, Richardson TJ, Pugh JK, Ross PN. Electrochemical and Infrared Studies of the Reduction of Organic Carbonates. *J Electrochem Soc*. 2001;148(12):A1341. doi:10.1149/1.1415547

193. Ryu SW, Trapa PE, Olugebefola SC, Gonzalez-Leon JA, Sadoway DR, Mayes AM. Effect of Counter Ion Placement on Conductivity in Single-Ion Conducting Block Copolymer Electrolytes. *J Electrochem Soc*. 2005;152(1):A158. doi:10.1149/1.1828244

194. Zhou W, Wang Z, Pu Y, et al. Double-Layer Polymer Electrolyte for High-Voltage All-Solid-State Rechargeable Batteries. *Adv Mater*. 2019;31(4):1-7. doi:10.1002/adma.201805574

195. Hernandez-Maya R, Rosas O, Saunders J, Castaneda H. Dynamic Characterization of Dendrite Deposition and Growth in Li-Surface by Electrochemical Impedance Spectroscopy. *J Electrochem Soc*. 2015;162(4):A687-A696. doi:10.1149/2.0561504jes

196. Jiang Y, Yu H, Fu Y, Liu L. Redox potentials of trifluoromethyl-containing compounds. *Sci China Chem*. 2015;58(4):673-683. doi:10.1007/s11426-014-5178-8

197. Pożyczka K, Marzantowicz M, Dygas JR, Krok F. IONIC CONDUCTIVITY AND LITHIUM TRANSFERENCE NUMBER OF POLY(ETHYLENE OXIDE):LiTFSI SYSTEM. *Electrochim Acta*. 2017;227:127-135. doi:10.1016/j.electacta.2016.12.172

198. Lin D, Liu W, Liu Y, et al. High Ionic Conductivity of Composite Solid Polymer Electrolyte via in Situ Synthesis of Monodispersed SiO_2 Nanospheres in Poly(ethylene oxide). *Nano Lett*. 2016;16(1):459-465. doi:10.1021/acs.nanolett.5b04117

199. Song C, Li Z, Peng J, et al. Enhancing Li ion transfer efficacy in PEO-based solid polymer electrolytes to promote cycling stability of Li-metal batteries. *J Mater Chem A*. 2022;10(30):16087-16094. doi:10.1039/d2ta03283j

200. Wang N, Wei Y, Yu S, et al. A flexible PEO-based polymer electrolyte with cross-linked network for high-voltage all solid-state lithium-ion battery. *J Mater Sci Technol*. 2024;183:206-214. doi:10.1016/j.jmst.2023.10.005

201. Shim J, Striebel KA. Cycling performance of low-cost lithium ion batteries with natural graphite and $LiFePO_4$. *J Power Sources*. 2003;119-121:955-958. doi:10.1016/S0378-7753(03)00297-0

Curriculum Vitae

Grégoire Vansse   gregoire.vansse@gmail.com

Date of birth: 23.07.1999

Place of birth: Lille, France

Nationality: French

Academic Career

11/2020 – 09/2024	**Karlsruhe Institute of Technology (KIT)**, Germany and **Laboratoire Electrochimie et Physicochimie des Materiaux et des Interfaces (LEPMI)**, France
	PhD candidate as part of a co-tutelle agreement in the group of Dr. Dominic Bresser (KIT) and the group of Dr. Cristina Iojiou (LEPMI)
	Single-ion conducting polymer and hybrid electrolyte for high-energy density lithium-metal batteries
09/2016 - 08/2020	**National Graduate School of Chemistry of Montpellier**, France
	Chemical engineer Diploma
	Master of sciences "Materials science and chemistry for energy and sustainable development"
	Master thesis: ‹‹Recycling of the material of lithium-ion batteries. Post mortem and Operando Electrochemical and XPS characterization of the interactions between Ionic Liquid and anode/cathode materials››
09/2014 - 07/2016	**Lycée Georges Clemenceau**, Nantes, France
	Classes Préparatoires aux Grandes Ecoles PCSI/PC*
09/2011 - 07/2014	**Lycée Jean Dautet**, La Rochelle, France
	Baccalauréat and Abitur